Electronic Thesis and Dissertation Repository

4-26-2011 12:00 AM

Particle Attrition with Supersonic Nozzles in a High Temperature Fluidized Bed

Feng Li, *The University of Western Ontario*

Supervisor: Dr. Cedric Briens, *The University of Western Ontario*
Joint Supervisor: Dr. Franco Berruti, *The University of Western Ontario*
A thesis submitted in partial fulfillment of the requirements for the Doctor of Philosophy degree in Chemical and Biochemical Engineering
© Feng Li 2011

Follow this and additional works at: https://ir.lib.uwo.ca/etd

 Part of the Petroleum Engineering Commons

Recommended Citation

PARTICLE ATTRITION WITH SUPERSONIC NOZZLES IN A HIGH
TEMPERATURE FLUIDIZED BED

(Spine title: Particle Attrition with Supersonic Nozzles in a High Temperature Fluidized
Bed)

(Thesis format: Integrated Article)

by

Feng <u>Li</u>

Graduate Program in Engineering Science
Department of Chemical and Biochemical Engineering

A thesis submitted in partial fulfillment
of the requirements for the degree of
Doctoral of Philosophy

The School of Graduate and Postdoctoral Studies
The University of Western Ontario
London, Ontario, Canada

THE UNIVERSITY OF WESTERN ONTARIO
School of Graduate and Postdoctoral Studies

CERTIFICATE OF EXAMINATION

Joint-Supervisor   Examiners

_____   _____
Dr. Cedric Briens   Dr. Paul Chapentier

Joint-Supervisor

                                                   _____
                                                   Dr. Ajay Ray

_____
Dr. Franco Berruti

                                                   _____
                                                   Dr. Raouf E. Baddour

Supervisory Committee

                                                   _____
                                                   Dr. Nicolas Abatzoglou
_____
Dr. Jennifer McMillan

The thesis by

Feng Li

entitled:

Particle attrition with supersonic nozzles in a high temperature fluidized bed

is accepted in partial fulfillment of the
requirements for the degree of
Doctor of Philosophy

_____   _____
           Date   Chair of the Thesis Examination Board

Abstract

Fluidized beds are widely used for a variety of processes such as food, pharmaceutical, petrochemical and energy production. As a typical application of fluidized beds, the fluid coking process uses thermal cracking reactions to upgrade heavy oils and bitumen from oil sands. In order to maintain a well fluidized bed and a satisfactory operation, a series of supersonic nozzles are used to inject high pressure steam in the bed to maintain the coke particle within an optimal range. Currently, the attrition nozzles consume a large florwrate of high pressure and superheated steam, which accounts for about 40 % of the total energy consumption in fluid coking reactors. Improving the efficiency of the attrition process would increase energy efficiency and reduce sour waste water production, reducing the environmental impact of heavy oil upgrading. Therefore, the main objective of the present thesis is an experimental and numerical study of particle attrition with supersonic nozzles in high temperature fluidized beds. The specific objective is to improve particle grinding efficiency and reduce the steam consumption in the fluid coking process.

To achieve the research objective, the primary investigations focused on the solids entrainment and penetration of jets issuing from supersonic nozzles, which have significant effects on particle attrition. Novel measuring techniques, therefore, were developed to accurately measure the flowrate of solids entrained into the jet and its penetration length. The numerical and experimental studies reveal that the jet penetration lengths are related to the two-phase Froude number. A new correlation was developed to predict the penetration length of jets issuing from supersonic nozzles in high temperature fluidized beds, based on Benjelloun's correlation and the Froude number. The attrition experimental results demonstrate that larger scale nozzles, operating with a high flowrate of a low molecular weight gas at high temperature provide the highest grinding efficiency.

A jet-induced attrition model in fluidized beds at high temperature has been proposed and developed. The model is a coupled Eulerian-Eulerian multiphase model with a population balance method. The particle-particle interactions are described with the kinetic theory of granular flow. Experimental results were used to determine and modify

iii

the critical parameters of the model. The best prediction was obtained using the Ghadiri breakage kernel, generalized daughter size distribution function, and discrete solution method.

Finally, the research focused on the enhancement of jet-induced attrition in fluidized bed. A twin-jet nozzle gave a grinding efficiency that is about 35% higher than with a single nozzle. The benefits of the twin-jet nozzle seem stronger at higher nozzle pressures and high temperature. It is likely that the twin-jet nozzle entrains more solids into the jets when compared with a single nozzle with the same gas flowrate.

Keywords

Co-Authorship Statement

Chapter 2

Article Title:
Study of Solids Entrainment into Attrition Jets in Fluidized Beds
Authors:
Feng Li, Cedric Briens, Franco Berruti, and Jennifer McMillan
Status:
Published by Fluidization Conference XIII Proceeding
Feng Li conducted all experiments and data analysis related to this paper. The article was written by Feng Li who also developed the novel technique to measure solids entrainment. The work was jointly supervised by Cedric Briens, Franco Berruti and Jennifer McMillan. The draft of article was reviewed by Cedric Briens and Franco Berruti.

Chapter 3

Article Title:
Penetration of High Velocity Horizontal Gas Jets Into A Fluidized Bed at High Temperature
Authors:
Feng Li, Cedric Briens, Franco Berruti, and Jennifer McMillan
Status:
Published by Fluidization Conference XIII Proceeding
Feng Li conducted all experiments and data analysis related to this paper. The article was written by Feng Li who also developed the novel technique to measure penetration length of supersonic nozzles. The work was jointly supervised by Cedric Briens, Franco Berruti and Jennifer McMillan. Various drafts of article were reviewed by Cedric Briens and Franco Berruti.

Chapter 4

Article Title:
Particle Attrition with Supersonic Nozzles in A Fluidized Bed at High Temperature
Authors:
Feng Li, Cedric Briens, Franco Berruti, and Jennifer McMillan
Status:
Prepare to publish at *Powder Technology*
The experimental apparatus was designed by Cedric Briens, Franco Berruti, and Ed Chan. Feng Li joined the design of the tertiary cyclone and the sampling set. Feng Li also conducted all experiments and data analysis related to this paper. The article was written by Feng Li and reviewed by Cedric Briens and Franco Berruti. The work was jointly supervised by Cedric Briens, Franco Berruti and Jennifer McMillan.

Chapter 5

Article Title:
Modeling of Penetration of Horizontal Supersonic Nozzles in High Temperature Fluidized Beds
Authors:
Feng Li, Cedric Briens, Franco Berruti, and Jennifer McMillan
Status:
Prepare to publish at *The Canadian Journal of Chemical Engineering*
Feng Li conducted all CFD simulation work and experimental work related to this paper. The article was written by Feng Li and reviewed by Cedric Briens and Franco Berruti. The work was jointly supervised by Cedric Briens, Franco Berruti and Jennifer McMillan.

Chapter 6

Article Title:
Numerical Simulation of Particle Attrition with Convergent Divergent Nozzles in High Temperature Fluidized Beds
Authors:
Feng Li, Cedric Briens, Franco Berruti, and Jennifer McMillan
Status:
Prepare to publish at *AIChE Journal*
Feng Li conducted all CFD simulation work and experimental work related to this paper. The article was written by Feng Li and reviewed by Cedric Briens and Franco Berruti. The work was jointly supervised by Cedric Briens, Franco Berruti and Jennifer McMillan.

Chapter 7

Article Title:
Experimental and Numerical Study of Twin-Jet Nozzle in Particle Attrition Process
Authors:
Feng Li, Cedric Briens, Franco Berruti, and Jennifer McMillan
Status:
Prepare to publish at *Chemical Engineering and Processing: Process Intensification*
Feng Li conducted all CFD simulation work and experimental work related to this paper. The twin-jet nozzles in this paper were designed by Feng Li. The article was written by Feng Li and reviewed by Cedric Briens and Franco Berruti. The work was jointly supervised by Cedric Briens, Franco Berruti and Jennifer McMillan.

Acknowledgements

Table of Contents

List of Tables

List of Figures

Chapter 1

1   Introduction

The research work discussed in this dissertation deals with experimental and numerical studies involving particle attrition with a convergent-divergent nozzle in fluidized beds. The integrated-article format was chosen for the dissertation.

In this chapter, a brief description of the development of oil sands and fluid coking upgrading process in Canada is first introduced, which is a major motivation for present project. Introductions are then presented on fluidized bed reactors, turbulent jets, particle attrition theory and the application of computational fluid dynamics to the simulation of multiphase system. A review of recent studies involving jet-induced particle attrition at high temperature follows. This chapter concludes with an outline of the thesis research objectives.

1.1   Oil sands and the Fluid coking upgrading process

The oil sands in Canada have become a focus of intense development in recent decades. The oil sands are a highly dense and viscous tar-like form of petroleum, a mixture of sand, clay, and bitumen. Most of the resource is located in northeastern Alberta, Canada. The Albertan oil sands reserve is estimated to exceed 1.8 trillion barrels; about 300 billion barrels can be recovered by current technologies, ranking Canada second only to Saudi Arabia in world capacity (Government of Alberta, 2009). In 2009, Alberta totally produced about 1.35 million bbls/d crude bitumen from oil sands, representing about 70 percent of Alberta's and 49 percent of Canada's total crude oil and equivalent production. Oil sands production is different from conventional oil production. For the resources within about 100 meters of the surface, oil sands are mined and then processed in facilities where the bitumen they contain is extracted. For the deeper deposits, the most common technology of in-situ is steam-assisted gravity drainage (SAGD). In SAGD, a pair of horizontal wells is drilled, where hot steam is injected into the upper one, heating bitumen to a temperature at which it can flow into the lower well. The bitumen from either mining or in situ operations contains 50 − 60 wt% vacuum residues. Vacuum

residue is the fraction of petroleum that does not distill under vacuum, and typically has a normal boiling point of over 525°C (Gray, 1994). As the bitumen cannot be processed in refineries, upgrading is essential to convert the bitumen from oil sands to synthetic crude oil (SCO). This reduces the viscosity to allow shipment by pipeline without solvent addition and converts the bitumen into a crude oil substitute of high quality. There are two upgrading approaches, coking and hydrotreating.

In the hydrotreating process, hydrogen is used to crack the bitumen to produce light crude oil. The reaction requires involving a catalyst and high pressure, but the temperature is relatively lower at 420°C. The hydrotreating process can efficiently remove impurities, such as nitrogen, sulphur, and trace metals in heavy crude feedstock. It is not widely used because of its high capital and operating costs.

Thermal cracking or coking process is a non-catalytic process that uses thermal cracking reactions to upgrading bitumen to light synthetic crude oil (Gray, 2002). In coking process, the long chain hydrocarbon molecules are broken down into small molecules at high operating temperature. There are two main types of thermal cracking processes, delayed coking and fluid coking. Delayed coking has a wide application in treating heavy residues, which uses long reaction times in the liquid phase to convert the residue fraction of the feed to gases, distillates, and coke. The delayed coking process is a semi-batch process that gives rise to a highly aromatic coke product that retains sulfur, nitrogen and metals (Gray, 1994). The bitumen is heated to approximately 500°C through a heating coil and sprayed into a coking drum where it is maintained until it is converted into the vapors and coke. The operation is continuous until the coking drum is substantially full of coke. Once the first drum is full of coke, the delayed coking reaction is switched to another coking drum.

The fluid coking process, developed by ExxonMobil, is a continuous fluid technology that thermally converts heavy oil from oil sands or FCC bottoms to synthetic crude oil. Currently, fluid coking process is used commercially in refineries for deep conversion and as the resource to upgrade oil sands bitumen. Since its continuous fluid bed process,

flexibility, high reliability, and large capacity, the fluid coking process has been shown to perform better than delayed coking (Gray, 1994). It is also characterized by a much lower greenhouse gas emissions than delayed coking.
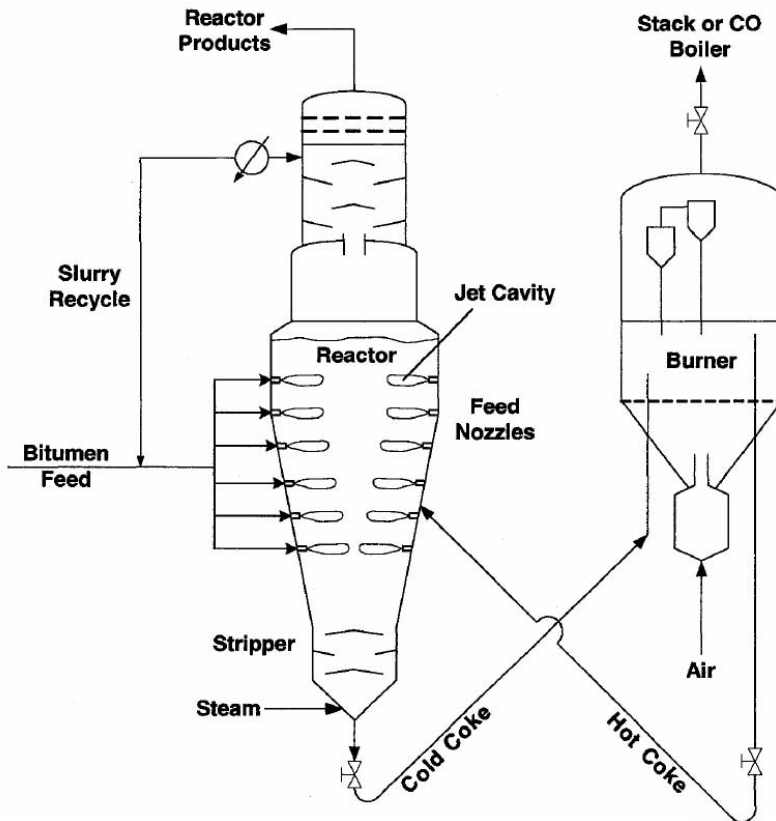
Figure 1.1 Flow diagram of the fluid coking process (House, 2007)

As shown in Figure 1.1 (House, 2007), fluid coking uses two main vessels, a reactor and a burner. The coker reactor is the primary equipment in the upgrading of bitumen to synthetic crude oil, which can be divided into three sections: scrubber section, reaction section, and stripper section. Bitumen feedstock is atomized and sprayed into the reaction section of the reactor through a number of high efficiency liquid-gas nozzles. It is crucial to make the feeding heavy oil be distributed quickly and uniformly over the individual particles of the bed for a stable and satisfied reaction rate. The feed vaporizes in the bed and leaves behind on the particles a sticky residue that forms a new layer of coke. The volume of vapor increases gradually up through the reactor dense bed due to the formation of cracked vapor products. In the reactor, the coke particles flow downwards through the dense bed into the stripping section at the bottom of vessel. The

gases and vapors, including fluidizing and stripping steam and vapors and gases formed by coking of the feed, rise and maintain a turbulent fluidized condition. Stripping steam is also used to displace the hydrocarbon product vapors contained between the coke particles. To maintain fluidization and effect the desired stripping, the average superficial velocity of the rising gases is ranged 0.3m/s to 1.0 m/s depending upon the coke size (Pfeiffer et al., 1959). The preferred coking temperature at coking zone is maintained by the rate of circulation of solids between the coker and burner.

Syncrude Canada, a leading manufacturer in Canada's oil sands industries, has a productive capacity equivalent to over 15 percent of the nation's crude oil production. In 2010, Syncrude produced totally 107 million barrels or about 300,000 barrels per day of sweet crude oil (COS, Canadian Oil Sands Trust, 2011). For about 350,000 bbls/d productive capacity, Syncrude has three of the largest Fluid Cokers operating in the world. In fluid coking operation at Syncrude, the oil sands bitumen is preheated and fed the fluid coker reactor through a series of feeding nozzles. These spray feeding nozzles use 600 psig steams to atomize the bitumen and spray the droplets into the reactor dense coke bed. The bitumen feed at approximately $350^{\circ}C$ is thermally cracked using the heat provided by $500^{\circ}C$ coke particles. In the fluid coking process, a stable range of particle size distribution is crucial for operation control. If the particle size distribution deviates from the range, for example, too many fine particles less than 50 μm or large particles more than 600μm, the fluidized bed behavior is erratic or can begin to defluidize. Then the coke circulation rate, the flow rate of coke between the reactor and burner, is hard to maintain. Therefore, the coke particle size distribution is controlled by the use of a series of attrition nozzles that use high pressure and supersonic superheated steam as seen in Figure 1.2. The attrition nozzle is a type of convergent-divergent nozzle, which can accelerate the superheated steam to supersonic speeds which fractures the coke particles by impact.
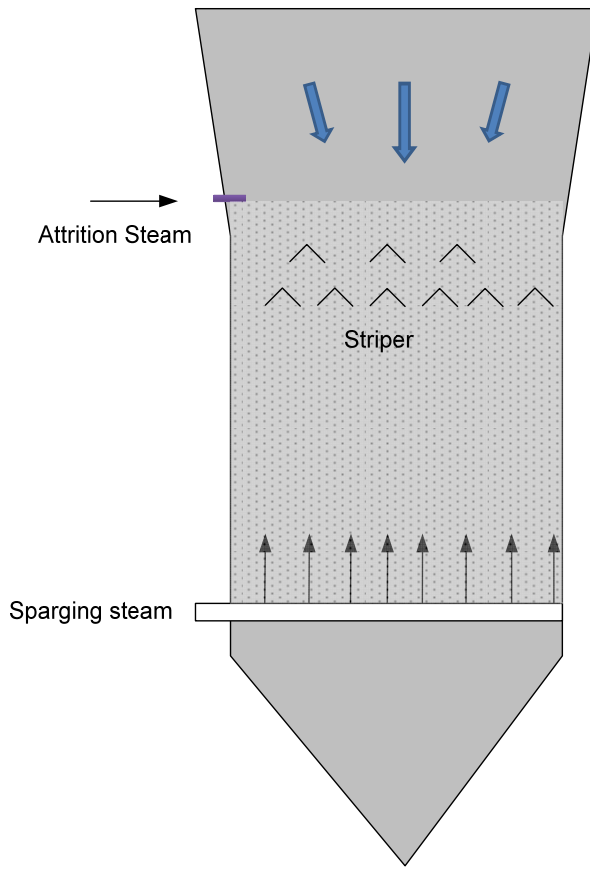
Figure 1.2 Located position of attrition jets in fluid coking process

1.2 **Motivation for research**

The motivation for the research comes from the fluid coking process, which is popularly used in upgrading of heavy oil. To maintain a well fluidized bed and a satisfactory reaction rate, it is desirable to keep the coke particle size distribution at a required range, since particles that are too large or fine will result in slugging or poor fluidization. In fluid cokers, a series of attrition nozzles are used to control coke particle size, with high pressure, superheated steam. Due to the high pressure and superheated temperature, attrition nozzles consume much steam, accounting for 40% of the total steam usage in fluid coking reactors. Improving the attrition nozzles to cut the required steam flow would reduce energy consumption, increase reactor throughput, and reduce sour wastewater production.

1.3 **Fundamentals of particle attrition**

Particle attrition is an important issue for a number of industrial applications such as crystallization, granulation, grinding and milling, Fluid catalytic cracking, and Fluid coking processes. The breakage of particles can be required or unwanted dependent upon the application. In many fluidized bed processes, the particle breakage from inter-particle collisions or particle-wall interactions has a detrimental effect on operation. Meanwhile, the fines produced by attrition in fluidized bed reactors often increase the cost of downstream processing in order to meet environmental regulations. On the other hand, the attrition rate must be maximized for grinding or milling processes. For instance, in the fluid coking process, a series of attrition nozzles are introduced to break particles and maintain their size within an ideal range. Whether particle attrition is required or unwanted, a better understanding of particle breakage mechanism is useful in the application and design of fluidized bed reactors.

1.3.1   **Particle attrition in Fluidized bed process**

Fluidized bed reactors are widely applied in a number of industrial areas due to their excellent abilities for heat exchange and multiphase contacting. The vigorous motion of the bed particles is such that attrition is a vital problem in the application of many fluidized bed reactors. Forsythe and Hertwig (1949) first developed a laboratory accelerated attrition test method for catalyst attrition in fluid cracking. The attrition rate is calculated from collected fines. Vaux and Keairns (1980) proposed the mechanism for particle attrition in fluidized beds, which includes thermal, chemical, kinetic and static mechanical stresses. In a fluidized bed, sources of particle attrition were identified as grid jets, gas bubbles attrition, and cyclones. Zenz and Kelleher (1980) proposed that attrition could occur in the following locations:

- o Particle attrition caused by the grid jets
- o Fine particle occurred in bubble wake
- o Particle attrition at the cyclone entrance and spiral route
- o Attrition at the conveying line, such as at elbows.

In hot fluidized beds, thermal shock or calcination is another main source of particle attrition. Bemrose and Bridgwater (1987) asserted that particle attrition is affected by a

great many variables, mostly influenced by particle and fluidized bed properties. Gwyn (1969) reported that both the average particle size and the spread of the initial particle size distribution affect the attrition rate. Patel et al. (1986) classified two main categories as main effects for particle breakage in a fluidized bed: properties of particle and properties of the environment (the fluidization velocity, operating temperature, and pressure).

In addition, material characteristics such as the fracture strength, and deformation behavior also play critical roles in particle breakage.

1.3.1.1   Material properties

Particle size and population balance

Although it is undoubted that the size distribution of the particles has a great impact on their attrition, its effects varies with the breakage mechanism. For example, Gwyn (1969) reported that both the average particle size and the spread of the initial particle size distribution affect the attrition rate. When Arena et al. (1983) studied the coal attrition in a mixture with sand at high temperature; they found that a larger sand particle size would significantly improve the coal attrition rate. Ray and Jiang (1987a) believe that the share of particles in the breakage energy is proportional to their surface areas. The analysis by Zhang and Kavetsky (1993) demonstrates that the breakage distribution function correlates to material property and particle size, and the breakage rate function also changes with material type and with particle size distribution. Lin (2005) argued that particle attrition increases with decreasing average particle size, because fine particles have a larger specific surface area, which increases the collision probability. On the other hand, an amount of fines in the system results to a lower attrition rate because fines are typically harder to grind.

Particle fracture energy

The fracture energy is defined as the energy required for particles to create a first point of fracture. King and Bourgeois (1993) found that the particle breakage depends on the probability of the impact energy reaching the particle fracture energy. Study by Tavares (2007) demonstrated that the breakage probability of limestone is affected by the fracture energies distribution.

Other material properties

No matter what kind of attrition modes, the material properties, including particle strength, Young's module, and hardness, also result in various breakage intensity.

1.3.1.2   Bed properties

Particle velocity

Particle velocity is an important factor in generating mechanical stress by inter-particle collision and particle-wall interaction.

Operating temperature

Thermal shock, particle properties, gas properties, can influence the particle attrition dramatically, and will be changed by temperature. For example, particle properties such as strength, hardness, and fracture energy can be affected by the temperature. Meanwhile, gas properties such as density and viscosity are changed with operating temperature.

Operating pressure

The operating pressure has small influence on particle attrition. In contrast, the upstream pressure of the attrition gas plays an important role in particle attrition.

Chemical reaction

Chemical reactions of particulate material may generate stress within the particle leading to fracture.

1.3.2   Jet-induced particle attrition

Air jet milling, which is the most popular commercial application of jet-induced particle attrition, uses high velocity gas jets to impact particles for size reduction. In 1882, Goessling first invented a modern jet mill to grind materials, with a jet and a grinding chamber. During the process of air jet milling, the high pressure fluid is converted to either sonic or supersonic jet as it expands to the mill. Two common forms of nozzle are employed in jet milling, abrupt type nozzle and the convergent-divergent nozzle (Albus, 1964). In convergent-divergent nozzle, supersonic conditions can be reached as the gas expand fully in the divergent section. In fluidized bed opposed jet mills, a typical jet mill, air jets are used to give high-energy impacts to collide the particles in the bed (Chamayou and Dodds, 2007).
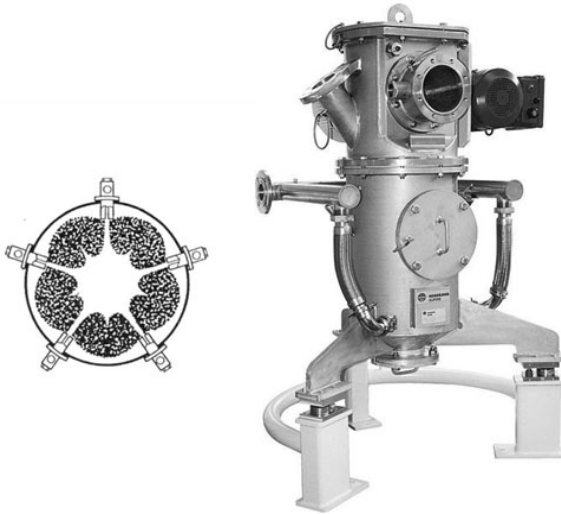
Figure 1.3 Fluidized bed opposed jet mill (Hosokawa Alpine)

Many studies have been performed to focus on the jet-induced particle attrition in fluidized beds, using subsonic jets. De Michele et al. (1976) developed a model to describe the axisymmetric jets in fluidized beds based on the theory of submerged turbulent jet. Merry suggested a scheme of the particle tracks in the void vicinity of the jet, with the most solids entrainment occurring at the potential zone region and particles accelerating at jet region (Merry, 1971). Bentham et al. (2004) also asserted that the particle breakage mechanism of subsonic jets involves the particles entrained in the jet.

A number of researches have been worked on the effects of attrition gas properties on jet-induced attrition in fluidized beds. The investigation by Chen et al. (1980) found that the jet would lose much of its high initial velocity as a result of jet expansion and energy transfer. They further developed an attrition model in which the attrition rate was proportional to the kinetic energy of the attrition gas and the particle surface area. Werther and Xi (1993) found that high velocity gas jets contribute high attrition rates, which is proportional to $\rho_0 d_0^2 u_0^3$. Ghadiri et al. (1992, 1994) stressed that the attrition rate is related to the orifice velocity raised to a power up to 5. A summary of the correlations of attrition rate for subsonic horizontal jets is list in Table 1.1.

Table 1.1 Correlations to predict particle attrition rate with subsonic jets

Model equation	Operating conditions	Authors
$R = C \cdot S \cdot \dfrac{\rho_0 Q (\beta u_0)^2}{W d_p \rho_p}$ (1.1)	u_0 = 25-300 m/s, 142-274μm iron ore, 3940kg/m3; lignite char, 1250 kg/m3	Chen et al., 1980
$R = C \rho_0 d_0^2 u_0^3$ (1.2)	u_0 =25-100 m/s; FCC: 106μm, 1500 kg/m3; catalyst HA-HPV: 125 μm, 650 kg/m3.	Werther and Xi, 1993
$R = C d_0^{\,n} u_0^{\,m}$ (1.3) n: 0.6-0.76 for FCC; 0.44-1.11 for NaCl m: 3.31 for FCC; 5.1 for NaCl	u_0 =25-125 m/s; FCC: 425-600 μm NaCl: 90-106 μm	Ghadiri et al., 1994
$R = C (u_0 \sqrt{\rho_0})^{2.5} \dfrac{\pi d_0^2}{4}$ (1.4)	u_0 =33-303 m/s, Silica-Alumina FCC Catalyst	Zenz and Kelleher, 1980

McMillan et al. (2007a) studied the performance of supersonic jets in a particle attrition process. They proposed a new criterion for characterizing particle attrition, and defined a grinding efficiency, which was defined as the total increasing surface area per attrition gas consumption. The definition of particle grinding efficiency is close to the term of energy utilization in jet mill industry, which names as the ratio of the new surface area and the input energy. Based on experimental results with supersonic jets, an empirical correlation was developed to predict the grinding efficiency of solids (McMillan et al., 2007a):

$$\eta = 7.81 \times 10^{-7} \alpha \beta d_0^{1.131} u_o^{0.55} (\rho_0 u_o^2)^{1.635} \left(\frac{u_g - u_{mf}}{u_{mf}} \right)^{0.494}$$

(1.5)

where α and β are coefficients that depend on particles properties and nozzle geometry, respectively. The characteristic study of jet-attrition in fluidized beds by McMillan et al. (2007b) suggested that most particle attritions are occurred in jet area, where, the entrained particles from ambient fluid are accelerated by the supersonic jet, and then these particles would collide with slow velocity particles near the jet boundary layer.

1.3.3   Particle breakage modes

Two types of breakage mechanisms abrasion and fragmentation have been proposed by Blinicheve et al. (1968). Abrasion is defined as that fine particles are removed from the particles' surface. Particle fragmentation is a process of particle breakage into similarly sized daughter particles. Ray and Jiang (1987) argued that the breaking mechanism

depends upon the particle strength and the breaking force in fluidized beds. They further noted that the breakage mode could shift from abrasion mode to fragmentation mode if impact force was increased. Pis et al. (1991) suggested that the two attrition modes have different effects on the daughter particle size distribution, as shown in Figure 1.4.
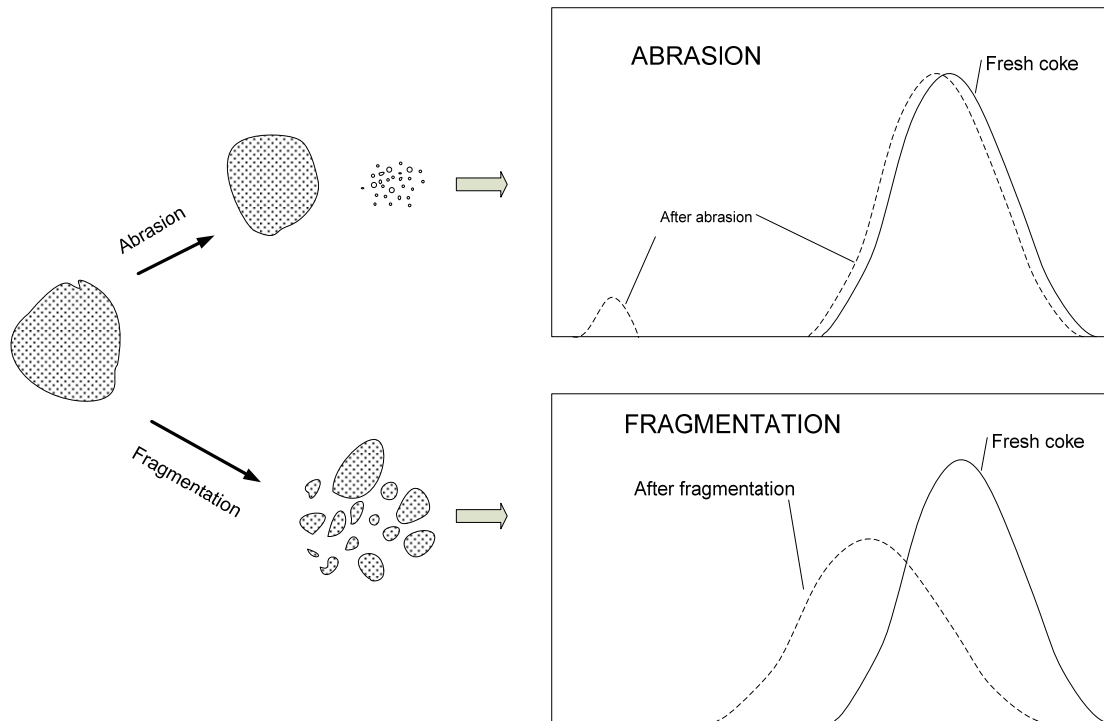
Figure 1.4 Attrition modes and the effects on the particle size distribution (retrieved from Pis et al., 1991)

1.4 Characteristics of attrition nozzles in fluidized bed

1.4.1 Convergent-divergent nozzles

Convergent-divergent nozzles have been widely applied to various fluidized bed processes, such as the production of pharmaceutical powders, fluid catalytic cracking process, jet milling, and the fluid coking process. As a type of attrition nozzle used in the jet-induced attrition process, the convergent-divergent nozzle is assumed as an isentropic process, which has physical characteristics such as area ratio (the ratio of the exit area to the throat area), and pressure ratio (the ratio of the stagnation pressure to the ambient pressure). In supersonic nozzles as shown in Fig.1.5, the fluid reaches the sonic velocity at the throat, and supersonic velocity is obtained in the divergent section (Smith, 2005). As shown in Figure 1.6, the velocity, pressure and temperature vary with Mach number

along the converging-diverging flow path according to (Liepmann, 1957, and Perry, 2008):

$$\frac{A}{A^*} = \frac{1}{M}\left[\frac{2}{\gamma+1}\left(1+\frac{\gamma-1}{2}M^2\right)\right]^{(\gamma+1)/2(\gamma-1)} \qquad (1.6)$$

$$\frac{p_0}{p} = \left[1+\frac{\gamma-1}{2}M^2\right]^{\gamma/(\gamma-1)} \qquad (1.7)$$

$$\frac{T_0}{T} = 1+\frac{\gamma-1}{2}M^2 \qquad (1.8)$$

The sonic mass flux through the throat is given by:

$$G = p_0\sqrt{\left(\frac{2}{\gamma+1}\right)^{(\gamma+1)/(\gamma-1)}\left(\frac{\gamma M_w}{RT_0}\right)}\,(kg/m^2 \cdot s) \qquad (1.9)$$

If A is the nozzle exit area, the exit temperature, pressure, and Mach number may be calculated.

Figure 1.5 Convergent-divergent attrition nozzle
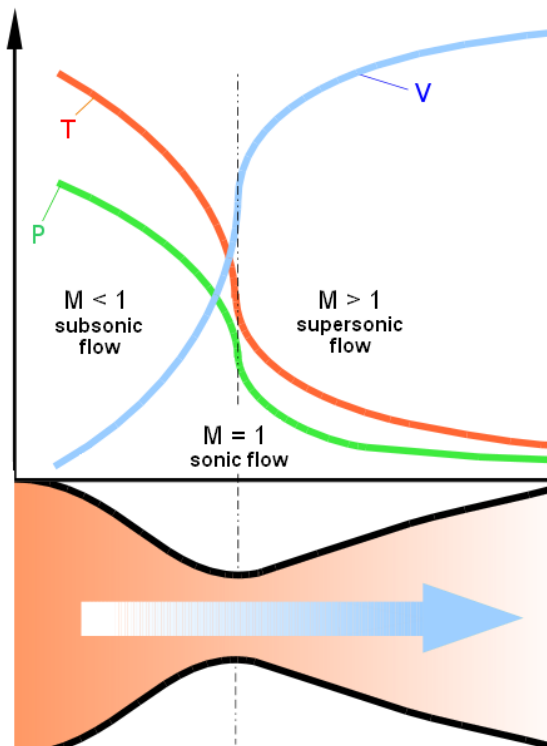
Figure 1.6 Effect of Mach number on velocity, temperature, and pressure in a convergent-divergent nozzle
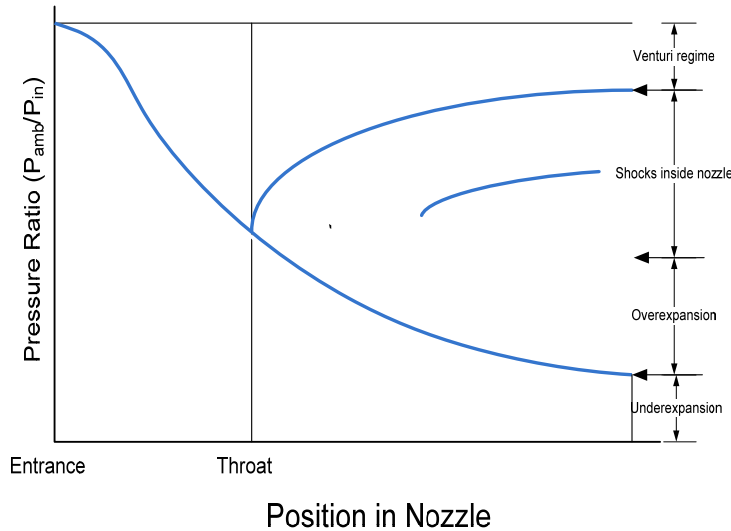
Figure 1.7 Operating modes for convergent-divergent nozzle (Adapted from Zucker and Biblarz, 2002)

For a specific nozzle geometry, the location and strength of the shock depend on the operating pressure ratio (Zucker and Biblarz, 2002). It can be seen there are three critical points in Fig. 1.7. The normal shock forms downstream of the nozzle throat but in the nozzle, if the pressure ratio is between the first critical point and the second critical point. Once the pressure ratio is at the second critical point, the shock is located at the exit of the nozzle. The overexpansion occurs when the pressure ratio is between the second and third critical points. If the operating pressure ratio is below the third critical point, an underexpansion occurs outside the nozzle. In some cases, the shock wave of a convergent-divergent nozzle acts a crucial role in attrition process because it can produce high turbulence to intensify collision and impact between the particles.

1.4.2   Jet properties

A convergent-divergent nozzle injected horizontally in a fluidized bed with sonic or supersonic velocity can be assumed to behave as a submerged jet, similar to a turbulent jet spreading through a liquid medium at rest. If a nozzle with a uniform velocity of U_0 is injected into a large stagnant mass of the same fluid, the size of the velocity boundary is as shown in Figure 1.8.
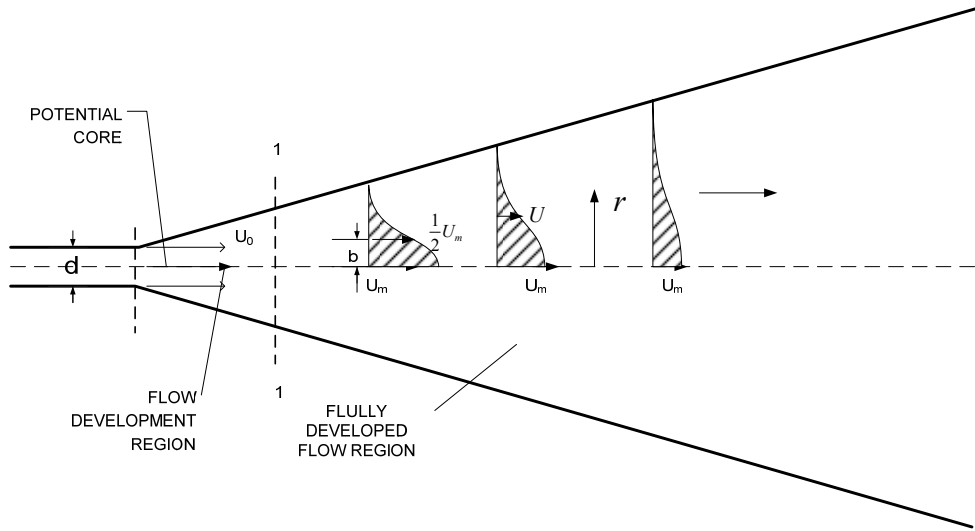
Figure 1.8 The velocity profile of circular turbulent jet (adapted from Rajaratnam, 1976)

In a free turbulent jet, the universal jet axial velocity profile is expressed as (Abramovich, 1963) :

$$\frac{u}{u_m} = \left(1 - \xi^{1.5}\right)^2$$

(1.10)

where

$$\xi = \frac{y}{b}$$

(1.11)

The dimensionless velocity profiles at different cross sections of a jet boundary layer b can be represented with the equation:

$$\frac{u - u_b}{u_m - u_b} = \left(1 - \xi^{1.5}\right)^2$$

(1.12)

where u_m is the velocity at axis, u_b is the interstitial jet velocity on the thickness b of boundary layer, and $\xi = y / b$.

De Michele et al. (1976) developed the turbulent jet model for axisymmetric jets in beds, which extended the theory of turbulent submerged jets to the gas injection in fluidized beds. In the initial region of jet, as shown in Figure 1.8, there exists a core region, known as the potential core, where the turbulence has not developed. Davies (1972) suggests that the length of the potential core is about 6.4 jet diameters, followed by a transition core of about 8 jet diameters. An equation was developed by De Michele et al. (1976) to predict the length of the potential core:

$$\frac{L_{core}}{d_0} = \frac{2.64}{\log \rho_B / \rho_0} \tag{1.13}$$

As turbulent jets in conventional fluids, jets in fluidized beds have a "potential" core where the gas momentum; temperature and composition are the same as at the mouth of the orifice. Merry (1971) suggested that the majority of entrainment occurs at the potential core region, as seen in Figure 1.9.
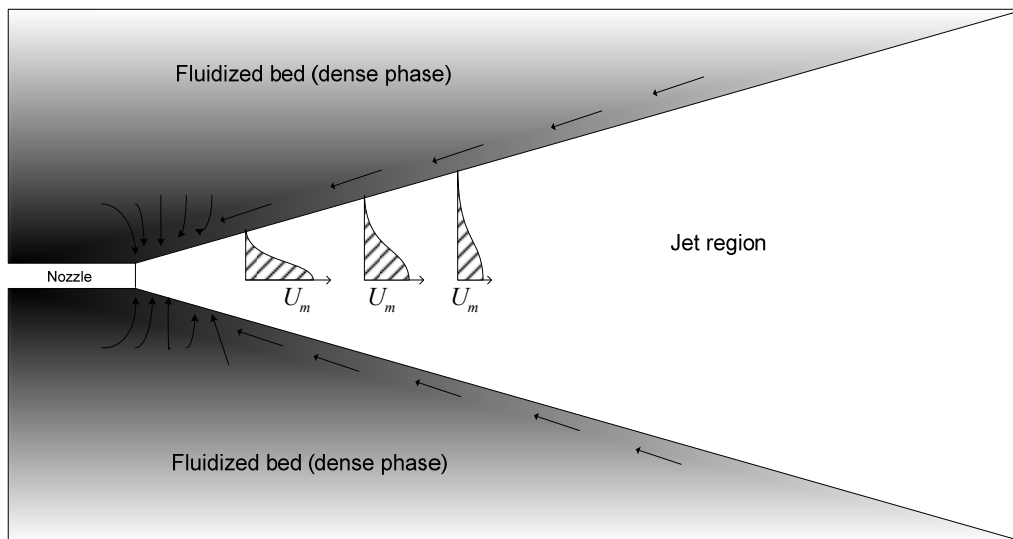
Figure 1.9 Solid entrainment track in the injection region (adapted from Merry, 1971)

1.4.3   Jet penetration

The penetration length of the jet issuing from an attrition nozzle is a critical property for the investigation of attrition in fluidized beds. Table 1.2 provides examples of published correlations for jet penetration length. It can be observed that the jet penetration length is related to the gas density and gas velocity. However, all these correlations were developed from data obtained with nozzle operating at subsonic velocities. Furthermore, the definitions of penetration length are various. Massimilla (1985) compared all of the existing empirical and semi-empirical correlations and found it is hard to develop a global expression to predict jet penetration length for different operation conditions.

Table 1.2 Correlations for jet penetration length

Correlation	Variables	U_0(m/s)	Reference
$\dfrac{L_j}{d_0} = 7.8\left(\dfrac{\rho_f U_0}{\rho_p \sqrt{g d_p}}\right)$	Copolymer $1 < \dfrac{d_0}{d_p} < 1.5$	83-192	Shakhova (1968)
$\dfrac{L_j}{d_0} + 4.5 = 5.25\left(\dfrac{\rho_0 U_0^2}{(1-\varepsilon)\rho_P g d_P}\right)^{0.4}\left(\dfrac{\rho_f}{\rho_P}\right)^{0.2}\left(\dfrac{d_p}{d_0}\right)^{0.2}$	Sand, steel shot, and Kale seeds $1.5 < \dfrac{d_0}{d_p} < 80$ $1.6\times10^{-4} < \dfrac{\rho_f}{\rho_p} < 12\times10^{-4}$	40-200	Merry (1971)
$0.044\dfrac{L_j}{d_0} + 1.48 = 0.5\log(0.67\rho_f U_0^2)$	FCC	32-64	Zenz (1968)
$\dfrac{L_j}{d_0} + 3.80 = 1.64\times10^6\left(\dfrac{\rho_0 U_0^2}{(1-\varepsilon)\rho_P g d_P}\right)^{0.327}\left(\dfrac{\rho_f}{\rho_P}\right)^{1.974}$	Millet, silica sand $2.2 < \dfrac{d_0}{d_p} < 7$ $7.5\times10^{-4} < \dfrac{\rho_f}{\rho_p} < 8\times10^{-4}$	6-190	Hong (1997)
$\dfrac{L_j}{d_0} = 5.52\left(\dfrac{\rho_0 U_0^2}{(\rho_p - \rho_f) g d_0}\right)^{0.27}$	Catalyst, glass, sand $1 < Fr < 380$	15-300	Benjelloun (1991)
$\dfrac{L_j}{d_0} = 2.8\left(\dfrac{\rho_0 U_0^2}{(\rho_p - \rho_f) g d_0}\right)^{0.4}$	Calcined alumina powder $1 < Fr < 180$		Yates (1991)

The penetration length of a jet depends on its momentum dissipation. Yang and Keairns (1981) provided the following equation to calculate momentum dissipation of vertical jets:

$$\frac{u_m}{u_0} = 3.84\frac{d_0}{x}$$

(1.14)

Considering the effects of the distance from the nozzle, the gas injection velocity, the fluidization velocity, and the nozzle shape on the gas velocity profile, Xuereb et al. (1991) proposed a correlation for horizontal jets:

$$\frac{u_m}{u_0} = 6.30 \frac{d_0}{x} \qquad\qquad\qquad (1.15)$$

Meanwhile, Yang and Keairns (1978) first suggested that a two-phase Froude number, defined as $(\rho_f U_j^2)/(\rho_s - \rho_f)g d_0$, could be used to predict the jet penetration length. Benjelloun et al. (1991) used the Froude number to describe the relation between the jet momentum and the gravity forces acting on the jet:

$$\frac{L}{d_o} = 5.52 Fr^{0.27} \qquad\qquad\qquad (1.16)$$

Ariyapadi et al. (2004) modified the Benjelloun's Correction to predict the penetration length of gas-liquid jets in a fluidized bed. Cruz et al. (2009) found the jet penetration length could be predicted with the jet thrusts, where the jet thrust is defined as a mechanical force generated through accelerating a mass of gas.

For measuring the penetration length accurately, many techniques were developed to determine jet penetrations in fluidized beds. Visual observation of the jet performance in the beds is a most common. The radiation densimeter, Pitot tube probe, optical probe, and capacitance probe are also utilized to measure the jet penetration (Raghunathan et al., 1988). Vaccaro et al. (1997) analyzed and classified the various techniques into two main groups. The first group includes visual observations of the phenomenon, photographic or high-speed film analysis, optical probes, capacitance probes, and X-ray image analysis. The second group involves Pitot tube probes and γ-ray. In the study by Hong et al. (1997), a high-speed video was employed for measuring the jet penetration length. Zhu et al. (2000) used a thermal method to measure the jet penetration length in a study of liquid jets in a gas-solid system. The thermal measurement technique was also adapted and developed to study the liquid-gas jet in fluidized beds by many researches (Ariyapadi et., 2005; McMillan et al., 2005). Typically, a triboelectric technique was developed successfully to measure gas jet boundaries, the penetration length, and expansion angle of jets (Dawe et al., 2008; Cruz et al., 2009).

1.4.4   Solid entrainment

Since the velocity of a supersonic jet is much higher than the fluidization velocity in fluidized beds, previous studies have found that the jet velocity profiles of gas and solids for horizontal jets in fluidized beds, as for homogeneous jets, are of the Schlichting or Tollmien type (Shakhova, 1968; Donadono *et al.*, 1980; Filla *et al.*, 1983; De Michele *et al.*, 1976). Thereby, the theory of turbulent gas jets (Abramovich, 1963) can be applied to solids entrainment with supersonic jets. Shakhova (1968) suggested that both a pure gas zone and a gas-solid zone exist within a turbulent jet in a fluidized bed. The zone boundaries are determined by the gas velocity and voidage of the dense bed area. The solids entrainment illustrates maximum at the potential core of the jet, eventually decreasing as the distance from the nozzle increases (Felli, 2002; Xuereb et al., 1991). De Michele et al. (1976) developed a modified model of the submerged turbulent theory to interpret mass transfer associated with gas injection, horizontal injection and large temperature differences between the bed and injected gases of various thermal properties. Yang and Keriarns (1982) proposed a numerical model for prediction of solids entrainment into a flame-like jet in a fluidized bed. Xuareb et al. (1992) proposed a model to predict the solids entrainment and suggested the most of solid entrainment occurred near the tip of the nozzle. They also found that increasing gas flowrate through the jet leads to a significant increase in particle velocity on the jet axis. In previous studies by Briens et al. (2008) and Hulet et al. (2008a), a specific technique was employed to measure the solids entrainment rate into submerged gas and gas-liquid jets.

1.5 Effect of temperature on attrition

Many studies have been carried out on particle attrition in fluidized beds. The mechanisms proposed for particle attrition in fluidized beds include thermal, chemical, kinetic and static mechanical stresses (Vaux and Keairns, 1980). In the case of bubbling fluidized beds, sources of particle attrition were identified as jets attrition, gas bubbles and cyclones. Bemrose and Bridgwater (1987) stated that particle attrition is affected by a great many variables, mostly influenced by particle and fluidized beds properties. Earlier studies have revealed that the operating temperature has a dramatic effect on the particle

attrition in fluidized beds, because it affects material strength, Young' modulus of the solid, and thermal diffusivity of the gas. Arena et al. (1983) suggested that bed temperature is related to the production of carbon fines. With the study of the effect of thermal shock, Vaux and Keairns (1980) found that the particle breakage rate increased with increasing temperature difference between the particles and the surrounding gas. Lin and Wei (2005) reported that the attrition rate increases with increasing temperature, decreases with particle size, and increases with fluidization velocity. Chirone et al. (1985) and Lee et al. (2002) claimed that a higher temperature causes a higher inner pressure and a higher thermal stress, resulting in enhanced particle fragmentation. So far, most of these studies on jet attrition in fluidized beds have used subsonic nozzles or have been conducted at ambient temperature.

1.6 Research objectives

The main objective of the present research is to numerically and experimentally study particle attrition using supersonic nozzles in high temperature fluidized beds. The specific objective is to improve particle grinding efficiency, and finally reduce the attrition gas consumption in the fluid coking process.

1.6.1   Study of solids entrainment into attrition jets in fluidized beds

Supersonic nozzles are applied to various fluidized bed processes, such as the production of pharmaceutical powders, fluid catalytic cracking, and fluid coking. In applications such as jet milling, it is essential to entrain a maximum flow-rate of solids from the fluidized bed into the jet cavity. Studies of solid entrainment rate into gas jets have been mostly conducted with subsonic jets. The purpose of this research is to study solids entrainment into jets issuing from supersonic convergent-divergent nozzles, and particularly the influences of nozzle size, nozzle mass flow-rate, the properties of injection gas, and the bed properties. A novel accurate technique is developed to measure solids entrainment into jets. This investigation can be found in Chapter 2.

1.6.2 Penetration of high velocity horizontal gas jets into a fluidized bed at high temperature

High velocity horizontal gas jets are applied to various industrial processes. In this work, an optimized thermal technique has been developed to measure the penetration length of horizontal gas jets. Experiments were carried out in a fluidized bed with a height of 1.23m and a rectangular cross section of 0.10m × 0.50m. The fluidized bed particles, which were either petroleum coke or sand, were heated by an in-bed electrical heater to temperatures between 300°C and 500°C. Cold gases, such as helium, nitrogen, carbon dioxide, were injected into the hot fluidized bed via a horizontal nozzle operating over a range of velocities. Based on the experimental results, a new empirical correlation was developed to predict the penetration length of jets issuing from the horizontal sonic nozzle at high temperature. The details of this study are discussed in Chapter 3.

1.6.3 Particle attrition with supersonic nozzles in a fluidized bed at high temperature

Fluidized beds are used for a variety of processes such as food, pharmaceutical, petrochemical and energy production. The fluid coking process, a typical application of fluidized beds, uses thermal cracking reactions to upgrade heavy oils and bitumen from oil sands. Supersonic nozzles injecting steam are used in the fluid coking process to control coke particle size, which is essential to maintain a well-fluidized bed and a satisfactory reaction rate. Maintaining a high attrition rate with a lower steam flowrate would reduce energy consumption, increase reactor throughput, and reduce sour wastewater production. The objective of the present research is, therefore, to study particle attrition with supersonic convergent-divergent nozzles in a fluidized bed at high temperatures, under conditions such as encountered in the fluid coking process. According to the experimental results, the grinding efficiency is significantly affected by fluidized bed temperature, attrition gas properties, and nozzle size. The experimental data further suggests that particle fragmentation is the dominant attrition process using supersonic nozzles in a hot fluidized bed. The results of this study are presented in Chapter 4.

1.6.4 Modeling of horizontal jet penetration in fluidized beds at high temperature

Supersonic nozzles as a type of efficient jet have been applied in various jet-induced attrition processes such as jet milling and the fluid coking processes. In jet-induced particle attrition, the penetration length of the supersonic nozzles is a critical property to investigate the attrition mechanism in the fluidized bed. A numerical model was developed to predict the penetration length of the horizontal supersonic nozzle in a high temperature fluidized beds, based on an Eulerian-Eulerian multiphase model and granular kinetic theory. The predicted results of the jet penetration length are in very good agreements with the experimental data and the predictions of Li's correlation. The simulation results have also demonstrated that the fluidization velocity and bed temperature have a little influence on jet penetration length. This research work is detailed in Chapter 5.

1.6.5 Numerical simulation of particle attrition with a convergent divergent nozzle in fluidized beds at high temperature

The attrition process is a critical step in the fluid coking process to control the particle size distribution. Previous studies have shown that some particle and bed properties affect jet-induced particle attrition in a fluidized bed. Because of the multiphase interactions and the complex flow behavior in the bed and jet system, it is desirable to develop a numerical model for the attrition process that combines theoretical and experimental techniques. Therefore, a model for jet-induced attrition in fluidized beds at high temperature has been proposed and developed. The model is a coupled Eulerian-Eulerian multiphase model coupled with a population balance method. Moreover, particle-particle interactions are described with the kinetic theory of granular flow. The model is solved using the discrete method and the quadrature method of moments. The vital adjustable parameters of the model were determined from experimental data. It is found that the best prediction was obtained using the Ghadiri breakage kernel, the Diemer-Austin generalized daughter size distribution function, and the discrete solution method. The details of this study can be found in Chapter 6.

1.6.6 Experimental and numerical study of twin-jets nozzle in particle attrition process

The convergent-divergent nozzle is popularly used in a number of industrial applications. For example, in the fluid coking process, a convergent-divergent nozzle is employed to control the particle size distribution in a reacting system. Studies for aerospace applications have found that twin-jet nozzles enhance flow mixing, entrainment, and jet thrust. Therefore, the aim of the present study is to investigate the fluid dynamic mechanism of twin-jet nozzles and their practical application to particle attrition in fluidized beds. The details of this study are described in Chapter 7.

1.7 **Notation**

A	Area of nozzle exit (m^2) (Eq. 1.8)
A*	Area of nozzle throat (m^2) (Eq. 1.8)
b	Radial of jet region (m) (Eq. 1.13)
C	Attrition constant (Table 1.1)
d_0	Diameter of nozzle (m)
d_p	Diameter of particles (m)
E	Young's modulus (Pa)
E$_p$	The diameter of column (m, Eqn. 1.27)
Fr	Froude number
H	Hardness (Pa)
K$_c$	Fracture toughness (Nm$^{-3/2}$)\
l	Cube dimension (m)
L_j	Length of jet penetration (m)
L_{core}	Length of potential core (m)
M	Mach number
M$_w$	Molar weight (kg/mol)
p$_0$	Upstream pressure of nozzle (Pa)
p	Pressure (Pa)
r_c	Indentation fracture (Eqn. 1.6)
S	Excess surface area per unit mass after attrition (m^2/kg, Eqn. 1.1)
T$_0$	Absolute temperature at nozzle throat (K)
T	Temperature at nozzle exit (K)
u_m	Jet velocity along x-axis (m/s)
u_{mf}	Minimum fluidization velocity (m/s)
u_g	Bed fluidization velocity (m/s)
U$_0$	Gas velocity at nozzle exit (m/s)
v	Impact velocity (m/s, Eqn. 1.7)
W$_j$	Solids entrainment rate (kg/s)
Y	Yield stress

Greek letters

α	Volume fraction
α	Correlation Constant (Eq. 1.5)
α'	Constant dimensionless (Eq. 1.7)
β	Correlation Constant (Eq. 1.5)
γ	Ratio of specific heat cp/cv (dimensionless)
ε	Volume fraction
Γ	Interface energy (Eqn. 1.6)
η	Grinding efficiency (Eqn. 1.5)
η	Attrition propensity parameter dimensionless (Eqn. 1.7)
θ	Jet half-angle
ξ	The dimensionless ratio (y/b)

ρ	Density (kg/m^3)
ρ_B	Bed density (kg/m^3)
ρ_o	Gas density at nozzle exit (kg/m^3)
ρ_f	Density of fluid in bed (kg/m^3)
ρ_p	Particle density (kg/m^3)

1.8 **References**

Alberta, G. o. *Alberta's Energy Industry (An Overview 2009)*; 2009.

Alberta, G. o. *Alberta Oil Sands Industry - Quarterly Update*; Edmonton, Alberta, 2010.

Albus, F. E., the modern fluid energy mill. *Chemical Engineering Progress* **1964,** *60* (6), 102.

ANSYS, ANSYS FLUENT 12.0 User's Guide. April 2009 ed.; ANSYS, Inc.: 2009a.

Arena, U.; Damore, M.; Massimilla, L., Carbon Attrition During the Fluidized Combustion of a Coal. *Aiche Journal* **1983,** *29* (1), 40-49.

Ariyapadi, S. Interaction between horizontal gas-liquid jets and gas-solid fluidized beds. The University of Western Ontario, London, 2004.

Bemrose, C. R.; Bridgwater, J., A Review of Attrition and Attrition Test Methods. *Powder Technology* **1987,** *49* (2), 97-126.

Benjelloun, F. V., J. In *Determination des longueurs de jets de gaz horizontaux dans des lits fluidises*, textes des communications presentees a l'occasion des 6emes journees europeenenes sur la fluidisation, Toulouse, Laguerie, C. G., P., Ed. Toulouse, 1991.

Bentham, A. C.; Kwan, C. C.; Boerefijn, R.; Ghadiri, A., Fluidised-bed jet milling of pharmaceutical powders. *Powder Technology* **2004,** *141* (3), 233-238.

Blinichev, V. N.; Strel'tsov, V. V.; Lebedeva, E. S., An investigation of the size reduction of granular materials during their processing in fluidized beds. *International Chemical Engineering* **1968,** *8* (8), 615.

Briens, C.; Berruti, F.; Felli, V.; Chan, E., Solids entrainment into gas, liquid, and gas-liquid spray jets in fluidized beds. *Powder Technology* **2008,** *184* (1), 52-57.

Chamayou, A.; Dodds, J. A.; Agba D. Salman, M. G.; Michael, J. H., Chapter 8 Air Jet Milling. In *Handbook of Powder Technology*, Elsevier Science B.V.: 2007; Vol. Volume 12, pp 421-435.

Chen, T.; Sishtla, C.; Punwani, H.; Arastoopour, H., A model for attrition in fluidized beds. In *Fluidization*, Grace, J. R.; Matsen, J., Eds. Engineering Foundation: New York, 1980; p 445.

Chirone, R. D. a., M.; Massimilia, L.; Mazza, A., Char attrition during the batch fluidized bed combustion of a coal. *AlChE* **1985,** *31* (5), 812-820.

Davies, J. T., *Turbulence phenomena; an introduction to the eddy transfer of momentum, mass, and heat particularly at interfaces*. Academic Press: New York, 1972.

Dawe, M.; Briens, C.; Berruti, F., Study of horizontal sonic gas jets in gas-solid fluidized beds. *Canadian Journal of Chemical Engineering* **2008,** *86* (3), 506-513.

De Michele, G.; Elia, A.; Massimilla, L., Interaction between Jets and Fluidized-Beds. *Quaderni Dell Ingegnere Chimico Italiano* **1976,** *12* (6), 155-162.

Donadono, S.; Maresca, A.; Massimilla, L., GAS INJECTION IN SHALLOW BEDS OF FLUIDIZED, COARSE SOLIDS. *Quaderni Dell Ingegnere Chimico Italiano* **1980,** *16* (1-2), 1-10.

Felli, V. Solids entrainment from a fluidized bed into a gas-liquid jet: effect of the draft tube. The university of western ontario, London, 2002.

Filla, M.; Massimilla, L.; Vaccaro, S., GAS JETS IN FLUIDIZED-BEDS - THE INFLUENCE OF PARTICLE-SIZE, SHAPE AND DENSITY ON GAS AND SOLIDS ENTRAINMENT. *Int. J. Multiph. Flow* **1983,** *9* (3), 259-267.

Forsythe, W. L.; Hertwig, W. R., Attrition Characteristics of Fluid Cracking Catalysts. *Industrial & Engineering Chemistry* **1949,** *41* (6), 1200-1206.

Ghadiri, M.; Cleaver, J. A. S.; Tuponogov, V. G.; Werther, J., Attrition of FCC powder in the jetting region of a fluidized bed. *Powder Technology* **1994,** *80* (2), 175-178.

Ghadiri, M.; Cleaver, J. A. S.; Yuregir, K. R.; O.E., Y. I., Attrition of sodium chloride crystals in a fluidized bed. In *Fluidization* Potter, O. E.; Nicklin, D. J., Eds. Engineering Foundation: Brisbane, Australia, 1992; Vol. VII, p 603.

Ghadiri, M.; Zhang, Z., Impact attrition of particulate solids. Part 1: A theoretical model of chipping. *Chemical Engineering Science* **2002,** *57* (17), 3659-3669.

Gray, M. R., *Upgrading petroleum residues and heavy oils*. M. Dekker: New York, 1994.

Gray, M. R., Fundamentals of bitumen coking processes analogous to granulations: A critical review. *Canadian Journal of Chemical Engineering* **2002,** *80* (3), 393-401.

Gwyn, J. E., On Particle Size Distribution Function and Attrition of Cracking Catalysts. *Aiche Journal* **1969,** *15* (1), 35-&.

Hong, R. Y.; Li, H. Z.; Li, H. B.; Wang, Y., Studies on the inclined jet penetration length in a gas-solid fluidized bed. *Powder Technology* **1997,** *92* (3), 205-212.

House, P. Interaction of gas-liquid jets with gas-solid fluidized beds: Effect on liquid-solid contact and impact on fluid coker operation. The University of Western Ontario, London, Canada, 2007.

Hulet, C.; Briens, C.; Berruti, F.; Chan, E. W., Experimental and analytical study of the solids circulation loop of a compartmented fluidized bed. *Powder Technology* **2008,** *185* (2), 131-143.

King, R. P.; Bourgeois, F., Measurement of fracture energy during single-particle fracture. *Minerals Engineering* **1993,** *6* (4), 353-367.

Lee, S. H.; Kim, S. D.; Lee, D. H., Particle size reduction of anthracite coals during devolatilization in a thermobalance reactor. *Fuel* **2002,** *81*, 1633-1639.

Liepmann, H. W.; Roshko, A., *Elements of Gasdynamics*. John Wiley & Sons: New York, 1957.

Lin, C. L.; Wey, M. Y., Influence of hydrodynamic parameters on particle attrition during fluidization at high temperature. *Korean Journal of Chemical Engineering* **2005,** *22* (1), 154-160.

Lin, L. S., J. T.; Wen, C. Y., Elutriation and Attrition of Char a Large Fluidized Bed. *Powder Technology* **1980,** (27), 105-115.

Massimilla, L. In *Gas jets in fluidized beds*, Fluidization 1985; Davidson, J. F. C., R.; Harrison, D. , Ed. Academic Press: 1985; p 733.

McMillan, J.; Briens, C.; Berruti, F.; Chan, E., High velocity attrition nozzles in fluidized beds. *Powder Technology* **2007a,** *175* (3), 133-141.

McMillan, J.; Briens, C.; Berruti, F.; Chan, E., Particle attrition mechanism with a sonic gas jet injected into a fluidized bed. *Chemical Engineering Science* **2007b,** *62* (14), 3809-3820.

Merrick, D. H., J., In *Particle size reduction and elutriation in a fluidized bed process*, AIChE Symp. Ser. , 1974; 1974; pp 366-378.

Merry, J. M. D., Penetration of a Horizontal Gas Jet into a Fluidised Bed. *Transactions of the Institution of Chemical Engineers and the Chemical Engineer* **1971,** *49* (4), 189.

Patel, K.; Nienow, A. W.; Milne, I. P., Attrition of urea in a gas-fluidised bed. *Powder Technology* **1986,** *47* (3), 257-261.

Perry, R. H.; Green, D. W., *Perry's chemical engineering' handbook.* 8th ed.; McGraw-Hill: New York, 2008.

Pfeiffer, R. W.; Borey, D. S.; Jahnig, C. E. Fluid coking of heavy hydrocarbons US2881130, 1959.

Pis, J. J.; Fuertes, A. B.; Artos, V.; Suarez, A.; Rubiera, F., Attrition of coal ash particle in a fluidized bed. *Powder Technology* **1991,** *66*, 41-46.

Raghunathan, K.; Mori, H.; Whiting, W. B., A technique for measurement of jet penetration in hot fluidized beds with a modified Pitot-tube probe. *Industrial & Engineering Chemistry Research* **1988,** *27* (6), 1011-1016.

Rajaratnam, N., *Turbulent jets*. Elsevier Scientific Pub. Co.: Amsterdam ;; New York, 1976; p 304.

Ray, Y.-C.; Jiang, T.-S.; Wen, C. Y., PARTICLE ATTRITION PHENOMENA IN A FLUIDIZED BED. *Powder Technology* **1987,** *49* (3), 193-206.

Salman, A. D.; Ghadiri, M.; Hounslow, M. J., *Particle breakage*. Elsevier: Amsterdam London, 2007; Vol. 12.

Shakhova, N. A., Discharge of turbulent jets into a fluidized bed. *Inzhenerno-Fizicheskii Zhurnal* **1968,** *14* (1), 61-69.

Shamlou, P. A.; Liu, Z.; Yates, J. G., Hydrodynamic Influences on Particle Breakage in Fluidized-Beds. *Chemical Engineering Science* **1990,** *45* (4), 809-817.

Sishtla, C. F., J.; Chan, I.; Knowlton, T. M. In *The Effect of Temperature and Gas Velocity on Fines Generation in Non-reactive Fluidized Beds of Coal Char*, Fluidization VI, Banff, Alberta, Canada, Grace, J. R. S., L. W.; Bergougnou, M. A., Ed. Banff, Alberta, Canada, 1989.

Smith, J. M.; Van Ness, H. C.; Abbott, M.; Van Ness, H., *Introduction to Chemical Engineering Thermodynamics*. McGaw-Hill: 2005.

Soskind, D. M.; Spektor, G. S.; Kasatkin, D. F.; Zenchenkova, M. G., FLUID COKING OF HEAVY RESIDS. *Chem. Tech. Fuels Oils* **1982,** *18* (9-10), 483-488.

Tavares, L. M.; Agba D. Salman, M. G.; Michael, J. H., Chapter 1 Breakage of Single Particles: Quasi-Static. In *Handbook of Powder Technology*, Elsevier Science B.V.: 2007; Vol. Volume 12, pp 3-68.

Truner, J. S., *Buoyancy Effects in Fluids*. Cambridge University Press: New York, 1973.

Vaccaro, S.; Musmarra, D.; Petrecca, M., Evaluation of the jet penetration depth in gas-fluidized beds by pressure signal analysis. *Int. J. Multiph. Flow* **1997,** *23* (4), 683-698.

Vaux, W. G., *Attrition of particles in the bubbling zone of a fluidized bed*. 1978; p Medium: X; Size: Pages: 793-802.

Vaux, W. G. K., Dale L. In *Particle attrition in fluid-bed processes*, Fluidization Grace, J. R. M., J. M. , Ed. Plenum Press: 1980.

Werther, J., Measurement techniques in fluidized beds. *Powder Technology* **1999,** *102* (1), 15-36.

Werther, J.; Hartge, E. U., Modeling of industrial fluidized-bed reactors. *Industrial & Engineering Chemistry Research* **2004,** *43* (18), 5593-5604.

Werther, J.; Reppenhagen, J., Catalyst attrition in fluidized-bed systems. *Aiche Journal* **1999,** *45* (9), 2001-2010.

Werther, J.; Xi, W., Jet attrition of catalyst particles in gas fluidized beds. *Powder Technology* **1993,** *76* (1), 39-46.

Xuereb, C.; Laguerie, C.; Baron, T., Behavior of Horizontal or Inclined Continuous Jets Gas-Injected into a Fluidized-Bed .1. Morphology of the Jets. *Powder Technology* **1991a,** *67* (1), 43-56.

Xuereb, C.; Laguerie, C.; Baron, T., Behavior of Horizontal or Inclined Continuous Jets Introduced to a Fluidized-Bed by a Gas .2. Gas Velocity Profiles in Horizontal Jets. *Powder Technology* **1991b,** *64* (3), 271-283.

Xuereb, C.; Laguerie, C.; Baron, T., Behavior of Horizontal or Inclined Continuous Gas Jets Introduced into a Fluidized-Bed .3. Model of the Developed Flow Zone of the Jet. *Powder Technology* **1992,** *72* (1), 7-16.

Yang, W. C., JET PENETRATION IN A PRESSURIZED FLUIDIZED-BED. *Industrial & Engineering Chemistry Fundamentals* **1981,** *20* (3), 297-300.

Yang, W. C.; Keairns, D. L. In *Design and operating parameters for a fluidized bed agglomerating combustor/gsifier*, Fluidization, Cambridge University Press: 1978.

Yates, J. G.; Cobbinah, S. S.; Cheesman, D. J.; Jordan, S. P. In *Particle attrition in fluidized beds containing opposing jets*, New York, NY, USA, Publ by AIChE: New York, NY, USA, 1991; pp 13-19.

Zenz, F. A., Bubble Formation and Grid Design. *Inst. Chem. Eng. Symp.* **1968,** *30*, 136-139.

Zenz, F. A.; Kelleher, E. G., STUDIES OF ATTRITION RATES IN FLUID-PARTICLE SYSTEMS VIA FREE FALL, GRID JETS, AND CYCLONE IMPACT. *Journal of powder & bulk solids technology* **1980,** *4* (2-3), 8.

Zhang, Y. M.; Kavetsky, A., Investigation of particle breakage mechanisms in a batch ball mill using back-calculation. *International Journal of Mineral Processing* **1993,** *39* (1-2), 41-60.

Zhu, C.; Wang, X. H.; Fan, L. S., Effect of solids concentration on evaporative liquid jets in gas-solid flows. *Powder Technology* **2000,** *111* (1-2), 79-82.

Zucker, R. D.; Biblarz, O., *Fundamentals of gas dynamics*. John Wilery & Sons, INC: 2002.

Chapter 2

2 Study of Solids Entrainment into Attrition Jets in Fluidized Beds

2.1 Abstract:

Supersonic nozzles are applied to various fluidized bed processes, such as the production of pharmaceutical powders, fluid catalytic cracking, and fluid coking. In applications such as jet milling, it is essential to entrain a maximum flow-rate of solids from the fluidized bed into the jet cavity. Studies of solid entrainment rate into gas jets have been mostly conducted with subsonic jets and none with convergent-divergent nozzles. The purpose of this research is to study solids entrainment into jets issuing from supersonic convergent-divergent nozzles, and particularly the effects of nozzle size, nozzle mass flow-rate, injection gas properties and fluidization velocity. A novel accurate technique is developed to measure solids entrainment into jets.

Keywords: supersonic nozzle, Fluidized bed, solids entrainment, turbulent jet theory

2.2 Introduction

Supersonic nozzles, a type of convergent-divergent nozzle, are applied to various fluidized bed processes, such as the production of pharmaceutical powders, fluid catalytic cracking process, and fluid coking process (Figure 2.1). For instance, in fluid coking it is very important to control the size of coke particles because large particles will cause poor fluidization and reaction (Dunlop et al, 1958). Therefore, De Laval convergent-divergent nozzles are used to inject steam into fluid cokers, causing particle breakage and preventing net particle growth resulting from coke deposition. Predicting the effects of nozzle mass flow-rate, nozzle size, and gas properties on solids entrainment into supersonic jets is essential to optimize the attrition process and, especially, to minimize the consumption of attrition gas.
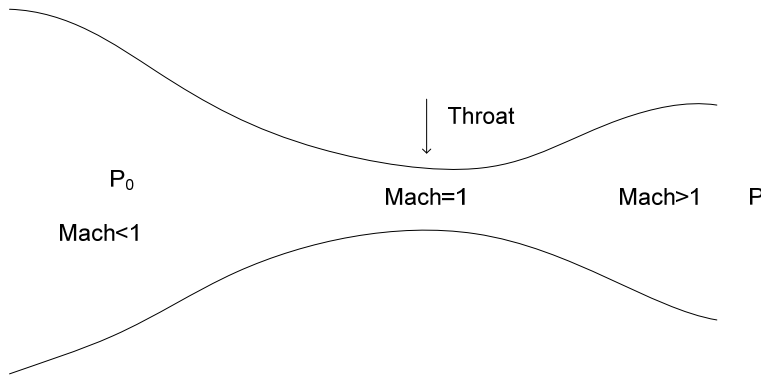
Figure 2.1 The convergent-divergent nozzle

In supersonic nozzles, the fluid reaches the sonic velocity at the throat, and supersonic velocity is obtained in the divergent section (Smith, 2005). The cross-sectional area, pressure and temperature vary with the Mach number along the converging-diverging flow path according to (Liepmann, 1975, and Perry, 2008):

$$\frac{A}{A^*} = \frac{1}{M}\left[\frac{2}{\gamma+1}\left(1+\frac{\gamma-1}{2}M^2\right)\right]^{(\gamma+1)/2(\gamma-1)} \tag{2.1}$$

$$\frac{p_0}{p} = \left[1+\frac{\gamma-1}{2}M^2\right]^{\gamma/(\gamma-1)} \tag{2.2}$$

$$\frac{T_0}{T} = 1+\frac{\gamma-1}{2}M^2 \tag{2.3}$$

The sonic mass flux through the throat is given by:

$$G = p_0\sqrt{\left(\frac{2}{\gamma+1}\right)^{(\gamma+1)/(\gamma-1)}\left(\frac{\gamma M_w}{RT_0}\right)}(kg/m^2 \cdot s) \tag{2.4}$$

If A is set equal to the nozzle exit area, the exit Mach number, pressure, and temperature may be calculated. Expansion will be incomplete if the exit pressure exceeds the ambient discharge pressure; in this case, shock waves will occur downstream of the nozzle. If the calculated exit pressure is less than the ambient discharge pressure, the nozzle is over expanded and compression shocks will occur within the expanding section of the nozzle. The relation between area and any other flow data can be obtained through the Mach number, as shown in Figure 2.2.
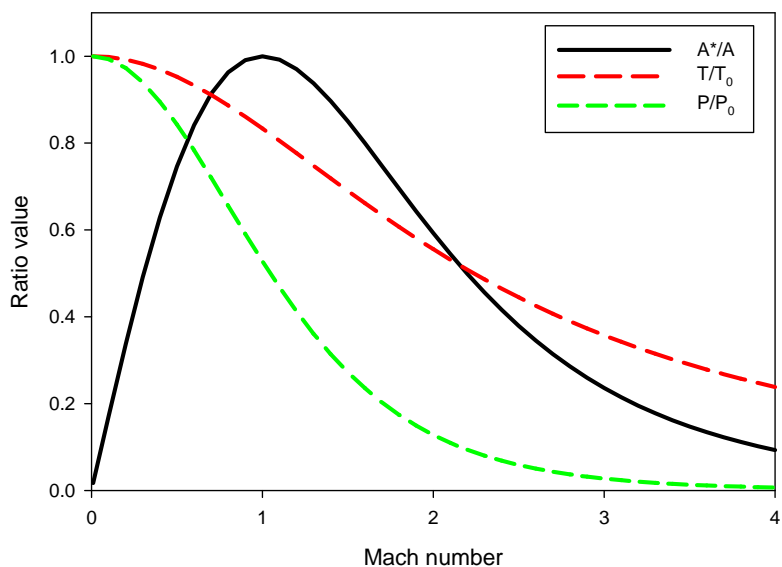
Figure 2.2 Effects of the Mach number on the area ratio, pressure ratio, and temperature ratio in a convergent-divergent nozzle.

The jet velocity is much higher than the superficial gas velocity. Previous studies have found that the transverse gas and solids velocity profiles in horizontal jets in fluidized beds are of the Schlichting or Tollmien type, as for homogeneous jets (Shakhova, 1968; Donadono *et al*., 1980; Filla *et al*., 1983; De Michele *et al*., 1976). De Michele et al. (1976) extended the theory of turbulent submerged jet to the gas injection in fluidized beds, to describe the axial profiles for gas velocity and gas temperature. Donadono et al. (1980) propose that the SCHLICHING's and SCHLICHTING-TAYLOR's correlations can be used to describe the radial gas profile, particle velocity profile, and radial temperature profile. Xuareb et al. (1992) and Ariyapadi et al. (2003) have developed a model to predict gas and solids entrainment in subsonic or sonic jets. In previous studies by Briens et al. (2008) and Hulet et al. (2008a), a specific technique was employed to measure the solids entrainment into submerged gas and gas-liquid jets.

The objective of this work was to study the effects of nozzle mass flow-rate, nozzle size, injection gas properties, and superficial gas velocity of bed on solids entrainment, using supersonic nozzles in fluidized beds. A novel technique has been developed for the accurate measurement of solids entrainment into jets in fluidized beds.

2.3 **Experimental setup**

A fluidized bed with two compartments, shown in Figure 2.3, was used for the solids entrainment measurements. The fluidized bed is constructed of polycarbonate, has a rectangular cross-section of 1.2 m × 0.1 m, and is 2.3 m tall. The bed is divided into two equal compartments by a partition wall, with an opening fitted with a draft tube. The fluidization velocity in each compartment is independently controlled by sonic nozzles and pressure regulators. Two differential pressure transducers are used to measure the pressure difference between the two compartments. A VTL (vertical transport line) unit is installed in the fluidized bed; it is comprised of a nozzle, a vertical riser, an elbow, a disengaging cyclone, and a downer with one 1 m length of sight glass and one pinch valve. A shroud installed around the VTL nozzle was used to maximize solids flow through the VTL (Hulet et al., 2008b). The bed solids could, thus, be pneumatically transported from the left side of bed to the right side through the VTL, while solids were conveyed back from the right side to left side by the supersonic nozzle through the draft tube connecting the two compartments. Coke particles, with a Sauter mean diameter of 135 μm and a density of 1450 kg/m^3, were used for the study. Several convergent-divergent supersonic nozzles, of various dimensions, were tested.
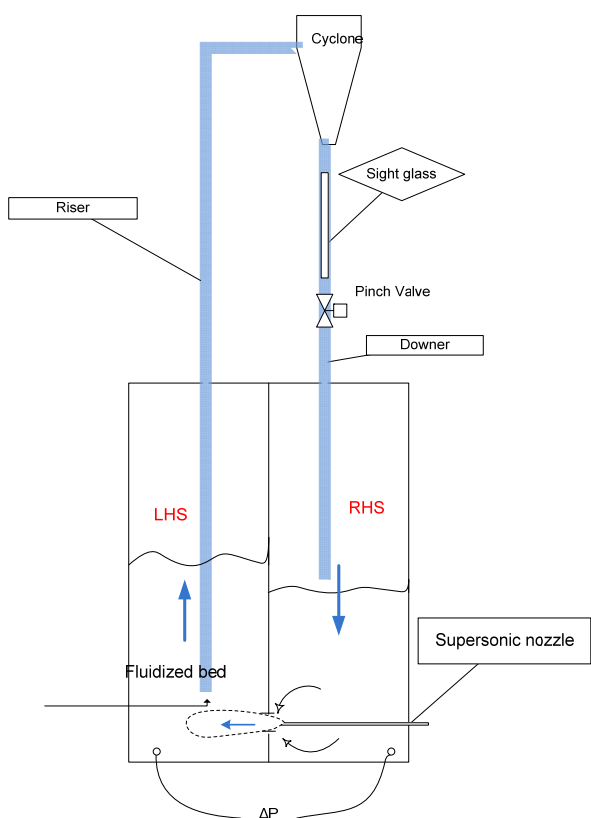
Figure 2.3 The Vertical transport line in a fluidized bed
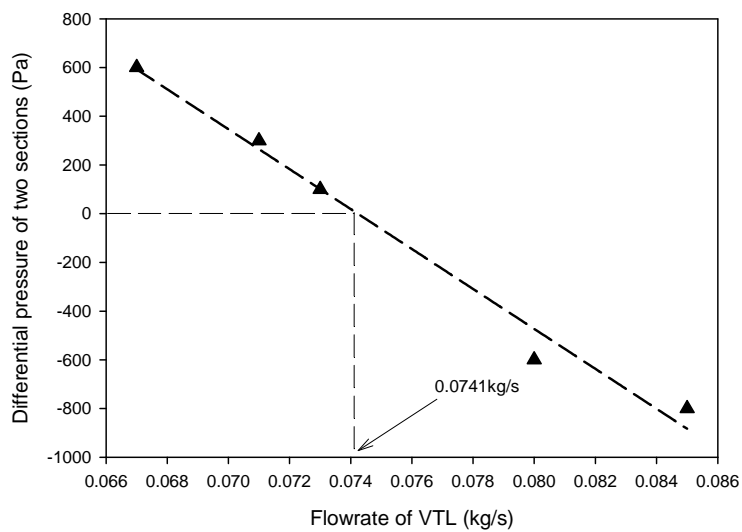
Figure 2.4 Estimate of jet solids entrainment rate.

In each experiment, the gas flow through the VTL nozzle was adjusted until the bed levels in both compartments of the column became the same, as indicated by a zero differential pressure between the two compartments, and remained steady. The flowrate of solids entrained into the jet and carried from the right hand side compartment to the left hand side compartment was, then, equal to the solids flowrate through the VTL, which could be accurately measured by closing the pinch valve and monitoring the rise of the solids level through the sight glass, using a camera. In practice, it was difficult to exactly achieve a steady differential pressure of 0 between the two compartments. Several experiments were, therefore, conducted with different gas flows to the VTL and the resulting solids flowrate through the VTL was measured. The exact solids flowrate corresponding to a zero pressure differential was then obtained by interpolation, as shown by Figure 2.4.

2.4 Results and discussion

Figure 2.5 illustrates the configuration of a turbulent jet, in which a core of flow with undiminished velocity equals to U_0 reaches section 1-1, on the jet axis (Rajaratnam, 1976). This core is known as the potential core. Davies (1972) suggests that the length of potential zone is about 6.4 jet diameters, followed by a transition zone of about 8 jet diameters. In the fully developed flow region, as shown in Figure 2.5, the universal jet axial velocity profile is expressed (Abramovich, 1963):

$$u = u_m \left(1 - \xi^{1.5}\right)^2 \tag{2.5}$$

$$\xi = \frac{y}{r} \tag{2.6}$$

where u is the axial gas velocity, u_m is the gas velocity on jet axis, y is radial distance from jet axis. In Eq. 2.6, r is defined as the large value of y where u equals to zero.
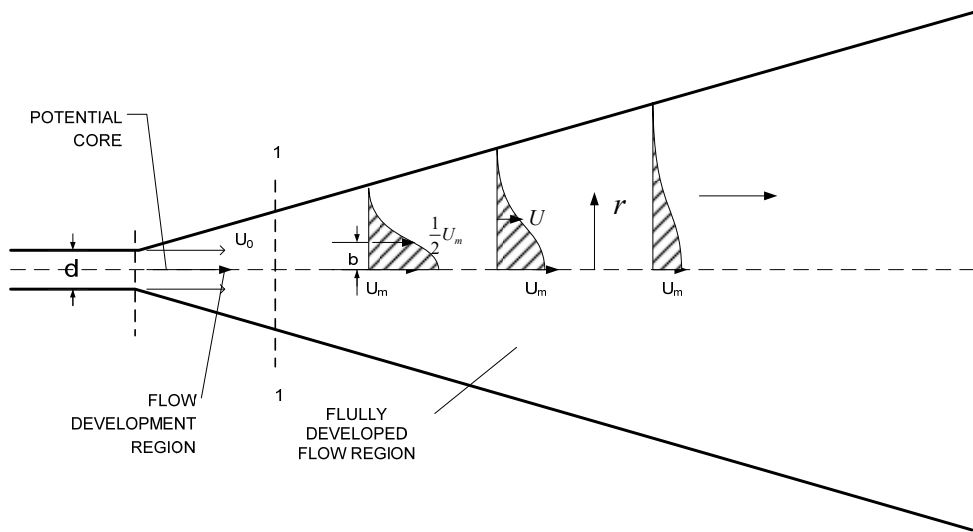
Figure 2.5 Configuration of a turbulent jets (adapted from Rajaratnam, 1976)

Behie et al. (1971) concluded that the radial distribution of axial momentum for vertical air jets in a fluidized bed could be interpreted with the theory of turbulent jets. De Michele et al. (1976) extended the theory of turbulent submerged jest to gas injection in fluidized beds, to describe the axial profiles for gas velocity and temperature. Donadono et al. (1980) proposed that the SCHLICHING's and SCHLICHTING-TAYLOR's correlations can be used to portray the radial gas profile, particle velocity profile, and radial temperature profile of jets in fluidized beds. Merry (1971) suggested a scheme of the particle tracks in the vicinity of the jet, shown in Figure 2.6, with the majority of entrainment occurring near the nozzle tip in the potential zone region.
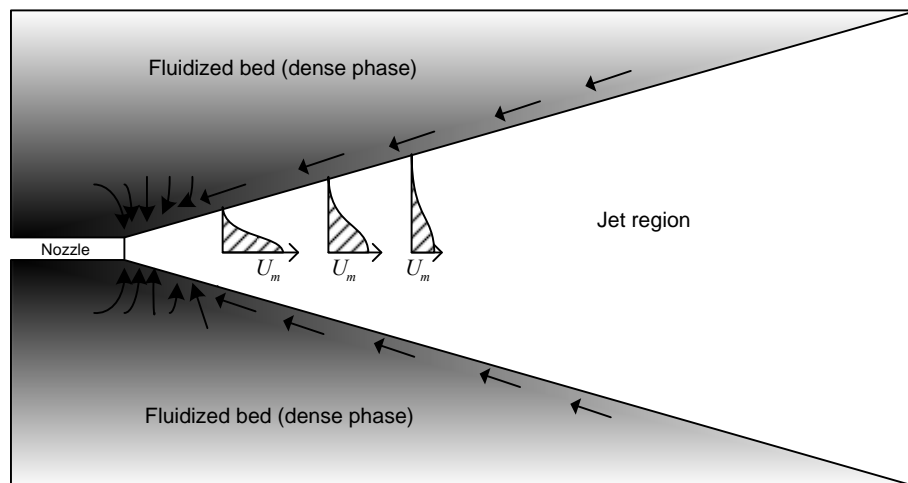
Figure 2.6 Solid entrainment track in the injection region (adapted from Merry, 1971)

Briens et al. (2008) found that the superficial gas velocity has little effect on the solids entrainment rate into a sonic jet. Preliminary experiments in this work confirmed these results. The constant superficial gas velocity for both compartments was, therefore, set to a constant value of 0.11 m/s for all experiments.

Draft tubes have been proposed to enhance jet attrition in fluidized beds. Segraves (1958) used a small draft tube located near the nozzle tip to stabilize the supersonic shock waves. McMillan et al. (2005) used a draft tube to enhance particle mixing and acceleration. Both studies used draft tubes which had a smaller diameter, were longer and were closer to the attrition nozzle tip than the draft tubes used to measure entrainment in this paper.

In the present study, the effect the draft tube on solids entrainment is supposed to be negligible because the draft tube diameter is too large to affect the flow of supersonic jet. However, the draft tube has an obvious influence on solids entrainment issuing into the jet in some conditions. Figure 2.7 shows that the maximum solids flowrate was obtained when the diameter of the connecting tube between the two compartments was between 0.0191 and 0.0254 m (3/4 and 1 inch). At smaller diameters, the jet was too constricted and could not carry all entrained solids through the tube. At larger diameters, the jet did not occupy the whole cross-section of the tube and solids could flow back near the wall of the tube.
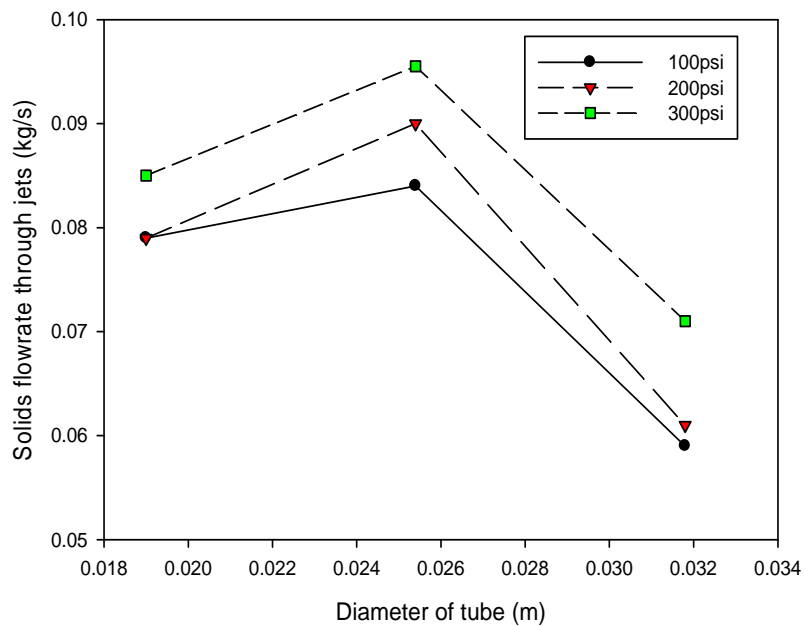
Figure 2.7 Effect of connecting tube diameter on measured solids flowrate
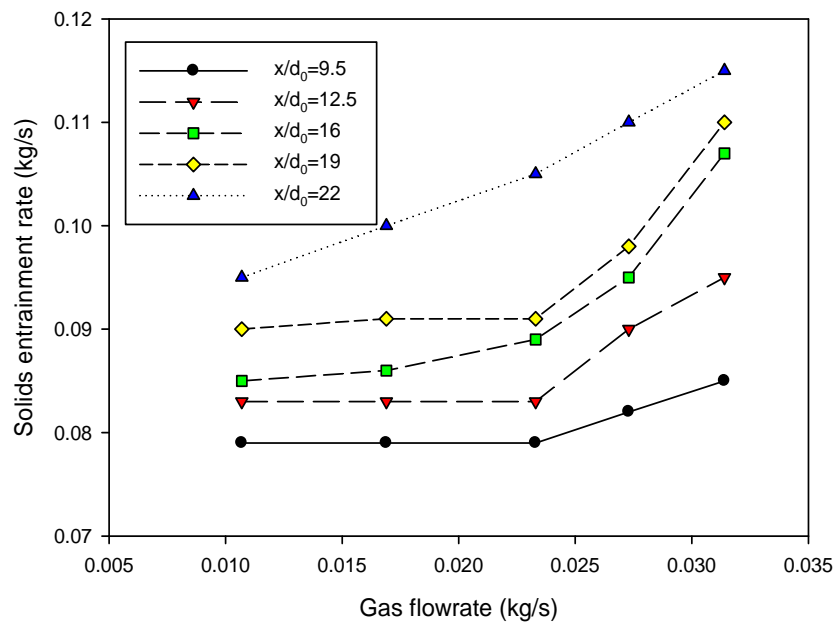
Figure 2.8 Effect of nozzle air flowrate on solids entrainment rate for varying distance x from the nozzle (2.4mm nozzle, air, 19mm draft tube).

Figure 2.8 shows that the solids entrainment rate was affected by the nozzle gas flowrate. It also shows that the solids entrainment rate into the jet steadily increases with increasing distance between the nozzle tip and connecting tube.

Because a prime objective is to reduce the consumption of nozzle gas, the dimensionless entrainment efficiency is defined as:

$$entrainmen\,t\;efficiency\;=\;\frac{solids\;entrainmen\,t\;(kg\,/\,s)}{flowrate\;of\;gas\;injection\;(kg\,/\,s)}\;=\;\frac{W_s}{W_g}$$

A comparison of Figures 2.8 and 2.9 shows that increasing the gas flowrate through the nozzle increases the solids entrainment rate, it dramatically reduces the entrainment efficiency. Increasing the gas flowrate through the nozzle does not greatly increase the size of the jet cavity, which suggests that the entrainment rate may be limited by phenomena occurring at the jet-bed interface.
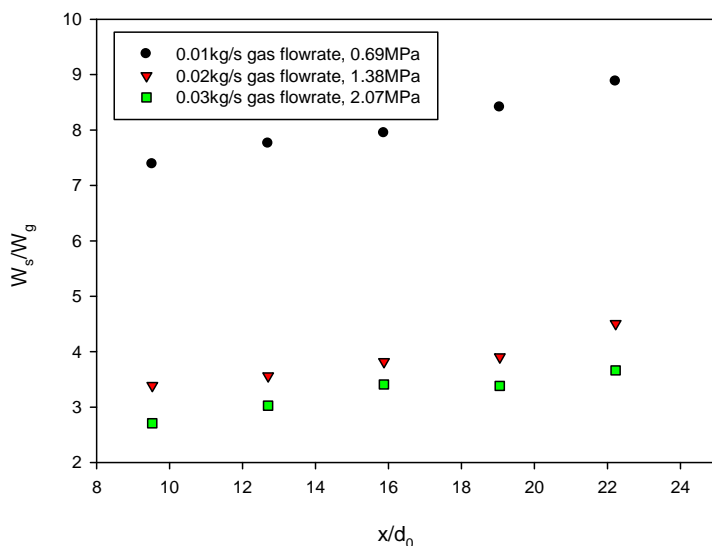
Figure 2.9 Effect of nozzle air flowrate on the entrainment efficiency at varying distance from the nozzle (2.4mm nozzle, air)
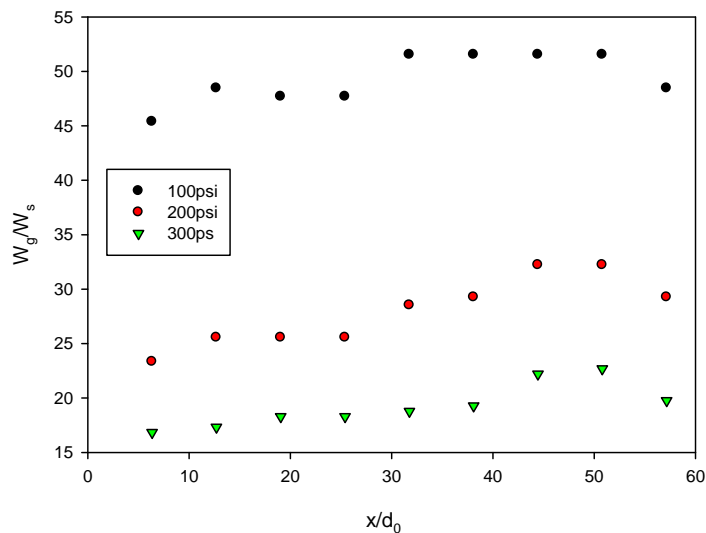
Figure 2.10 Effect of nozzle air flowrate on the entrainment efficiency at varying distance from the nozzle (1.2mm nozzle, air)

In order to study the effect of the nozzle size, two different nozzle sizes were tested. A comparison of Figures 2.9 and 2.10 demonstrates that smaller nozzles are much more efficient at entraining solids: reducing the nozzle diameter by a factor of two increases the entrainment efficiency by a factor of about 5.

Three different gases, helium, carbon dioxide, and air, were used in the experiments to determine the effect of nozzle gas properties on entrainment efficiency. Figure 2.11 shows that decreasing the gas molecular weight increases the solids entrainment efficiency. One explanation is the gas with lower molecular weight has a higher exit velocity compared to higher molecular weight when they have the same mass flowrates.
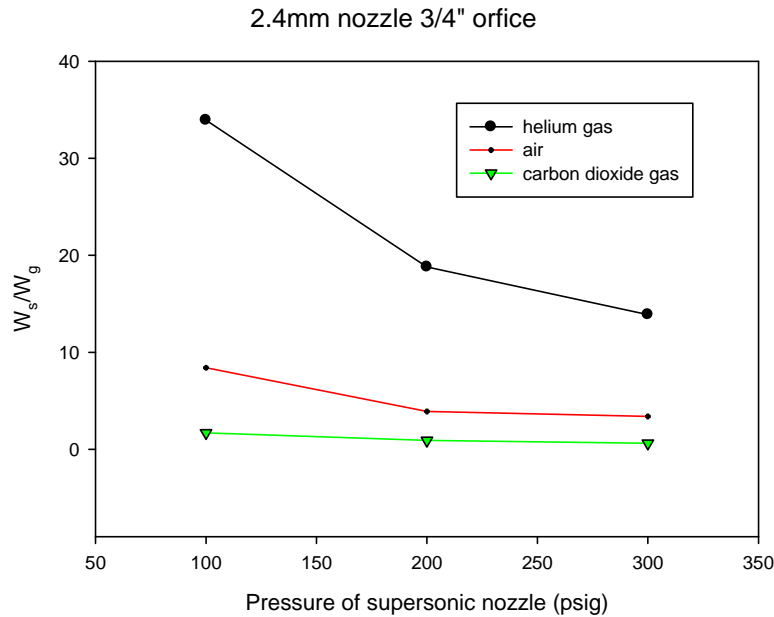
Figure 2.11 Effect of nozzle gas density on the entrainment efficiency (2.4mm nozzle, 19mm orifice).

2.5 **Conclusions**

A novel technique has been developed to reliably measure the solids entrainment rate into jets issuing from supersonic convergent-divergent nozzles in fluidized beds. If the objective is to increase the entrainment efficiency, i.e. the ratio of the mass flowrate of entrained solids to the mass flowrate of nozzle gas, then it is better to operate with smaller nozzles, at lower nozzle gas flowrates and a low nozzle gas density.

2.6 **Notation**

A   Area of nozzle exit (m^2)

A*   Area of nozzle throat (m^2)

d_0 Diameter of nozzle exit (m^2)

G   Mass flux (kg/m^2s)

M   Mach number

M_w Molar weight (kg/mol)

p_0 Upstream pressure of nozzle   (Pa)

p_1 Pressure at throat (Pa)

p_2 Pressure at nozzle exit (Pa)

p_3 Ambient pressure (Pa)

r	Large value of y where u equals to zero (m)
R	Ideal gas universal constant
T_0	Absolute temperature at nozzle throat (K)
T	Absolute temperature at nozzle exit (K)
u	Axial gas velocity (m/s)
U_0	Gas velocity at nozzle exit (m/s)
u_m	Velocity on jet axis (m/s)
u*	Gas velocity at nozzle throat (m/s)
W_s	Solid entrainment rate through nozzle (kg/s)
$W_{g.}$	Flow-rate of gas injection (kg/s)
x	Distance to nozzle exit (m)
y	Radial distance from jet axis (m)

Greek letters

ρ	Gas density at nozzle exit (kg/m^3)
ρ*	Gas density at nozzle throat (kg/m^3)
γ	Ratio of specific heat

2.7 **References**

Abramovich, The theory of turbulent jets. M. I. T. Press: Cambridge, Mass.,, 1963.

Ariyapadi, S.; Berruti, F.; Briens, C.; Griffith, P.; Hulet, C., Modeling the injection of gas-liquid jets into fluidized beds of fine particles. Can. J. Chem. Eng. 2003, 81 (3-4), 891-899.

Briens, C.; Berruti, F.; Felli, V.; Chan, E., Solids entrainment into gas, liquid, and gas-liquid spray jets in fluidized beds. Powder Technol. 2008, 184 (1), 52-57.

Davies, J. T., Turbulence phenomena; an introduction to the eddy transfer of momentum, mass, and heat particularly at interfaces. Academic Press: New York, 1972.

De Michele, G.; Elia, A.; Massimilla, L., INTERACTION BETWEEN JETS AND FLUIDIZED-BEDS. Quaderni Dell Ingegnere Chimico Italiano 1976, 12 (6), 155-162.

Donadono, S.; Maresca, A.; Massimilla, L., GAS INJECTION IN SHALLOW BEDS OF FLUIDIZED, COARSE SOLIDS. Quaderni Dell Ingegnere Chimico Italiano 1980, 16 (1-2), 1-10.

Dunlop, D. D.; Griffin, J. L. I.; Moser, J. J. F., Particle size control in fluid coking. Chemical Engineering Progress 1958, 54 (8), 39-42.

Filla, M.; Massimilla, L.; Vaccaro, S., GAS JETS IN FLUIDIZED-BEDS - THE INFLUENCE OF PARTICLE-SIZE, SHAPE AND DENSITY ON GAS AND SOLIDS ENTRAINMENT. International Journal of Multiphase Flow 1983, 9 (3), 259-267.

Hulet, C.; Briens, C.; Berruti, F.; Chan, E. W., Experimental and analytical study of the solids circulation loop of a compartmented fluidized bed. Powder Technol. 2008a, 185 (2), 131-143.

Hulet, C.; Briens, C.; Berruti, F.; Chan, E. W., Effect of a shroud on entrainment into a submerged jet within a fluidized bed. Chemical Engineering and Processing 2008b, 47 (9-10), 1435-1450.

Liepmann, H. W., Elements of gasdynamics. John Wiley & Sons, Inc. : New York, 1957.

Massimilla, L. In Gas jets in fluidized beds, Fluidization 1985; Davidson, J. F. C., R.; Harrison, D. , Ed. Academic Press: 1985; p 733.

McMillan, J.; Zhou, D.; Ariyapadi, S.; Briens, C.; Berruti, F.; Chan, E., Characterization of the Contact between Liquid Spray Droplets and Particles in a Fluidized Bed. Industrial & Engineering Chemistry Research 2005, 44 (14), 4931-4939.

Merry, J. M. D., Penetration of a Horizontal Gas Jet into a Fluidised Bed. Transactions of the Institution of Chemical Engineers and the Chemical Engineer 1971, 49 (4), 189-&.

Merry, J. M. D., Fluid and Particle Entrainment into Vertical Jets in Fluidized-Beds. Aiche Journal 1976, 22 (2), 315-323.

Perry, R. H. G., Don W.; et al. , Perry's chemical engineers' handbook. -- McGraw-Hill's Access Engineering 8th ed.; McGraw-Hill: New York, 2008.

Rajaratnam, N., TURBULENT JETS. ELSEVIER SCIENTIFIC PUBLISHING COMPANY: NEW YORK, 1976.

Shakhova, N. A., Discharge of turbulent jets into a fluidized bed. Inzhenerno-Fizicheskii Zhurnal 1968, 14 (1), 61-69.

Smith, J. M., Introduction to Chemical Engineering Thermodynamics. 7 ed.; McGraw-Hill Companies, Inc: 2005.

Xuereb, C.; Laguerie, C.; Baron, T., Behavior of Horizontal or Inclined Continuous Gas Jets Introduced into a Fluidized-Bed .3. Model of the Developed Flow Zone of the Jet. Powder Technol. 1992, 72 (1), 7-16.

Segraves, W. B.; Rouge, B. Supersonic jet grinding means and method. US2832545, 1958.

Chapter 3

3 Penetration of High Velocity Horizontal Gas Jets into A Fluidized Bed at High Temperature

Feng Li, Cedric Briens, Franco Berruti
Department of Chemical and Biochemical Engineering
Institute for chemicals and Fuels from Alternative Resources (ICFAR)
The University of Western Ontario
London, ON, Canada N6A 5B9
and
Jennifer McMillan
Edmonton Research Centre
Syncrude Canada Ltd.
Edmonton, AB, Canada T6N 1H4

3.1 Abstract:

High velocity horizontal gas jets are applied to various industrial processes. In this work, a new thermal technique has been developed to measure the penetration length of horizontal gas jets. Experiments were conducted in a fluidized bed with a height of 1.23m and a rectangular cross section of 0.10m × 0.50m. The fluidized bed particles, which were either petroleum coke or sand, were heated by an in-bed electrical heater to temperatures between 300°C and 500°C. Cold gases, such as helium, nitrogen, carbon dioxide, were injected into the hot fluidized bed via a horizontal nozzle operating over a range of velocities. Based on the experimental results, a new empirical correlation was developed to predict the penetration length of jets issuing from the horizontal sonic nozzle at high temperature.

Keywords: Jet Penetration, Fluidized bed, Penetration Length, Supersonic Nozzle

3.2 Introduction

A number of industrial processes, such as fluid coking, use high velocity horizontal gas jets for particle attrition in high temperature fluidized beds. In the fluid coking process, the size of coke particles must be controlled because large particles cause poor

fluidization and degrade the operation of the coke transport lines (Dunlop et al., 1958). This is achieved by injecting steam into the fluidized bed through high velocity nozzles. According to McMillan et al. (2007b), the high velocity gas jet issuing from these nozzles entrains bed particles and accelerates them to a high speed; due to their inertia, these particles slam on slow moving bed particles near the jet tip, causing breakage and thus, reducing the particle size. Minimizing steam consumption is essential to maximize reactor throughout and reduce wastewater volumes. Typically, convergent-divergent nozzles are more efficient than regular nozzles, i.e. they require less steam to achieve the same attrition rate (McMillan et al., 2007a). Knowing the penetration depth of the high velocity jets is important to maximize their attrition efficiency and avoid the erosion of fluidized bed internals, because most of the particles attrition and collision occurs in the void area of the horizontal jets in fluidized beds.

However, the current knowledge of the hydrodynamics and fundamental phenomena of high velocity horizontal gas jets is mostly limited to ambient temperature conditions. Among the published correlations for penetration length, many are unreliable for jets issuing from convergent-divergent nozzles, particularly at high temperature. A high velocity jet injected horizontally in a fluidized bed can be assumed to behave as a submerged jet, similar to a turbulent jet spreading through a liquid medium at rest (Abramovich, 1963; De Michele et al., 1976). Many studies confirmed that the model gives a good description of momentum, heat, and mass transfers (Behie et al., 1970, and 1975; Hong et al., 1997).

Table 3.1 provides examples of published correlations for jet penetration length. The jet penetration length increases with increasing gas density and gas velocity. However, all these correlations were developed from data obtained with nozzles operating at subsonic velocities.

Table 3.1 Correlations for horizontal jet penetration length

Correlation	Variables	U_0(m/s)	Reference
$\dfrac{L_j}{d_0} = 7.8\left(\dfrac{\rho_f U_0}{\rho_p \sqrt{g d_p}}\right)$	Copolymer $1 < \dfrac{d_0}{d_p} < 1.5$	83-192	Shakhova (1968)
$\dfrac{L_j}{d_0} + 4.5 = 5.25\left(\dfrac{\rho_0 U_0^2}{(1-\varepsilon)\rho_P g d_P}\right)^{0.4}\left(\dfrac{\rho_f}{\rho_P}\right)^{0.2}\left(\dfrac{d_p}{d_0}\right)^{0.2}$	Sand, steel shot, and Kale seeds $1.5 < \dfrac{d_0}{d_p} < 80$ $1.6\times10^{-4} < \dfrac{\rho_f}{\rho_p} < 12\times10^{-4}$	40-200	Merry (1971)
$0.044\dfrac{L_j}{d_0} + 1.48 = 0.5\log(0.67\rho_f U_0^2)$	FCC	32-64	Zenz (1968)
$\dfrac{L_j}{d_0} + 3.80 = 1.64\times10^6\left(\dfrac{\rho_0 U_0^2}{(1-\varepsilon)\rho_P g d_P}\right)^{0.327}\left(\dfrac{\rho_f}{\rho_P}\right)^{1.974}$	Millet, silica sand $2.2 < \dfrac{d_0}{d_p} < 7$ $7.5\times10^{-4} < \dfrac{\rho_f}{\rho_p} < 8\times10^{-4}$	6-190	Hong (1997)
$\dfrac{L_j}{d_0} = 5.52\left(\dfrac{\rho_0 U_0^2}{(\rho_p - \rho_f)g d_0}\right)^{0.27}$	Catalyst, glass, sand $1 < Fr < 380$	15-300	Benjelloun (1991)
$\dfrac{L_j}{d_0} = 2.8\left(\dfrac{\rho_0 U_0^2}{(\rho_p - \rho_f)g d_0}\right)^{0.4}$	Calcined alumina powder $1 < Fr < 180$		Yates (1991)

For measuring the penetration length accurately, many techniques were developed to determine jet penetrations in fluidized beds. Visual observation of the jet performance in the beds is a most common. The radiation densimeter, Pitot tube probe, optical probe, and capacitance probe are also utilized to measure the jet penetration (Raghunathan et al., 1988). Vaccaro et al. (1997) analyzed and classified the various techniques into two main groups. The first group includes visual observations of the phenomenon, photographic or high-speed film analysis, optical probes, capacitance probes. The second group involves Pitot tube probes and γ-ray. In the study by Hong et al. (1997), a high-speed video was employed for measuring the jet penetration length. Zhu et al. (2000) used a thermal method to measure the jet penetration length in a study of liquid jets in a gas-solid system.

The thermal measurement technique was also adapted and developed to study the liquid-gas jet in fluidized beds by many researches (Ariyapadi et al., 2005; McMillan et al., 2005). A triboelectric technique was successfully developed to measure gas jet boundaries, the penetration length, and the expansion angle of jets (Dawe et al., 2008; Cruz et al., 2009).

The objective of the study illustrated in this paper was the development of a correlation to predict the penetration of horizontal jets issuing from convergent-divergent nozzles at high temperature, operating under supersonic conditions.

3.3 **Experimental Setup**

Experiments were performed in a hot fluidized bed with a height of 1.23m and a rectangular cross section of 0.10m × 0.50m (Figure 3.1). The bed particles were heated with an in-bed electrical heater to temperatures between 200°C to 500 °C. Cold gases, such as helium, nitrogen, carbon dioxide, or mixtures of these gases, were injected into the hot fluidized bed via a horizontal nozzle at a distance of 0.127m above the gas distributor. Two different types of particles were used in the experiments, silica sand with a Sauter-mean diameter of 200 μm and petroleum coke with a Sauter-mean diameter of 120 μm. Tests were conducted with a range of nozzle flowrates dependent on the temperature and injection pressure. Several different sizes of convergent-divergent nozzles were used to test the effects of nozzle size on the penetration length of supersonic gas jets.
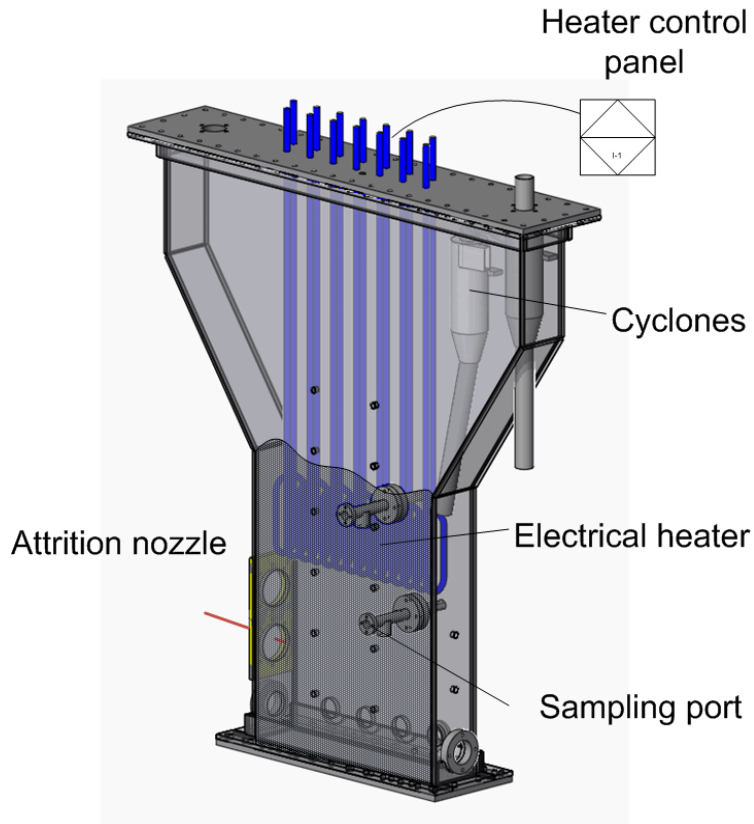
Figure 3.1 The scheme of the hot fluidized bed
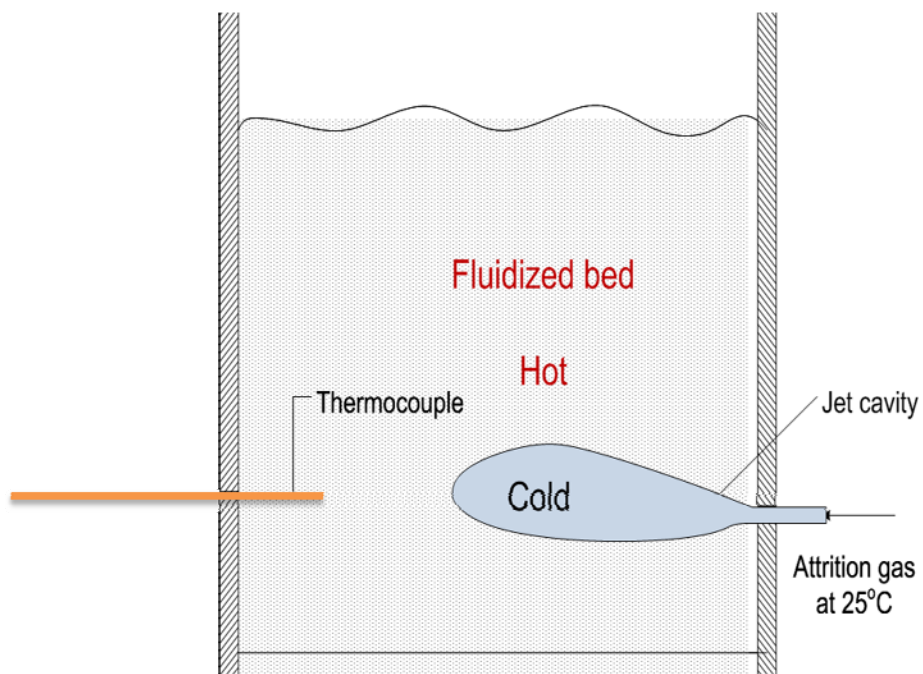
Figure 3.2 Diagram of the thermal method to measure penetration length in fluidized beds at high temperature
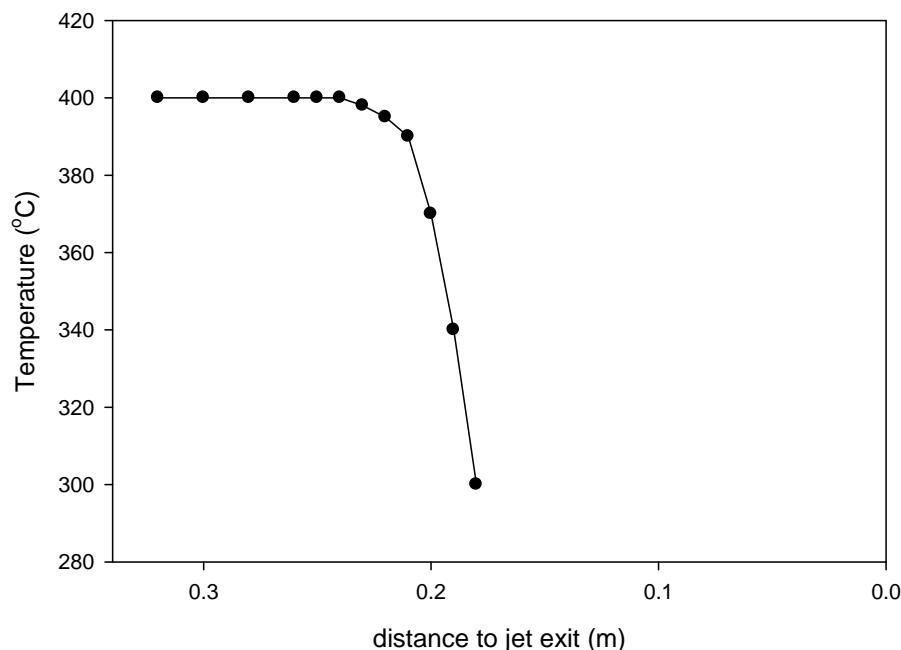
Figure 3.3 Temperature profile of jet cavity with a supersonic nozzle in fluidized beds

An optimized method was developed to measure the penetration length of the high velocity horizontal gas jets. The method used the observation that, because cold gas was used to form the jet, the jet cavity was always at a temperature below that of the hot fluidized bed, and that the bed temperature was nearly uniform. The thermal method used a fast thermocouple, which was inserted along the axis of the jet from the opposite wall (Figure 3.2), a series of temperature signals were recorded while moving the thermocouple progressively towards the jet. The end of the jet cavity could be detected from the sharp decrease in temperature at the boundary of the jet cavity, due to the cold jet cavity (Figure 3.3). The penetration length of the high velocity gas jet L_j is defined as the distance from the jet tip to the end of jet cavity, where the temperature of jet end boundary is assumed to be 20^oC lower than the bed temperature.

3.4 **Results and discussion**

Figure 3.4 shows the results of measurements obtained using the thermal method at various bed operating temperatures. The results demonstrate that the bed temperature has a minimal influence on the jet penetration length. On the other hand, it was observed that

the jet penetration length increased with increasing nozzle exit diameter, as illustrated in Figure 3.5.

Influence of operating temperatures on jet penetration (silica sands, d_0=4mm, compressed air)
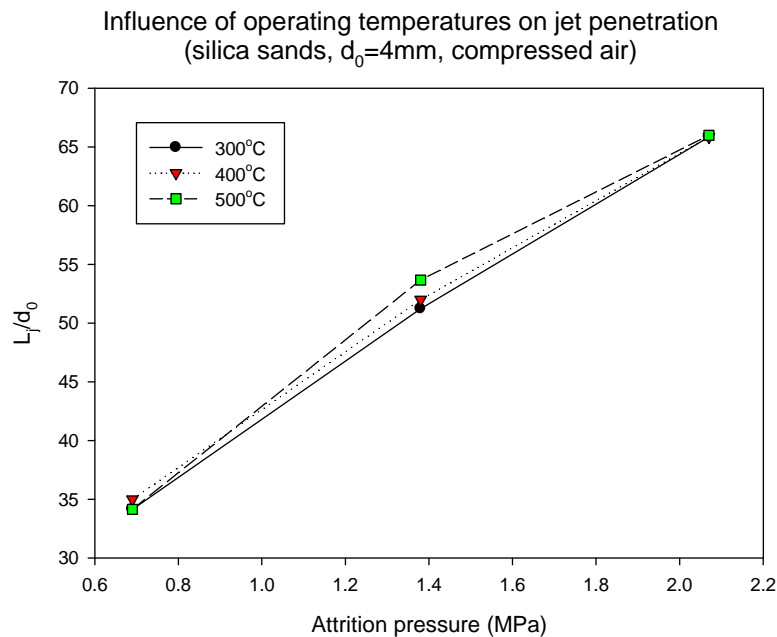
Figure 3.4 Comparison of experimental results with various temperatures (sand, d_0=4mm, air)
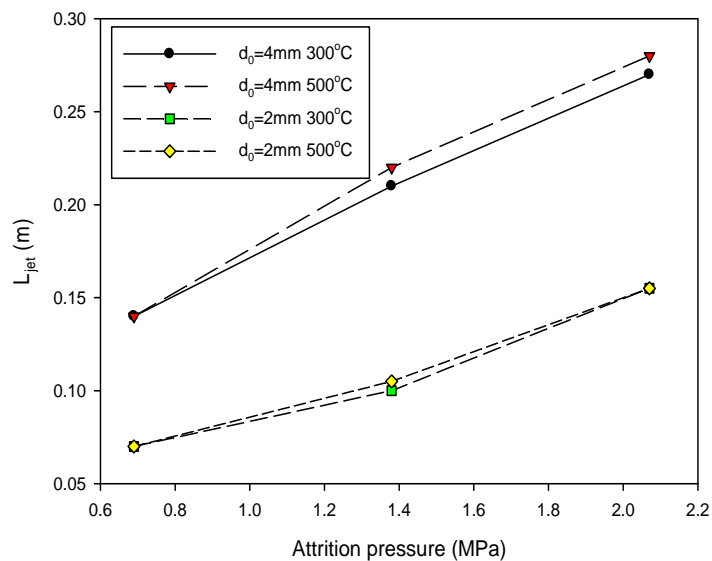
Figure 3.5 Comparison the experimental results with various nozzle size (Sand, air)
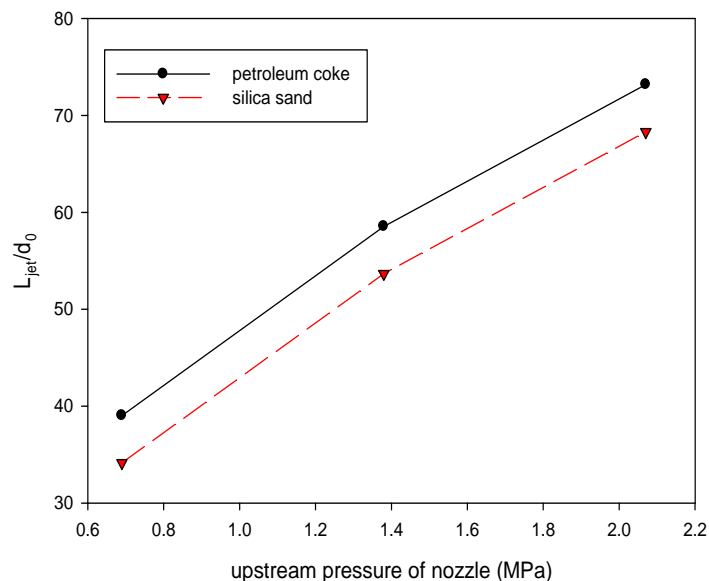
Figure 3.6 Influence of particle size and density on penetration length
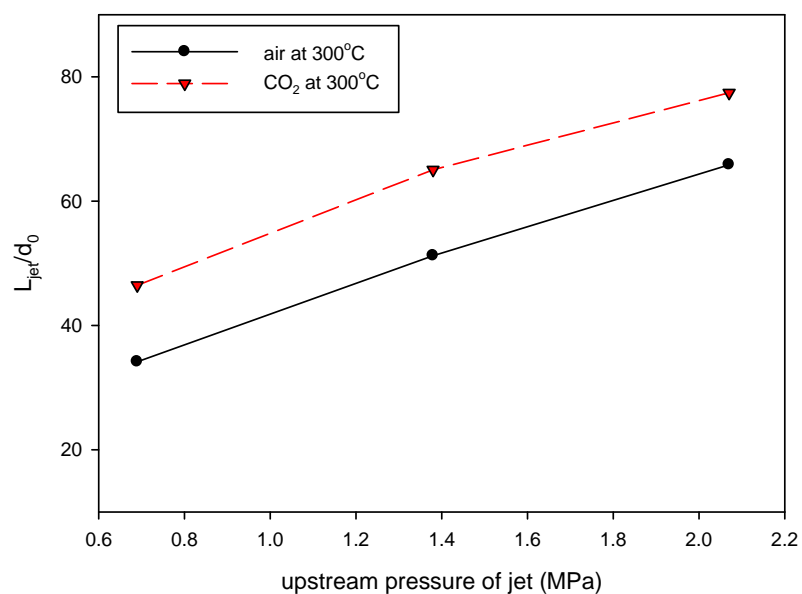
Figure 3.7 Influence of the attrition gas properties on the penetration length

The influence of the particle density on the penetration length was studied using two different types of particles, i.e. petroleum coke and silica sand. It was observed that the jet penetrated further in a bed of coke (ρ_p=1450 kg/m^3) than in a bed of silica sand (ρ_p=2650 kg/m^3), as shown in Figure 3.6. Similar results were reported by Dawe et al. (2008) and Musmarra (2000).   Figure 3.7 illustrates that the jet penetration length

increased as the gas density increased, in agreement with other literature data (Dawe et al., 2008; Vaccaro, 1997).

Table 3.2 lists all experimental conditions for the measurements of the jet penetration length by the thermal measurement method. In addition, the experimental data have been compared to the predictions derived from existing empirical correlations in the literature.

Table 3.2 Experimental conditions used for tests with typical divergent-convergent nozzles in a fluidized bed at high temperature

Attrition gas	Bed particles	Diameter of nozzle throat (mm)	Diameter of nozzle exit (mm)	Bed temperature (^{o}C)	Pressure Upstream of nozzle (MPa)	Froude number
helium	Coke	2.4	4	300, 500	0.7-2.0	25000-69222
helium	Coke	1.2	2	500	0.7-2.0	50000-140000
helium	sand	2.4	4	300, 500	0.7-2.0	25000-69222
Nitrogen	Coke	2.4	4	300, 400, 500	0.7-2.0	6500-18000
Nitrogen	Coke	1.2	2	300, 500	0.7-2.0	1200-35000
Nitrogen	Coke	2.4	5.2	210	0.7-2.0	7600-21000
Air	Sand	1.2	2	400, 500	0.7-2.0	1200-35000
Air	Sand	2.4	4	300, 400, 500	0.7-2.0	6500-18000
Air	Sand	2.4	4.85	300,400,500	0.7-2.0	5700-16000
Air	Sand	2.4	5.2	200,300,500	0.7-2.0	7600-21000
CO_2	coke	2.4	4	300,400,500	0.7-2.0	2500-6500
CO_2	Sand	2.4	4	300, 400, 500	0.7-2.0	2500-6500
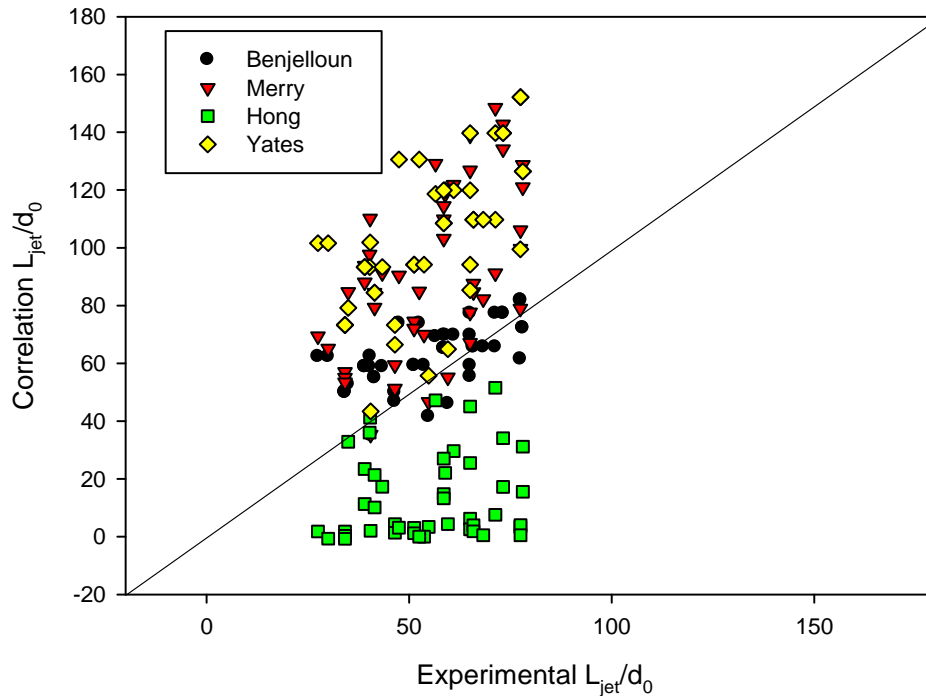
Figure 3.8 Comparison the experimental results with predicted data by empirical coefficients

The study shows that the empirical correlations listed in Table 3.2 are unable to predict the experimental data at high temperature, as shown by Figure 3.8. All these correlations were developed using data collected with low velocity, subsonic straight nozzles. Correlations from both Merry and Yates overestimated the jet penetration length, whereas Hong's correlation shows the predicted values are smaller than the experimental results. Only the predictions from Benjelloun's correlation are in relatively good agreement with the measurements. The majority of the correlations use dimensionless terms such as the Froude and Galileo numbers, shown in equations 3.1 and 3.2, respectively. The Froude number has been used in the empirical correlations of Yang-Keairn (1978), Yates (1991), Benjelloun (1991), and Ariyapadi (2003).

$$Fr = \frac{\rho_0 U_0^2}{(\rho_p - \rho_f)gd_0}$$

(3.1)

The Froude number integrates the effects of particle size, jet diameter and jet gas velocity, and represents the ratio of the inertial force of gas at the nozzle and the gravity force of

particles. Benjelloun (1991) suggested that the relationship between the gas momentum at the orifice and gravity forces acting on the jet can be written as a function of the Froude number, from which the penetration length can be obtained. Using the experimental data obtained in this study, a new empirical correlation is proposed based on the same basic concept as the one proposed by Benjelloun and adapting his correlation to supersonic nozzles discharging into hot fluidized beds. Assuming that the ratio of jet penetration length and nozzle diameter is proportional to the Froude number, a generic form of the relationship can be represented as:

$$\frac{L_j}{d_o} = \alpha Fr^\beta \tag{3.2}$$

Equation 3.3 can be rearranged to:

$$L_j = \frac{\alpha}{g^\beta} \frac{1}{(\rho_p - \rho_f)^\beta} \left(\rho_0 U_0^{\ 2}\right)^\beta d_0^{\ (1-\beta)} \tag{3.3}$$

The value of α and β vary according to the particle type and the bed temperature.

Table 3.3 Values of empirical constants of Equation 4 derived from experimental data

Bed Temperature (°C)	Particles	α	β
200~500	Sand	0.15	0.664
200~500	coke	0.38	0.540

The new empirical correlation shows a much better agreement with the experimental data, compared to existing correlations, as illustrated in Figures 3.9 and 3.10. The relationships among the horizontal jets, bed solids characteristics and operating conditions are complex. The effects of nozzle gas mass flow-rate, nozzle size, and operation temperature on the penetration length are well predicted by the new empirical correlation for supersonic horizontal nozzles proposed in this work.
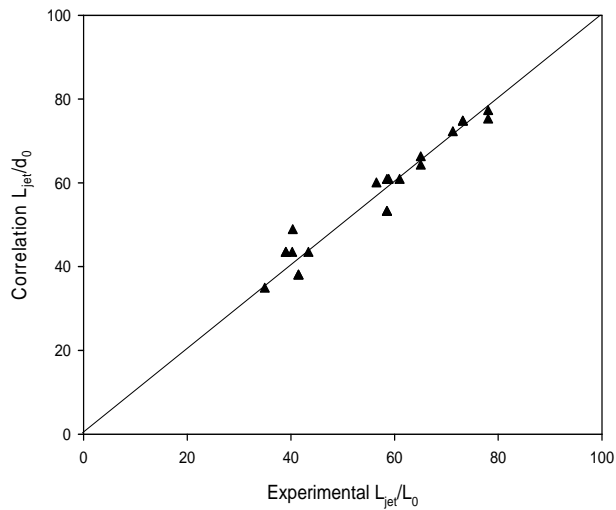
Figure 3.9 Comparison of new empirical correlation with experimental data (Petroleum coke, high temperature)
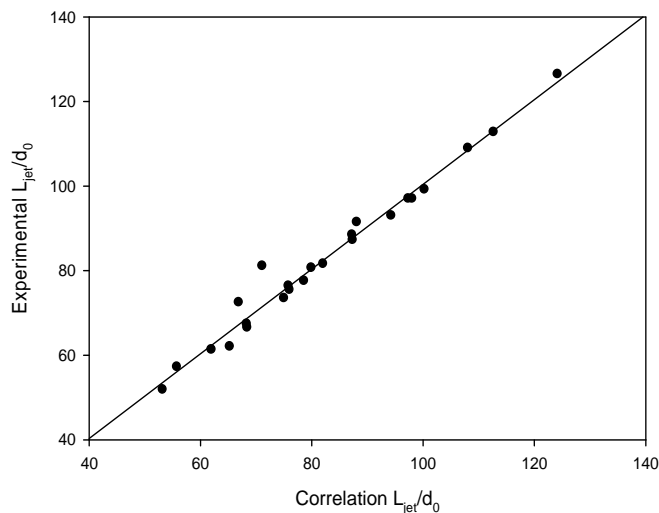
Figure 3.10 Comparison of new empirical correlation with experimental data (Silica sand, high temperature)

3.5 **Conclusion**

An optimized method has been developed to measure the penetration length of high velocity horizontal jets in fluidized beds at high temperatures. Based on the experimental data obtained, a new and improved empirical correlation has been proposed, derived with a variety of nozzle sizes, gas properties, and operating temperatures.

3.6 **Notation**

b radius of jet region(m)

d_0 nozzle exit diameter (m)

d_p particle diameter (m)

d_t nozzle thoat diameter (m)

g gravity constant (m/s^2)

h inclined nozzle position (m) (Hong correlation)

h_0 bed depth (m) (Hong correlation)

L_j Jet penetration depth (m)

U_0 gas velocity at nozzle (m/s)

u velocity at jet axis (m/s)

u_m velocity at radius (m/s)

Greek letters

α correlation constant

β correlation constant

ε Bed voidage (-)

ξ Specific heat ratio of the gas (-)

ρ_0 Gas density at the nozzle exit (kg/m^3)

ρ_f Gas density in the bed (kg/m^3)

ρ_p Particles density in the bed (kg/m^3)

3.7 **References**

Abramovich, *The theory of turbulent jets*. M. I. T. Press: Cambridge, Mass.,, 1963.

Ariyapadi, S.; Berruti, F.; Briens, C.; Griffith, P.; Hulet, C., Modeling the injection of gas-liquid jets into fluidized beds of fine particles. *Canadian Journal of Chemical Engineering* **2003,** *81* (3-4), 891-899.

Behie, L. A.; Bergougn.Ma; Baker, C. G. J.; Bulani, W., Jet Momentum Dissipation at a Grid of a Large Gas Fluidized Bed. *Canadian Journal of Chemical Engineering* **1970,** *48* (2), 158-&.

Behie, L. A.; Bergougnou, M. A.; Baker, C. G. J., Heat-Transfer from a Grid Jet in a Large Fluidized-Bed. *Canadian Journal of Chemical Engineering* **1975,** *53* (1), 25-30.

Benjelloun, F. V., J. In *Determination des longueurs de jets de gaz horizontaux dans des lits fluidises*, textes des communications presentee a l'occasion des 6emes journees europeenenes sur la fluidisation, Toulouse, Laguerie, C. G., P., Ed. Toulouse, 1991.

Chen, L. B.; Weinstein, H., Shape and Extent of the Void Formed by a Horizontal Jet in a Fluidized-Bed. *Aiche Journal* **1993,** *39* (12), 1901-1909.

Dawe, M.; Briens, C.; Berruti, F., Study of horizontal sonic gas jets in gas-solid fluidized beds. *Canadian Journal of Chemical Engineering* **2008,** *86* (3), 506-513.

De Michele, G.; Elia, A.; Massimilla, L., Interaction between Jets and Fluidized-Beds. *Quaderni Dell Ingegnere Chimico Italiano* **1976,** *12* (6), 155-162.

Dunlop, D. D.; Griffin, J. L. I.; Moser, J. J. F., Particle size control in fluid coking. *Chemical Engineering Progress* **1958,** *54* (8), 39-42.

Hong, R. Y.; Li, H. Z.; Li, H. B.; Wang, Y., Studies on the inclined jet penetration length in a gas-solid fluidized bed. *Powder Technology* **1997,** *92* (3), 205-212.

McMillan, J.; Briens, C.; Berruti, F.; Chan, E., High velocity attrition nozzles in fluidized beds. *Powder Technology* **2007a,** *175* (3), 133-141.

McMillan, J.; Briens, C.; Berruti, F.; Chan, E., Particle attrition mechanism with a sonic gas jet injected into a fluidized bed. *Chemical Engineering Science* **2007b,** *62* (14), 3809-3820.

Merry, J. M. D., Penetration of a Horizontal Gas Jet into a Fluidised Bed. *Transactions of the Institution of Chemical Engineers and the Chemical Engineer* **1971,** *49* (4), 189-&.

Merry, J. M. D., Penetration of Vertical Jets into Fluidized-Beds. *Aiche Journal* **1975,** *21* (3), 507-510.

Merry, J. M. D., Fluid and Particle Entrainment into Vertical Jets in Fluidized-Beds. *Aiche Journal* **1976,** *22* (2), 315-323.

Musmarra, D., Influence of particle size and density on the jet penetration length in gas fluidized beds. *Ind. Eng. Chem. Res.* **2000,** *39* (7), 2612-2617.

Perry, R. H. G., Don W.; et al. , Perry's chemical engineers' handbook. -- McGraw-Hill's Access Engineering 8th ed.; Don W. Green, a. l. e., Robert H. Perry, Ed. McGraw-Hill: New York, 2008. http://www.accessengineeringlibrary.com/html/viewbookdetails.asp?catid=B&bookid=200139d8.

Rajaratnam, N., *TURBULENT JETS*. ELSEVIER SCIENTIFIC PUBLISHING COMPANY: NEW YORK, 1976.

Shakhova, N. A., Discharge of turbulent jets into a fluidized bed. *Inzhenerno-Fizicheskii Zhurnal* **1968,** *14* (1), 61-69.

Vaccaro, S.; Musmarra, D.; Petrecca, M., Evaluation of the jet penetration depth in gas-fluidized beds by pressure signal analysis. *International Journal of Multiphase Flow* **1997,** *23* (4), 683-698.

Xuereb, C.; Laguerie, C.; Baron, T., Behavior of Horizontal or Inclined Continuous Jets Gas-Injected into a Fluidized-Bed .1. Morphology of the Jets. *Powder Technology* **1991,** *67* (1), 43-56.

Xuereb, C.; Laguerie, C.; Baron, T., Behavior of Horizontal or Inclined Continuous Jets Introduced to a Fluidized-Bed by a Gas .2. Gas Velocity Profiles in Horizontal Jets. *Powder Technology* **1991,** *64* (3), 271-283.

Xuereb, C.; Laguerie, C.; Baron, T., Behavior of Horizontal or Inclined Continuous Gas Jets Introduced into a Fluidized-Bed .3. Model of the Developed Flow Zone of the Jet. *Powder Technology* **1992,** *72* (1), 7-16.

Yates, J. G.; Cobbinah, S. S.; Cheesman, D. J.; Jordan, S. P. In *Particle attrition in fluidized beds containing opposing jets*, AIChE Annual Meeting, Chicago, 1991; Weimer, A. W., Ed. Americal Institute of Chemical Engineers (AIChE): Chicago, 1990; pp 13-19.

Zenz, F. A., Bubble Formation and Grid Design. *Inst. Chem. Eng. Symp.* **1968,** *30*, 136-139.

Chapter 4

4 Particle Attrition with Supersonic Nozzles in a Fluidized Bed at High Temperature

4.1 Abstract

Fluidized beds are used for a variety of processes such as food, pharmaceutical, petrochemical and energy production. The fluid coking process, a typical application of fluidized beds, uses thermal cracking reactions to upgrade heavy oils and bitumen from oil sands. Supersonic nozzles injecting steam are used in the fluid coking process to control coke particle size, which is essential to maintain a well-fluidized bed and a satisfactory reaction rate. Maintaining a high attrition rate with a lower steam flowrate would reduce energy consumption, increase reactor throughput, and reduce sour wastewater production. The purpose of the present research is to study particle attrition with supersonic convergent-divergent nozzles in a fluidized bed at high temperatures, under condition such as these encountered in the fluid coking process. According to the experimental results, the grinding efficiency is significantly affected by fluidized bed temperature, attrition gas properties, and nozzle size. The experimental data further suggest that particle fragmentation is the dominant attrition process using supersonic nozzles at a hot fluidized bed.

4.2 Introduction

Fluidized beds are used for a variety of processes such as food, pharmaceutical, petrochemical and energy production. An example is the fluid coking process, which uses thermal cracking reactions to upgrade heavy oils and bitumen from oil sands. In this process, hot coke particles provide the heat for the endothermic cracking reactions that convert the feed into vapor products and coke. To maintain a well fluidized bed and a constant reaction rate, it is desirable to maintain the coke particle size within its optimal range, since particles that are too large or fine will result in slugging or poor fluidization. In fluid cokers, supersonic attrition nozzles are used to control coke particle size, with

high pressure and superheated steam. Maintaining a high attrition rate with a lower steam flowrate would reduce energy consumption, increase reactor throughput, and reduce sour wastewater production upon its condensation.

Many studies have been conducted on particle attrition in fluidized beds. The mechanisms proposed for particle attrition in fluidized beds include thermal, chemical, kinetic and static mechanical stresses (Vaux and Keairns, 1980). In the case of bubbling fluidized beds, sources of particle attrition were identified as grid jets attrition, gas bubbles and cyclones. Bemrose and Bridgwater (1987) stated that particle attrition is affected by a great many variables, mostly influenced by particle and fluidized beds properties. Gwyn (1969) reported that both the average particle size and the spread of the initial particle size distribution affect the attrition rate. Formal researches indicated that the attrition rate is a function of the excess gas velocity $(u_g - u_{mf})$ (Merrick and Highely, 1974; Lin et al., 1980; Sishtla et al., 1989). On the contrary, Patel et al. (1986) stated that the attrition rate is proportional to the fluidization velocity rather than the excess velocity $(u_g - u_{mf})$, because attrition occurs mainly in the high velocity regions close to the distributor, where it is caused by the gas jets issuing from the distributor orifices.
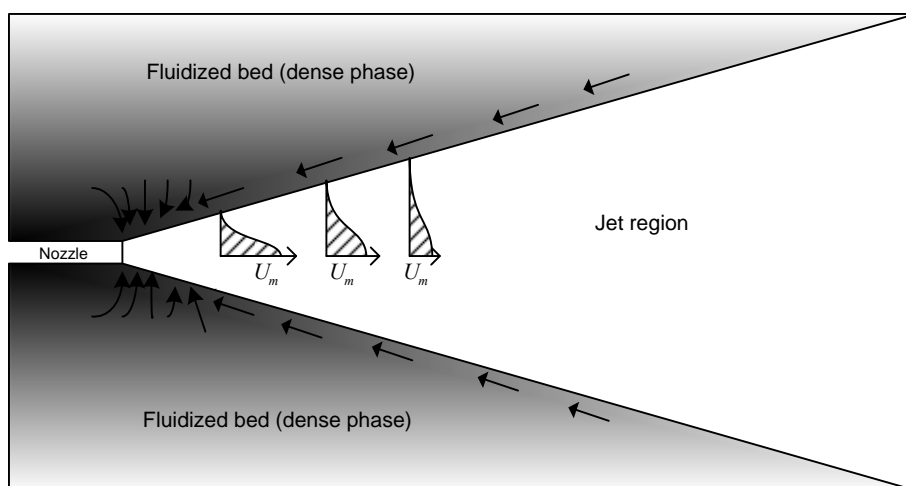
Figure 4.1 Solid entrainment track in the injection region (adapted from Merry, 1971)

A number of studies have been performed to focus on the jet-induced particle attrition in fluidized bed, using subsonic jets. Behie et al. (1971) concluded that the radial distribution of axial momentum for vertical air jets in a fluidized bed could be interpreted with the theory of turbulent jet. De Michele et al. (1976) extended the theory of turbulent

flow jet to the gas injection in fluidized beds, to describe the axial profiles for gas velocity and gas temperature. Donadono et al. (1980) propose that the SCHLICHING's and SCHLICHTING-TAYLOR's correlations can be used to describe the radial gas profile, particle velocity profile, and radial temperature profile. Merry (1971) suggested a scheme of the particle tracks in the vicinity of the jet, shown in Figure 4.1, with the majority of entrainment occurring near the nozzle tip in the potential core region. Bentham et al. (2004) further described that the breakage mechanism of subsonic jets involves the entrainment of particles from the dense phase region into the jet cavity area, where particles are accelerated by the high velocity gas and collide with each other as well as impact on the dense phase on the top of jet. Werther and Xi (1993) found that high-velocity gas jets produce high attrition rates and the attrition rate is proportional to $\rho_0 d_0^2 u_0^3$ (jet gas density, orifice diameter, and jet exit velocity respectively). Ghadiri et al. (1992, 1994) confirmed that the attrition rate is proportional to the orifice velocity raised the power up to 5. Table 4.1 lists the correlations of attrition rate for subsonic horizontal jets:

Table 4.1 Correlations to predict particle attrition rate with subsonic jets

Model equation	Operating conditions	Authors
$R = C \cdot S \cdot \dfrac{\rho_0 Q (\beta u_0)^2}{W d_p \rho_p}$ (4.1)	u_0 = 25-300 m/s, 142-274μm iron ore, 3940kg/m³; lignite char, 1250 kg/m³	Chen et al., 1980
$R = C \rho_0 d_0^2 u_0^3$ (4.2)	u_0 =25-100 m/s; FCC: 106μm, 1500 kg/m³; catalyst HA-HPV: 125 μm, 650 kg/m³.	Werther and Xi, 1993
$R = C d_0^n u_0^m$ (4.3) n: 0.6-0.76 for FCC; 0.44-1.11 for NaCl m: 3.31 for FCC; 5.1 for NaCl	u_0 =25-125 m/s; FCC: 425-600 μm NaCl: 90-106 μm	Ghadiri et al., 1994
$R = C (u_0 \sqrt{\rho_0})^{2.5} \dfrac{\pi d_0^2}{4}$ (4.4)	u_0 =33-303 m/s, Silica-Alumina FCC Catalyst	Zenz and Kelleher, 1980

McMillan et al. (2007a) studied the performance of supersonic jets in particle attrition process. They proposed a new criterion for characterizing particle attrition, and defined a grinding efficiency, which was defined as the amount of new surface area produced per unit mass of attrition gas used. Based on experimental results with supersonic jets, an empirical correlation was developed to predict the grinding efficiency of solids (McMillan et al., 2007a):

$$\eta = 7.81 \times 10^{-7} \alpha \beta d_0^{1.131} u_o^{0.55} (\rho_0 u_o^2)^{1.635} \left(\frac{u_g - u_{mf}}{u_{mf}} \right)^{0.494} \tag{4.5}$$

where α and β are coefficients that depend on particles properties and nozzle geometry, respectively.

According to another study of McMillan et al. (2007b), the high velocity gas jet issuing from an attrition nozzle entrains bed particles and accelerates them to a high speed; due to their inertia, these particles slam on slow moving bed particles near the jet tip, causing breakage and reducing the particle size. Typically, convergent-divergent nozzles are more efficient than regular nozzles, i.e. they require less steam to achieve the same attrition rate (McMillan et al., 2007a). A study by Li et al. (2010a) has demonstrated that the entrainment efficiency is affected significantly by gas jet properties. Operation of supersonic jets in beds with smaller nozzles, at lower nozzle gas flowrates, and a low nozzle gas density would contribute to increasing entrainment efficiency of particles through jets.

Earlier studies have revealed that the operating temperature has a significant influence on the particle attrition in fluidized beds, because it affects material strength, Young' modulus of the solid, and thermal diffusivity of the gas with temperature. Arena et al. (1983) suggested that bed temperature affects directly the mechanism of generation of carbon fines. With the study of the effect of thermal shock, Vaux and Keairns (1980) suggested that the particle attrition rate increased with increasing temperature difference between the particles and the surrounding gas. Lin and Wei (2005) reported that the attrition rate increases with increasing temperature, decreases with particle size, and increases with fluidization velocity. Chirone et al. (1985) and Lee et al. (2002) claimed that a higher temperature causes a higher inner pressure and a higher thermal stress, resulting in enhanced particle fragmentation. So far, most of these studies on jet attrition

in fluidized beds have used subsonic nozzles or have been conducted at ambient temperature. Therefore, the objective of the present research is to study the particle attrition with supersonic convergent-divergent nozzles in a fluidized bed at high temperature.

4.3 **Experimental setup**

Attrition experiments were carried out in a hot fluidized bed with a height of 1.23 m and a rectangular cross-section of 0.10 m × 0.50 m (Figure 4.2). The bed particles were typically heated up to 500°C with an in-bed electrical heater. Attrition gases, such as helium, nitrogen, carbon dioxide, or mixtures of these gases, were injected into the hot fluidized bed via a convergent-divergent attrition nozzle located on the sidewall of the fluidized bed at a distance of 0.127m above the gas distributor. Two different types of particles were used in the experiments: silica sand and petroleum coke (Table 4.2). The operating temperature was varied from ambient temperature to 500°C, while the cold gas pressure upstream of the supersonic nozzle ranged from 689kPa to 2068kPa. Two screw sampling ports were designed and located at two different positions under the bed height, as a result particle samples can be taken while the bed is still running. Three cyclones in series are used to collect all fines carried over in the attrition process.
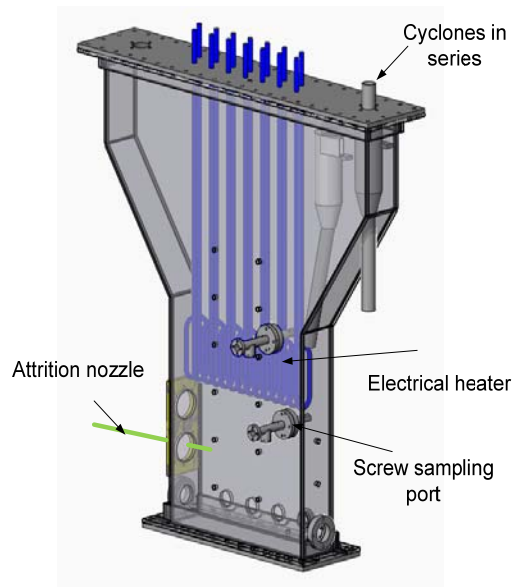
Figure 4.2 Schematic diagram of the hot fluidized bed

Table 4.2 Material and properties

Name	Particle Density (kg/m³)	Sauter diameter d_{psm} (μm)
Silica Sand	2650	209
Petroleum coke	1400	115

Typically, in convergent-divergent attrition nozzles, the fluid reaches sonic velocity at the throat, and supersonic velocity is obtained in the divergent channel (Smith, 2005). In order to focus on the influence of nozzle scale on particle attrition, only one nozzle geometry with Mach number of 2.5 was chosen in attrition tests, as shown in Fig. 4.3.

Figure 4.3 A kind of convergent-divergent Nozzle used in the experiments.

For each run, a specific quantity of material, silica sand or coke, was introduced in to the bed to provide the required bed height. The bed was then heated to the specified temperature, with a low superficial velocity, just above the minimum superficial velocity. Once the attrition temperature had been reached, the fluidization velocity was set to the required excess velocity (e.g. u_g-u_{mf}= 0.20m/s) for 15 minutes before the start of attrition process. High pressure gas supplied by cylinders was injected horizontally into the bed through the attrition nozzle for specified attrition duration. During each attrition run, bed particle samples were taken from the bed through screw sampling ports and fines samples were collected from cyclones at regular intervals. Before each sampling, the bed was mixed and elutriated at a fluidization superficial gas velocity of 0.30 m/s to 0.50 m/s for 15 minutes. The aim of the elutriation is to eliminate small particles from the bed, to ensure that fines observed after attrition could only have come from particle breakage. Preliminary study has demonstrated there is no significant attrition occurred during high velocity elutriation. After sampling, the laser diffraction sensor HELOS of Sympatec was used in analysis of particle size distribution. The laser diffraction of particles could be depicted by Mie or Fraunhofer theory. In order to assess the extent of particle attrition, the grinding efficiency was used in the study, which was defined as the amount of new surface area created per unit mass of attrition gas used (McMillan et al., 2007a). The

calculation of grinding efficiency was determined from the bed particle and cyclone fines samples.

$$\eta(m^2/kg) = \frac{a_{bed}^f + a_{fines}^f - a_{bed}^i}{m_{attr}}$$
(4.6)

where:

a_{bed}^f = Surface area of bed particles after attrition (m^2);

a_{fines}^f = Surface area of cyclone fines after attrition (m^2);

a_{bed}^i = Surface area of bed particles before attrition (m^2)

m_{attr} = Mass of attrition gas (kg/s)

4.4 Results and discussion

4.4.1 Influence of bed properties on grinding efficiency at high temperature

4.4.1.1 Fluidized bed properties at high temperature

Most fluidization studies that have been published in the open literature were carried out at ambient temperature, although most of the industrial applications are at high temperature. Figure 4.4 shows that the voidage of bed, at a constant excess fluidization gas velocity, varied with the temperature. Figure 4.5 indicates the change of the minimum fluidization velocity varying temperatures, which further confirms that the current empirical equations such as Wen & Yu, Leva, and Richardson overpredicted the minimum fluidization velocity at high temperature, as first reported by Wu and Baeyens (1991). The decrease in bed voidage with temperature, with excess gas velocity, confirms previous observations that the emulsion phase voidage decreases with increasing temperature (Cui et al., 2003; Llop et al., 2000; Geldart and Kapoor, 1976; and Stubington et al., 1984).

u_g=0.15m/s, petroleum coke, d_{psm}=120um
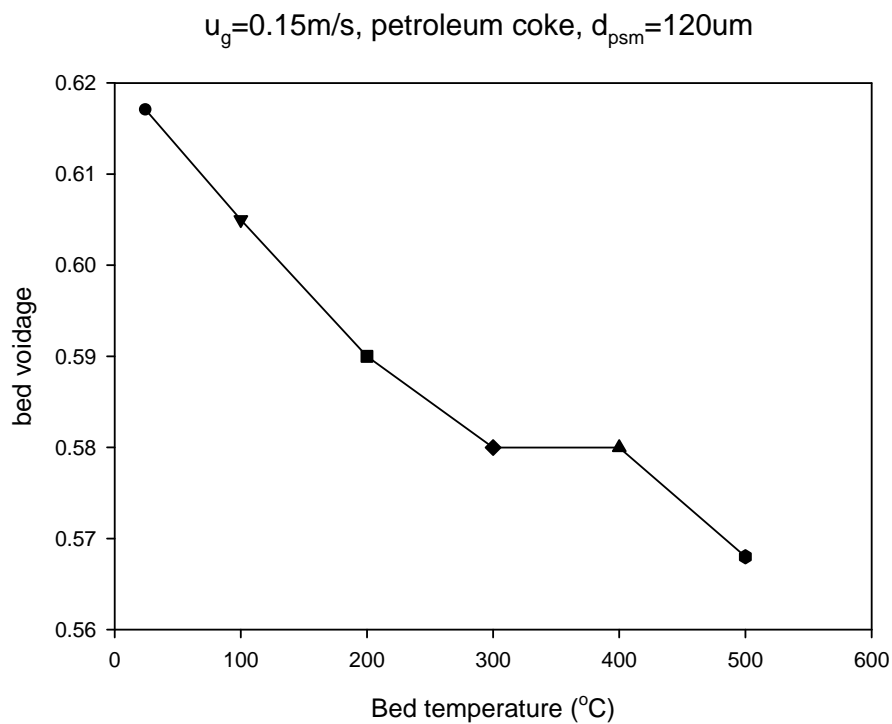
Figure 4.4 Influence of temperature on bed voidage (V_g=0.15m/s, petroleum coke, d_{psm}=120μm, M_{bed}=21kg)

M_{bed}=21kg Petroleum coke, d_{psm}=120um

predicted by Wen & Yu correlation
predicted with Leva correlation
predicted with Richardson correlation
experimental data
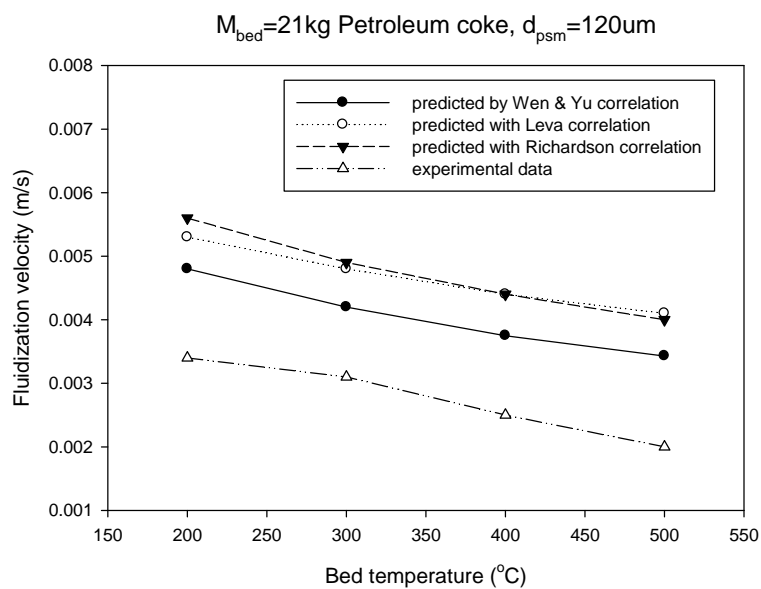
Figure 4.5 Comparison of measured and predicted value of minimum fluidization velocity of petroleum coke

4.4.1.2   Effect of gas superficial velocity on the grinding efficiency

Both Fig. 4.6 and Fig. 4.7 illustrate that the grinding efficiency increases with gas superficial velocity. It was originally suspected that increasing the superficial gas velocity would increase the solid entrainment into the attrition jet cavity, but Li et al. (2010a) found that the superficial gas velocity has little effect on the solids entrainment rate into a supersonic nozzle, as was also reported by Briens et al. (2008). The explanation might be that the bed acts as an effective classifier at higher fluidization velocity, with elutriation at high velocity removing small particles before they can be ground further: eliminating the fines from the bed, which are harder to grind, would increase the average grinding efficiency.
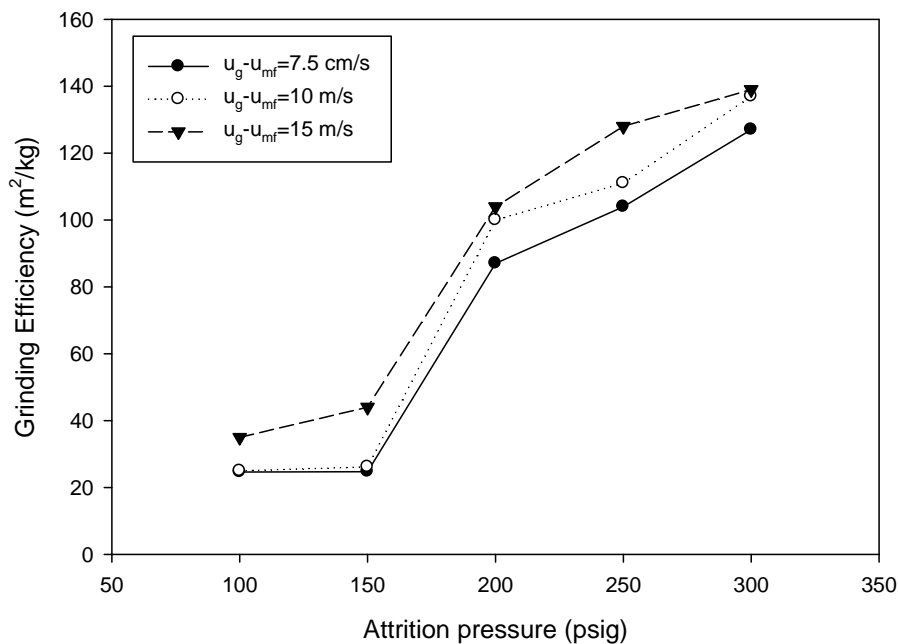
Figure 4.6 Influence of attrition pressure on grinding efficiency at different excess fluidization velocity (Mbed=27kg, Silica sand, ambient temperature)
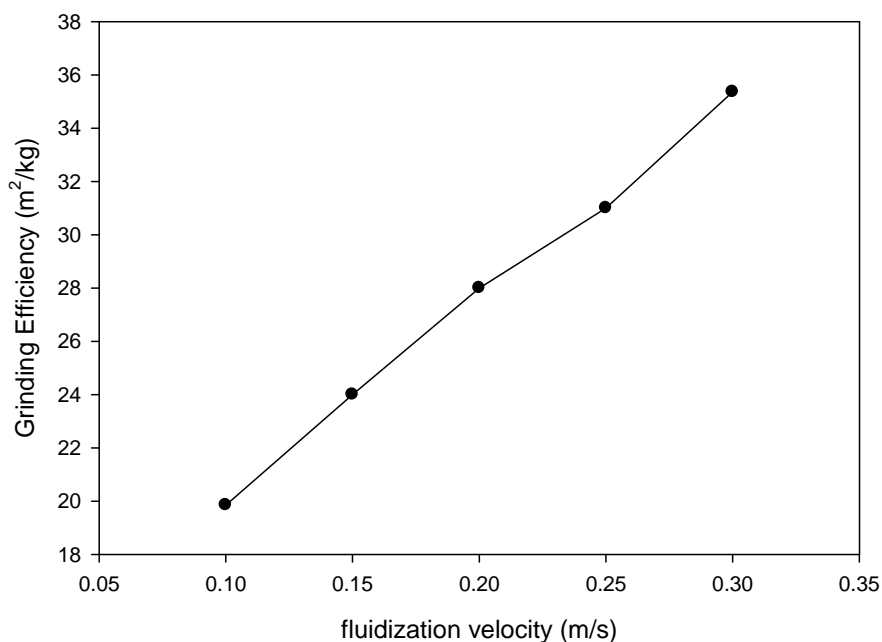
Figure 4.7 Influence of fluidization velocity on grinding efficiency (M_{bed}=21kg, petroleum coke, T_{bed}=300°C, 200psi attrition pressure)

4.4.1.3   Effect of bed mass on the grinding efficiency

To determine the effect of bed mass on the grinding efficiency, experiments were conducted with various bed masses. Fig. 4.8 and Fig. 4.9 show that the grinding efficiency increases with the bed mass, for both silica sand and petroleum coke. The influence of bed mass on the grinding efficiency is small but not negligible in this study, although former studies stated that the particle mass has been shown to have little effect on the horizontal jet induced particle attrition. The effect of bed mass in this study probably is because fresh particles usually have an initial period of rapid attrition before the attrition pace slows down to a certain steady level. Ray and Jiang (1987) reported the similar phenomenon in their results. If attrition duration was long enough, as seen in Fig. 4.10, the grinding efficiency of silica sand reaches to a maximum value at the beginning of attrition and then eventually decreased to a constant value. In contrast, Fig. 4.11 shows

that petroleum coke has a stable grinding efficiency throughout the experiment in a short attrition time.
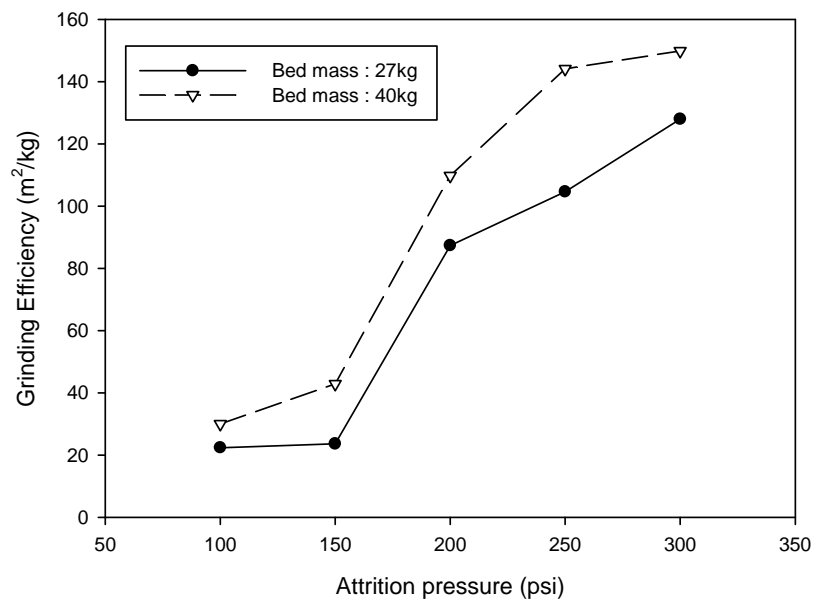
Figure 4.8 Influence of mass of bed on the grinding efficiency with silica sand.
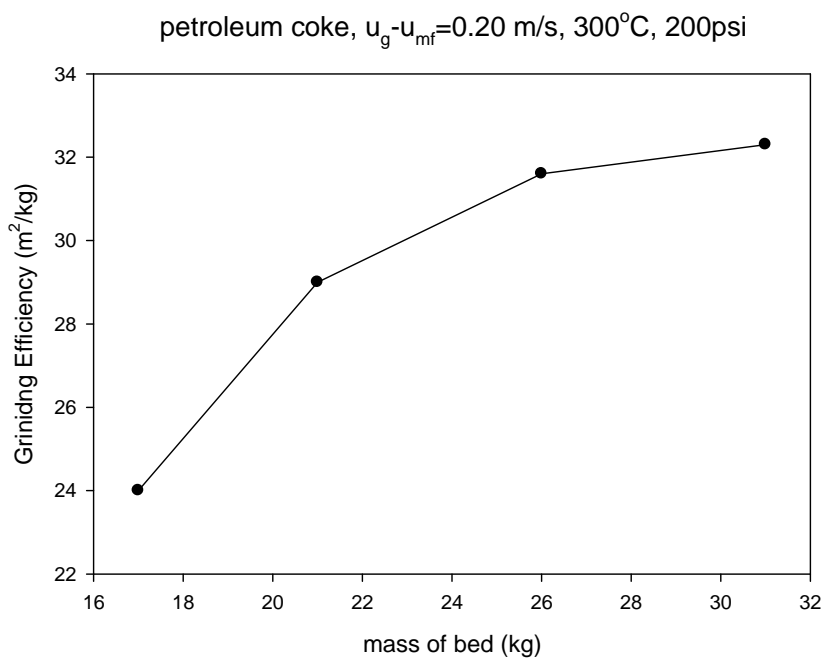
Figure 4.9 Influence of bed mass on the grinding efficiency with petroleum coke.

Silica sands, attrition pressure: 150psi
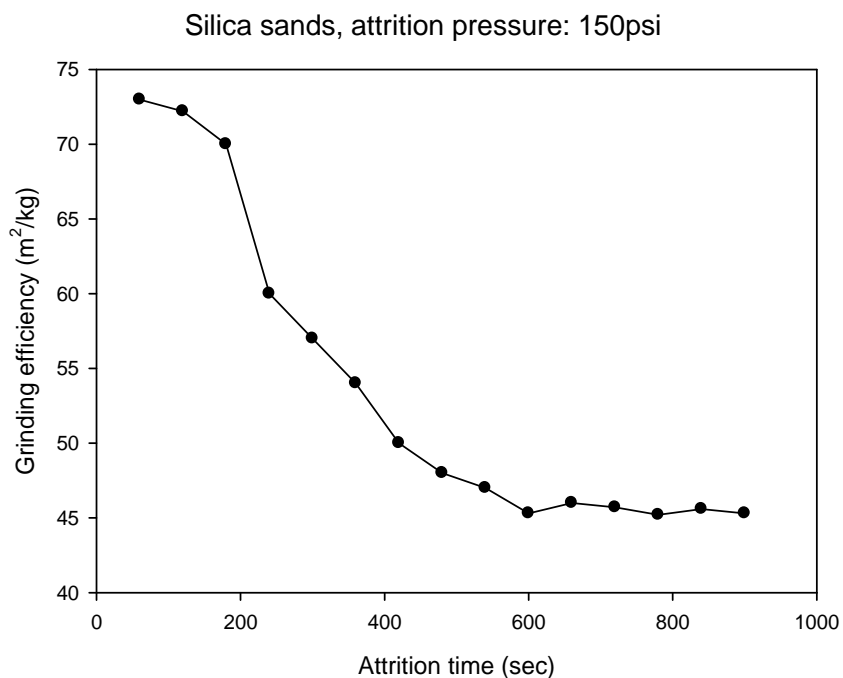
Figure 4.10 Influence of attrition time on grinding efficiency . (silica sand).

Influence of attrition time on grinding efficiency
(Petroleum coke, 300°C, 200psi, U$_g$-U$_{mf}$=0.20m/s)
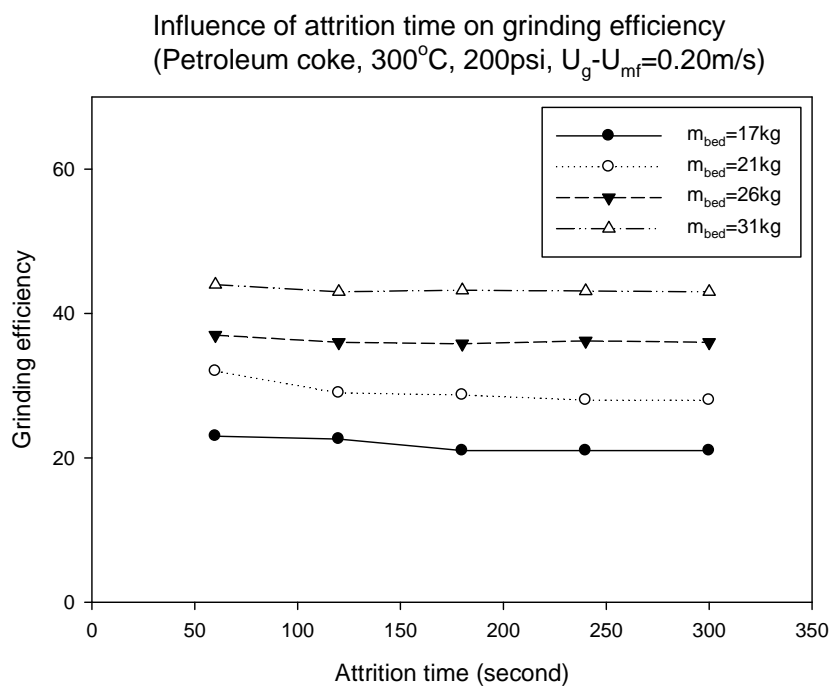
Figure 4.11 Influence of attrition time on grinding efficiency. (petroleum coke).

4.4.2   The effect of high temperature on grinding efficiency

In order to determine the effect of temperature on the grinding efficiency, experiments were carried out with varied attrition temperature in the same operating excess fluidization velocities (u_g-u_{mf}) and bed particle size distribution. Results shown in Fig. 4.12 and Fig. 4.13, the maximum efficiency was obtained at the highest bed temperature with both silica sand and petroleum coke. The experimental data demonstrate clearly that the grinding efficiency increases with increasing temperature. One explanation is that higher temperature increases the thermal stress to which the particles are subjected when contacting the cold injection gas, resulting in higher breakage rates. Lee et al. (2002) studied the phenomenon of coal fragmentation in a fluidized bed reactor, and reported a similar effect of the temperature. A number of researchers have worked on studies of the mechanism of particle breakage in a fluidized jet bed. Ghadiri and Zhang (2002) developed a mechanistic model of impact attrition of particulate solids, where the fragmentation is the dominant role in the particle breakage process.   The Ghadiri breakage model is related to the material properties and impact conditions. The breakage frequency f, the fraction of particles to breakage per unit time, is defined as (Moreno-Atanasio and Ghadiri, 2006):

$$f = \frac{\rho_p E^{2/3}}{\Gamma^{5/3}} v^2 d_p^{\,5/3} \tag{4.7}$$

where ρ_p is the particle density, E is the Young's modulus of the granule, Γ is the interface energy, v is the impact velocity, and d_p is the particle diameter prior to breaking. Emmerich (1994) pointed out the Young's modulus of petroleum coke (a graphitizable carbon) increases with increasing temperature, and the maximum of the modulus of petroleum coke is at a temperature of about $1200^{\circ}C$. Γ is the interface energy, which equals 2 times the surface energy (γ) (Israelachvili, 1991). The surface energy of a particle decreases dramatically with increasing temperature and particle diameter (Wiederhorn, 1969; Bikeman, 1978). Since $E^{2/3}/\Gamma^{5/3}$ increases with increasing temperature while the values of particle density, impact velocity, and particle diameter are independent of the operation temperature, a high attrition temperature therefore would promote particle attrition in fluidized beds.

Additionally, it is interesting that high temperature attrition produced coarser particles than low temperature attrition when petroleum coke was used as the bed material, as seen in Fig. 4.14. In contrast to petroleum coke, silica sand created more fines particles with high temperature attrition compared to the attrition at low temperature, as shown in Fig. 4.15.
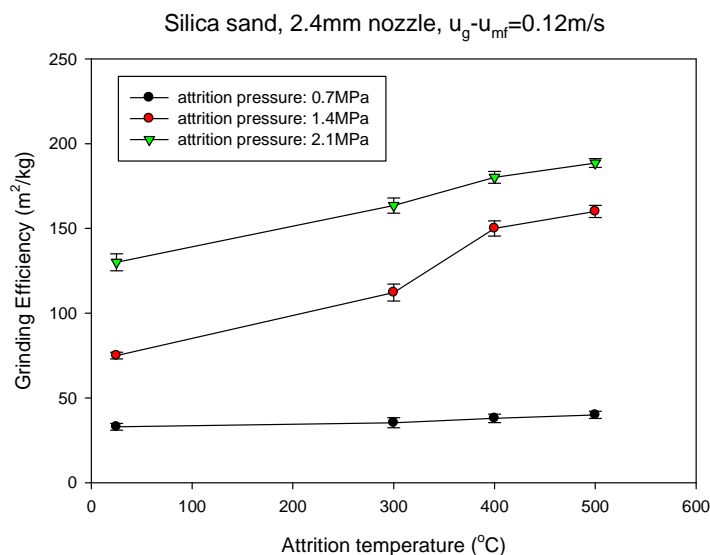
Figure 4.12 Influence of attrition Temperature on attrition rate at various pressures (W_{bed}=30kg, U_g-U_{mf}=0.12m/s, silica sand, air).
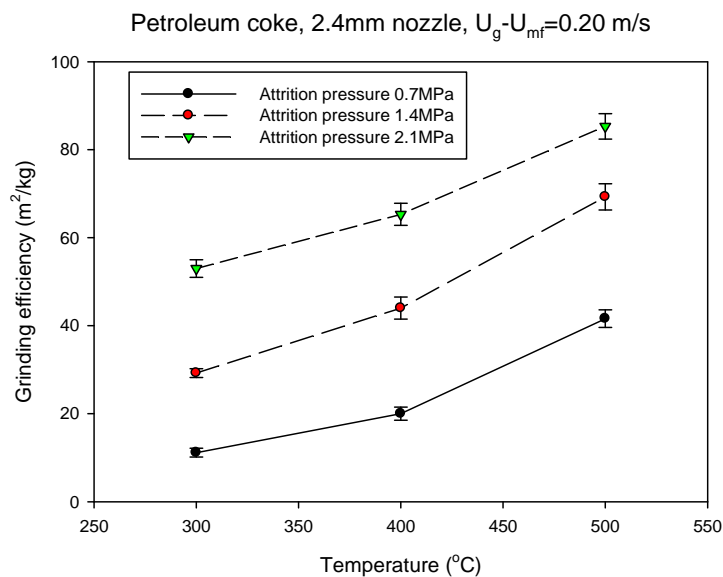
Figure 4.13 Influence of operation temperature on the grinding efficiency at various pressures (Wbed=21kg, Ug-Umf=0.20m/s, petroleum coke, Nitrogen gas).

Petroleum coke, 1.4MPa attrition pressure, u_g-u_{mf}=0.20 m/s
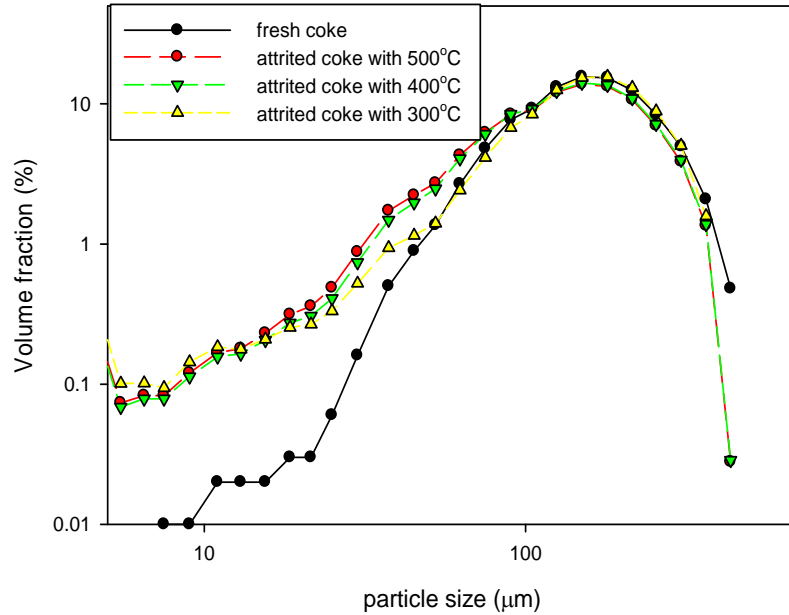
Figure 4.14 Particle size distribution of petroleum coke attrited at various operating temperatures.

Silica sand, 2.4mm nozzle, u_g-u_{mf}=0.12 m/s, P_{att}= 1.4MPa
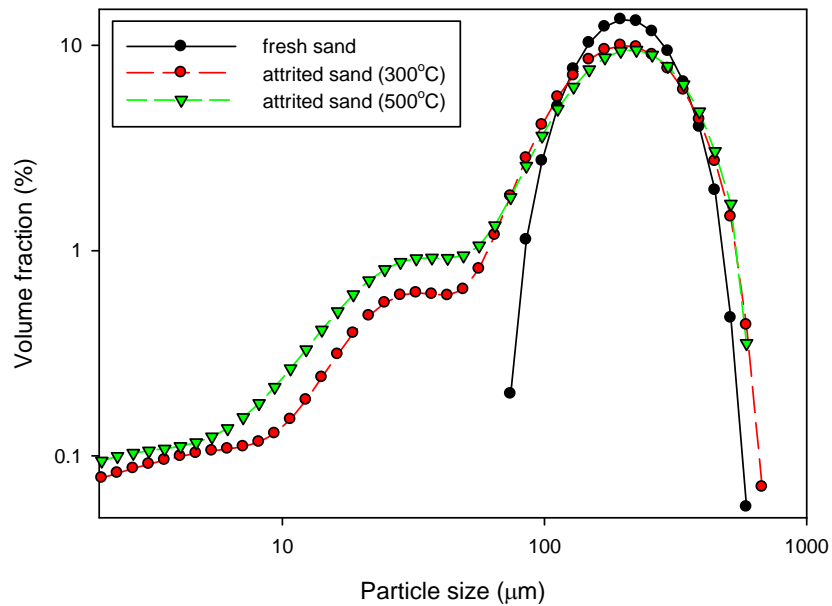
Figure 4.15 Particle size distribution of silica sand attrited at various operating temperatures.

4.4.3 The influences of properties of attrition gas on the grinding efficiency

4.4.3.1 The effect of attrition gas flowrate on the grinding efficiency

As shown in Fig. 4.16 and Fig. 4.17, the influences of attrition gas pressure and flowrate on the jet attrition were investigated. It can be seen that the grinding efficiency increases with increasing attrition gas pressure. For a specific convergent-divergent nozzle operating in the supersonic regime, the gas mass flowrate through the nozzle is proportional to the static pressure. Therefore, as seen in Fig. 4.17, increasing the flowrate of attrition gas through the supersonic nozzle improves the grinding efficiency at various temperatures. The results illustrated in Figure 4.18 further show the influence of nozzle scale on the grinding efficiency. Larger scale nozzles operating at larger gas flowrates resulted in significantly higher grinding efficiencies, as previously reported by McMillan et al. (2007a).
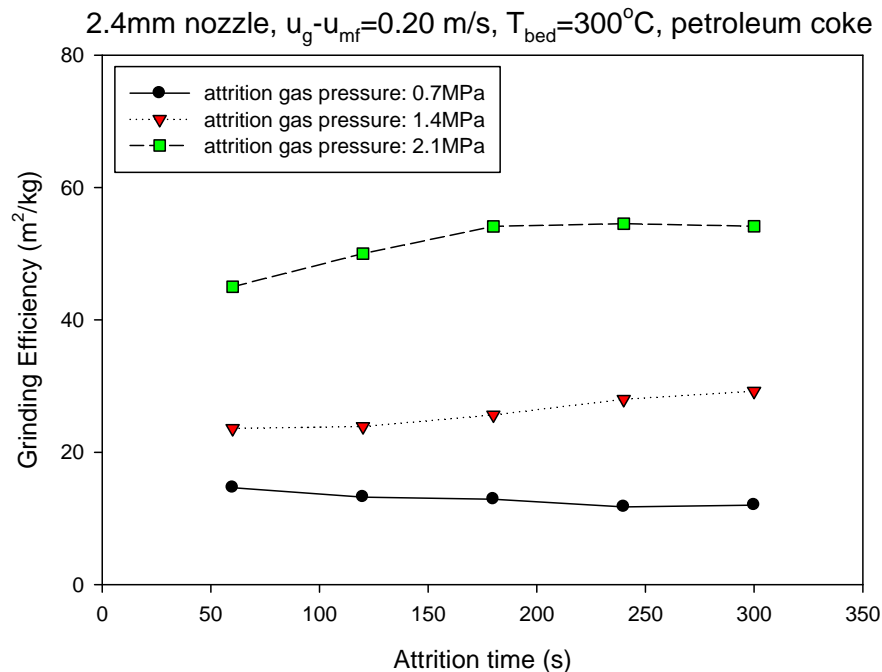
Figure 4.16 influence of attrition pressure on grinding efficiency (petroleum coke, air, 2.4mm nozzle, u_g-u_{mf}=0.20m/s).

Petroleum coke, N$_2$, 2.4mm nozzle, U$_g$-U$_{mf}$=0.20m/s
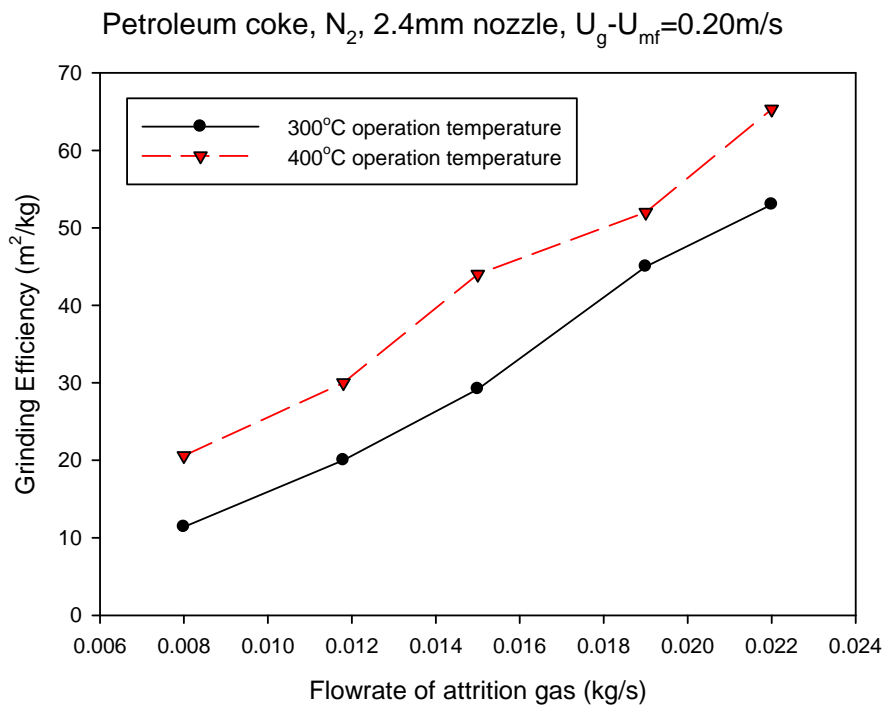
Figure 4.17 influence of flowrate of attrition gas on the grinding efficiency (petroleum coke, 2.4mm nozzle, u$_g$-u$_{mf}$=0.20m/s)

petroleum coke, Air, u$_g$-u$_{mf}$=0.20m/s, P$_{attr}$=2.1MPa
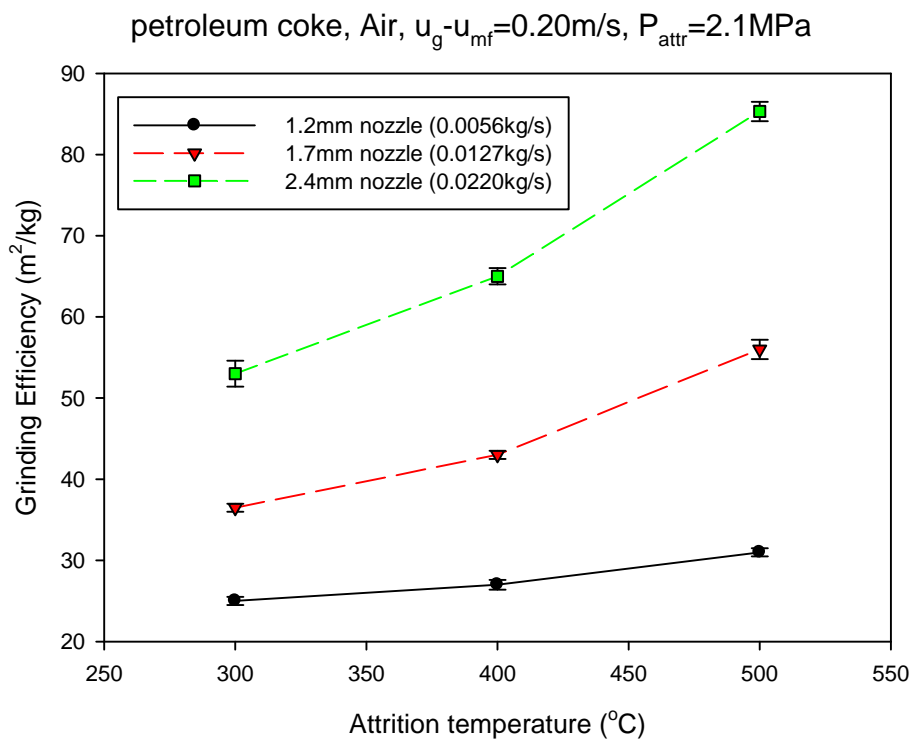
Figure 4.18 Influence of nozzle scale on the grinding efficiency (petroleum coke, U$_g$-U$_{mf}$=0.20m/s, P$_{attr}$=2.1MPa)

4.4.4 The effects of attrition gas temperature and density on grinding efficiency

The properties of attrition gas also acts in an important role in jet-induced particle attrition. More attrition experiments were carried out to inspect the influences of attrition gas properties. As shown in Figures 4.19 and 4.20, it can be seen clearly that increasing the temperature of the attrition gas or reducing its molecular weight enhances the grinding efficiency.
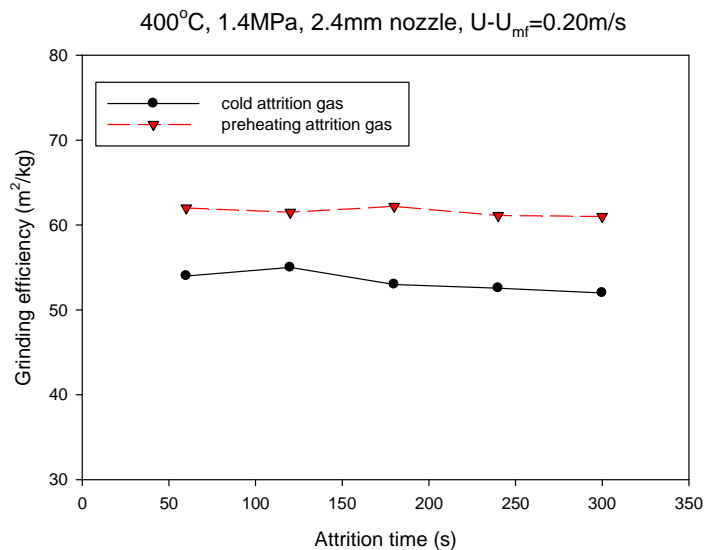
Figure 4.19 influence of attrition gas temperature on particle grinding efficiency (petroleum coke)
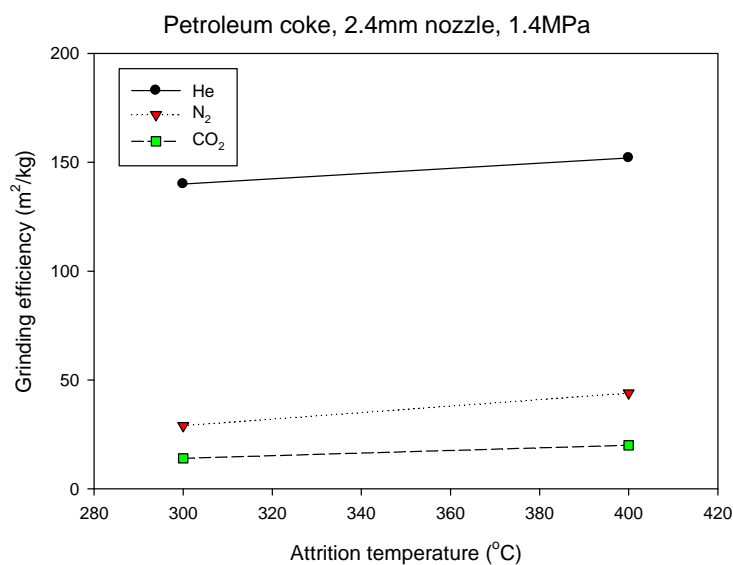
Figure 4.20 influence of gas molecular weight on the grinding efficiency.

In convergent-divergent nozzles, the fluid reaches sonic velocity at the throat, and supersonic velocity is obtained in the divergent section (Smith, 2005). The cross-sectional area, pressure and temperature vary with Mach number along the converging-diverging flow path according to (Liepmann, 1957, and Perry, 2008):

$$\frac{A_e}{A^*} = \frac{1}{M}\left[\frac{2}{\gamma+1}\left(1+\frac{\gamma-1}{2}M^2\right)\right]^{(\gamma+1)/2(\gamma-1)} \tag{4.8}$$

$$\frac{p_0}{p_e} = \left[1+\frac{\gamma-1}{2}M^2\right]^{\gamma/(\gamma-1)} \tag{4.9}$$

$$\frac{T_0}{T_e} = 1+\frac{\gamma-1}{2}M^2 \tag{4.10}$$

The sonic mass flux through the throat is given by:

$$G = p_0\sqrt{\left(\frac{2}{\gamma+1}\right)^{(\gamma+1)/(\gamma-1)}\left(\frac{\gamma M_w}{RT_0}\right)}(kg/m^2\cdot s) \tag{4.11}$$

If A is set equal to the nozzle exit area, the exit Mach number, pressure, and temperature may be calculated. The relation between gas temperature and exit velocity can be obtained through the Mach number, as shown in Fig. 4.21. The exit velocity of the attrition gas at the nozzle tip increases with increasing gas temperature and decreasing gas molar mass.

Li et al. (2010b) developed an empirical correlation to predict the penetration length of jets issuing from a horizontal sonic nozzle into a fluidized bed of petroleum coke at high temperature:

$$L_j = 0.11\frac{1}{(\rho_p-\rho_g)^{0.540}}\left(\rho_0 U_0^2\right)^{0.540} d_0^{0.460} \tag{4.12}$$

The jet penetration length increases with increasing nozzle exit velocity as well as with nozzle size. The grinding efficiency increases with increasing jet penetration length because of the greater probability for particle-particle collision due to the larger jet boundary area. On the other hand, the term $\rho_0 U_0^2$ could be related to the energy input, which to some degree is proportional to the impact energy near the jet cavity. Consequently, it is reasonable to expect that larger scale nozzles with a high gas flowrate,

operating at high attrition gas temperature with lower molar mass gas would show a greater grinding efficiency.
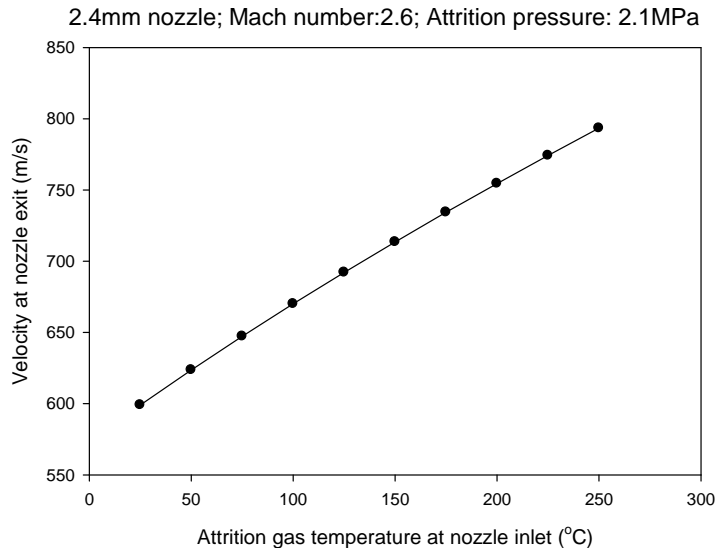
Figure 4.21 the relationship between temperature of attrition gas and gas velocity at nozzle exit

4.4.5 The breakage mechanism of particle attrition at high temperature

Two breakage modes have been proposed for particle attrition in fluidized beds: fragmentation and surface abrasion. Abrasion of the particles surface produces significant amounts of elutriated fines, while fragmentation yields similarly sized pieces. Pis et al. (1991) proposed that the two attrition modes have different effects on the particle size distribution. As shown in Fig. 4.22, the particle size distribution of parent particles changes slightly after abrasion, while very small fines are produced. On the other hand, fragmentation produces daughter particles with a broader particle size distribution and smaller mean diameter compared to their parent particles, and no fines are generated.

To determine the breakage modes in this study, the attrition experiments were carried out with the same excess fluidization velocity and varying operating temperature. Fig. 4.23 and Fig. 4.24 show the particle size distributions obtained in these attrition experiments, which indicates clearly that the particle fragmentation mechanism predominated. Note that the measurements were performed after a small fraction of the bed particles were

attrited, which means that only a small fraction of attrited particles were exposed to the attrition jet more than once.

In order to further study the attrition mode at high temperature, scanning electron microscope (SEM) was used. In Figure 4.25, four SEM images represent the particle sizes and shapes at different attrition stages. Before attrition, the fresh coke particles had a smooth shape (Fig. 4.25a); in contrast, some attrited coke particles have sharp corners and edges (Fig 4.25c). A typical crack caused by jet attrition is shown in Fig.4.25d. The experimental results suggest fragmentation is a dominant fact in particle attrition by convergent-divergent nozzles in a fluidized bed at high temperature.
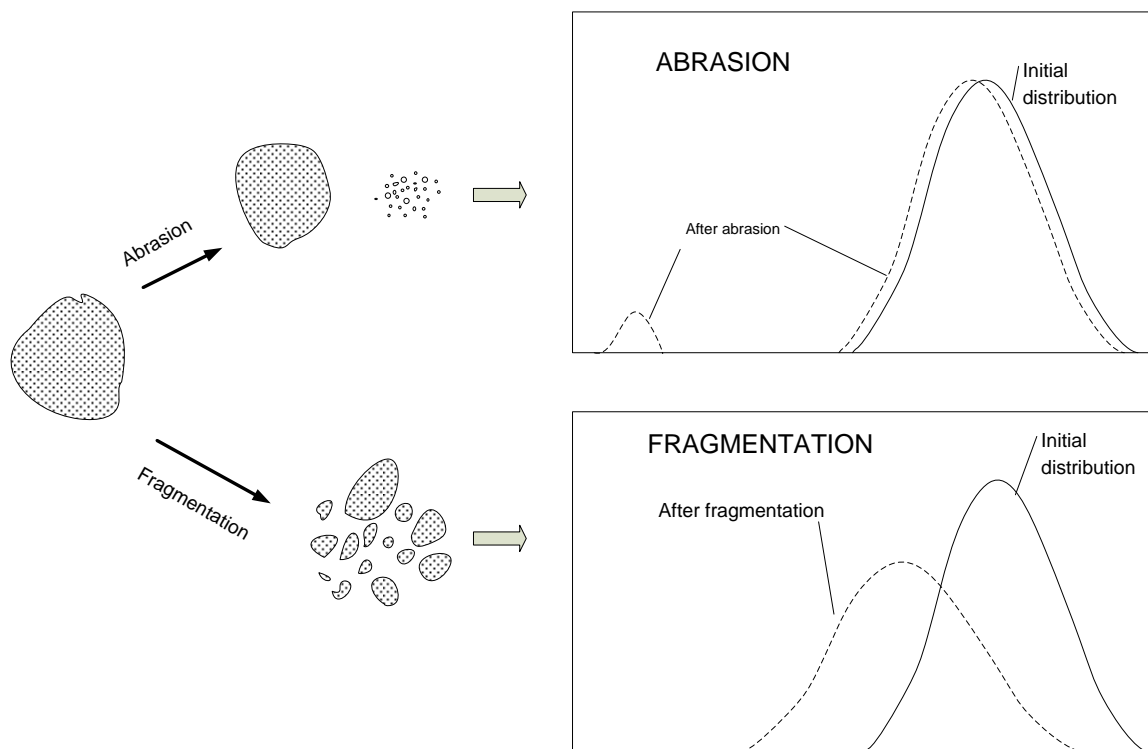
Figure 4.22 Attrition modes and the effects on the particle size distribution (retrieved from Pis et al., 1991)
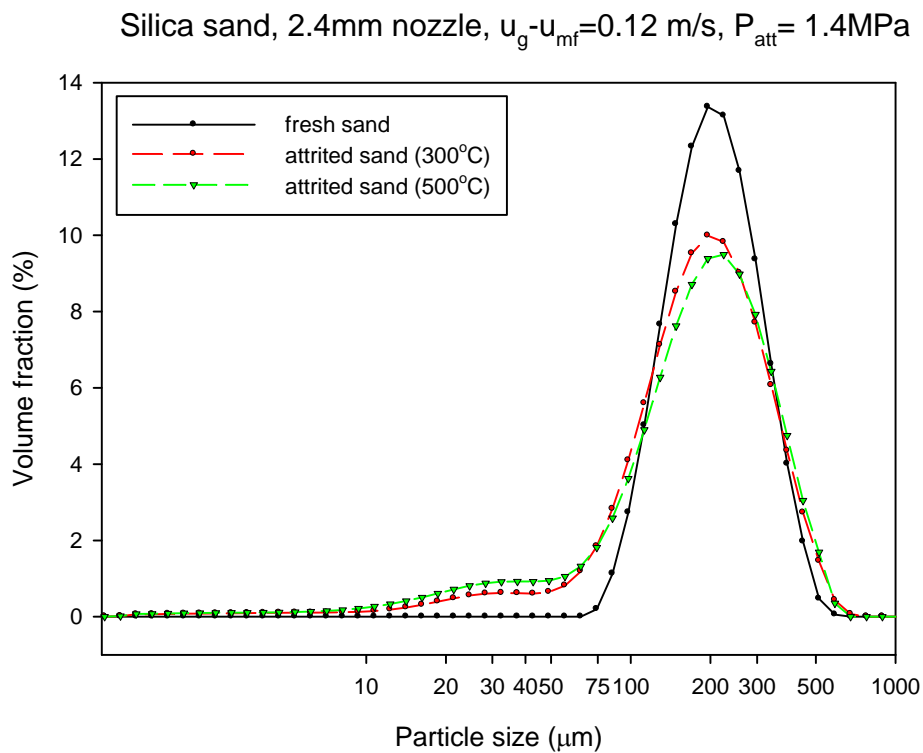
Figure 4.23 Particle size distributions of silica sand with attrition processes at various temperature
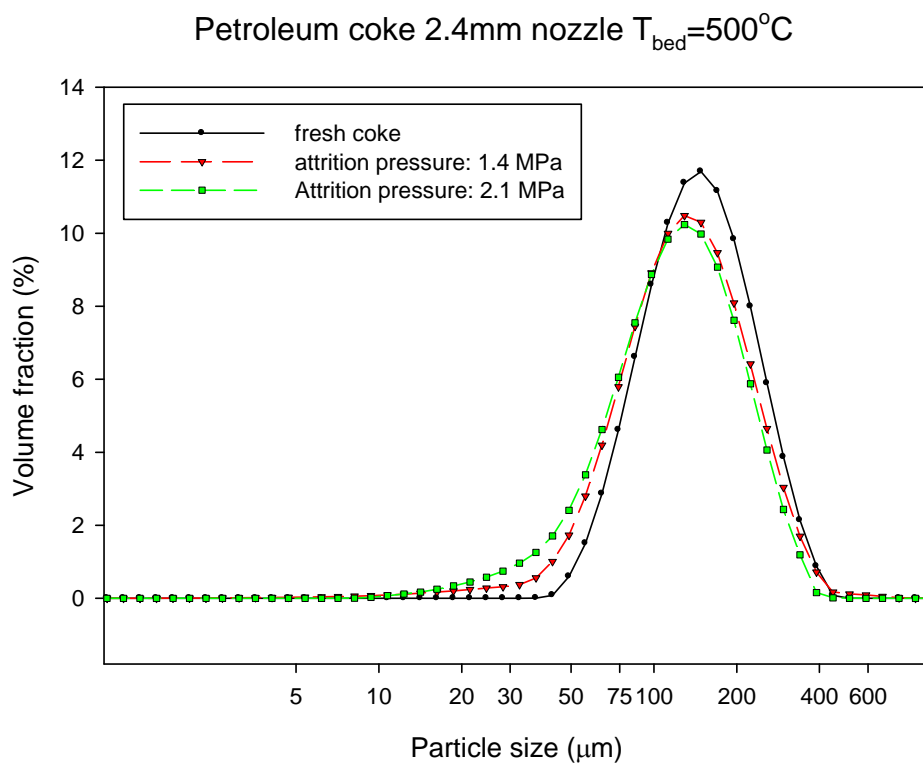
Figure 4.24 Particle size distributions of petroleum coke with attrition processes at various pressure

(a)SEM image of petroleum coke particles before attrition (90 times magnification)

(b)SEM image of Petroleum coke after 3 min attrition (90 times magnification)

(c)SEM image of Petroleum coke after 3 min attrition (150 times magnification)

(d)SEM image of a crack at one attrited coke particle(1000 times magnification)
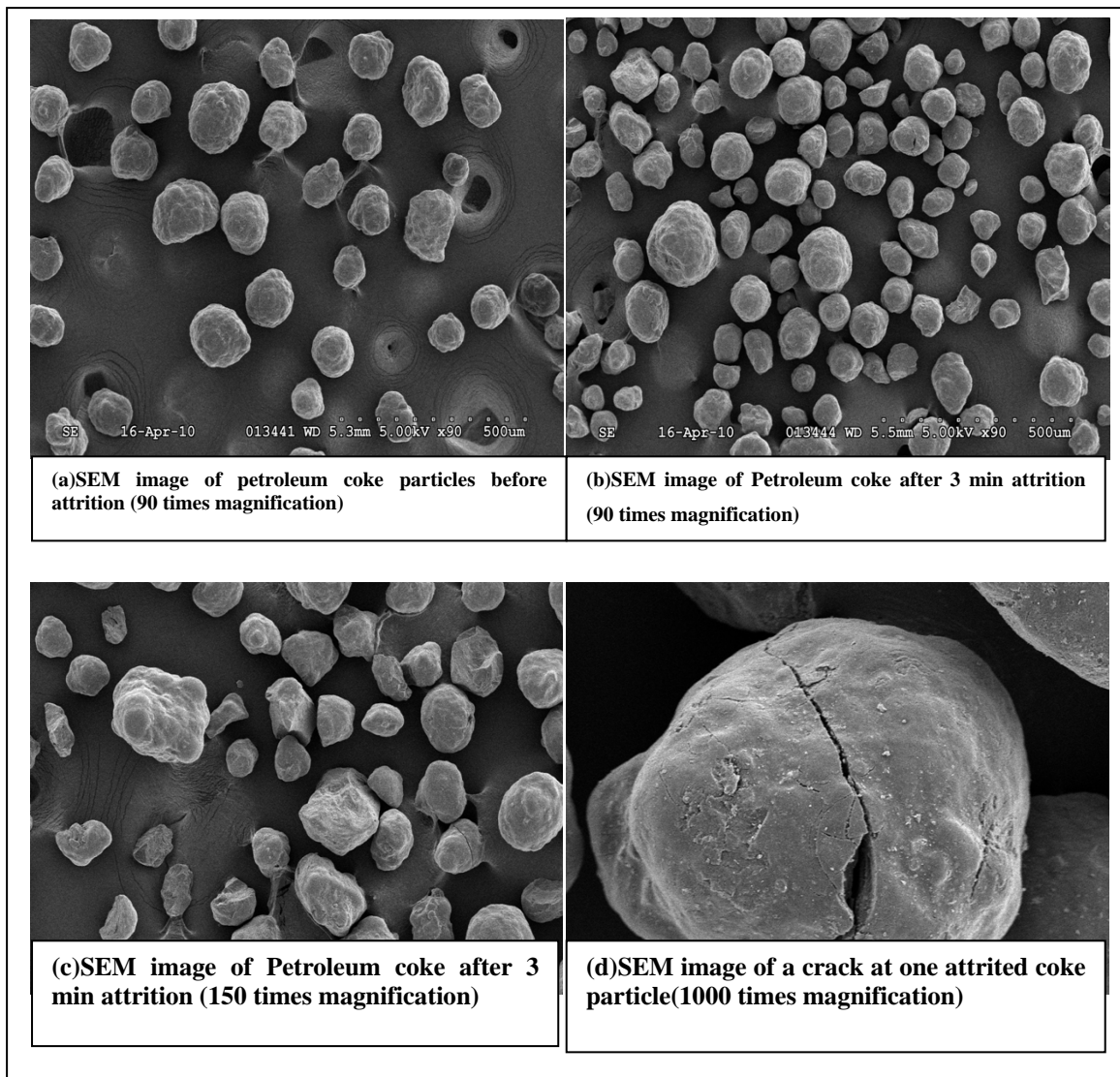
Figure 4.25 SEM images of particles before and after the attrition process

4.5 Conclusion

To study the particle attrition with attrition nozzles, attrition experiments were conducted with convergent-divergent nozzles in a fluidized bed at high temperature, using various gases, at various operating conditions. The experimental results demonstrate that the grinding efficiency is significantly and positively affected by operation temperatures. The Ghadiri breakage model was used to give an explanation of particle attrition at high temperature. Moreover, attrition gas properties and nozzle sizes also have a considerable impact on the grinding efficiency. Larger scale nozzles with a high gas flowrate,

operating at high attrition gas temperature with lower molar mass gas, contribute to achieving the highest grinding efficiency. The experimental results further suggest that fragmentation is the dominant mechanism in supersonic induced particle attrition at high temperature.

4.6 **Notation**

a_{bed}^i Surface area of bed particles before attrition (m^2)

a_{bed}^f Surface area of bed particles after attrition (m^2)

a_{fine}^f Surface area of cyclone fines after attrition (m^2)

A_e Area of nozzle exit (m^2)

A^* Area of nozzle throat (m^2)

C   Attrition constant (Table 4.1)

d_0 Diameter of nozzle exit (m)

d_p Diameter of particle (m, Eqn.4.1)

E   Young's modulus (Pa, Eqn. 4.7)

f   Breakage frequency

L_{jet} Penetration length of attrition nozzle

G   Mass flux (kg/m^2s)

m Mass (g, kg)

m   Power index (Eq. 4.3)

m_{attr} Mass of attrition gas (kg/s) (Eqn. 4.6)

M   Mach number

M_w Molar weight (kg/mol)

n   Power index (Eqn. 4.3)

p_0 Upstream pressure of nozzle   (Pa)

p_e Pressure at nozzle exit (Pa)

p   Pressure (Pa)

Q   Volumetric flow rate at nozzle exit (m^3/s)

R   Ideal gas universal constant

R   Attrition rate (kg/s)

S   Excess surface area per unit mass after attrition (m^2/kg, Eqn. 4.1)

T_0 Absolute temperature at nozzle throat (K)

T_e Absolute temperature at nozzle exit (K)

t   Time (s)

u_0 Gas velocity at nozzle exit (m/s)

u_g Fluidization velocity (m/s)

u_m Gas velocity on jet axis (m/s)

u_{mf} Minimum fluidization velocity (m/s)

v   Impact velocity (m/s, Eqn. 4.7)

W   Residue bed weight (kg, Eqn. 4.1)

Greek letters

α Particle coefficient (Eqn. 4.5)

β Correction factor (Eqn. 4.1)

β Geometry coefficient of nozzle (Eqn.4.5)

ε Volume fraction

Γ Interface energy (Eqn. 4.7)

$\rho*$ Gas density at nozzle throat (kg/m^3)

ρ_g Density of fluidization gas (kg/m^3)

ρ_0 Gas density at nozzle exit (kg/m^3)

ρ_p Particle density (kg/m^3)

γ Ratio of specific heat c_p/c_v (dimensionless)

η Grinding efficiency (m^2/kg)

μ Viscosity (Ns/m^2)

4.7 **References**

Arena, U.; Damore, M.; Massimilla, L., Carbon Attrition During the Fluidized Combustion of a Coal. *Aiche Journal* **1983,** *29* (1), 40-49.

Bemrose, C. R.; Bridgwater, J., A Review of Attrition and Attrition Test Methods. *Powder Technology* **1987,** *49* (2), 97-126.

Bentham, A. C.; Kwan, C. C.; Boerefijn, R.; Ghadiri, A., Fluidised-bed jet milling of pharmaceutical powders. *Powder Technology* **2004,** *141* (3), 233-238.

Briens, C.; Berruti, F.; Felli, V.; Chan, E., Solids entrainment into gas, liquid, and gas-liquid spray jets in fluidized beds. *Powder Technology* **2008,** *184* (1), 52-57.

Chen, T.; Sishtla, C.; Punwani, H.; Arastoopour, H., A model for attrition in fluidized beds. In *Fluidization*, Grace, J. R.; Matsen, J., Eds. Engineering Foundation: New York, 1980; p 445.

Chen, Z. X.; Lim, C. J.; Grace, J. R., Study of limestone particle impact attrition. *Chemical Engineering Science* **2007,** *62* (3), 867-877.

Chirone, R. D. a., M.; Massimilia, L.; Mazza, A., Char attrition during the batch fluidized bed combustion of a coal. *AlChE* **1985,** *31* (5), 812-820.

Cui, H. P.; Sauriol, P.; Chaouki, J., High temperature fluidized bed reactor: measurements, hydrodynamics and simulation. *Chemical Engineering Science* **2003,** *58* (3-6), 1071-1077.

De Michele, G.; Elia, A.; Massimilla, L., Interaction between Jets and Fluidized-Beds. *Quaderni Dell Ingegnere Chimico Italiano* **1976,** *12* (6), 155-162.

Emmerich, F. G., Application of a cross-linking model to the Young's modulus of graphitizable and non-graphitizable carbons. *Carbon* **1995,** *33* (1), 47-50.

Geldart, D.; Kapoor, D. S., Bubble Sizes in a Fluidized-Bed at Elevated-Temperatures. *Chemical Engineering Science* **1976,** *31* (9), 842-843.

Ghadiri, M.; Cleaver, J. A. S.; Tuponogov, V. G.; Werther, J., Attrition of FCC powder in the jetting region of a fluidized bed. *Powder Technology* **1994,** *80* (2), 175-178.

Ghadiri, M.; Cleaver, J. A. S.; Yuregir, K. R.; O.E., Y. I., Attrition of sodium chloride crystals in a fluidized bed. In *Fluidization* Potter, O. E.; Nicklin, D. J., Eds. Engineering Foundation: Brisbane, Australia, 1992; Vol. VII, p 603.

Ghadiri, M.; Zhang, Z., Impact attrition of particulate solids. Part 1: A theoretical model of chipping. *Chemical Engineering Science* **2002,** *57* (17), 3659-3669.

Gwyn, J. E., On Particle Size Distribution Function and Attrition of Cracking Catalysts. *Aiche Journal* **1969,** *15* (1), 35-&.

Israelachvili, J. N., *Intermolecular and surface forces*. Second ed.; Academic Press: Toronto, 1991.

Lee, S. H.; Kim, S. D.; Lee, D. H., Particle size reduction of anthracite coals during devolatilization in a thermobalance reactor. *Fuel* **2002,** *81*, 1633-1639.

Li, F.; Briens, C.; Berruti, F.; McMillan, J., Study of solids entrainment into attrition jets in fluidized beds. In *Fluidization XIII*, Kim, S. D.; Kang, Y.; Lee, J. K.; Seo, Y. C., Eds. Engineering Conferences International: Gyeong-ju, Korea, 2010a.

Li, F.; Briens, C.; Berruti, F.; McMillan, J., Penetration of high velocity horizontal gas jets into a fluidized bed at high temperature. In *Fluidization XIII*, Kim, S. D.; Kang, Y.; Lee, J. K.; Seo, Y. C., Eds. Engineering Conferences International: Gyeong-ju, Korea, 2010b; Vol. XIII.

Liepmann, H. W.; Roshko, A., *Elements of Gasdynamics*. John Wiley & Sons: New York, 1957.

Lin, C. L.; Wey, M. Y., Influence of hydrodynamic parameters on particle attrition during fluidization at high temperature. *Korean Journal of Chemical Engineering* **2005,** *22* (1), 154-160.

Lin, L. S., J. T.; Wen, C. Y., Elutriation and Attrition of Char a Large Fluidized Bed. *Powder Technology* **1980,** (27), 105-115.

Llop, M. F.; Casal, J.; Arnaldos, J., Expansion of gas-solid fluidized beds at pressure and high temperature. *Powder Technology* **2000,** *107* (3), 212-225.

McMillan, J.; Briens, C.; Berruti, F.; Chan, E., High velocity attrition nozzles in fluidized beds. *Powder Technology* **2007a,** *175* (3), 133-141.

McMillan, J.; Briens, C.; Berruti, F.; Chan, E., Particle attrition mechanism with a sonic gas jet injected into a fluidized bed. *Chemical Engineering Science* **2007b,** *62* (14), 3809-3820.

Merrick, D. H., J., In *Particle size reduction and elutriation in a fluidized bed process*, AIChE Symp. Ser. , 1974; 1974; pp 366-378.

Merry, J. M. D., Penetration of a Horizontal Gas Jet into a Fluidised Bed. *Transactions of the Institution of Chemical Engineers and the Chemical Engineer* **1971,** *49* (4), 189-&.

Moreno-Atanasio, R.; Ghadiri, M., Mechanistic analysis and computer simulation of impact breakage of agglomerates: Effect of surface energy. *Chemical Engineering Science* **2006,** *61* (8), 2476-2481.

Patel, K.; Nienow, A. W.; Milne, I. P., Attrition of urea in a gas-fluidised bed. *Powder Technology* **1986,** *47* (3), 257-261.

Perry, R. H.; Green, D. W., *Perry's chemical engineering' handbook*. 8th ed.; McGraw-Hill: New York, 2008.

Pis, J. J.; Fuertes, A. B.; Artos, V.; Suarez, A.; Rubiera, F., Attrition of coal ash particle in a fluidized bed. *Powder Technology* **1991,** *66*, 41-46.

Ray, Y.-C.; Jiang, T.-S.; Wen, C. Y., PARTICLE ATTRITION PHENOMENA IN A FLUIDIZED BED. *Powder Technology* **1987,** *49* (3), 193-206.

Sishtla, C. F., J.; Chan, I.; Knowlton, T. M. In *The Effect of Temperature and Gas Velocity on Fines Generation in Non-reactive Fluidized Beds of Coal Char*, Fluidization VI, Banff, Alberta, Canada, Grace, J. R. S., L. W.; Bergougnou, M. A., Ed. Banff, Alberta, Canada, 1989.

Smith, J. M.; Van Ness, H. C.; Abbott, M.; Van Ness, H., *Introduction to Chemical Engineering Thermodynamics*. McGaw-Hill: 2005.

Stubington, J. F.; Barrett, D.; Lowry, G., Bubble-Size Measurements and Correlation in a Fluidized-Bed at High-Temperatures. *Chem. Eng. Res. Des.* **1984,** *62* (3), 173-178.

Svoboda, K.; Hartman, M., Influence of Temperature on Incipient Fluidization of Limestone, Lime, Coal Ash, and Corundum. *Industrial & Engineering Chemistry Process Design and Development* **1981,** *20* (2), 319-326.

Vaux, W. G. K., Dale L. In *Particle attrition in fluid-bed processes*, Fluidization Grace, J. R. M., J. M. , Ed. Plenum Press: 1980.

Werther, J.; Xi, W., Jet attrition of catalyst particles in gas fluidized beds. *Powder Technology* **1993,** *76* (1), 39-46.

Wiederhorn, S. M., Fracture Surface Energy of Glass. *Journal of the American Ceramic Society* **1969,** *52* (2), 99-105.

Wu, S. Y.; Baeyens, J., EFFECT OF OPERATING TEMPERATURE ON MINIMUM FLUIDIZATION VELOCITY. *Powder Technology* **1991,** *67* (2), 217-220.

Zenz, F. A.; Kelleher, E. G., STUDIES OF ATTRITION RATES IN FLUID-PARTICLE SYSTEMS VIA FREE FALL, GRID JETS, AND CYCLONE IMPACT. *Journal of powder & bulk solids technology* **1980,** *4* (2-3), 8.

Chapter 5

5 Modeling of Penetration of Horizontal Supersonic Nozzles in High Temperature Fluidized Beds

5.1 Abstract

Supersonic nozzles as a type of most efficient jet have been applied in various jet-induced attrition processes such as jet mill and fluid coking processes. In jet-induced particle attrition, the penetration length of supersonic nozzle is a critical property to investigate the attrition mechanism in fluidized bed. A numerical model was developed to predict the penetration length of horizontal supersonic nozzle in a high temperature fluidized bed, based on an Eulerian-Eulerian multiphase model and Granular kinetic theory. The predicted results of jet penetration lengths are in very good agreement with the experimental data and the predictions of Li's correlation. The simulation results have also demonstrated that the fluidization velocity and bed temperature have a minor influence on jet penetration length.

5.2 Introduction

Convergent-divergent attrition nozzles have been popularly applied to various industrial applications, such as the production of pharmaceutical powders, fluid catalytic cracking process, jet milling, and fluid coking process. For example, it is desired to control the size of coke particles in a satisfied range in the fluid coking process, because large particles cause poor fluidization and degrade the operation of the coke transport lines (Dunlop et al., 1958). This is achieved by injecting steam into the fluidized bed through a series of convergent-divergent nozzles. As a type of attrition nozzle used in jet-induced attrition process, the convergent-divergent nozzle has two characteristic physical parameters, the ratio of the exit area to the throat area, and the ratio of the stagnation pressure to the ambient pressure. The fluid reaches the sonic velocity at the throat, and supersonic velocity is obtained in the divergent section (Smith, 2005).). Bentham et al. (2004)

asserted that the particle breakage mechanism of subsonic jets involves the particles entrained in the jet. According to another study of McMillan et al. (2007b), the entrained particles in the jet are accelerated by the supersonic jet, and then these particles would collide with slow velocity particles near the jet boundary layer. Since the convergent-divergent nozzles demonstrate more efficiency than a regular nozzle, they require less steam to achieve the same attrition rate (McMillan et al., 2007a). Knowing the penetration depth of the high velocity jets is important to maximize their attrition efficiency and avoid the erosion of fluidized bed internals, as most of the particles attrition and collision occurs in the void cavity area of the horizontal jets.

The penetration length of attrition jets is a critical property to investigate the attrition mechanism in a fluidized bed. Table 5.1 provides examples of published correlations for jet penetration length. The jet penetration length is strongly related to the gas density and gas velocity. However, all these correlations were developed from data obtained with nozzles operating at subsonic velocities.

Although many studies have been done in jet penetration, the knowledge of the hydrodynamics and fundamental phenomena of high velocity horizontal gas jets is mostly limited to ambient temperature conditions. Among the published correlations for penetration length, many are unreliable for jets issuing from convergent-divergent nozzles, particularly at high temperature. A supersonic jet injected horizontally in fluidized beds can be assumed to behave as a submerged jet, similar to a turbulent jet spreading through a liquid medium at rest. The study by Li et al. (2010b) found that the empirical correlations listed in Table 5.1 are unable to predict the jet penetration at high temperature. Only the predictions from the Benjelloun's correlation are in relatively good agreement with the experimental data. Therefore, a new and improved empirical correlation was proposed by Li et al. (2010b) to predict the penetration length of jets issuing from the horizontal supersonic nozzle at high temperature.

Table 5.1 Correlations for jet penetration length

Correlation	Variables	U_0(m/s)	Reference
$$\frac{L_j}{d_0} = 7.8\left(\frac{\rho_f U_0}{\rho_p \sqrt{gd_p}}\right)$$	Copolymer $$1 < \frac{d_0}{d_p} < 1.5$$	83-192	Shakhova (1968)
$$\frac{L_j}{d_0} + 4.5 = 5.25\left(\frac{\rho_0 U_0^2}{(1-\varepsilon)\rho_P gd_P}\right)^{0.4}\left(\frac{\rho_f}{\rho_P}\right)^{0.2}\left(\frac{d_p}{d_0}\right)^{0.2}$$	Sand, steel shot, and Kale seeds $$1.5 < \frac{d_0}{d_p} < 80$$ $$1.6\times10^{-4} < \frac{\rho_f}{\rho_p} < 12\times10^{-4}$$	40-200	Merry (1971)
$$0.044\frac{L_j}{d_0} + 1.48 = 0.5\log(0.67\rho_f U_0^2)$$	FCC	32-64	Zenz (1968)
$$\frac{L_j}{d_0} + 3.80 = 1.64\times10^6\left(\frac{\rho_0 U_0^2}{(1-\varepsilon)\rho_P gd_P}\right)^{0.327}\left(\frac{\rho_f}{\rho_P}\right)^{1.974}$$	Millet, silica sand $2.2 < \dfrac{d_0}{d_p} < 7$ $$7.5\times10^{-4} < \frac{\rho_f}{\rho_p} < 8\times10^{-4}$$	6-190	Hong (1997)
$$\frac{L_j}{d_0} = 5.52\left(\frac{\rho_0 U_0^2}{(\rho_p - \rho_f)gd_0}\right)^{0.27}$$	Catalyst, glass, sand $$1 < Fr < 380$$	15-300	Benjelloun (1991)
$$\frac{L_j}{d_0} = 2.8\left(\frac{\rho_0 U_0^2}{(\rho_p - \rho_f)gd_0}\right)^{0.4}$$	Calcined alumina powder $1 < Fr < 180$		Yates (1991)

With the dramatic development of computation technologies, Computational Fluid Dynamics (CFD) has become a powerful tool for studying and designing fluidized bed reactors. Hong et al. (1996) proposed a two-phase model to simulate the aspects of an inclined nozzle in a gas-solid bubbling fluidization. Tyler and Mees (1999) used CFD to model the hydrodynamics of horizontal gas jet in a fluidized bed. In the investigation of ESE nozzle system by Cui et al. (2005), a three-dimensional computational model of the nozzle was developed to explore the influence of nozzle geometries on the entrainment of solid. Hulet et al. (2008) further developed a numerical simulation model to investigate the interaction between the jet and the fluidized bed. The studies suggested that both a shroud around the nozzle tip and a draft tube can promote the entrainment rate of solids into a horizontal gas jet. In the work by Li et al. (2008), a computational model was

developed to focus on the study of the horizontal jet penetration of subsonic nozzles into a fluidized bed. Li and colleagues (2009) continued the numerical simulation work on the multiple gas jets in bubbling fluidized bed. Although many research projects have been carried out to study the interaction between horizontal jets and fluidized bed by numerical simulation, all these studies were conducted with nozzles operating at subsonic velocity and at ambient temperature conditions.

The main objective of this work is to develop a computational model, based on an Eulerian-Eulerian multiphase model and Granular kinetic theory, for the simulation of the jet penetration of a convergent-divergent nozzle in a high temperature fluidized bed.

5.3 Numerical approaches

5.3.1   Modeling of fluidized bed reactor with an Eulerian-Eulerian multiphase model

Two different approaches have been taken in the numerical calculation of multiphase fluids: the Eulerian-Lagrangian approach and the Eulerian-Eulerian approach. In the Eulerian-Lagrangian approach, the gas phase is treated as a continuous phase and calculated with Navier-Stokes equations, while the solids phase is solved as a discrete phase. On the contrary, the Eulerian-Eulerian approach treats all phases in the system as continuous. Chiesa et al. (2005) found that the Eulerian-Lagrangian approach agrees well with the experimental results compared the Eulerian-Eulerian approach. The major disadvantage of the Eulerian-Lagrangian approach is its numerical cost. In their study, the CPU time needed for Eulerian-Lagrangian approach is usually four orders of magnitude higher than the time needed for Eulerian-Eulerian approach. The kinetic theory of granular flow (KTGF) can be used to describe particle interactions in a bubbling fluidized bed where particles are in random motion state and can collide with other particles in binary collisions (Ding and Gidaspow, 1990; Gidaspow, 1994). The particles in a gas-solid system can be solved as a continuous fluid by the Eulerian-Eulerian approach when the particle properties are described with KTGF (Boemer et al., 1998). Therefore, the Eulerian-Eulerian model and KTGF are adopted in the present work.

5.3.1.1 Conservation of Mass

Because no mass transfer occurs between the two phases (gas and solid), the continuity equation is

$$\frac{\partial}{\partial t}(\varepsilon_q \rho_q) + \nabla(\varepsilon_q \rho_q \vec{u}_q) = 0$$

(5.1)

5.3.1.2 Conservation of Momentum

The momentum equation is expressed as:

$$\frac{\partial}{\partial t}(\varepsilon_s \rho_s \vec{u}_s) + \nabla(\varepsilon_s \rho_s \vec{u}_s \vec{u}_s) = -\varepsilon_s \nabla p + \nabla \cdot \overline{\overline{\tau}}_s + \varepsilon_s \rho_s \vec{g} +$$

$$\sum_{p=1}^{n} K_{ls}(\overline{u_l} - \overline{u_s})$$

(5.2)

where $\overline{\overline{\tau}}_q$ is the qth phase stress-strain tensor

$$\overline{\overline{\tau}}_q = \varepsilon_q \mu_q (\nabla \vec{u}_q + \nabla \vec{u}_q^T) + \varepsilon_q (\lambda_q - \frac{2}{3}\mu_q)\nabla \cdot \vec{u}_q \overline{\overline{I}}$$

(5.3)

Here μ_q and λ_q are the shear and bulk viscosity of phase q.

$K_{ls}(= K_{sl})$ is the interphase momentum exchange coefficient, more details described at next section.

5.3.1.3 Fluid-Solid Momentum Transfer and Exchange Coefficient

The fluid-solid exchange coefficient K_{sl} can be written in the following general form:

$$K_{sl} = \frac{\varepsilon_s \rho_s f}{\tau_s}$$

(5.4)

where f is defined differently for the different exchange-coefficient models, and τ_s, is defined as

$$\tau_s = \frac{\rho_s d_s^2}{18\mu_l}$$

(5.5)

where d_s is the particle diameter

Syamlal-O'Brien model (Syamlal, 1987)

$$K_{ls} = \frac{3}{4} \frac{C_D}{\upsilon_{r,s}^2} \frac{\rho_g \left| \vec{v}_s - \vec{v}_g \right|}{d_s} \alpha_g \alpha_s \qquad (5.6)$$

$$f = \frac{C_D \, \text{Re}_s \, \varepsilon_g}{24 v_{r,s}^2} \qquad (5.7)$$

$$C_D = \left(0.63 + \frac{4.8}{\sqrt{\text{Re}_s / v_{r,s}}} \right)^2 \qquad (5.8)$$

$$\text{Re}_s = \frac{\rho_g d_s \left| \vec{v}_s - \vec{v}_g \right|}{\mu_g} \qquad (5.9)$$

$$\upsilon_{r,s} = 0.5(A - 0.06 \, \text{Re}_s + \sqrt{(0.06 \, \text{Re}_s)^2 + 0.12 \, \text{Re}_s (2B - A) + A^2})$$

$$A = \alpha_g^{4.14}$$

$$(5.10) \quad B = \begin{cases} \varepsilon_g^{C1} & \varepsilon_g \geq 0.85 \\ C_2 \varepsilon_g^{1.28} & \varepsilon_g < 0.85 \\ default \ value: \ C_1 = 2.65 \ and \ C_2 = 0.8 \end{cases}$$

Wen and Yu model

$$K_{ls} = \frac{3}{4} C_D \frac{\alpha_s \alpha_l \rho_l \left| \vec{v}_s - \vec{v}_l \right|}{d_s} \alpha_l^{-2.65} \qquad (5.11)$$

$$C_D = \frac{24}{\alpha_l \, \text{Re}_s} \left[1 + 0.15 (\alpha_l \, \text{Re}_s)^{0.687} \right] \qquad (5.12)$$

Gidaspow model

when $\alpha_g > 0.8$ then:

$$K_{sl} = \frac{3}{4} C_D \frac{\alpha_s \alpha_l \rho_l \left| \vec{v}_s - \vec{v}_l \right|}{d_s} \alpha_l^{-2.65} \qquad (5.13)$$

Where

$$C_D = \frac{24}{\alpha_l \, \text{Re}_s} \left[1 + 0.15 (\alpha_l \, \text{Re}_s)^{0.687} \right] \qquad (5.14)$$

When $\alpha_l \leq 0.8$ then:

$$K_{sl} = 150 \frac{\alpha_s (1-\alpha_l)\mu_l}{\alpha_l d_s^2} + 1.75 \frac{\rho_l \alpha_s |\vec{v}_s - \vec{v}_l|}{d_s}$$

(5.15)

5.3.1.4 The conservation of Energy

$$\frac{\partial}{\partial t}(\varepsilon_q \rho_q h_q) + \nabla(\varepsilon_q \rho_q \vec{u}_q h_q) = -\varepsilon_q \frac{\partial p_q}{\partial t} + \overline{\overline{\tau}}_q : \nabla \vec{u}_q - \nabla \vec{q}_q + S_q +$$

$$\sum_{p=1}^{n} (Q_{pq} + \dot{m}_{pq} h_{pq} - \dot{m}_{qp} h_{qp})$$

(5.16)

In fluidized beds, the energy transfer between particles and gas is more complex than in a fixed bed because of the motion of the suspended particles and gas bubbles (Chen, 2005). Three heat transfer mechanisms are involved in fluidized beds: gas-particle convection, particle-particle conduction, and particle radiation. The heat transfer coefficient of a bubbling fluidized bed is used for all three cases, with the surface area of particles defined as:

$$h_p = \frac{Q}{A(T_p - T_g)}$$

(5.17)

A dimensionless Nusselt number, $Nu_p = h_p D / k$, indicates the relationship of the fluid thermal conductivity k and a characteristic length D specified for each flow system (Bird et al, 2002). Ranz and Marshall (1952) presented a correlation for estimating the Nusselt number in fixed beds:

$$Nu_p = 2 + 0.6 \operatorname{Re}_p^{0.5} \operatorname{Pr}_g^{0.33}$$

(5.18)

The Nusselt number correlation developed by Gunn (1978) could estimate the heat transfer for the fixed and fluidized beds, typically for a porosity range of 0.35-1.0 and Reynolds number of up to 1×10^5.

$$Nu = (7 - 10\alpha_f + 5\alpha_f^2)(1 + 0.7 \operatorname{Re}_p^{0.2} \operatorname{Pr}^{1/3}) + (1.33 - 2.4\alpha_f + 1.2\alpha_f^2) \operatorname{Re}_p^{0.7} \operatorname{Pr}^{1/3}$$

(5.19)

In the present investigation, the Gunn correlation was used in all numerical simulation involving energy exchange.

5.3.1.5 Constitutive Equation

Solid pressure

The solid pressure is composed of a kinetic term and a second term due to particle collision:

$$p_s = \alpha_s \rho_s \Theta_s + 2\rho_s(1+ess)\alpha_s^2 g_{0,ls}\Theta_s \qquad (5.20)$$

Radial Distribution Function

$$g_0 = \left[1-\left(\frac{\alpha_s}{\alpha_{s,max}}\right)^{\frac{1}{3}}\right]^{-1} \qquad (5.21)$$

Kinetic Viscosity

There are two options for prediction of the Kinetic viscosity by FLUENT:

Syamlal et al:

$$\mu_{s,kin} = \frac{\alpha_s d_s \rho_s \sqrt{\Theta_s \pi}}{6(3-e_{ss})}\left[1+\frac{2}{5}(1+e_{ss})(3e_{ss}-1)\alpha_s g_{0,ss}\right] \qquad (5.22)$$

Gidaspow et al:

$$\mu_{s,kin} = \frac{10 d_s \rho_s \sqrt{\Theta_s \pi}}{96\alpha_s(1+e_{ss})g_{0,ss}}\left[1+\frac{4}{5}\alpha_s g_{0,ss}(1+e_{ss})\right]^2 \alpha_s \qquad (5.23)$$

Bulk Viscosity (Lun et al)

$$\lambda_s = \frac{4}{3}\alpha_s d_s \rho_s g_{0,ss}(1+e_{ss})\left(\frac{\Theta_s}{\pi}\right)^{1/2} \qquad (5.24)$$

Frictional viscosity

In present work, Schaeffer's expression was used:

$$\mu_{s,fr} = \frac{p_s \sin\phi}{2\sqrt{I_{2D}}} \qquad (5.25)$$

where p_s is the solids pressure, ϕ is the angle of internal friction, and I_{2D} is the second invariant of the deviatoric stress tensor.

Granular Temperature

The granular temperature of solid phase is defined to be is proportional to the kinetic energy of the random motion of the particles.

$$\frac{3}{2}\left[\frac{\partial}{\partial t}(\rho_s \alpha_s \Theta_s) + \nabla \cdot (\rho_s \alpha_s \vec{v}_s \Theta_s)\right] = (-p_s \bar{I} + \bar{\tau}s) : \nabla \vec{v}_s + \nabla \cdot \left(k_{\Theta_s} \nabla \Theta_s\right) - \gamma_{\Theta_s} + \phi_{ls} \tag{5.26}$$

where

$(-p_s \bar{I} + \bar{\tau}s) : \nabla \vec{v}_s$ = the generation of energy by the solid stress tensor

$k_{\Theta_s} \nabla \Theta_s$ = the diffusion of energy (k_{Θ_s} is the diffusion coefficient)

γ_{Θ_s} = the collisional dissipation of energy

ϕ_{ls} = the energy exchange between the gas phase and the solid phase

The diffusion coefficient of granular temperature calculated according Syamlal-O'Briens is:

$$k_{\Theta_s} = \frac{15 d_s \rho_s \alpha_s \sqrt{\Theta_s \pi}}{41(41 - 33\eta)}\left[1 + \frac{12}{5}\eta 2(4\eta - 3)\alpha_s g_{0,ss} + \frac{16}{15\pi}(41 - 33\eta)\eta \alpha_s g_{0,ss}\right] \tag{5.27}$$

The diffusion coefficient of granular temperature calculated according to Gidaspow is:

$$k_{\Theta_s} = \frac{150 d_s \rho_s \sqrt{\Theta_s \pi}}{384(1 + e_{ss})g_{0,ss}}\left[1 + \frac{6}{5}\alpha_s g_{0,ss}(1 + e_s)\right]^2 + 2\rho_s \alpha_s^2 d_s(1 + e_{ss})g_{0,ss}\sqrt{\frac{\Theta_s}{\pi}} \tag{5.28}$$

Lun et al. (1984) developed the following expression for calculating the collisional dissipation energy:

$$\gamma_{\Theta m} = \frac{12(1 - e_{ss}^2)g_{0,ss}}{ds\sqrt{\pi}}\rho_s \alpha_s^2 \Theta_s^{3/2} \tag{5.29}$$

5.3.1.6   Turbulence Models

The *k-ε* dispersed turbulence model was used in the present work because the concentration of the secondary phase is dilute. The model is applicable when there is a primary continuous phase and other phases dispersed.

Turbulence in the primary phase

The turbulent predictions are obtained:

$$\frac{\partial}{\partial t}\left(\alpha_q\rho_q k_q\right)+\nabla\cdot\left(\alpha_q\rho_q\vec{U}_q k_q\right)=\nabla\cdot\left(\alpha_q\frac{\mu_{t,q}}{\sigma_k}\nabla k_q\right)+\alpha_q G_{k,q}-\alpha_q\rho_q\varepsilon_q+\alpha_q\rho_q\Pi_{kq}$$

(5.30)

$$\frac{\partial}{\partial t}\left(\alpha_q\rho_q\varepsilon_q\right)+\nabla\cdot\left(\alpha_q\rho_q\vec{U}_q\varepsilon_q\right)=\nabla\cdot\left(\alpha_q\frac{\mu_{t,q}}{\sigma_\varepsilon}\nabla\varepsilon_q\right)+\alpha_q\frac{\varepsilon_q}{k_q}\left(C_{1\varepsilon}G_{k,q}-C_{2\varepsilon}\rho_q\varepsilon_q\right)+\alpha_q\rho_q\Pi_{\varepsilon q}$$

(5.31)

Here Π_{kq} *and* $\Pi_{\varepsilon q}$ represent the effect of the dispersed phases on the continuous phase, and $G_{k,q}$ is the production of turbulent kinetic energy.

$$\Pi_{kq}=\sum_{p=1}^{M}\frac{K_{pq}}{\alpha_q\rho_q}\left(k_{pq}-2k_q+\vec{v}_{pq}\cdot\vec{v}_{dr}\right)$$

(5.32)

$$\Pi_{\varepsilon q}=C_{3\varepsilon}\frac{\varepsilon_q}{k_q}\Pi_{kq}$$

(5.33)

where $C_{3\varepsilon}=1.2$

Turbulence in the Dispersed Phase

$$\tau_{F,pq}=\frac{\alpha_q\rho_q}{K_{pq}}\left(\frac{\rho_p}{\rho_q}+C_V\right)$$

(5.34)

There are three common turbulent *k-ε* models: the standard, RNG; and realizable. In the present work, the standard k-ε model is used for simulation due to excellent performance for a wide range of turbulent flows. The standard k-ε model consists by the turbulence kinetic energy k and dissipation rate ε.

$$\frac{\partial}{\partial t}\left(\rho k\right)+\frac{\partial}{\partial x_i}\left(\rho k u_i\right)=\frac{\partial}{\partial x_i}\left[\left(\mu+\frac{\mu_t}{\sigma_k}\right)\frac{\partial k}{\partial x_j}\right]+G_k+G_b-\rho\varepsilon-Y_M+S_k$$

(5.35)

$$\frac{\partial}{\partial t}\left(\rho\varepsilon\right)+\frac{\partial}{\partial x_i}\left(\rho\varepsilon u_i\right)=\frac{\partial}{\partial x_i}\left[\left(\mu+\frac{\mu_t}{\sigma_\varepsilon}\right)\frac{\partial\varepsilon}{\partial x_j}\right]+C_{1\varepsilon}\frac{\varepsilon}{k}(G_k+C_{3\varepsilon}G_b)-C_{2\varepsilon}\rho\frac{\varepsilon^2}{k}+S_\varepsilon$$ (5.36)

5.4 **Experimental setup**

Experiments were performed in a hot fluidized bed with 1.23 m of bed height, 0.10 m of bed width, and 0.50 of bed length (Figure 5.1). The bed particles were heated with an in-

bed electrical heater to temperatures between 300°C to 500°C. Cold gases, such as compressed air, helium, nitrogen, carbon dioxide, were injected into the hot fluidized bed through a horizontal nozzle inserted in the side wall of the fluid bed at a distance of 0.127 m above the gas sparger. Two different particles were used in the tests: silica sand with a Sauter-mean diameter of 205 µm, and petroleum coke with a Sauter-mean diameter of 120 µm. Tests were conducted with a range of nozzle flowrates dependent on the temperature and injection pressure. Three different sizes of convergent-divergent nozzles were used to assess the influences of nozzle size on the penetration length of supersonic gas jets.
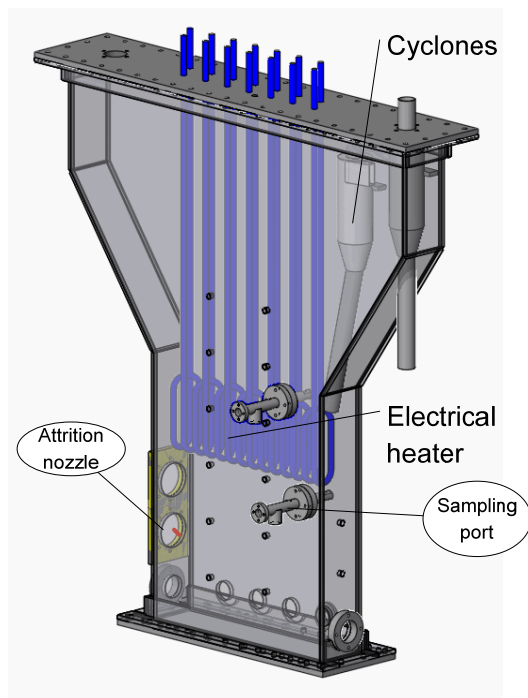
Figure 5.1 Schematic diagram of the hot fluidized bed
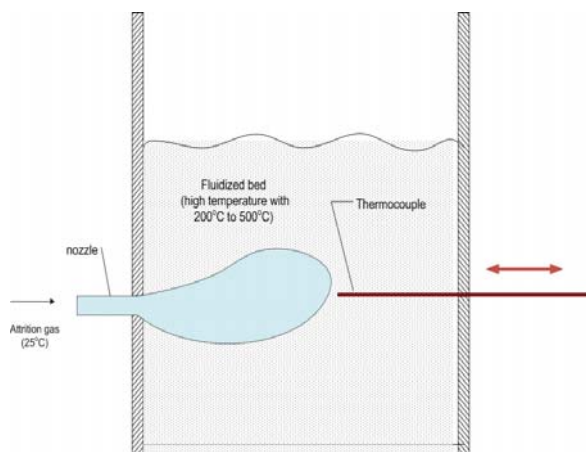
Figure 5.2 Diagram of the thermal method to measure penetration length in fluidized beds at high temperature

A novel thermal method was developed to measure the penetration length of the high velocity horizontal gas jets. It used the observation that, because cold gas was used to form the jet, the jet cavity was always at a temperature below that of the hot fluidized bed, and that the bed temperature was nearly uniform. The thermal method used a fast thermocouple, which was inserted along the axis of the jet from the opposite wall (Figure 5.2), a series of temperature signals were recorded while moving the thermocouple progressively towards the jet. The end of the jet cavity could be detected from the sharp decreasing temperature at the boundary of the jet cavity, due to the presence of the colder gas jet.

5.5 Computational model and parameters

5.5.1 Computational domains

A three-dimension computational domain, consisting of a nozzle, was used to model the gas-solid two phase flow and the hydrodynamic properties of jet-bed interaction. The computational domain is the same as the dimensions of hot fluidized bed used in the experiments, with a height of 1.23 m and a rectangular cross-section of 0.10 m × 0.50 m. Figure 5.3 illustrates the 3-D computational domain developed by Gambit 2.4.
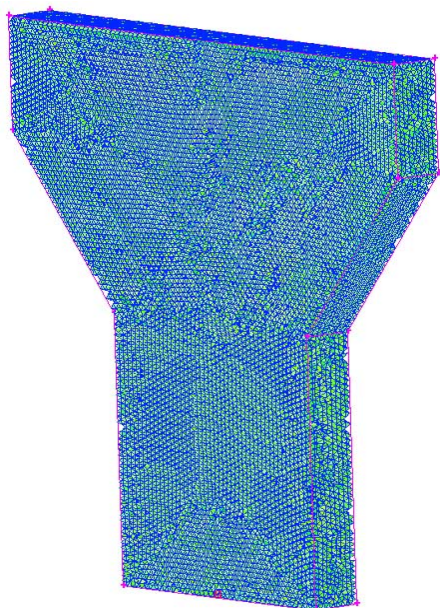
Figure 5.3 Scheme of the 3-dimensionalcomputational domain

5.5.2 Operating parameters of the hot bed

Table 5.2 Simulation model parameters

Description	Value
Gas density	Incompressible & compressible
Particle density	Silica sand: 2650 kg/m^3
	Petroleum coke: 1450 kg/m^3
Mean particle diameter	Silica sand: 205 μm
	Petroleum coke: 120 μm
Restitution coefficient	0.80 – 0.99
Initial solids packing	0.60
Superficial gas velocity	0.1 m/s – 0.5 m/s
Bed width	0.50 m
Bed height	1.3 m
Static bed height	0.4 m
Time step size	0.001 s
Maximum number of iterations	100
Convergence criteria	10^{-6}

Table 5.3 Configuration of secondary phase

Primary phase	Air or Nitrogen gas
Secondary Phase	Petroleum coke or Silica sand
Granular	Activate
Granular temperature model	Phase property
Particle diameter	120 μm, 205 μm
Granular viscosity	Gidaspow
Granular bulk viscosity	Lun-et-al
Friction viscosity	Schaeffer
Angle of internal friction	30
Friction pressure	Based-ktgf
Frictional modulus	Derived
Friction packing limit	0.61
Granular temperature	Algebraic
Solids pressure	Syamlal-O'Brien
Radial distribution	Lun-et-al
Elasticity modulus	derived
Packing limit	0.63

5.5.3   Boundary and initial conditions

The boundary conditions for the gas and solid phases are summarized in Table 5.4 and Table 5.5, respectively.

Table 5.4 Gas phase boundary conditions in Attrition Model

Name	Type	Value
Fluidization gas inlet	Mass flowrate inlet (mass flux)	V_g=0.10 -0.50 m/s
	Intensity and hydraulic diameter	5% Turbulent intensity; 0.17 m Hydraulic diameter
Bed out	Pressure outlet	P_{out} = 0 psig
	Intensity and hydraulic diameter	2% backflow turbulent intensity; 0.17 m Backflow hydraulic diameter
Nozzle inlet	Mass flow inlet	Vary with attrition pressures and attrition nozzles
	Pressure inlet	0.7 MPa - 2.1 MPa
	Turbulent intensity	5%
	Diameter (throat)	1.2 mm to 2.4 mm
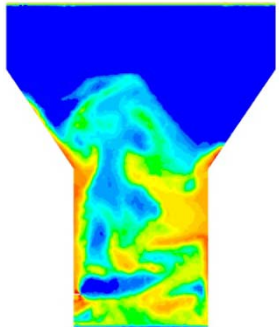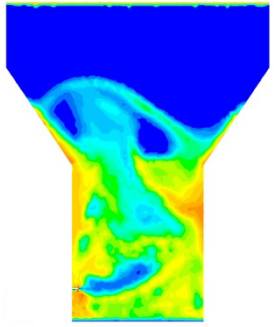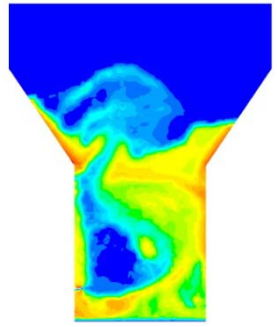
Table 5.5 Solid phase boundary conditions in Attrition Model

Name	Type	Value
Fluidization gas inlet	Mass flowrate inlet (mass flux)	0
	Intensity and hydraulic diameter	5% Turbulent intensity; 0.17 m Hydraulic diameter
Bed out	Pressure outlet	P_{out} = 0 psig
	multiphase	Backflow volume fraction: 0
Nozzle inlet	Mass flow inlet	0
	Pressure inlet	0
	Volume fraction	0

5.5.4   Sensitivity study of mesh sizes

In the present work, the behavior of the jet penetration was used to study the sensitivity of the mesh size selection. The simulations ran for a 10 s of real-time to make certain the bed is in a quasi-steady state. All the simulations were performed at a fluidization velocity of 0.20 m/s, with the Gidaspow drag law and a restitution coefficient equal to 0.90. The jet penetration in the present study is defined as the distance from the nozzle tip to the end of the jet cavity, where the solids volume fraction ε is more than 0.20. As shown in Table 5.6, the results were obtained with numerical simulations using a 2.4 mm diameter nozzle and the operating conditions of 200 psig attrition pressure and 0.20 m/s fluidization velocity. The experimental jet penetration length of the 2.4 mm nozzle at 200 psig attrition pressure is 0.280 m. It can be observed that all the three different grids chosen can verify very well the accuracy of the numerical simulation of the jet penetration in the fluidized bed, with a particularly good agreement between the medium mesh sizes of 282K and the finer mesh sizes of 353K cells.   Considering the computational cost, mesh sizes of 282K cells was deemed sufficiently fine for the numerical simulation of jet penetration in a fluidized bed for this investigation. Thereby, the mesh size of 282,978 cells grid was used to generate most of the subsequent simulation results.

Table 5.6 Jet penetration length at time of 10 s for V_g = 0.20 m/s, P = 200psi, diameter of nozzle: 4mm

Size	Fine	Medium	coarse
Grid cells	353,384	282,978	114,128
Grid nodes	71,645	58,157	23,192
Contour of solid volume fraction			
Penetration (m)	0.277	0.276	0.285

5.5.5 Time step

An excessively long time step will make the calculations unstable; on the other hand, a time step that is too short will make the calculations needlessly slow. The most commonly used time step in gas-solid fluidized bed simulations is 0.001s (Taghipour et al., 2005; Hulet, 2006; Cornelissen et al., 2007). Similarly, in the present research, 0.001s was found to be adequate to generate a stable and precise simulation of the jet penetration and of the dynamics of the fluidized bed.

5.5.6 Adjustment of the drag law model and restitution coefficient

The drag coefficient, a function of a particle's Reynolds number, is defined as the ratio of the forces on the particle and the fluid dynamics pressure. Three drag law methods are most common in CFD simulation. There are: the Gidaspow model, the Wu and Yu model, and the Syamlal-O'Brien model. To predict the drag coefficient more accurately, Syamlal and O'Brien (1987) proposed an approach to adjust drag law based on the minimum fluidization velocity in a gas-solid fluidized bed. The former work by Vejahati et al. (2009) and Hulet (2006) suggested that adjustment using minimum fluidization velocity improves the simulation of the gas-solid two phase system

The adjusted way of Syamlal and O'Brien drag law equation is:

$$\left\{ U_{mf}^{experiment} - \mathrm{Re}_t \frac{\alpha_g \mu_g}{d_s \rho_g} \right\} \to 0 \tag{5.37}$$

$$where \ C_D = \left(0.63 + \frac{4.8}{\sqrt{\mathrm{Re}_s / \upsilon_r}} \right)^2 \tag{5.38}$$

$$\mathrm{Re}_t = \upsilon_r \, \mathrm{Re}_{ts} \tag{5.39}$$
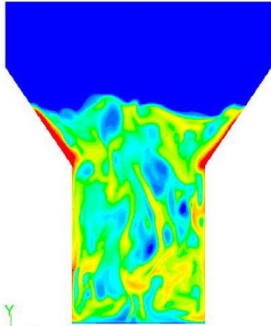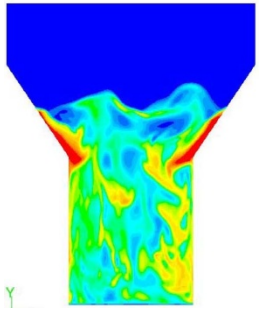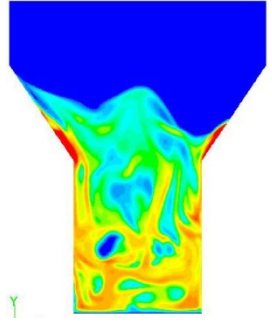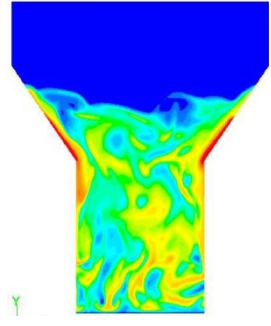
$$\upsilon_r = \frac{A + 0.06B \, \mathrm{Re}_{ts}}{1 + 0.06 \, \mathrm{Re}_{ts}} \tag{5.40}$$

$$\mathrm{Re}_{ts} = \left(\frac{\sqrt{23.04 + 2.52\sqrt{4Ar/3}} - 4.8}{1.26} \right)^2 \tag{5.41}$$

The bed expansion of a fluidized bed was used to verify the sensitivities of various drag law models due to its virtual characteristic in bed dynamics performance. The bed expansion ratio is defined as

$$\delta = \frac{H - H_{mf}}{H}$$

where H and H_{mf} are the bed heights at operating conditions and minimum fluidization respectively.

Gidaspow model	Wen-Yu model	Syamlal-O'Brien model	Syamlal-O'Brien adjusted model
Vg=30cm/s, e=0.90	Vg=30cm/s, e=0.90	Vg=30cm/s, e=0.90	Vg=30cm/s, e=0.90

| Vg=20cm/s, e=0.90 | Vg=20cm/s, e=0.90 | Vg=20cm/s, e=0.90 | Vg=20cm/s, e=0.90 |

Comparison of simulation results with experimental data

A comparison of experimental bed expansion results with those predicted by the Syamlal-O'Brien drag model, which can modify the C_1 and C_2 (Eq. 5.17) depending on the value of the experimental minimum fluidization velocity, shows the best agreement. So, the adjusted Syamlal-O'Brien drag model was used in most of the subsequent simulation work.

5.6 Results and discussions

5.6.1   Properties of convergent-divergent nozzles

As mentioned earlier, the convergent-divergent nozzle is characterized by two important parameters: the area ratio (the ratio of the exit area to the throat area), and the pressure ratio (the ratio of the stagnation pressure to the ambient pressure). In supersonic nozzles, the fluid reaches the sonic velocity at the throat, and supersonic velocity is obtained in the divergent section (Smith, 2005). The cross-sectional area, pressure and temperature vary with Mach number along the converging-diverging flow path according to (Liepmann, 1957, and Perry, 2008):

$$\frac{A}{A^*} = \frac{1}{M}\left[\frac{2}{\gamma+1}\left(1+\frac{\gamma-1}{2}M^2\right)\right]^{(\gamma+1)/2(\gamma-1)}$$

(5.42)

$$\frac{p_0}{p} = \left[1+\frac{\gamma-1}{2}M^2\right]^{\gamma/(\gamma-1)}$$

(5.43)

$$\frac{T_0}{T} = 1+\frac{\gamma-1}{2}M^2$$

(5.44)

The sonic mass flux through the throat is given by:

$$G = p_0\sqrt{\left(\frac{2}{\gamma+1}\right)^{(\gamma+1)/(\gamma-1)}\left(\frac{\gamma M_w}{RT_0}\right)}\ (kg/m^2\cdot s)$$

(5.45)

If A is set equal to the nozzle exit area, the exit pressure, temperature, Mach number may be obtained. The relation between area and any other flow data can be obtained through the Mach number, as shown in Fig. 5.4.
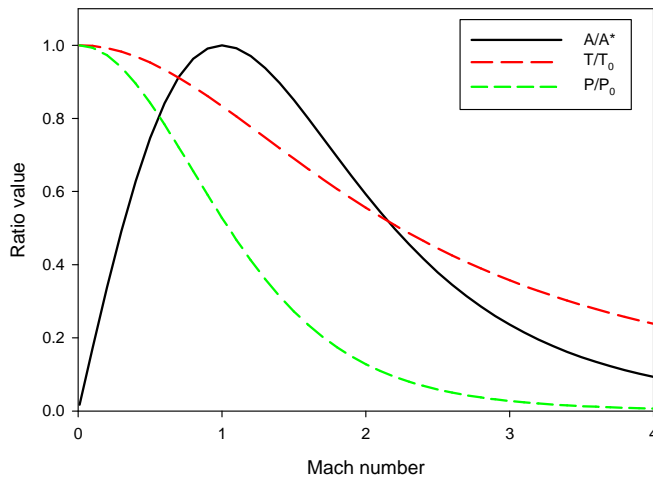
Figure 5.4 Effect of the Mach number on area ratio, temperature ratio, and pressure ratio in a convergent-divergent nozzle
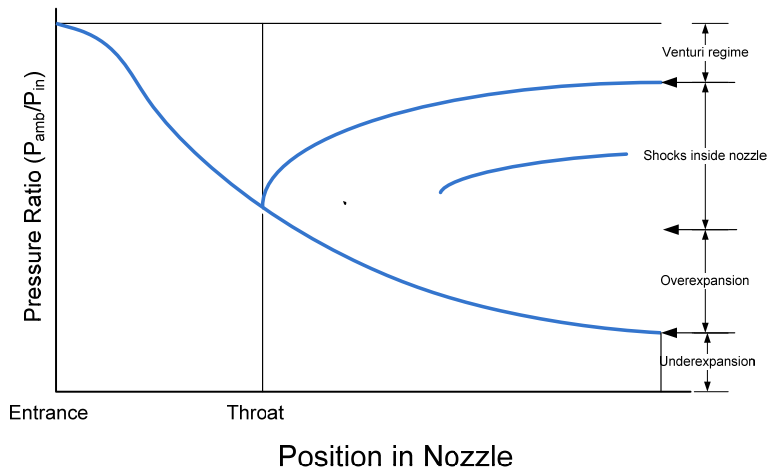
Figure 5.5 Shock wave modes for convergent-divergent nozzle (Adapted from Zucker and Biblarz, 2002)

For specific nozzle geometry, the location and strength of the shock are depended on the operating pressure ratio (Zucker and Biblarz, 2002). It can be seen there are three critical points in Fig. 5.5. The normal shock forms downstream of the nozzle throat but in the nozzle, if the pressure ratio is between the first critical point and the second critical point. Once the shock is located at the exit of nozzle, the pressure ratio is at the second critical point. The overexpansion occurs when the pressure ratio is between the second and third critical points. If the operating pressure ratio is below the third critical point, an underexpansion occurs outside the nozzle. Since the operation pressure ratios are range from 0.04 to 0.14 in the present study, the under-expansion would occur for all operation

conditions. The underexpansion of shock wave can be observed in Figures 5.6 and 5.7, with pressure ratios 0.14 and 0.05, respectively.
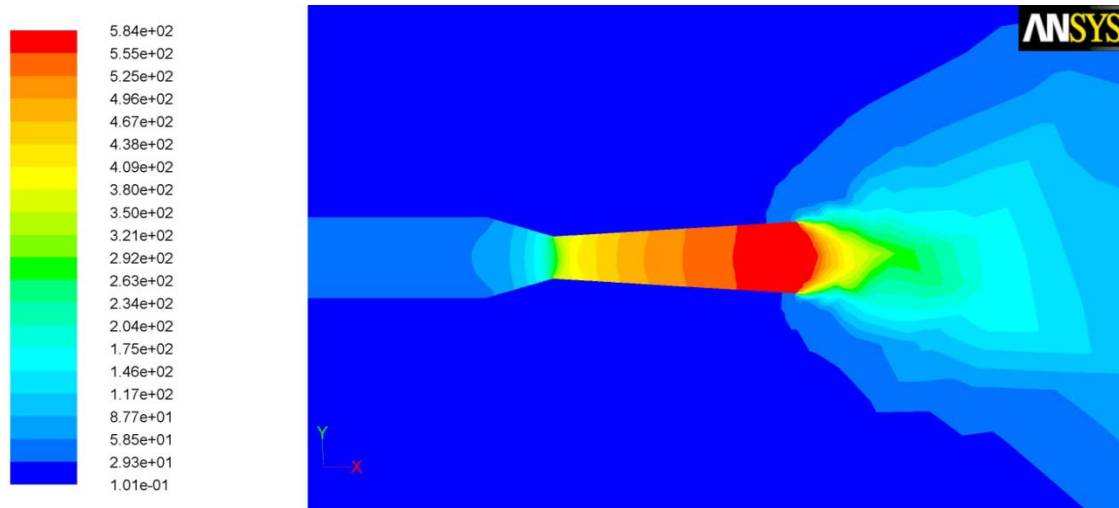
Figure 5.6 Contours of velocity of supersonic nozzle (P/Pin=0.14)
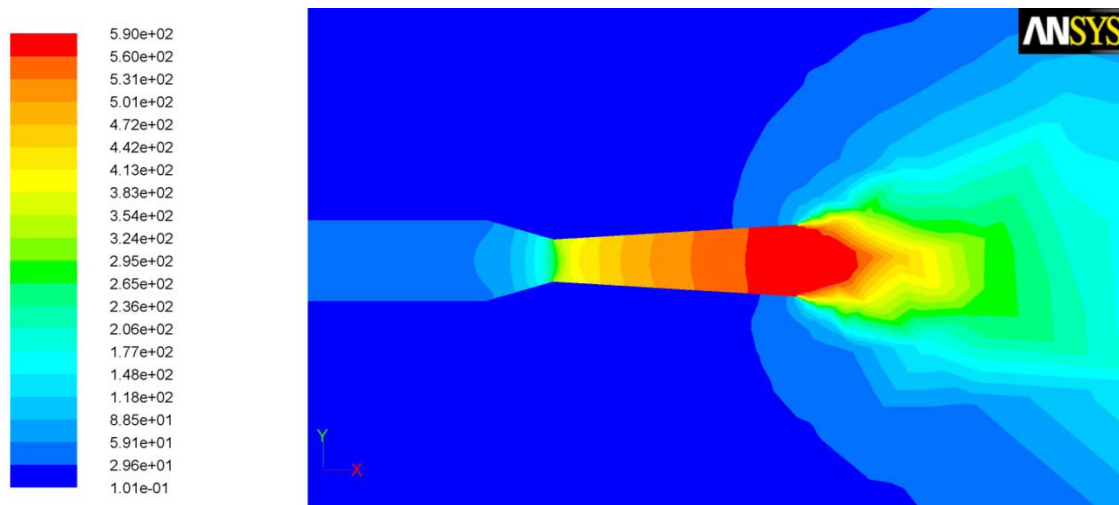
Figure 5.7 Contours of velocity of nozzle with underexpansion (P/Pin=0.05)

Figure 5.8 shows the shape of the convergent-divergent attrition nozzle used in the present research, which was located inside the bed at a 0.127 m height above the fluidizing gas distributor. A convergent-divergent nozzle injecting a jet horizontally in a fluidized bed with sonic or supersonic velocity can be assumed to behave as a submerged jet, similar to a turbulent jet spreading through a liquid medium at rest. If a nozzle with a uniform velocity of U_0 injects fluid into a large stagnant mass of the same fluid, the velocity profiles shown in Figure 5.9 are expected.

Figure 5.8 Convergent-divergent attrition nozzle used in this work
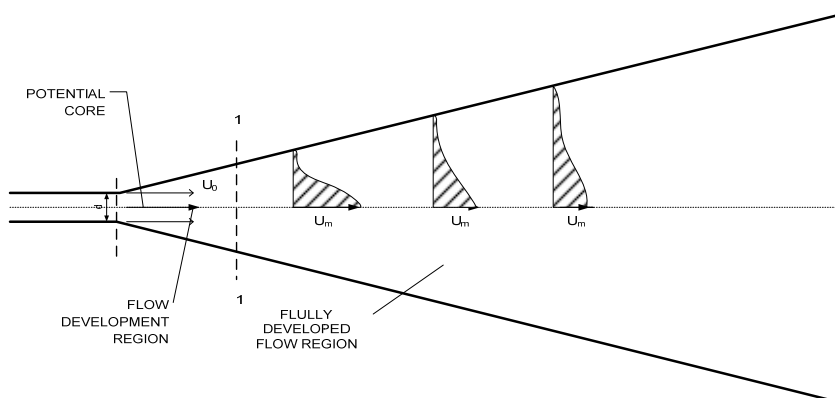
Figure 5.9 Velocity profile of circular turbulent jet (adapted from Rajaratnam, 1976)

De Michele et al. (1976) developed the turbulent jet model for axisymmetric jets in beds, which is extended the theory of turbulent submerged jet to the gas injection in fluidized beds. In the initial region of jet, as shown in Figure 5.9, there exists a core region, known as the potential core, where the turbulence flow is developing. Davies (1972) suggests that the length of potential core is about 6.4 jet diameters, followed by a transition core of about 8 jet diameters. An equation was developed by De Michele et al. (1976) to predict the length of potential core:

$$\frac{L_{core}}{d_0} = \frac{2.64}{\log \rho_B / \rho_g} \tag{5.46}$$

As for turbulent jets in conventional fluids, jets in fluidized beds have a "potential" core within which gas momentum, temperature and composition are the same as at the mouth of the orifice. As seen in Figure 5.10, Merry suggested the majority of entrainment occurrsin the potential core region (Merry, 1971).
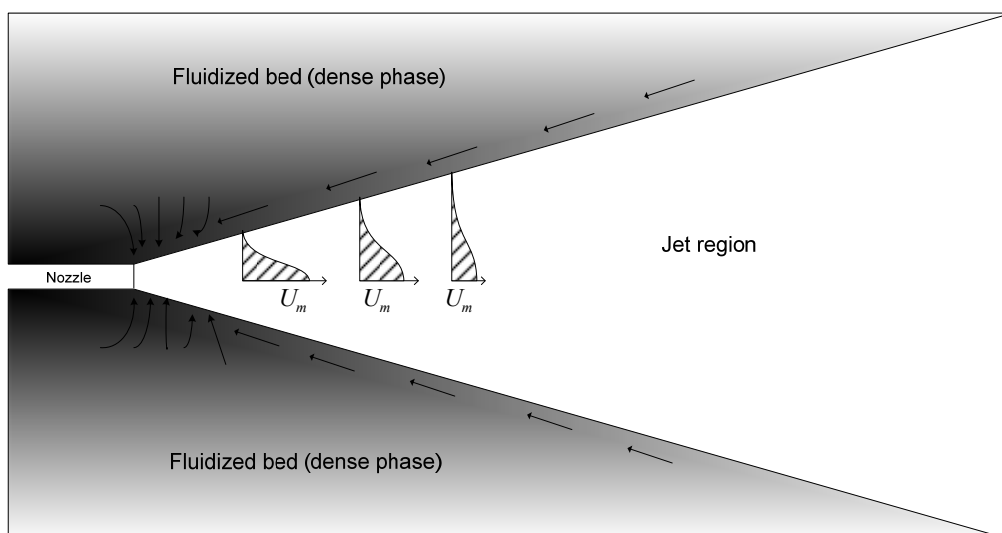
Figure 5.10 Solid entrainment track in the injection region (adapted from Merry, 1971)

According to the study by McMillan et al. (2007b), the entrained particles in the jet are accelerated by the supersonic jet, and these particles would collide with slow velocity particles near the jet boundary layer. Since the convergent-divergent nozzles demonstrate higherefficiency than a regular nozzle, they require less steam to achieve the same attrition rate (McMillan et al., 2007a).
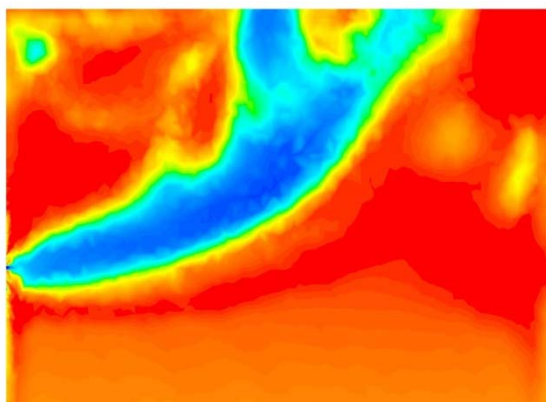
Figure 5.11 The jet geometry of convergent-divergent nozzles in fluidized beds (high gas flowrate)
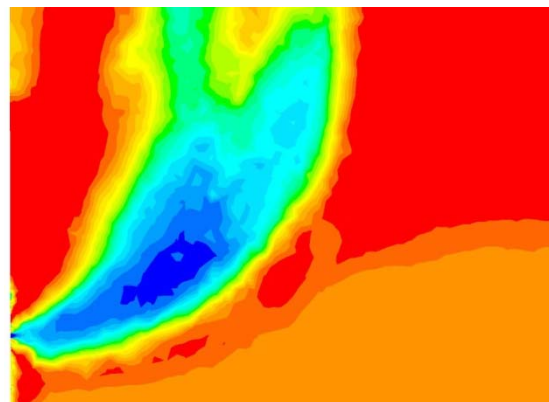
Figure 5.12 The jet geometry of convergent-divergent nozzles in fluidized beds (low gas flowrate)
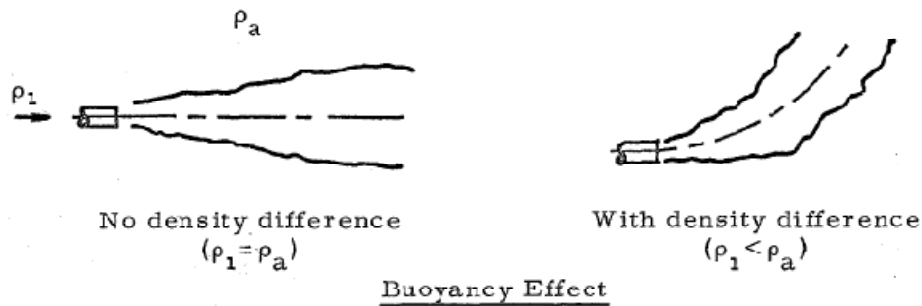
Figure 5.13 Buoyancy effect on jet geometry in a fluidized bed

There are some key assumptions for the analysis of the jet characteristics of the convergent-divergent nozzles in fluidized beds:

- The two-phase fluidized bed is assumed to have a specific steady density.

- The turbulent jet into a fluidized bed is fully developed.

- The fluids are incompressible

- The two phases gas-solids system is integrated as a continuous phase with a uniform density in the bed

Due to the high momentum of convergent-divergent nozzles and to the lower density of the jet compared with the bed itself, the performance of a supersonic jet in the bed is similar to a buoyant jet in a stagnant uniform environment. The simulation results of a supersonic jet in a fluidized bed can be seen in Figures 5.11 and 5.12, with higher gas flowrate and lower gas flowrate, respectively. It can be seen that the jets are issuing horizontally from the tip of nozzles horizontally. The jet axis eventually is deflected upwards because of the increase of vertical momentum flux due to the action of the buoyancy force. The cause of this buoyancy force is the differential density between the jet fluid and the bed, as shown in Figure 5.13.

5.6.2   Correlation to predict the jet penetration

Yang and Keairns (1978) first suggested that a two-phase Froude number, defined as $(\rho_f U_j^2)/(\rho_s - \rho_f)g d_0$, could be used to predict the jet penetration length. Benjelloun et al. (1991) used the Froude number to describe the relationship between the jet momentum and the forces of gravity acting on the jet:

$$\frac{L_j}{d_o} = f\left(\frac{Fr}{(1-\varepsilon)}\right) \tag{5.47}$$

$$Fr = \frac{\rho_g U_0^2}{(\rho_s - \rho_g)g} \tag{5.48}$$

Considering that the term of $(1-\varepsilon)$ in the correlation does not change significantly, they developed a new simple correlation with the Froude number to predict the penetration length of a horizontal nozzle:

$$\frac{L_j}{d_o} = 5.52 Fr^{0.27} \tag{5.49}$$

As described in the last section, a supersonic jet through a convergent-divergent nozzle in a fluidized bed can be assumed as a buoyant jet. Yang (1998) suggested that the length of jet penetration is depended on the two-phase Froude number based on the buoyancy theory of Turner (1973). The momentum flux at the jet, M_0 is given by:

$$M_0 = \frac{\pi}{4} d_0^2 U_0^2 \tag{5.50}$$

The buoyancy flux at the orifice, J, can be expressed as:

$$J_0 = \frac{\pi}{4} d_0^2 U_0 g\left(\frac{\rho_b}{\rho_f} - 1\right) \tag{5.51}$$

The characteristic length scale L, assumed here to be the jet penetration length, is expressed as:

$$\frac{L}{d_0} = \frac{M_0^{3/4}}{J^{1/2} d_0} = Fr^{0.5} \tag{5.52}$$

If a convergent-divergent nozzle is described as a turbulent jet, then the universal jet axial velocity profile is expressed (Abramovich, 1963):

$$u = u_m \left(1 - \xi^{1.5}\right)^2 \tag{5.53}$$

where

$$\xi = \frac{y}{b} \tag{5.54}$$

In the work by Fan (1969), the velocity profile of a supersonic jet is described as Gaussian distribution:

$$u = u_m e^{-r^2/b^2} \tag{5.55}$$

where $\sqrt{2}b$ is defined to be the nominal half width of the jet, r is the diameter of the jet. The profiles of density deficiency respecting to the ambient density are assumed to obey the Gaussian distribution:

$$\frac{\rho_a - \rho}{\rho_0} = \left(\frac{\rho_a - \rho_m}{\rho_0}\right) e^{-r^2/(\lambda^2 b^2)} \tag{5.56}$$

where, λb is the characteristic length of the profile; λ^2 is the turbulent Schmidt number which is assumed to be constant and is larger than 1 (Fan, 1969).

If the rate of entrainment is proportional to the local velocity (Fan, 1967), u_m, then the equation of continuity is expressed as:

$$\frac{d}{ds} \int_0^{2\pi} \int_0^{\infty} u r \, dr \, d\varphi = 2\pi \alpha b u_m \tag{5.57}$$

The left-hand side can be integrated from Eq. 5.62, then,

$$\frac{d}{ds}(u_m b^2) = 2\alpha b u_m \tag{5.58}$$

The x-momentum flux should be conserved:

$$\frac{d}{ds} \int_0^{2\pi} \int_0^{\infty} \rho u(u \cos\theta) r \, dr \, d\varphi = 0 \tag{5.59}$$

$$\frac{d}{ds}(\frac{u^2 b^2}{2} \cos\theta) = 0 \tag{5.60}$$

The y-momentum flux should be conserved:

$$\frac{d}{ds}\int_0^{2\pi}\int_0^{\infty}(\rho uu\sin\theta)rdrd\varphi = g\int_0^{2\pi}\int_0^{\infty}(\rho_a-\rho)rdrd\varphi \tag{5.61}$$

$$\frac{d}{ds}(\frac{u^2b^2}{2}\sin\theta) = g\lambda^2b^2\frac{\rho_0-\rho}{\rho} \tag{5.62}$$

Fan (1969) final proposed a formula to predict the x/d:

$$X_j/d_0 = \alpha\cdot Fr^{0.4} \tag{5.63}$$

Therefore, the hypothesis of buoyant jet and Gaussian distribution of velocity profile is useful to justify why the penetration length of a horizontal supersonic nozzle can be predicted by the Froude number.

5.6.3   Effect of fluidization velocity on the jet penetration

In the subsequent work, jet penetration lengths were predicted by the simulation model and validated by experimental results by Li et al. (2010b). Figure 5.14 illustrates the different penetration lengths with various attrition pressures through the jets but under the same other operation conditions by the present simulation model. The jet penetration in bed simulation is defined as the distance from the nozzle tip to the end of jet cavity, where solids volume fraction ε is more than 0.20, as shown in Figure 5.15.
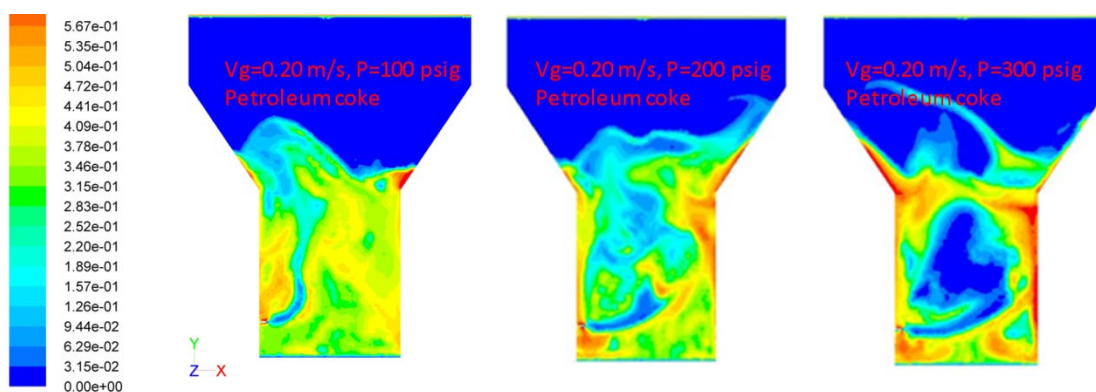
Figure 5.14 Penetration length measurement using the contour of solids volume fraction in fluidized beds (2.4mm nozzle)
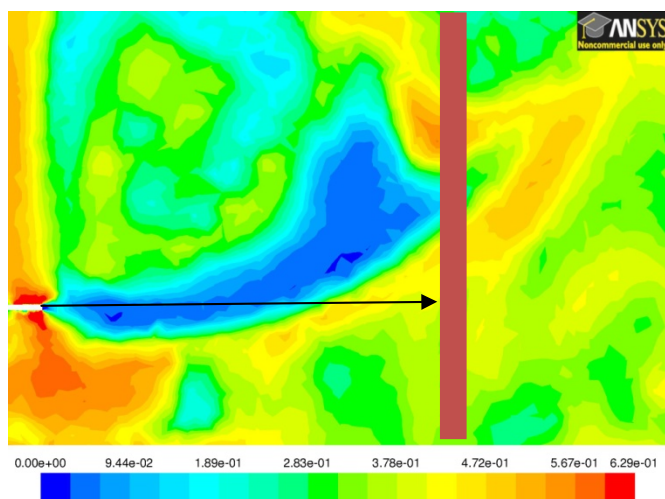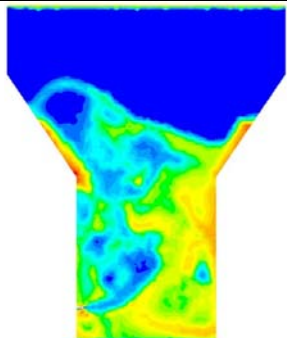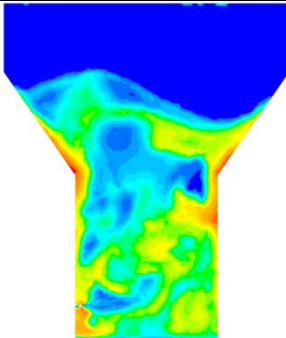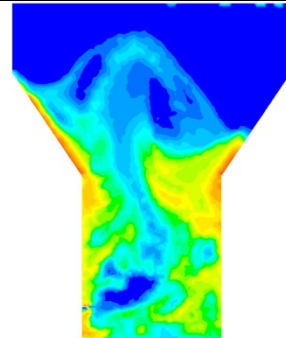
Figure 5.15 Definition of penetration length in simulation work

The influence of gas fluidization velocity on the jet penetration is shown in Table 5.7. Obviously, the gas fluidization velocity has a small effect on the jet penetration length, however, the influence on the bed expansion and bed solid voidage is shown clearly. The simulation result agrees with the experimental data reported by Li et al. (2010b) that the fluidization velocity has a minimum influence on the jet penetration length.

Table 5.7 Effect of fluidization velocity on the jet penetration

	Vg=0.10m/s	Vg=0.20m/s	Vg=0.30m/s
Volume fraction			
Penetration length(m)	0.265	0.260	0.255
Bed height	0.80	0.85	0.88

5.6.4   Effect of bed temperature

Figure 5.16 illustrates the effect of bed temperature on the jet penetration. It is seen that the operating temperature has a small influence on the jet penetration. The simulation results show a good agreement with the experimental results by Li et al. (2010b), indicating that the bed temperature has a minimum influence on the jet penetration length.
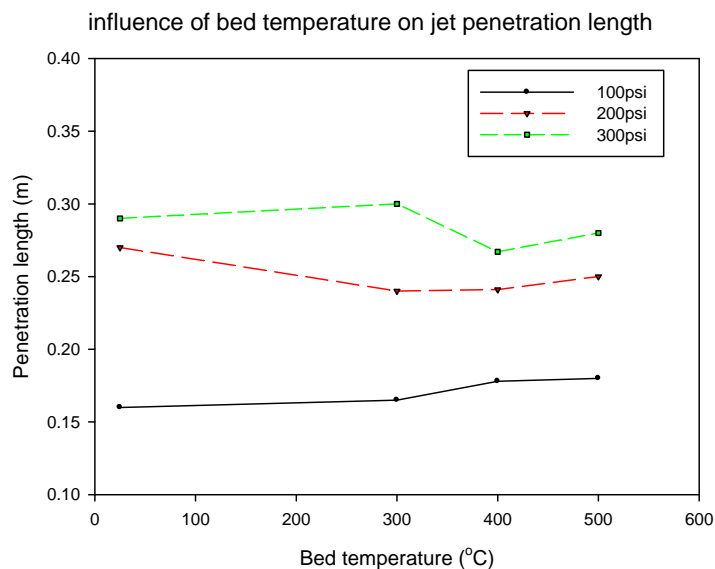
Figure 5.16 Influence of bed temperature on jet penetration length

5.6.5   Jet penetration length of convergent-divergent nozzle

In order to study the jet-induced attrition process in a fluidized bed, knowing the penetration depth of the high velocity jets is important to maximize their attrition efficiency and avoid the erosion of fluidized bed internals, because most of a particles attrition and collision occur in the void area of the horizontal jets in fluidized beds, especially at the tip of the cavity (McMillan et al., 2007b).   Abramovich (1963) developed a submerged jet model. This model has been adapted to fluidized beds of fine particles by De Michele et al. (1976). Many studies confirmed that this model gives a good explanation of momentum, energy, and mass transfers (Behie et al., 1970, and 1975; Hong et al., 1997).

Li et al. (2010a) investigated the penetration length of convergent-divergent nozzles in a fluidized bed at high temperature and found that the empirical correlations listed in Table 5.1 are unable to predict the experimental data at high temperature. This is probably because all these correlations were developed using data collected with low velocity, subsonic straight nozzles at room temperature.   Correlations from both Merry and Yates overestimated the jet penetration length, whereas Hong's correlation shows predicted values that are smaller than experimental results. Only the predictions from the Benjelloun's correlation, based on a two-phase Froude number $\left(\rho_f U_j^2\right)/\left(\rho_s - \rho_f\right)g d_0$, are in relatively good agreement with the measurements. The Froude number has been used

in the empirical correlations of Merry, Benjelloun (1991), and Ariyapadi (2003). Li et al. (2010a) proposed a new empirical correlation based on experimental data collected from supersonic nozzles discharging into hot fluidized beds:

$$\frac{L_{jet}}{d_o} = \alpha \left(\frac{\rho_0 U_0^2}{(\rho_p - \rho_f)gd_0} \right)^{\beta}$$

(5.64)

where both α and β vary according to the particle type and the bed temperature.

Table 5.8 summarizes the penetration length results for simulation work. Figure 5.17 and Figure 5.18 show that jet penetration lengths predicted from the attrition model agree well with the experimental data and predictions of Li's correlation.

Table 5.8 Summary of part predicted results from the numerical model

L_j/d_0	Simulation Model	Li's Correlation	Experimental
case 1	42	44	40
case 2	66	62	65
case 3	70	76	71
case 4	45	44	43
case 5	55	62	59
case 6	60	76	65
case 7	59	34	46
case 8	70	51	65
case 9	75	66	71
case 10	60	38	41
case 11	56	52	55
case 12	70	58	60
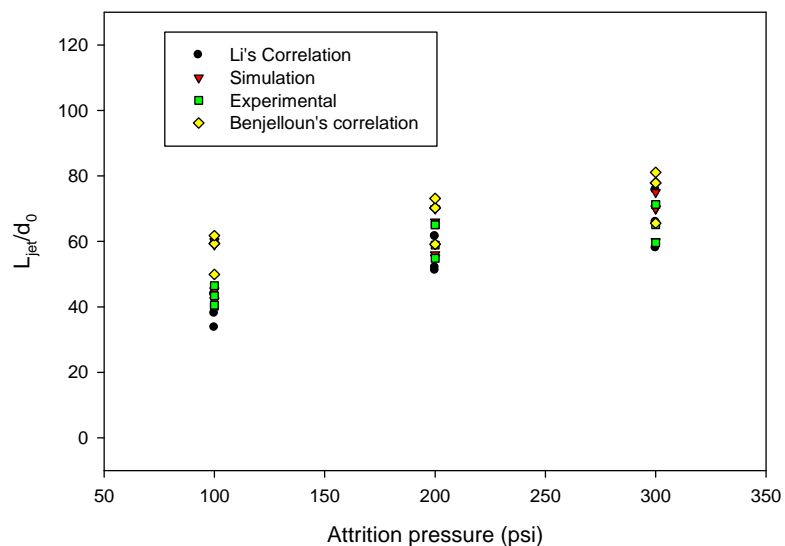
Figure 5.17 Comparison of experimental data and simulation results of the jet penetration lengths for convergent-divergent nozzles at high temperature
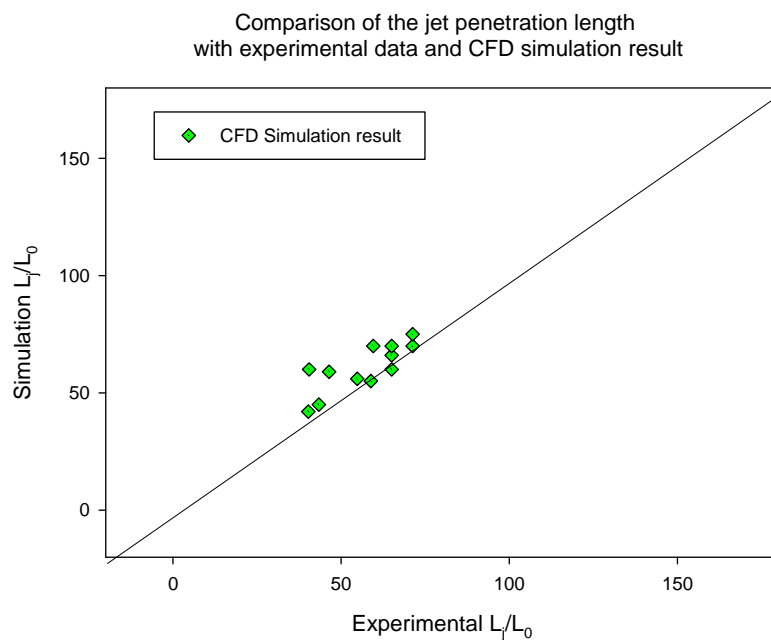
Figure 5.18 CFD simulation model for jet penetration in a high temperature bed.

5.7 Conclusion

A three-dimensional numerical model was developed to simulate a horizontal convergent-divergent attrition nozzle in a high temperature fluidized bed. The simulation model was optimized with adjustments of drag laws, heat transfer coefficients, and turbulent modes. The predicted results of jet penetration lengths are in very good agreements with the

experimental data and the predictions of Li's correlation. The simulation results have also demonstrated that the fluidization velocity and bed temperature have a little influence on jet penetration length. Finally, the hypothesis was proposed that the behavior of a horizontal convergent-divergent nozzle is similar to an inclined buoyant jet in a uniform stagnant environment. The velocity and density profiles follow the Gaussian function distributions.

5.8 Acknowledgements

5.9 **Notation**

a	Surface area of particles
A	Area of nozzle exit (m^2)
A*	Area of nozzle throat (m^2)
b	Radius of jet region (m)
C_D	Drag coefficient
c_p, c_v	Heat capacity at constant pressure, volume (J/kg·K)
d	Diameter (m)
d_0	Diameter of nozzle (m)
d_p	Particle diameter (m)
d_s	Diameter of solid (m)
D	Characteristic length
e_{ss}	Coefficient of restitution
f	Breakage frequency ($1/m^3$·s)
g	Gravity constant (m/s^2)
$g_{0,ss}, g_0$	Radial distribution function
G	Mass flux (kg/m^2s)
G_b	Generation of turbulence kinetic energy due to buoyancy
G_k	Generation of turbulence kinetic energy due to the mean velocity
h	Heat transfer coefficient (W/M^2·K)
H	Bed height at operating conditions (m)
H_{mf}	Bed height at minimum fluidization (m)
L	Particle diameter (m)
L_j	Jet penetration length (m)
L_{core}	Length of the jet potential core (m)
J_0	Buoyancy flux at the orifice
k	Thermal conductivity
K_{sl}, K_{ls}	Fluid-solid exchange coefficient
K_{gs}	Gas-solid exchange coefficient
$k_{\Theta_s} \nabla \Theta_s$	Diffusion of energy
m	Mass (g, kg)
m	Mass (g, kg)
$\dot{m}$	Mass flow rate (kg/s)

M	Mach number
M_0	Momentum flux at the jet
M_w	Molar weight (kg/mol)
p	Pressure (Pa)
p_0	Upstream pressure of nozzle (Pa)
p_a	Ambient pressure of fluid (Pa)
p_s	Solid pressure
Pr	Prandtl number
Q	Flow rate of enthalpy (W)
q	Heat flux (W/m^2)
R	Ideal gas universal constant
Re	Reynolds number
S	Total entropy (J/K)
T_0	Absolute temperature at nozzle throat (K)
T	Absolute temperature at nozzle exit(K)
t	Time (s)
u, v, w	Velocity (m/s)
u_m	Jet velocity along x-axis (m/s)
u_{mf}	Minimum fluidization velocity (m/s)
u_g	Bed fluidization velocity (m/s)
v	Impact velocity (m/s)
U_0	Gas velocity at nozzle exit (m/s)
U_m	Gas velocity on jet axis (m/s)
U_{mf}	Minimum fluidization velocity (m/s)
V_g	Fluidization velocity (m/s
$v_{r,s}$	The terminal velocity correlation for the solid phase
y	Radial distance from jet axis (m) (Eq. 5.61)
Y_M	Contribution of the fluctuating dilatation in compressible turbulence to the overall dissipation rate

Greek letters

α	Volume fraction
α	Correlation Constant (Eq. 5.71)

β	Correlation Constant (Eq. 5.71)
γ	Ratio of specific heats
γ_{Θ_s}	Collisional dissipation of energy
δ	Bed expansion ratio
ε	Volume fraction
ε	Turbulent dissipation rate (m^2/s^3)
η	Grinding efficiency
θ	Angle of inclination of the jet axis (with respect ot x-axis)
Θ_s	Granular temperature
λ^2	Turbulent Schmidt number (Eq. 5.63)
λb	The characteristic length (m) (Eq. 5.63)
λ_q	Bulk viscosity
λ_s	Bulk Viscosity
μ	Dynamic viscosity (Pa-s)
μ_q	Shear viscosity
$\mu_{s,kin}$	Kinetic Viscosity
$\mu_{s,fr}$	Frictional viscosity
ξ	The dimensionless ratio (y/b)
τ_s	Particle relaxation time (Eq. 7.5)
$\overline{\overline{\tau_q}}$	Stress-strain tensor
ρ	density (kg/m3)
ρ_B	Bed density (kg/m3)
ρ_f	Density of fluid in bed (kg/m3)
ρ_p	Particle density (kg/m3)
ρ_s	Particle density (kg/m3)
σ	Turbulent Prandtl number
ϕ	Angle of internal friction

ϕ_{ls} Energy exchange between the gas phase and the solid phase

φ Angular coordinate on a cross section normal to the jet axis

5.10 **References**

Abramovich, G. N., *The Theory of Turbulent Jets*. Leon H. Schinder ed.; M.I.T. Press: Cambridge, Mass., 1963.

ANSYS, ANSYS FLUENT 12.0 User's Guide. April 2009 ed.; ANSYS, Inc.: 2009a.

Ariyapadi, S.; Berruti, F.; Briens, C.; Griffith, P.; Hulet, C., Modeling the injection of gas-liquid jets into fluidized beds of fine particles. *Canadian Journal of Chemical Engineering* **2003,** *81* (3-4), 891-899.

Behie, L. A.; Bergougn.Ma; Baker, C. G. J.; Bulani, W., Jet Momentum Dissipation at a Grid of a Large Gas Fluidized Bed. *Canadian Journal of Chemical Engineering* **1970,** *48* (2), 158-&.

Behie, L. A.; Bergougnou, M. A.; Baker, C. G. J., Heat-Transfer from a Grid Jet in a Large Fluidized-Bed. *Canadian Journal of Chemical Engineering* **1975,** *53* (1), 25-30.

Benjelloun, F. V., J. In *Determination des longueurs de jets de gaz horizontaux dans des lits fluidises*, textes des communications presentees a l'occasion des 6emes journees europeenenes sur la fluidisation, Toulouse, Laguerie, C. G., P., Ed. Toulouse, 1991.

Bentham, A. C.; Kwan, C. C.; Boerefijn, R.; Ghadiri, A., Fluidised-bed jet milling of pharmaceutical powders. *Powder Technology* **2004,** *141* (3), 233-238.

Bird, R. B. B.; Warren E. Stewart; Lightfoot, E. N., *Transport phenomena*. John Wiley & Sons, Inc: New York : , c2007. , 2002.

Boemer, A.; Qi, H.; Renz, U., Verification of Eulerian simulation of spontaneous bubble formation in a fluidized bed. *Chemical Engineering Science* **1998,** *53* (10), 1835-+.

Chen, J. C.; Grace, J. R.; Golriz, M. R., Heat transfer in fluidized beds: design methods. *Powder Technology* **2005,** *150* (2), 123-132.

Chiesa, M.; Mathiesen, V.; Melheim, J. A.; Halvorsen, B., Numerical simulation of particulate flow by the Eulerian-Lagrangian and the Eulerian-Eulerian approach with application to a fluidized bed. *Computers & Chemical Engineering* **2005,** *29* (2), 291-304.

Cornelissen, J. T.; Taghipour, F.; Escudi, R.; Ellis, N.; Grace, J. R., CFD modelling of a liquid-solid fluidized bed. *Chemical Engineering Science* **2007,** *62* (22), 6334-6348.

Cui, M. P.; Straatman, A. G.; Zhang, C., A Computational Study of Gas-solid Flow in an Enhanced Solid Entrainment (ESE) Nozzle System. *International Journal of Chemical Reactor Engineering* **2005,** *3*, Article A7.

Davies, J. T., *Turbulence phenomena; an introduction to the eddy transfer of momentum, mass, and heat particularly at interfaces*. Academic Press: New York, 1972.

De Michele, G.; Elia, A.; Massimilla, L., Interaction between Jets and Fluidized-Beds. *Quaderni Dell Ingegnere Chimico Italiano* **1976,** *12* (6), 155-162.

Ding, J.; Gidaspow, D., A Bubbling Fluidization Model Using Kinetic-Theory of Granular Flow. *Aiche Journal* **1990,** *36* (4), 523-538.

Dunlop, D. D.; Griffin, J. L. I.; Moser, J. J. F., Particle size control in fluid coking. *Chemical Engineering Progress* **1958,** *54* (8), 39-42.

Ergun, S.; Orning, A. A., Fluid Flow through Randomly Packed Columns and Fluidized Beds. *Industrial & Engineering Chemistry* **1949,** *41* (6), 1179-1184.

Fan, L.-N. *Turbulent buoyant jets into stratified or flowing ambient fluids*; **CaltechKHR:KH-R-15**; California Institute of Technology: Pasadena, CA. , June 1967, 1967.

Fan, L.-N.; Brooks, N. H. *Numerical solutions of turbulent buoyant jet problems*; CaltechKHR:KH-R-18; California Institute of Technology: Pasadena, California, 1969.

Gidaspow, D., *Multiphase flow and fluidization : continuum and kinetic theory descriptions*. Academic Press: Boston, 1994; p xx, 467 p.

Gunn, D. J., Transfer of heat or mass to particles in fixed and fluidised beds. *International Journal of Heat and Mass Transfer* **1978,** *21* (4), 467-476.

Hong, R. Y.; Guo, Q. J.; Luo, G. H.; Zhang, J. Y.; Ding, J., On the jet penetration height in fluidized beds with two vertical jets. *Powder Technology* **2003,** *133* (1-3), 216-227.

Hong, R. Y.; Li, H.; Maoyu, C.; Jiyu, Z., Numerical simulation and verification of a gas-solid jet fluidized bed. *Powder Technology* **1996,** *87* (1), 73-81.

Hong, R. Y.; Li, H. Z.; Li, H. B.; Wang, Y., Studies on the inclined jet penetration length in a gas-solid fluidized bed. *Powder Technology* **1997,** *92* (3), 205-212.

Hulet, C.; Briens, C.; Berruti, F.; Chan, E. W., Effect of a shroud on entrainment into a submerged jet within a fluidized bed. *Chem. Eng. Process.* **2008,** *47* (9-10), 1435-1450.

Li, F.; Briens, C.; Berruti, F.; McMillan, J. In *Study of solids entrainment into attrition jets in fluidized beds*, Fluidization XIII, Gyeong-ju, Korea, Kim, S. D.; Kang, Y.; Lee, J. K.; Seo, Y. C., Eds. Engineering Conferences International: Gyeong-ju, Korea, 2010a; pp 201-208.

Li, F.; Briens, C.; Berruti, F.; McMillan, J. In *Penetration of high velocity horizontal gas jets into a fluidized bed at high temperature.*, Fluidization XIII, Gyeong-ju, Korea, 2010; Kim, S. D.; Kang, Y.; Lee, J. K.; Seo, Y. C., Eds. Engineering Conferences International: Gyeong-ju, Korea, 2010b; pp 893-900.

Li, T.; Pougatch, K.; Salcudean, M.; Grecov, D., Numerical simulation of horizontal jet penetration in a three-dimensional fluidized bed. *Powder Technology* **2008,** *184* (1), 89-99.

Li, T.; Pougatch, K.; Salcudean, M.; Grecov, D., Numerical simulation of single and multiple gas jets in bubbling fluidized beds. *Chemical Engineering Science* **2009,** *64* (23), 4884-4898.

Liepmann, H. W., *Elements of gasdynamics*. John Wiley & Sons, Inc. : New York, 1957.

McMillan, J.; Briens, C.; Berruti, F.; Chan, E., High velocity attrition nozzles in fluidized beds. *Powder Technology* **2007a,** *175* (3), 133-141.

McMillan, J.; Briens, C.; Berruti, F.; Chan, E., Particle attrition mechanism with a sonic gas jet injected into a fluidized bed. *Chemical Engineering Science* **2007b,** *62* (14), 3809-3820.

Merry, J. M. D., Penetration of a Horizontal Gas Jet into a Fluidised Bed. *Transactions of the Institution of Chemical Engineers and the Chemical Engineer* **1971,** *49* (4), 189.

Perry, R. H. G., Don W.; et al. , Perry's chemical engineers' handbook. -- McGraw-Hill's Access Engineering 8th ed.; Don W. Green, a. l. e., Robert H. Perry, Ed. McGraw-Hill: New   York, 2008. http://www.accessengineeringlibrary.com/html/viewbookdetails.asp?catid=B&bookid=200139d8.

Ranz, W. E., Friction and transfer coefficients for single particle and packed beds. *Chem Eng Progress* **1952,** *48* (5), 247-253.

Shakhova, N. A., Discharge of turbulent jets into a fluidized bed. *Inzhenerno-Fizicheskii Zhurnal* **1968,** *14* (1), 61-69.

Smith, J. M.; Van Ness, H. C.; Abbott, M.; Van Ness, H., *Introduction to Chemical Engineering Thermodynamics*. McGaw-Hill: 2005.

Syamlal, M.; O'Brien, T. J. *The Derivation of a Drag Coefficient Formula from Velocity–Voidage Correlations*; 1987.

Taghipour, F.; Ellis, N.; Wong, C., Experimental and computational study of gas-solid fluidized bed hydrodynamics. *Chemical Engineering Science* **2005,** *60* (24), 6857-6867.

Truner, J. S., *Buoyancy Effects in Fluids*. Cambridge University Press: New York, 1973.

Tyler, J.; Mees, P., Using CFD to model the interaction of a horizontal feed jet on fluidized bed hydrodynamics, , (1999), pp. 113–117. In *Second International Conference on CFD in the Minerals and Process Industries,CSIRO*, Melbourne, Australia, 1999; pp 113-117.

Vejahati, F.; Mahinpey, N.; Ellis, N.; Nikoo, M. B., Cfd Simulation of Gas-Solid Bubbling Fluidized Bed: a New Method for Adjusting Drag Law. *Canadian Journal of Chemical Engineering* **2009,** *87* (1), 19-30.

Yang, W.-c., *Handbook of fluidization and fluid-particle systems*. Marcel Dekker: New York, 2003; p 861.

Yang, W. C., *30-years of industrial research on fluidization - Bridging the gap between theory and practice*. United Engineering Foundation: New York, 1998; p 31-43.

Yang, W. C.; Keairns, D. L. In *Design and operating parameters for a fluidized bed agglomerating combustor/gsifier*, Fluidization, Cambridge University Press: 1978.

Yates, J. G.; Cobbinah, S. S.; Cheesman, D. J.; Jordan, S. P. In *Particle attrition in fluidized beds containing opposing jets*, New York, NY, USA, Publ by AIChE: New York, NY, USA, 1991; pp 13-19.

Zenz, F. A., Bubble Formation and Grid Design. *Inst. Chem. Eng. Symp.* **1968,** *30*, 136-139.

Zucker, R. D.; Biblarz, O., *Fundamentals of gas dynamics*. John Wilery & Sons, INC: 2002.

Chapter 6

6   Numerical Simulation of Particle Attrition with Convergent Divergent Nozzles in High Temperature Fluidized Beds

6.1 Abstract

Attrition process is a critical step in the fluid coking process to control the particle size distribution in a system. Previous studies have shown that some particle and bed properties affect jet-induced particle attrition in a fluidized bed. Because of the multiphase interactions and the complex flow behavior in both the bed and jet, it is desirable to develop a numerical model for the attrition process that combines theoretical and experimental approaches. This paper presents such a model, which is an Eulerian-Eulerian multiphase model coupled with a population balance method. Particle-particle interactions are described with the kinetic theory of granular flow (KTGF). The model is solved using the discrete method and the quadrature method of moments. The adjustable parameters of the model were determined from experimental data. It is found that the best prediction was obtained using the Ghadiri breakage kernel, the Diemer-Austin generalized daughter size distribution function, and the discrete solution method.

6.2 **Introduction**

The fluid coking process is a popular approach to upgrade heavy oil to light synthetic crude oil for transporting and processing in existing conventional refineries. During the fluid coking process, thermal cracking reactions take place inside fluidized bed reactors, where hot coke provides the heat for endothermic cracking reactions of the feed to vapor products and coke.

It is desirable to maintain the size distribution of the coke particles within a well-defined range, since particles that are either too large or fine will result in slugging or poor fluidization. A series of attrition nozzles are, therefore, used to control the coke particle size, with high pressure, high velocity, and superheated steam. Maintaining the required attrition rate of the coke particles with lower steam consumption would reduce energy consumption, increase the reactor throughput, and reduce sour wastewater volumes.

Many studies have been carried out on particle attrition in fluidized beds. The mechanism proposed for particle attrition in fluidized beds includes thermal, chemical, kinetic and static mechanical stresses (Vaux and Keairns, 1980). In the case of bubbling fluidized beds, sources of particle attrition were identified as grid jets attrition, gas bubbles and cyclones. Bemrose and Bridgwater (1987) stated that particle attrition is affected by a great many variables, mostly influenced by particle and fluidized beds properties. Gwyn (1969) reported that both the average particle size and the spread of the initial size distribution affect the attrition rate.

More recently, a number of papers have been published about the jet-induced particle attrition in fluidized bed, using subsonic jets. De Michele et al. (1976) developed the turbulent jetting region and jet model for axisymmetric jets in fluid beds, which is based on the extension of the theory of turbulent, submerged jets to the injection of gas in fluidized beds. Merry proposed that the majority of entrainment occurs near the nozzle tip in the potential zone region (Merry, 1971). Bentham et al. (2004) asserted that the particle breakage mechanism of subsonic jets involves the particles entrained in the jet. Werther and Xi (1993) found that high velocity gas jets create high attrition rates. In addition, they developed an attrition model in which the attrition rate is proportional to $\rho_0 d_0{}^2 u_0{}^3$, which denote jet gas density, orifice diameter, and nozzle exit velocity respectively. Most of the

correlations for the attrition rate use a power law function of the nozzle exit velocity, as shown in Table 6.1.

Table 6.1 Correlations to predict particle attrition rate with subsonic jets.

Model equation	Operating conditions	Authors
$R = C \cdot S \cdot \dfrac{\rho_0 Q (\beta u_0)^2}{W d_p \rho_p}$ (6.1)	u_0 = 25-300 m/s, 142-274μm iron ore, 3940kg/m^3; lignite char, 1250 kg/m^3	Chen et al., 1980
$R = C \rho_0 d_0^2 u_0^3$ (6.2)	u_0 =25-100 m/s; FCC: 106μm, 1500 kg/m^3; catalyst HA-HPV: 125 μm, 650 kg/m^3.	Werther and Xi, 1993
$R = C d_0^n u_0^m$ (6.3) n: 0.6-0.76 for FCC; 0.44-1.11 for NaCl m: 3.31 for FCC; 5.1 for NaCl	u_0 =25-125 m/s; FCC: 425-600 μm NaCl: 90-106 μm	Ghadiri et al., 1994
$R = C(u_0 \sqrt{\rho_0})^{2.5} \dfrac{\pi d_0^2}{4}$ (6.4)	u_0 =33-303 m/s, Silica-Alumina FCC Catalyst	Zenz and Kelleher, 1980

Recent studies have focused on convergent-divergent nozzles with sonic or supersonic velocities. McMillan et al. (2007a) found that nozzle scale, gas properties, and bed properties, had a significant effect on the grinding efficiency. The grinding efficiency is defined as the increasing particle surface area per mass of attrition gas. To predict the grinding efficiency, a correlation was developed and expressed as:

$$\eta = 7.81 \times 10^{-7} \alpha \beta d_0^{1.131} u_o^{0.55} (\rho_0 u_{sound,eq}^2)^{1.635} \left(\frac{u_0 - u_{mf}}{u_{mf}} \right)^{0.494} \tag{6.5}$$

where α and β are coefficients that depend on particles properties and nozzle geometry, respectively.

Moreover, an attrition model was developed by McMillan et al. (2007b) to predict the particle breakage frequency and daughter particle size distribution. Cruz et al. (2010) argued that the grinding efficiency is dependent on the thrust and equivalent velocity of the supersonic nozzle. The experimental data also suggested that the geometry of the attrition nozzle has a large impact on the grinding efficiency (Cruz, 2009). Meanwhile, more research work has focused on particle attrition at high temperature, since more

commercial applications of particle attrition and supersonic jets are conducted at high temperature (Li et al., 2010a, c). The results demonstrate that the operating temperature has a significant influence on the particle grinding efficiency, especially at high attrition gas velocities.

On the other hand, numerical models of the particle attrition or breakage have been developed by several research groups. In order to study the fundamental mechanism of jet-induced particle attrition in fluidized beds at high temperature, it is desired to consider the change of particle size distribution, in addition to momentum, mass, and energy balances. The population balance method, therefore, is introduced in the present study, because it represents the most fundamental method for simulating particle dynamics in a multiphase system. Hulburt and Katz (1964) firstly proposed the idea of the population balance. Randolph and Larson (1988) developed a population balance theory in particulate processes with associated mass, momentum, and energy transportations. Ramkrishna (2000) developed the concepts of population balance model on a variety of issues. The population balance equation consists of "external" coordinates and "internal" coordinates, which refer to its physical site and the internal attributes of the entity, respectively (Ramkrishna, 2000). Population balance equations can be used to model the evolution of particulate and other dispersed-phase systems (Randolph and Larson, 1988). The population balance model can take in account particle growth, aggregation, breakage and nucleation, when coupled with CFD. On the other hand, with the rapid development of computational ability, CFD has been emerged as a very useful tool in simulating and understanding the hydrodynamics of multiphase reactors. When numerical simulation work couples Euler-Euler multiphase model with the population balance method, it becomes a promising approach in simulating and evaluating the process of particle attrition.

The main objective of this part of the research is to develop an attrition model to describe the mechanisms of particle attrition with convergent-divergent nozzles in a fluidized bed at high temperature. Meanwhile, with coupling the population balance method with CFD simulation, the model for jet-induced particle attrition in fluidized beds based on CFD-PDM will be validated and modified with experimental data.

6.3 **Numerical approaches**

6.3.1   **Modeling of fluidized bed reactor with the Eulerian-Eulerian multiphase model (Ansys, 2009b, 2009c)**

Two different approaches have been taken in the numerical calculation of multiphase fluids: the Eulerian-Lagrangian approach and the Eulerian-Eulerian approach. The Eulerian-Lagrangian approach treats the gas phase as a continuous phase and calculated with Navier-Stokes equations, while the solids phase is solved as a discrete phase. On the contrary, the Eulerian-Eulerian approach solves all phases in system as a continuum. Chiesa et al. (2005) found that the Eulerian-Lagrangian approach agrees well with the experimental results compared the Eulerian-Eulerian approach. The major disadvantage of the Eulerian-Lagrangian approach is its numerical cost. In their study, the CPU time needed for Eulerian-Lagrangian approach is usually four orders of magnitude higher than the time needed for Eulerian-Eulerian approach. The kinetic theory of granular flow (KTGF) can be used to describe particle interactions in a bubbling fluidized bed where particles are in random motion state and can collide with other particles in binary collisions (Ding and Gidaspow, 1990; Gidaspow, 1994). The particles in a gas-solid system can be solved as a continuous fluid by the Eulerian-Eulerian approach when the particle properties are described with KTGF (Boemer et al., 1998). Therefore, the Eulerian-Eulerian model and KTGF are adopted in the present work.

6.3.1.1   **Conservation of Mass**

Since there is no mass transfer between the gas and solid phases, the continuity equation for two phases is:

$$\frac{\partial}{\partial t}(\varepsilon_q \rho_q) + \nabla(\varepsilon_q \rho_q \vec{u}_q) = 0$$

(6.6)

6.3.1.2   **Conservation of Momentum**

The momentum equation for two phases is:

$$\frac{\partial}{\partial t}(\varepsilon_s \rho_s \vec{u}_s) + \nabla(\varepsilon_s \rho_s \vec{u}_s \vec{u}_s) = -\varepsilon_s \nabla p + \nabla \cdot \overline{\overline{\tau}}_s + \varepsilon_s \rho_s \vec{g} +$$

$$\sum_{p=1}^{n} K_{ls}(\overline{u_l} - \overline{u_s})$$

(6.7)

where $\overline{\overline{\tau}}_q$ is the qth phase stress-strain tensor:

$$\overline{\overline{\tau}}_q = \varepsilon_q \mu_q (\nabla \vec{u}_q + \nabla \vec{u}_q^T) + \varepsilon_q (\lambda_q - \frac{2}{3}\mu_q) \nabla \cdot \vec{u}_q \overline{\overline{I}}$$

(6.8)

Here μ_q and λ_q are the shear and bulk viscosity of phase q.

$K_{ls}(=K_{sl})$ is the interphase momentum exchange coefficient, more details described at next section.

6.3.1.3 Fluid-Solid Momentum Transfer and Exchange Coefficient

The fluid-solid exchange coefficient K_{sl} can be expressed as:

$$K_{sl} = \frac{\varepsilon_s \rho_s f}{\tau_s}$$

(6.9)

where f is the drag coefficient function, defined for the various drag law model. τ_s is expressed as:

$$\tau_s = \frac{\rho_s d_s^2}{18\mu_l}$$

(6.10)

where d$_s$ is the diameter of the particle of phase s.

Syamlal-O'Brien model (Syamlal, 1987)

$$K_{gs} = \frac{3}{4}\frac{C_D}{v_{r,s}^2}\frac{\rho_g |\vec{v}_s - \vec{v}_g|}{d_s}\alpha_g \alpha_s$$

(6.11)

$$f = \frac{C_D Re_s \varepsilon_g}{24 v_{r,s}^2}$$

(6.12)

$$C_D = \left(0.63 + \frac{4.8}{\sqrt{Re_s/v_{r,s}}}\right)^2$$

(6.13)

$$Re_s = \frac{\rho_g d_s |\vec{v}_s - \vec{v}_g|}{\mu_g}$$

(6.14)

$$\upsilon_{r,s} = 0.5(A - 0.06\,\mathrm{Re}_s + \sqrt{(0.06\,\mathrm{Re}_s)^2 + 0.12\,\mathrm{Re}_s(2B - A) + A^2})$$

$$A = \alpha_g^{4.14}$$

(6.15)
$$B = \begin{cases} \varepsilon_g^{C1} & \varepsilon_g \geq 0.85 \\ C_2\varepsilon_g^{1.28} & \varepsilon_g < 0.85 \\ default\ value: \ C_1 = 2.65\ and\ C_2 = 0.8 \end{cases}$$

Wen and Yu model

$$K_{sl} = \frac{3}{4}C_D \frac{\alpha_s\alpha_l\rho_l|\vec{v}_s - \vec{v}_l|}{d_s}\alpha_l^{-2.65}$$

(6.16)

$$C_D = \frac{24}{\alpha_l\,\mathrm{Re}_s}\left[1 + 0.15(\alpha_l\,\mathrm{Re}_s)^{0.687}\right]$$

(6.17)

Gidaspow model

When $\alpha_g > 0.8$ then:

$$K_{sl} = \frac{3}{4}C_D \frac{\alpha_s\alpha_l\rho_l|\vec{v}_s - \vec{v}_l|}{d_s}\alpha_l^{-2.65}$$

(6.18)

where

$$C_D = \frac{24}{\alpha_l\,\mathrm{Re}_s}\left[1 + 0.15(\alpha_l\,\mathrm{Re}_s)^{0.687}\right]$$

(6.19)

When $\alpha_l \leq 0.8$ then:

$$K_{sl} = 150\frac{\alpha_s(1 - \alpha_l)\mu_l}{\alpha_l d_s^2} + 1.75\frac{\rho_l\alpha_s|\vec{v}_s - \vec{v}_l|}{d_s}$$

(6.20)

6.3.1.4   The conservation of Energy

$$\frac{\partial}{\partial t}(\varepsilon_q\rho_q h_q) + \nabla(\varepsilon_q\rho_q\vec{u}_q h_q) = -\varepsilon_q\frac{\partial p_q}{\partial t} + \overline{\overline{\tau}}_q : \nabla\vec{u}_q - \nabla\vec{q}_q + S_q +$$

$$\sum_{p=1}^{n}(Q_{pq} + \dot{m}_{pq}h_{pq} - \dot{m}_{qp}h_{qp})$$

(6.21)

In a fluidized bed, the heat transfer between particles and gas is more complex than in a fixed bed due to the motion of the suspended particles and gas bubbles (Chen, 2005). The

heat transfer in a fluidized bed involves three heat transfer mechanisms: gas-particle convection, particle-particle conduction, and particle radiation. The heat transfer coefficient of a bubbling fluidized bed is used for all three cases, with the surface area of particles as defined as:

$$h_p = \frac{Q}{A(T_p - T_g)} \tag{6.22}$$

A dimensionless Nusselt number, $Nu_p = h_p D / k$, indicates the relationship of the fluid thermal conductivity k and a characteristic length D that specific for each flow system (Bird et al, 2002). Ranz and Marshall (1952) presented a correlation to estimate the Nusselt number for heat transfer between fluid and particles in fixed beds:

$$Nu_p = 2 + 0.6 \, \mathrm{Re}_p^{0.5} \, \mathrm{Pr}_g^{0.33} \tag{6.23}$$

The Nusselt number correlation by Gunn (1978) is extended to describe the heat transfer for the fixed and fluidized beds. The Gunn correlation is applicable to granular flows with a porosity range of 0.35-1.0 and Reynolds number of up to 1×10^5 .

$$Nu = (7 - 10\alpha_f + 5\alpha_f^{\,2})(1 + 0.7 \, \mathrm{Re}_p^{0.2} \, \mathrm{Pr}^{1/3}) + (1.33 - 2.4\alpha_f + 1.2\alpha_f^{\,2}) \, \mathrm{Re}_p^{0.7} \, \mathrm{Pr}^{1/3} \tag{6.24}$$

In the present investigation, the Gunn correlation was used in all numerical simulation involving energy exchange.

6.3.1.5 Constitutive Equation

Solid pressure

The solid pressure is used to describe particle collisions:

$$p_s = \alpha_s \rho_s \Theta_s + 2\rho_s (1 + e_{ss})\alpha_s^{\,2} g_{0,ss} \Theta_s \tag{6.25}$$

where e_{ss} denotes the coefficient of restitution for particle collisions; $g_{0,ss}$ is the radial distribution function, and Θ_s is the granular temperature.

The radial distribution function is expressed as:

$$g_0 = \left[1 - \left(\frac{\alpha_s}{\alpha_{s,max}} \right)^{\frac{1}{3}} \right]^{-1} \tag{6.26}$$

Kinetic Viscosity

There are two options to predict the kinetic viscosity with FLUENT:

Syamlal et al:

$$\mu_{s,kin} = \frac{\alpha_s d_s \rho_s \sqrt{\Theta_s \pi}}{6(3 - e_{ss})} \left[1 + \frac{2}{5}(1 + e_{ss})(3e_{ss} - 1)\alpha_s g_{0,ss} \right]$$
(6.27)

Gidaspow et al:

$$\mu_{s,kin} = \frac{10 d_s \rho_s \sqrt{\Theta_s \pi}}{96 \alpha_s (1 + e_{ss}) g_{0,ss}} \left[1 + \frac{4}{5}\alpha_s g_{0,ss}(1 + e_{ss}) \right]^2 \alpha_s$$
(6.28)

Bulk Viscosity (Lun et al.)

$$\lambda_s = \frac{4}{3}\alpha_s d_s \rho_s g_{0,ss}(1 + e_{ss})\left(\frac{\Theta_s}{\pi}\right)^{1/2}$$
(6.29)

Frictional viscosity

In present work, Schaeffer's expression was used:

$$\mu_{s,fr} = \frac{p_s \sin\phi}{2\sqrt{I_{2D}}}$$
(6.30)

where p_s is the solids pressure, ϕ is the angle of internal friction, and I_{2D} is the second invariant of the deviatoric stress tensor.

Granular Temperature

$$\frac{3}{2}\left[\frac{\partial}{\partial t}(\rho_s \alpha_s \Theta_s) + \nabla \cdot (\rho_s \alpha_s \vec{v}_s \Theta_s) \right] = (-p_s \bar{I} + \bar{\tau}s) : \nabla\vec{v}_s + \nabla \cdot (k_{\Theta_s}\nabla\Theta_s) - \gamma_{\Theta_s} + \phi_{ls}$$
(6.31)

where

$(-p_s \bar{I} + \bar{\tau}s) : \nabla\vec{v}_s$ = the generation of energy by the solid stress tensor

$k_{\Theta_s}\nabla\Theta_s$ = the diffusion of energy

k_{Θ_s} = the diffusion coefficient

γ_{Θ_s} = the collisional dissipation of energy

ϕ_{ls} = the energy exchange in gas-solid phase

Diffusion coefficient of granular temperature

Syamlal-O'Brien:

$$k_{\Theta_s} = \frac{15 d_s \rho_s \alpha_s \sqrt{\Theta_s \pi}}{41(41 - 33\eta)} \left[1 + \frac{12}{5} \eta 2(4\eta - 3)\alpha_s g_{0,ss} + \frac{16}{15\pi}(41 - 33\eta)\eta \alpha_s g_{0,ss} \right]$$ (6.32)

Gidaspow:

$$k_{\Theta_s} = \frac{150 d_s \rho_s \sqrt{\Theta_s \pi}}{384(1 + e_{ss})g_{0,ss}} \left[1 + \frac{6}{5} \alpha_s g_{0,ss}(1 + e_s) \right]^2 + 2\rho_s \alpha_s^2 d_s (1 + e_{ss})g_{0,ss} \sqrt{\frac{\Theta_s}{\pi}}$$ (6.33)

Lun et al. (1984) developed the collisional dissipation of energy, expressed as:

$$\gamma_{\Theta m} = \frac{12(1 - e_{ss}^2)g_{0,ss}}{ds\sqrt{\pi}} \rho_s \alpha_s^2 \Theta_s^{3/2}$$ (6.34)

6.3.2   Modeling particle breakage with population balance method

The birth rate of particles of volume V due to breakage is given by:

$$B_{br} = \int_{\Omega_V} pg(x')\beta\langle x|x'\rangle n(x')dx'$$ (6.35)

The death rate of particles of volume V due to breakage is given by:

$$D_{br} = g(x)n(x)$$ (6.36)

therefore, the populations balance equation for the breakage process:

$$\frac{\partial n(x,t)}{\partial t} = B_{br} - D_{br} = \int_x^\infty pg(x')\beta(x/x')n(x')dx - g(x)n(x)$$ (6.37)

where $g(x')$: breakage frequency

$\beta\langle x|x'\rangle$: Probability density function (PDF) of daughter particles from x diameter

parent particle to x' daughter particle.

p :number of child particles produced per parent

$n(x,t)$: number density function

The Ghadiri model is used to model the breakage frequency of the solid particles (Ghadiri and Zhang, 2002; Moreno-Atanasio and Ghadiri, 2006). The breakage frequency is related to the material properties and impact conditions:

$$g(x') = \frac{\rho_s E^{2/3}}{\Gamma^{5/3}} v^2 d^{5/3} = K_b v^2 d^{5/3} \qquad (6.38)$$

where ρ_s denotes the particle density, E denotes the elastic modulus of the granule, and Γ denotes the interface energy. While, v is the impact velocity and d is the particle diameter prior to breaking.

The biggest challenge is to set the relationship with temperature of the breakage constant of petroleum coke, which is based on the values of particle density, the elastic modulus of the granule, and the interface energy.

After selecting the Ghadiri-model for calculation of particle breakage frequency, the probability density function would be used to calculate the breakage rate with either a parabolic, generalized, or user-defined function. A lot of PDFs have been used to explain the daughter size distribution of the breakage process. Kostoglou et al. (1997) studied the problem of breakage processes in steady size and proposed Parabolic and Equal-size breakage distribution functional of binary breakage kernels. Hill and Na (1995, 1996) presented a method to generate theoretical breakage distribution functions for multiple particle breakage. Diemer and Olson (2002c) developed a simple generalized analytical expression to describe the size distribution of fine particles. The generalized form of the PDF could be used in simulation of multiple breakage fragments (>2) and to specify the attrition of the daughter distribution (ANSYS, 2009c).

6.4 Experimental setup

Attrition experiments were carried out in a high temperature fluidized bed with a height of 1.23 m and a rectangular cross-section of 0.10 m × 0.50 m (Figure 6.1). The bed particles were typically heated up to 500°C with an in-bed electrical heater. Cold gases, such as helium, nitrogen, carbon dioxide, or mixtures of these gases, were injected into the hot fluidized bed via a convergent-divergent attrition nozzle located on the sidewall of the fluidized bed at a distance of 0.127m above the gas sparger. Two different particles were used in the experiments: silica sand with and petroleum coke (Table 6.2). The operating temperature was varied from ambient temperature to 500°C, while the cold gas pressure upstream of the supersonic nozzle ranged from 689kPa to 2068kPa. Three

different sizes nozzles, in convergent-divergent type, were chosen in attrition tests, as seen in Fig. 6.2.

Table 6.2 Material and properties

Name	Particle Density (kg/m^3)	Sauter diameter d$_{psm}$ (μm)
Silica Sand	2650	209
Petroleum coke	1400	115
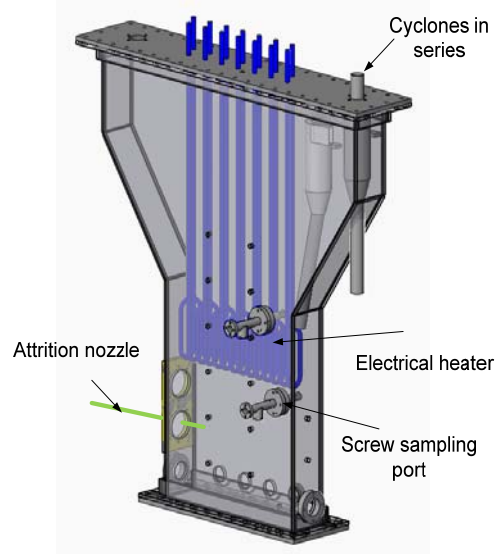
Figure 6.1 Schematic diagram of the hot fluidized bed
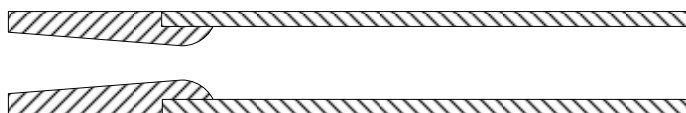
Figure 6.2 Convergent-divergent nozzle used in present study

During each attrition run, bed particle samples were taken from the bed through screw sampling ports and fines samples were collected from cyclones at regular intervals. After sampling, the particle size distribution of sample was measured by the laser diffraction sensor (HELOS of Sympatec Ltd).

6.5 Computational domains and parameters

6.5.1   Computational domains

The commercial CFD software FLUENT 12.0 was used in the attrition model to simulate the hydrodynamics of gas-solid interaction in a fluidized bed. A two-dimensional model, as illustrated in Figure 6.3, was used to simulate the gas-solid two phase flow in a hot

fluidized bed for preliminary studies, such as determining mesh size, the turbulence model, drag law, and coefficient of restitution. The two-dimension computational domain of a fluidized bed had the similar dimensions as the hot fluidized bed used in the experiments. Considering that the 2-D model cannot simulate the hydrodynamics of a convergent-divergent nozzle in fluidized bed, a 3-dimensional model was developed to simulate a horizontal convergent-divergent nozzle in fluidized beds, which was further used to numerical simulate jet-induced particle attrition model at high temperature. Figure 6.4 illustrates the 3-D computational domain developed by Gambit 2.4.6 (Ansys Fluent Inc).
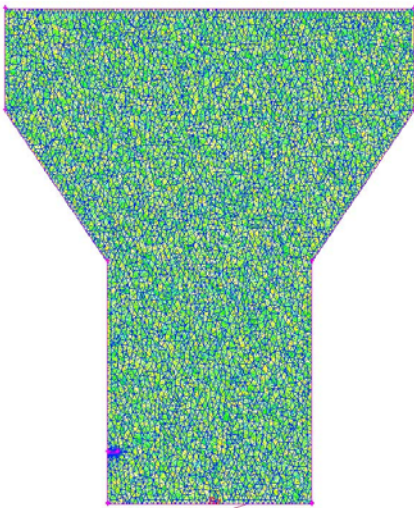
Figure 6.3 Scheme of the 2-dimension computational domain
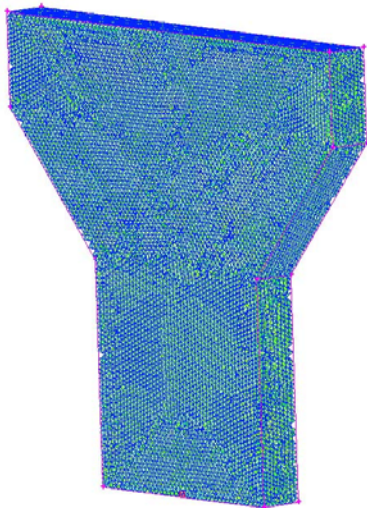
Figure 6.4 Scheme of the 3-dimensional computational domain

6.5.2   Primary settings of Attrition model

Table 6.3 Simulation model parameters

Description	Value
Gas density	incompressible
Particle density (kg/m^3)	Silica sand: 2650 Petroleum coke: 1450
Mean particle diameter (μm)	Silica sand: 205 Petroleum coke: 120
Restitution coefficient	0.80 – 0.99
Initial solids packing	0.60
Superficial gas velocity (m/s)	0.1 – 1
Bed width (m)	0.50
Bed height (m)	1.2
Static bed height (m)	0.4
Time step size	0.001
Maximum number of iterations	20 or 100
Convergence criteria	10^{-6}

Table 6.4 FLUENT phase definitions

Primary phase	Air or Nitrogen gas
Secondary Phase	Petroleum coke, Silica sand
Granular	Activate
Granular temperature model	Phase property
Particle diameter	120 μm
Granular viscosity	Gidaspow
Granular bulk viscosity	Lun-et-al.
Friction viscosity	Schaeffer
Angle of internal friction	30
Friction pressure	Based-ktgf
Frictional modulus	Derived
Friction packing limit	0.61
Granular temperature	Algebraic
Solids pressure	Syamlal-O'Brien
Radial distribution	Lun-et-al.
Elasticity modulus	derived
Packing limit	0.63

6.5.3   Boundary and initial conditions

The boundary and initial conditions for the gas-solid phases are list in Table 6.5 and Table 6.6, respectively.

Table 6.5 Gas phase boundary conditions in Attrition Model

Name	Type	Value
Fluidization gas inlet	Mass flowrate inlet (mass flux)	Vg=0.10 -0.50 m/s
	Intensity and hydraulic diameter	5% Turbulent intensity; 0.17 m Hydraulic diameter
Bed out	Pressure outlet	Pout = 0 psig
	Intensity and hydraulic diameter	2% backflow turbulent intensity; 0.17 m Backflow hydraulic diameter
Nozzle inlet	Mass flow inlet	Vary with attrition pressures and attrition nozzles
	Pressure inlet	0.7 MPa - 2.1 MPa
	Turbulent intensity	5%
	Diameter	1.2 mm to 2.4 mm

Table 6.6 Solid phase boundary conditions in Attrition Model

Name	Type	Value
Fluidization gas inlet	Mass flowrate inlet (mass flux)	0
	Intensity and hydraulic diameter	5% Turbulent intensity; 0.17 m Hydraulic diameter
Bed out	Pressure outlet	P_{out} = 0 psig
	multiphase	Backflow volume fraction: 0
Nozzle inlet	Mass flow inlet	0
	Pressure inlet	0
	Volume fraction	0

6.5.4 Sensitivity study of mesh sizes

To study the sensitivities of the computational results on the mesh sizes of the simulation model, three different mesh sizes were chosen with the mesh cell sizes of 141 372, 279 146, and 392 515 respectively. The model was run with the Gidaspow drag model and 0.90 of restitution coefficient at 0.20 m/s velocity for 20 seconds. To assess the mesh size sensitivity, the bed expansions were used to evaluate the sensitivities of mesh sizes.

As shown in Figure 6.5 and Table 6.7, the simulation results demonstrate that the three different grids that were selected can all perform well for the numerical simulation of a fluidized bed. The agreement between the medium mesh sizes of 279K cells and the finer mesh sizes of 392K cells was particularly good. Considering the computational cost, mesh sizes of 279,146 cells are sufficiently fine for the numerical simulation of a fluidized bed at high temperature. To

determine the mesh sizes sensitivity, the bed pressure drop was used in three-dimensional fluidized bed model.

Table 6.7 Contours of solid voidage in the bed with various mesh sizes

Mesh size:392 515	Mesh size:279 146	Mesh size:141 372
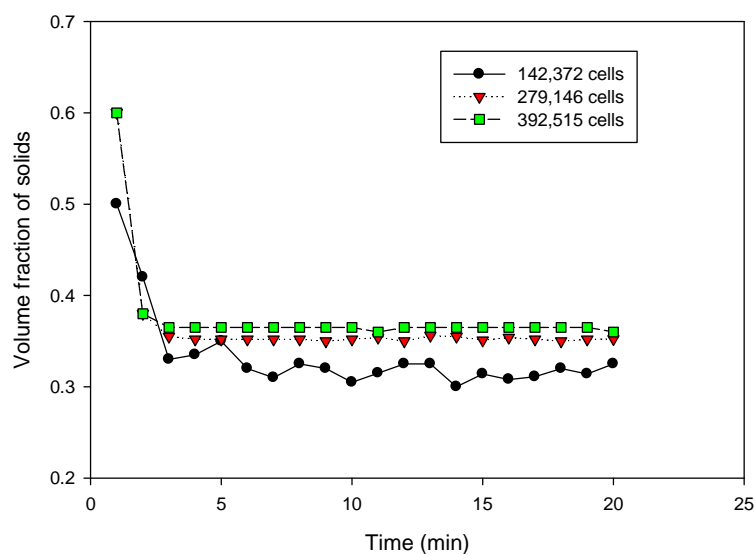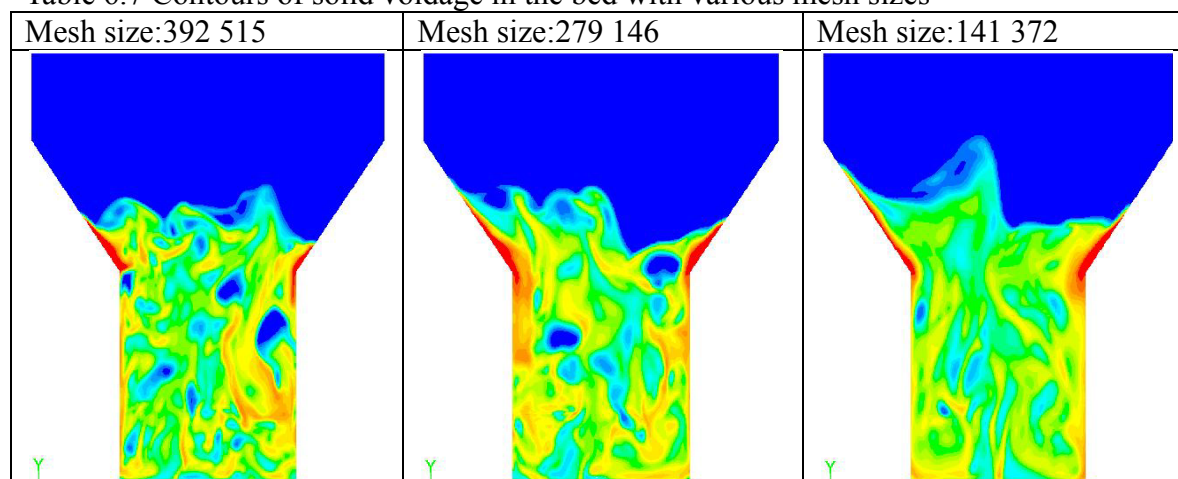
Figure 6.5 Grid size sensitivity results of solid void (Gidaspow drag model, Vg=0.20 m/s, Coke)

6.5.5   Time step

Too large a time step will make the calculations unstable; on the other hand, too small a time step will make the calculations needlessly slow. Most often used time step in gas-solid fluidized beds is 0.001s (Taghipour et al., 2005; Hulet, 2006; Cornelissen et al., 2007). In the present research, 0.001s and 0.005s time step were used as the base case setting due to its good time-step-independent results.

6.6 **Results and discussions**

There are too many facts related to hydrodynamics, kinetics, and transport properties in the present study system. For developing and evaluating the attrition model efficiently, a uniform gas-solid system and binary breakage were assumed in the attrition model. More details are described about the attrition model in the following sections.

6.6.1 **Solution Methods**

The most popular methods to solve the population balance equation include the discrete methods (DM), the classic method of moments (CM), and the quadrature method of moments (QMOM). Both DM and QMOM were used in simulation of particle attrition in fluidized bed.

6.6.1.1 **The discrete method**

In order to solve the PBE directly, a natural discretization of particle state space was used to represent derivatives and integrals (Ramkrishna, 2000).

$$B_b(i) = \sum_{k=i+1, i \neq N}^{N} \Omega_b(v_k, v_i) + \sum_{k=i, i \neq N}^{i} x_{i+1} \Omega_b(v_{i+1}, v_k) + \sum_{k=1, i \neq 1}^{i-1} (1 - x_{i,k}) g(v_i + 1) \Omega_b(v_i, v_k) \qquad (6.39)$$

here

$$\Omega_b(v_k, v_i) = N_k g(v_k) \beta(v_k, v_i) \qquad (6.40)$$

The discrete method of particles is based on representing the continuous particle size distribution in terms of a set of discrete size bins, as shown in Fig.6.6 and 6.7. The obvious benefits of the discrete method are it represents the PSD directly and it predicts correctly the rate of change of total particle number and voidage (Hounslow et al., 1988). The main drawbacks of DM are that the bins must be defined a priori and that the numerical cost may be expensive.
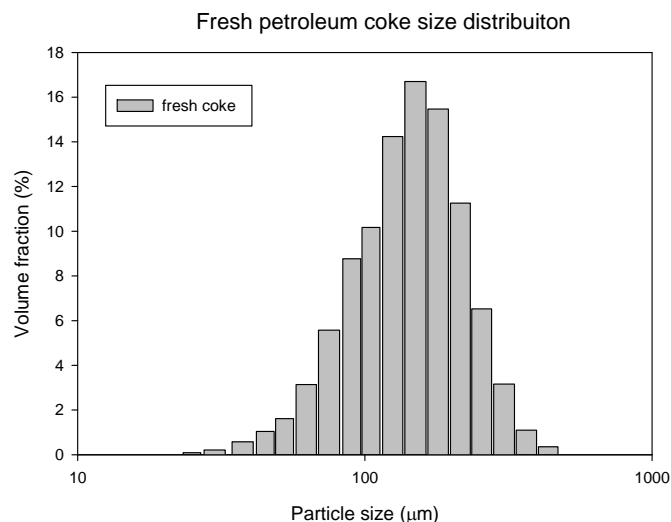
Figure 6.6 Particle size distribution, in volume fractions, of fresh petroleum coke by the discrete method
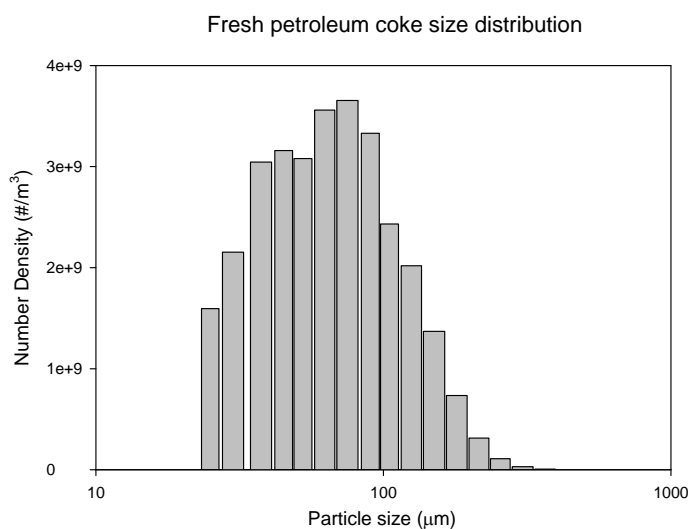
Figure 6.7 Particles size distribution, in number fractions, of fresh petroleum coke by the discrete method

6.6.1.2 The Quadrature Method of Moments (QMOM) (ANSYS, 2009c)

In order to portray the particle size distribution in a specific system such as particles in a fluidized bed that has typical internal and external coordinates, the number density function (NDF) is proposed to describe the distribution. For description of the general breakage process with QMOM, the number density function can be expressed with:

$$\frac{dm_k(t)}{dt} = \overline{B_k^b} - \overline{D_k^b}$$

(6.41)

where

$$\overline{B_k^b}(t) = \int_0^{+\infty} x^k \int_0^{+\infty} a(\lambda)b(x|\lambda)n(\lambda;t)d\lambda dx$$

$$\overline{D_k^b}(t) = \int_0^{+\infty} x^k a(x)n(x;t)dx$$

The QMOM uses a quadrature approximation to represent the distribution function by a set of delta functions with weight function and abscissas.

$$m_k = \int_0^\infty n(x)x^k dx \approx \sum_{i=1}^N \omega_i x_i^k \tag{6.42}$$

where weights (ω_i) and abscissas (x_i) are determined through the product-difference (PD) algorithm from the lower-order moments (Gordon, 1968). If the abscissas of the quadrature approximation are the nodes of the polynomial of order N, then the quadrature approximation:

$$\int_0^\infty f(x)n(x)dx \approx \sum_{i=1}^N f(x_i)\omega_i \tag{6.43}$$

is exact if f(x) is a polynomial of order N or smaller.

Thus, the birth and death of breakage process can be written:

$$B_{b,k} = \sum_{i=1}^N \omega_i \int_0^\infty x_k g(x_i)\beta(x|x_i)dx \tag{6.44}$$

$$D_{b,k} = \sum_{i=1}^N \omega_i x_i^k g(x_i) \tag{6.45}$$

$$m_k = \int_0^\infty n(x)x^k dx \tag{6.46}$$

where m_k is a moment of the particle size distribution; n(x) is the number density, which is a function of characteristic length x. The moment m_k has different physical meanings depending on the value of k.

$$m_0(t) = \int_0^\infty n(x,t)dx \tag{6.47}$$

$$m_1(t) = \int_0^\infty n(x,t)x dx \tag{6.48}$$

$$m_2(t) = \int_0^\infty n(x,t)x^2 dx \tag{6.49}$$

$$m_3(t) = \int_0^\infty n(x,t)x^3 dx \tag{6.50}$$

$$d_{32} = \frac{m_3(t)}{m_2(t)} \tag{6.51}$$

where $m_0(t)$, the first moment, is the total number of particles in system; while $m_1(t)$, $K_a m_2$, and $K_v m_3$ indicate the total diameter of particles, the total area of particles, and the total volume of particles, respectively. The Sauter mean diameter, the ratio of total volume and total area, can be attained through d_{32} in Eq. 6.56. McGraw (1997) suggested that a quadrature approximation could be used to modify the classic method of moments regarding to the closure problem. Marchiso et al. (2003) developed the quadrature method of moments (QMOM) for population balance equation based on the classic method of moments by approximation with a Gaussian quadrature. Previous results demonstrated it is enough for description of moment evolutions accurately to use a quadrature approximation with three nodes (Marchisio et al., 2003; Wan and Ring, 2006). In the present research, the particle size distribution of a particle was calculated using below equation which derived from Equation 6.50:

$$m_k = \sum_{i=1}^{100} n_i x_i^k = \sum_{i=1}^{100} \left(\frac{6\alpha_i}{\pi x_i^3} \right) x_i^k \tag{6.52}$$

n_i is the volumetric number of particles in class i with diameter L_i and volume fraction α_i. For example, the particle size distribution of fresh coke is illustrated as Figure 6.8. The size distribution of particles can be described with six moments, as shown in Table 6.8 and 6.9.

Table 6.8 QMOM method to describe PSD of fresh petroleum coke

moments	units	
$m_0 = 3.6052 \times 10^{11}$	#/m^3	$N_{total} = m_0$
$m_1 = 2.6770 \times 10^7$	m/m^3	$L_{total} = m_1$
$m_2 = 2616$	m^2/m^3	$A_{total} = \pi m_2$
$m_3 = 0.3260$	m^3/m^3	$V_{total} = \frac{\pi}{6} m_3$
$m_4 = 4.9933 \times 10^{-5}$	m	
$m_5 = 9.0877 \times 10^{-9}$	m^2	
$d_{psm} = 124$	μm	$d_{psm} = m_3(t)/m_2(t)$

Table 6.9 QMOM method to describe PSD of fresh silica sand

moments	units	
$m_0 = 1.6885 \times 10^{11}$	#/m^3	$N_{total} = m_0$
$m_1 = 2.724 \times 10^7$	m/m^3	$L_{total} = m_1$

$m_2 = 4985$	m^2/m^3	$A_{total} = \pi m_2$
$m_3 = 1.0482$	m^3/m^3	$V_{total} = \dfrac{\pi}{6} m_3$
$m_4 = 2.54 \times 10^{-4}$	m	
$m_5 = 7.0524 \times 10^{-8}$	m^2	
$d_{psm} = 210$	μm	$d_{psm} = m_3(t)/m_2(t)$
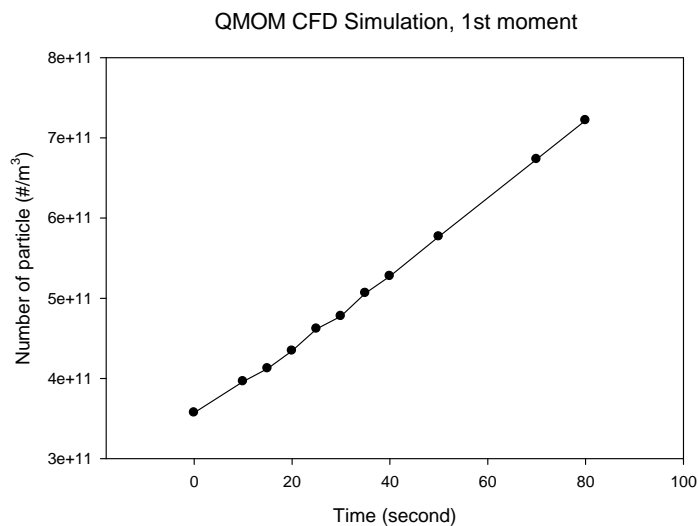
Figure 6.8 The trend of number of particle per volume (m_0) with time in attrition process
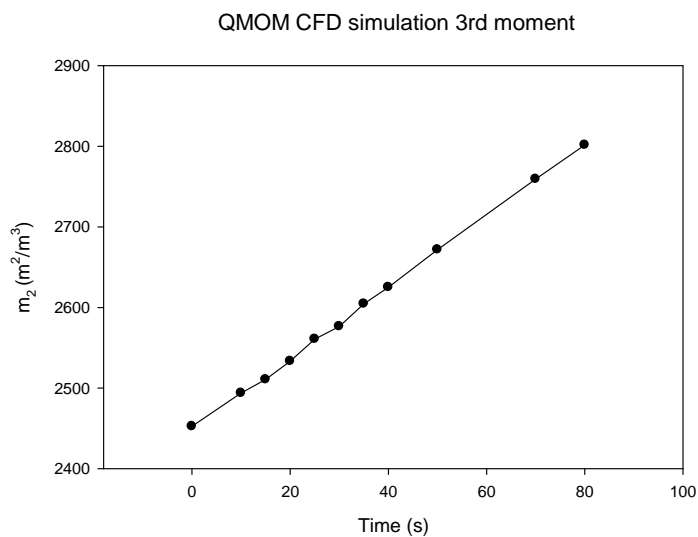
Figure 6.9 The trend of particle area per volume (m_2) with time in attrition process

6.6.2   Breakage kernel

The particle fragmentation may be viewed as the fracture of solids due to propagation of cracks. Griffith (1921), in his research of the phenomena of rupture and flow in solids, firstly introduced the importance of surface energy for the fracture process. He suggested that the increasing surface energy due to a crack must be compensated through the externally added or internally released energy:

$$S = \sqrt[2]{2E\gamma / \pi a} \tag{6.53}$$

where S the ultimate tensile stress applied on the solids, E is Young's modulus, γ is the specific surface energy, and a is the half crack length. The Ghadiri model is used to calculate the breakage frequency of the solid particles in this study (Ghadiri and Zhang, 2002; Moreno-Atanasio and Ghadiri, 2006), because it integrated the effects of particle material properties and environmental properties like impact velocity and attrition temperature. The breakage frequency f in the Ghadiri model is defined as:

$$f = \frac{\rho_s E^{2/3}}{\Gamma^{5/3}} v^2 d^{5/3} = K_b v^2 d^{5/3} \tag{6.54}$$

where ρ_s is the particle density, E is the elastic modulus of the granule, and Γ is the interface energy. v is the impact velocity and L is the particle diameter prior to breaking.

In order to describe the mechanism of particle jet-induced attrition mechanism, McMillan et al. (2007b) found that not all particles in bed involve in jet attrition in a fluidized bed because some particles never reach the attrition jet during the attrition process. Moreover, the other bed properties such the bed temperature, the bed dimensions and the fluidization velocity also play a vital role in particle attrition (Li et al., 2010c). As shown in Figure 6.10, breakage constant affect attrition rate directly in attrition model.

Comparison of different breakage constant on surface area of particle
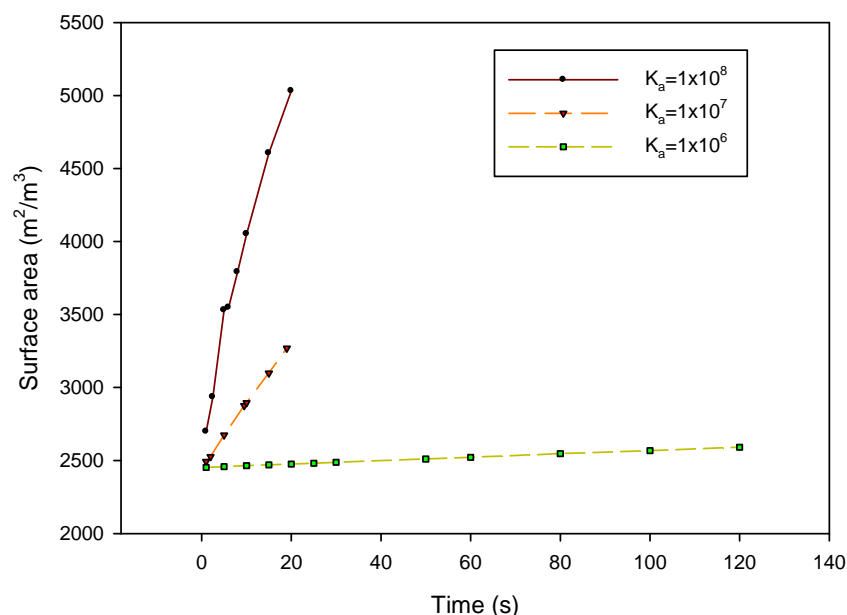
Figure 6.10 Comparison of different breakage constants K_b on surface area of particle.

Emmerich (1995) pointed out that the Young's modulus of petroleum coke (a graphitizable carbon) increases with increasing temperature, and the maximum of the modulus of petroleum coke is at a temperature of about 1200°C. Γ is the interface energy, which equals to 2 times of surface energy (γ) (Israelachvili, 1991). The surface energy of a particle decreases dramatically with increasing temperature and particle diameter (Wiederhorn, 1969; Bikeman, 1978). Since $E^{2/3}/\Gamma^{5/3}$ increases with increasing temperature while the values of particle density, impact velocity, and particle diameter are independent of the operation temperature, a high attrition temperature therefore would promote the particle attrition in fluidized beds. With experimental data, the breakage constant K_a was adjusted with various operation temperatures.

6.6.3   Particle breakage probability density function

The mechanisms of breakage are very difficult to determine in systems of multiphase and turbulent conditions, although particle breakage processes are very common phenomena in engineering and science (Kostoglou et al., 1997). A number of functions were used to describe the breakage daughter distributions. Kostoglou et al. (1997) proposed a numerical method to describe particle breakage and reviewed some specific types of breakage kernels, which are power type kernel, parabolic kernel, equal-size breakage kernel, and attrition kernel. Diemer and Olson (2002c) developed generalized distribution functions to simulate daughter distribution in

particle breakage or coagulation processes based on Hill-Ng distributions. The generalized PDF has the flexibility to represent a wide range of size distribution according the investigation by Diemer and Olson (2002c). Hill and Ng (1996) presented a method for description of theoretical breakage distribution functions for multiple particle breakage. The Hill-Ng particle breakage multiple PDF were simplified with the self-similar solution by Diemer and Olson (2002c). The self-similar solution presented by Ramkrishna (2000) is defined as those "invariant" domains in the space of the independent variables along which the solution remains the same or contains a part that is the same. For specific condition of pure breakage, the generalized PDF is expressed as:

$$p\beta(x|x') = \frac{\theta(z)}{x'} \tag{6.55}$$

where the similarity z is the ratio of daughter-to-parent size; and $\theta(z)$ can be expressed as follow:

$$\theta(z) = \sum_i w_i p_i \frac{z^{q_i-1}(1-z)^{r_i-1}}{\beta(q_i, r_i)} \tag{6.56}$$

where i can be 0 or 1.

Table 6.10 lists the most common breakage probability density functions to describe particle breakage.

Table 6.10 Summary of breakage probability density functions (Daughter distributions functions) (ANSYS, 2009c)

Type	$\theta(z)$	p	Constraints	Authors
Equisized	$p\delta(z-1/p)$	p	$p \geq 2$	Kostoglou et al. (1997)
Attrition	$\delta\{z-(1-\varepsilon)\}+\delta(z-\varepsilon)$	2	$\varepsilon << 1$	Kostoglou et al. (1997)
Power Law	$(v+1)z^{v-1}$	$(v+1)/v$	$0 < v \leq 1$	Vigil and Ziff (1989)
Parabolic	$(v+2)(v+1)z^{v-1}(1-z)$	$(v+2)/v$	$0 < v \leq 2$	Vigil and Ziff (1989)
Austin	$w_0(q_0+1)(z)^{q_0-1}+$ $w_1(q_1+1)(z)^{q_1-1}$	$w(1+1/q_1)$ $+(1-w)(1+1/q_2)$	$q_1, q_2 > 0$	Austin et al. (1976)

A number of researches have been conducted on grinding of material in a mill regarding a rate process (Austin et al., 1976; Hill and Ng, 1996). One population balance equation was developed to describe particle grinding in a mill by Austin et al. (1976), treating the grinding of a particular

size of material as a first-order kinetic process. Ziff (1991) developed scaling similarity solutions regarding a power-law breakage rate kernel following the work by Austin et al (1976).

$$\theta(z) = w(q_0 + 1)z^{q_0 - 1} + (1 - w)(q_1 + 1)z^{q_1 - 1} \tag{6.57}$$

Due to a similar mechanism of particle breakage and good performance of simulation results, Austin PDF was used to explain jet-induced attrition process in fluidized beds at high temperature. Only the binary breakage is considered in the present simulation work. The values of q_1 and q_2 vary with material but are similar in most operation conditions.

6.6.4 Initial simulation to optimize of parameters of attrition model with experimental results

The initial task consisted in the optimization of the attrition model by adjusting breakage constant value and the parameters of the daughter size distribution function.

By comparing the experimental data and the simulation results, the objective function shown below should be minimized (Rajniak et al., 2008):

$$\min\left\{ F = \sqrt{\sum_{i=0,1,2} \left(\frac{m_i^{\exp} - m_i^{\mathrm{mod}}}{m_i^{\exp}} \right)^2} \right\} \tag{6.58}$$

here $m_i^{\exp}$ are experimental results of moments from analysis results of particle analyzer; and m_i^{mod} are simulation results from the attrition model.

The experimental moments of the particle can be calculated with experimental data of particles size distributions by the particle analyzer. While, simulation moments of particle are predicted directly by the present attrition model. Fig. 6.11 illustrates the particle size distributions of petroleum coke before and after attrition process with various attrition pressures, which can be converted to experimental values of six moments in Table 6.11 to represent the particle size distribution.

On the other hand, first of all, several PDF functions were chosen in simulation for determining the best PDF function to fit the tests results. Before optimization, a uniform gas-solid system and binary breakage are assumed. In the case, the breakage constant in Ghadiri model simply set to a specific value. Table 6.12 lists the parameters for PDF in general form. It is apparent that Case 8 is the best fit to experimental results. Therefore, the parameters of Case 8 were used in the subsequent simulation work. With a number of simulation work, the grinding efficiency was

found to be proportional to log(K_b) for specific values of PDF. Figure 6.12 shows the effect of breakage constant K_b of Ghadiri model on the particle grinding efficiency using values of PDF in case 8. The further correlation of relationship between breakage constant and the grinding efficiency was developed and expressed as:

$$\eta = 537 \cdot \log K_b - 3215 \tag{6.59}$$

As a result, once the PDF and its parameters are chosen, the breakage constant of Ghadiri model can be determined by experimental data in Chapter 4.
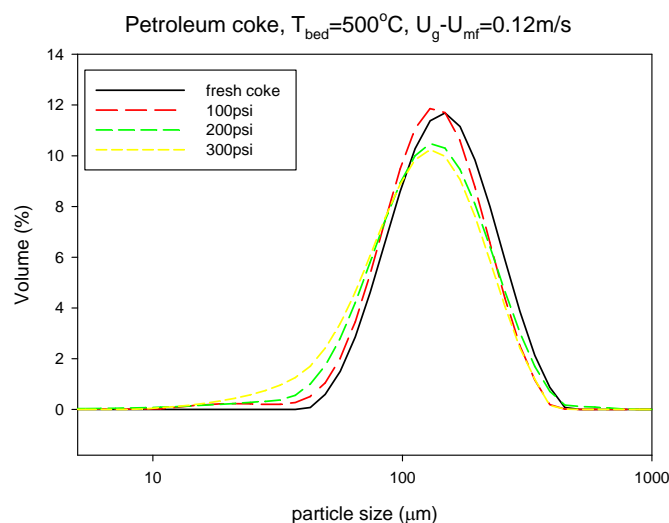
Figure 6.11 Particle sizes distributions of petroleum coke before and after attrition with various attrition pressures at 500°C.

Table 6.11 QMOM method to describe PSD of petroleum coke

moments	Fresh coke	P=100 psig	P=200 psig	P=300 psig
$m_0 (\#/m^3)$	4.34E+11	1.13E+13	2.24E+13	3.54E+12
$m_1 (m/m^3)$	39824023	1.02E+08	1.56E+08	1.06E+08
$m_2 (m^2/m^3)$	4316.111	5174.614	5635.294	5967.689
$m_3 (m^3/m^3)$	0.563135	0.563135	0.563134	0.563134
$m_4 (m^4/m^3)$	8.89E-05	8.04E-05	8.10E-05	7.48E-05
$m_5 (m^5/m^3)$	1.68E-08	1.38E-08	1.49E-08	1.25E-08
$d_{psm}=m_3(t)/m_2(t)(\mu m)$	130	108.8	99.9	94.3

Table 6.12 Parameters for PDF in general form

	ω_0	p_0	q_0	r_0	ω_1	p_1	q_1	r_1	f(m)
Case 1	1	2	1	2	N/A	N/A	N/A	N/A	0.92
Case 2	1	3	0.5	2	N/A	N/A	N/A	N/A	0.60
Case 3	1	2	0.01	0.01	N/A	N/A	N/A	N/A	1.23
Case 4	1	2	0.5	0.5	N/A	N/A	N/A	N/A	1.05
Case 5	1	2	1	1	N/A	N/A	N/A	N/A	0.35
Case 6	1	2	1.5	1.5	N/A	N/A	N/A	N/A	1.07
Case 7	0.5	2	0.1	1	0.5	2	1	0.1	0.50
Case 8	0.5	2	0.1	1	0.5	2	0.1	0.01	0.08
Case 9	0.5	2	0.01	1	0.5	2	0.01	0.0001	0.10
Case 10	0.5	2	0.001	1.00	0.5	2	1	0.001	0.25
Case 11	0.5	2	0.5	1	0.5	2	0.5	0.25	0.09
Case 12	0.5	2	0.4	1	0.5	2	0.4	0.16	0.09

General PDF (Case 8), P_{attr}=200 psig
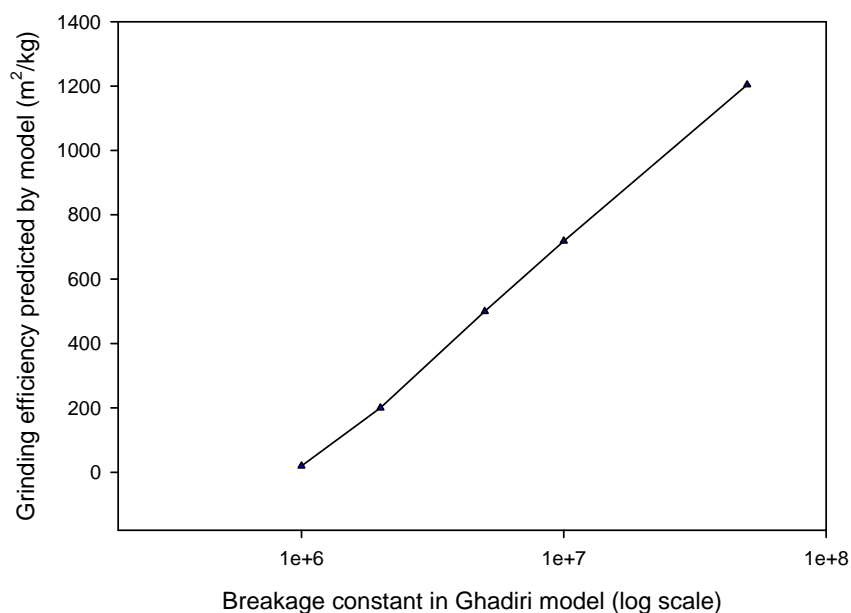
Figure 6.12 The effect of breakage constant in Ghadiri model on particle grinding efficiency.

6.6.5   Parameters of attrition model

In addition, the boundary conditions for the gas and solid phases have been summarized in Table 6.11 and Table 6.12, respectively. In the attrition model, the multiphase momentum equations, the turbulence equations and the volume fraction equations were solved by the FLUENT Phase coupled SIMPLE algorithm. When the Phase coupled SIMPLE algorithm is used in simulation, the velocities are solved coupled by phases in segregated fashion, while fluxes are reconstructed

at the faces of the control volume and then a pressure correction is built based on total continuity (ANSYS, 2009a). The solution methods and under relaxation factors used in Attrition Model are illustrated in Table 6.13, Table 6.14, respectively.

Table 6.13 Configuration of solution methods in Attrition Model

Scheme	Phase Coupled SIMPLE
Gradient	Least Squares Cell Based
Momentum	First order upwind
Volume fraction	QUICK
Turbulent kinetic energy	First order upwind
Turbulent dissipation rate	First order upwind
Energy	First order upwind
Solid-phase Bin	First order upwind
Transient Formulation	First order implicit

Table 6.14 under-relaxation factors in Attrition Model

Name	Value
Pressure	0.3
Density	0.5
Body forces	0.5
Momentum	0.4
Volume fraction	0.5
Granular temperature	0.2
Turbulent kinetic energy	0.4
Turbulent dissipation rate	0.4
Turbulent viscosity	0.2
Energy	0.2
Solid-phase bin	0.5

Table 6.15 Values for configuration of population balance model

Solution method	Discrete	
Breakage kernel	Ghadiri	
Breakage Constant (K_b) (Experimental estimation)	$300^{\circ}C$	1.12×10^6
	$400^{\circ}C$	1.18×10^6
	$500^{\circ}C$	1.30×10^6
Particle distribution function	General PDF $\omega_0 = 0.5,\ p_0 = 2,\ q_0 = 0.1,\ r_0 = 1;$ $\omega_1 = 0.5,\ p_1 = 2,\ q_1 = 0.1,\ r_1 = 0.01;$	

Sauter mean diameter of solid phase, as shown in Eq. 5.66, which represents the particle diameter of the secondary phase, is used to couple population balance modeling of the solid phase (ANSYS, 2009c). To solve the population balance model, both the discrete method and the QMOM were chosen, although most of simulation jobs were calculated with the discrete

method due to accurate prediction. In addition, Ghadiri breakage kernels and Generalized PDF were used to simulate the particle attrition in fluidized beds. Table 6.15 lists the most important parameters for configuration of population balance model.

6.6.6   Particle grinding efficiency

The particle grinding efficiency was first introduced by McMillan (2007a), as a ratio of the new surface area created per mass of attrition gas used. The grinding efficiency was determined from the bed particle and cyclone fines samples:

$$\eta(m^2/kg) = \frac{a^f_{bed} + a^f_{fines} - a^i_{bed}}{m_{attr}} \tag{6.60}$$

where:

a^f_{bed} = Surface area of bed particles after attrition (m^2);

a^f_{fines} = Surface area of cyclone fines after attrition (m^2);

a^i_{bed} = Surface area of bed particles before attrition (m^2)

m_{attr} = Mass of attrition gas (kg/s)

$$m_2(t) = \int_0^\infty n(L,t)L^2 dL$$

The total change of the surface area per unit volume can be obtained from the third moments, m_2, which can be estimated from the discrete method or the quadrature method of moments. The relationship between the third moment and the total surface area could be expressed:

$$A_{total} = K_a \cdot m_2 \tag{6.61}$$

where $K_a = \pi$ in the present work, due to assuming spherical particle for petroleum coke and silica sands. Therefore, the grinding efficiency in simulation work can be written:

$$\eta(m^2/kg) = \frac{K_a(m_2^f - m_2^i)}{m_{attr}} \tag{6.62}$$

As shown in Figure 6.13, after each simulation work done, the particle grinding efficiency could be calculated with the third moments (m$_2$) and simulation real time. Meanwhile, the most likely PSD can be obtained based on given a set of moments. After each numerical CFD simulation, the

number density function and length number density function for population balance model can be retrieved in FLUENT Post-processing.

200psi, 300°C Petroleum coke
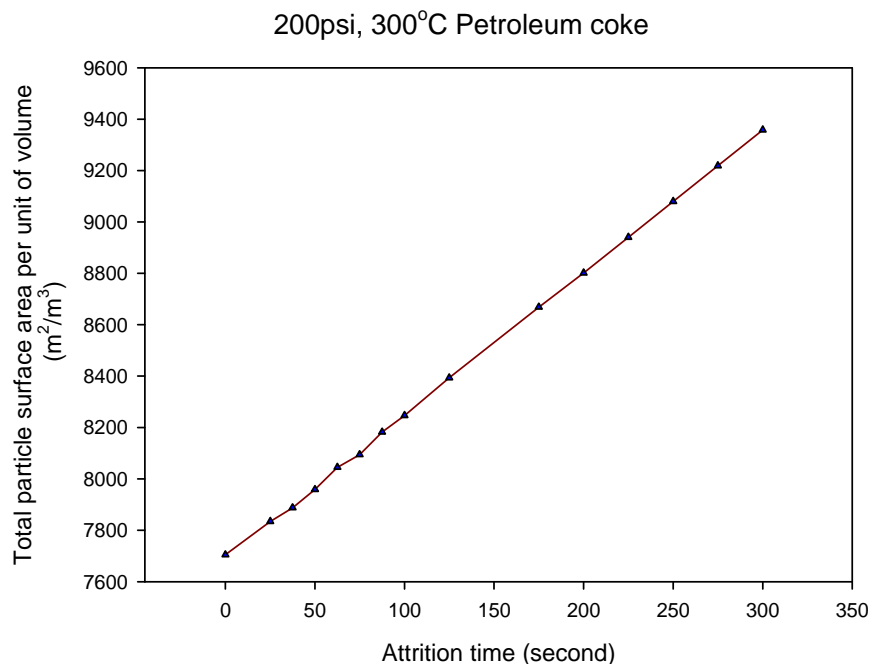
Figure 6.13 Modeling results of particle surface area per unit volume with attrition time.

6.6.7   The influence of attrition pressure on grinding efficiency

Previous studies have demonstrated that the grinding efficiency increases with increasing flowrate of attrition gas through the supersonic nozzle at various temperatures (Li et al., 2011a). In order to determine the influence of the gas flowrate on the grinding efficiency, the particle attrition process was simulated using various nozzle sizes and operation pressure by jet-induced attrition model. Fig. 6.14 illustrates the predicted results of grinding efficiency by attrition model and experimental results by a laboratory fluidized bed. It is obvious that the attrition model results display a good agreement with the experimental data; however the predicted grinding efficiencies are higher than the test's for high attrition pressure.

2.4mm nozzle, V_g=0.20 m/s, T_{bed}=300°C, Petroleum coke
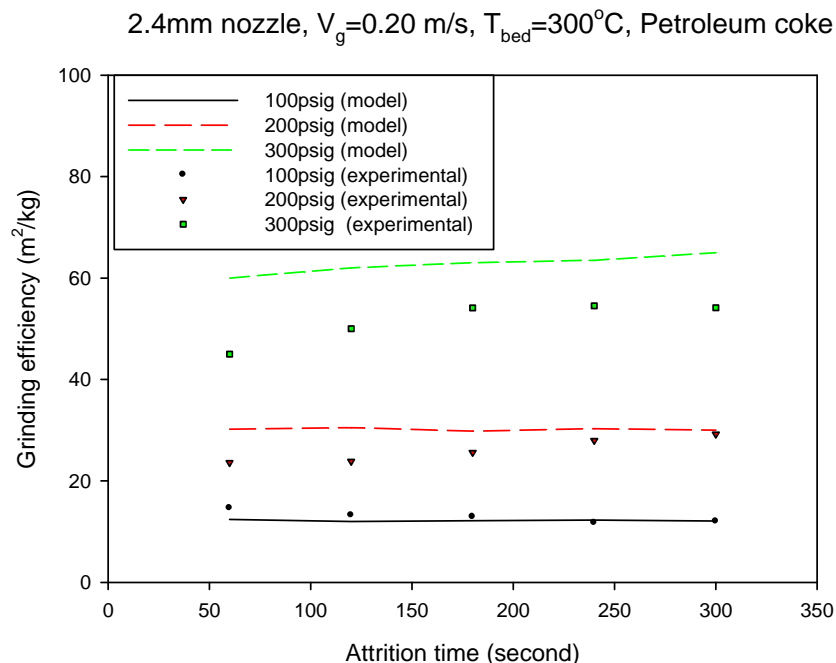
Figure 6.14 Comparison of prediction of grinding efficiency using attrition model with experimental results.

6.6.8 The influence of temperature on particle grinding efficiency

Li et al. (2011a) studied the jet-induced particle attrition in fluidized beds at high temperature to obtain that the higher temperature and higher pressure of attrition gas could contribute higher grinding efficiency with both silica and petroleum coke. To validate the experimental data with simulation results, a series of simulation work was conducted with attrition model by petroleum coke. The jet-induced particle attrition model was used to simulate the particle attrition with a convergent-divergent nozzle in fluidized beds, with various breakage frequencies depending on the properties of material and the operating temperature. It can be seen in Figure 6.15 that while most of model results on temperature trends are predicted well, the grinding efficiency predicted by attrition model at high pressure attrition is higher than the experimental data.
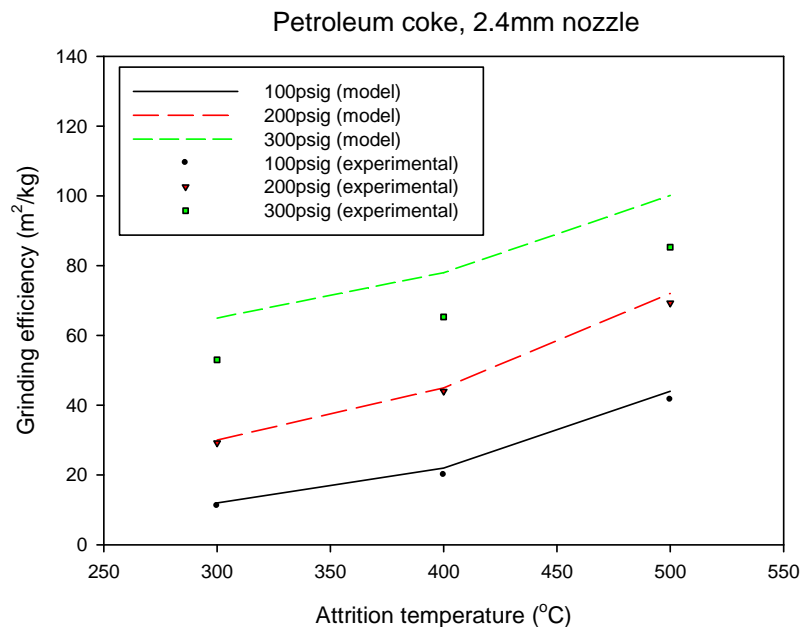
Figure 6.15 Comparison of predicted and experimental values with the effect of temperature on grinding efficiency..

6.6.9 The influence of nozzle size on particle grinding efficiency

Previous studies related to the effect of nozzle scale on the grinding efficiency claimed that either larger scale nozzles or higher gas flowrate resulted in significantly higher grinding efficiencies (McMillan et al., 2007a; Li, et al., 2010c). The experimental data shows that the nozzle with a throat diameter of 2.4 mm has a higher grinding efficiency than smaller nozzles. In order to validate the attrition model on nozzle scale, four different sizes nozzles were used in model simulation, there are throat diameters of 1.2mm, 1.7mm, 2.0mm, and 2.4mm, respectively. Figure 6.16 shows that the same trend can be found in simulation results by the Attrition Model in present research.

comparison of the influence of nozzle scale on grinding efficiency
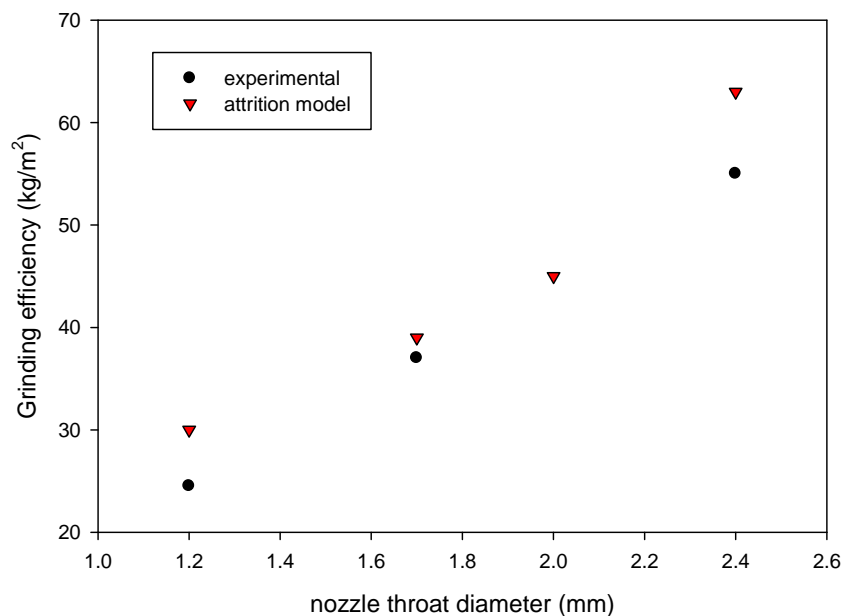
Figure 6.16 Comparison of the influence of nozzle scale on grinding efficiency (P_{attr}=300psi, T=300°C)

6.7 Conclusion

A jet-induced attrition model in fluidized beds at high temperature has been proposed and developed. The model is coupled Eulerian-Eulerian multiphase model with population balance method. Moreover, particle-particle interactions are described with the kinetic theory of granular flow. To optimize and validate attrition model, experimental results with hot fluidized bed were used to determine and modify the critical parameters of model. It is found that the best prediction was obtained using Ghadiri breakage kernel, generalized daughter size distribution function, and discrete solution method. Moreover, the breakage constant of Ghadiri breakage kernel increases with increasing temperature.

Future work is required to develop a semi-empirical breakage kernel and to improve optimization procedure for more precisely prediction of particle attrition through a convergent-divergent nozzle in fluidized bed at high temperature.

6.8 **Acknowledgements**

6.9 Notation

a	Surface area of particles
a	The half crack length (Eq.6.56)
A	Area (m^2)
B_{br}	Birth rate of particles in breakage process
$B_b(i)$	Breakage rate (Eq. 6.41)
C	Attrition constant in Table 6.1
C_D	Drag coefficient
D_{br}	Death rate of breakage process
d	Diameter (m)
d_p	Particle diameter (m)
d_{32}	The Sauter mean diameter (m)
E	Elastic modulus of the granule
e_{ss}	Coefficient of restitution
f	Breakage frequency (1/m^3·s) (Eq.6.57)
f	Drag coefficient function (Eq.6.9)
G_b	Generation of turbulence kinetic energy due to buoyancy
G_k	Generation of turbulence kinetic energy due to the mean velocity
$g(V')$	Breakage frequency
$g_{0,ss}, g_0$	Radial distribution function
h	Heat transfer coefficient (W/M^2·K)
L	Particle diameter (m)
k	Turbulence kinetic energy per unit mass (J/kg)
K_b	Breakage constant (in Ghadiri breakage kernel)
K_{sl}, K_{ls}	Fluid-solid exchange coefficient
K_{gs}	Gas-solid exchange coefficient
$k_{\Theta_s} \nabla \Theta_s$	Diffusion of energy (Eq. 6.31)
k_{Θ_s}	Diffusion coefficient (Eq. 6.31)
m	Mass (g, kg)
$\dot{m}$	Mass flow rate (kg/s)
m_i^{exp}	Moment calculated from experimental data (Eq.6.63)
m_i^{mod}	Moment predicted from attrition model (Eq.6.63)
m_k	The kth moment (Eq. 6.44,6.45)
M$_w$	Molar weight (kg/mol)
Nu	Nusselt number
N	Number of child particles
N	The nodes of the polynomial of order

$n(V,t)$	Number density function
p	Pressure (Pa)
p	Number of child particles produced per parent (Eq.6.35, 6.37)
P_s	Solid pressure
Pr	Prandtl number
Q	Volumetric flow rate at orifice (m^3/s) (Eq.6.1)
Q	Flow rate of enthalpy (W)
q	Heat flux (W/m^2)
R	Ideal gas universal constant
Re	Reynolds number
S	Total entropy (J/K)
S	The ultimate tensile stress (Eq. 6.56)
S	Excess surface area (m^2) (Eq..6.1)
T	Temperature (^{o}C or K)
t	Time (s)
u_q	Velocity for q phase (m/s)
U_0, u_0	Gas velocity at nozzle exit (m/s)
u_{mf}	Minimum fluidization velocity (m/s)
$u_{sound,eq}$	Equivalent speed of sound (m/s) (Eq.6.5)
u, v, w	Velocity (m/s)
V	Volume of parental particle (m^3)
V'	Volume of child particle (m^3)
v	Impact velocity (m/s)
$v_{r,s}$	The terminal velocity correlation for the solid phase
W	Residue bed weight (Eq.6.1)
x	Particle diameter (m)
Y_M	Contribution of the fluctuating dilatation to the overall dissipation rate

Greek letters

α	Solid coefficient (Eq.6.5)
β	Correction factor (Eq.6.1)
β	Geometry coefficient (Eq.6.5)
$\beta(V|V')$	Probability density function of particles breakage
γ	The specific surface energy (Eq.6.56)
γ_{Θ_s}	Collisional dissipation of energy (Eq. 6.31)
Γ	Interface energy
ε	Volume fraction
ε	Turbulent dissipation rate (m^2/s^3)
η	The grinding efficiency
Θ_s	Granular temperature

λ_q	Bulk viscosity
λ_s	Bulk Viscosity
μ_q	Shear viscosity
$\mu_{s,kin}$	Kinetic Viscosity
$\mu_{s,fr}$	Frictional viscosity
ρ	Density (kg/m^3)
ρ_0	Gas density at orifice (kg/m^3)
ρ_p	Particle density (kg/m^3)
ρ_s	Particle density (kg/m3) (Eq. 6.38)
$\overline{\overline{\tau_q}}$	Stress-strain tensor
ϕ	The angle of internal friction (Eq. 6.30)
ϕ_{ls}	Energy exchange between the gas phase and the solid phase (Eq. 6.31)

6.10 **References**

ANSYS, ANSYS FLUENT 12.0 User's Guide. April 2009 ed.; ANSYS, Inc.: 2009a.

ANSYS, ANSYS FLUENT 12.0 Theory Guide. April 2009 ed.; 2009b.

ANSYS, ANSYS FLUENT 12.0 Population Balance Module Manual. **2009c**.

Austin, L.; Shoji, K.; Bhatia, V.; Jindal, V.; Savage, K.; Klimpel, R., Some Results on the Description of Size Reduction as a Rate Process in Various Mills. *Industrial & Engineering Chemistry Process Design and Development* **1976,** *15* (1), 187-196.

Bemrose, C. R.; Bridgwater, J., A Review of Attrition and Attrition Test Methods. *Powder Technology* **1987,** *49* (2), 97-126.

Bentham, A. C.; Kwan, C. C.; Boerefijn, R.; Ghadiri, A., Fluidised-bed jet milling of pharmaceutical powders. *Powder Technology* **2004,** *141* (3), 233-238.

Bikerman, J. J., *Surface energy of solid*. Springer Berlin: Heidelberg, 1978; Vol. 77.

Bird, R. B. B.; Warren E. Stewart; Lightfoot, E. N., *Transport phenomena*. John Wiley & Sons, Inc: New York : , c2007. , 2002.

Boemer, A.; Qi, H.; Renz, U., Verification of Eulerian simulation of spontaneous bubble formation in a fluidized bed. *Chemical Engineering Science* **1998,** *53* (10), 1835-+.

Chen, J. C., Heat Transfer. In *Handbook of Fluidization and Fluid-particle systems*, Yang, W. C., Ed. Marcel Dekker, Inc.: New York, 2003.

Chen, J. C.; Grace, J. R.; Golriz, M. R., Heat transfer in fluidized beds: design methods. *Powder Technology* **2005,** *150* (2), 123-132.

Chen, T.; Sishtla, C.; Punwani, H.; Arastoopour, H., A model for attrition in fluidized beds. In *Fluidization*, Grace, J. R.; Matsen, J., Eds. Engineering Foundation: New York, 1980; p 445.

Chiesa, M.; Mathiesen, V.; Melheim, J. A.; Halvorsen, B., Numerical simulation of particulate flow by the Eulerian-Lagrangian and the Eulerian-Eulerian approach with application to a fluidized bed. *Computers & Chemical Engineering* **2005,** *29* (2), 291-304.

Cornelissen, J. T.; Taghipour, F.; Escudi, R.; Ellis, N.; Grace, J. R., CFD modelling of a liquid-solid fluidized bed. *Chemical Engineering Science* **2007,** *62* (22), 6334-6348.

Cruz, N. Interactions Between Supersonic Gas Jets and Gas-Solid Fluidized Beds

The University of Western Ontario, London, 2009.

Cruz, N.; Briens, C.; Berruti, F., Supersonic attrition nozzles in gas-solid fluidized beds. *Chemical Engineering and Processing: Process Intensification* **2010,** *49* (3), 225-234.

De Michele, G.; Elia, A.; Massimilla, L., Interaction between Jets and Fluidized-Beds. *Quaderni Dell Ingegnere Chimico Italiano* **1976,** *12* (6), 155-162.

Diemer, R. B.; Olson, J. H., A moment methodology for coagulation and breakage problems: Part 3--generalized daughter distribution functions. *Chemical Engineering Science* **2002c,** *57* (19), 4187-4198.

Ding, J.; Gidaspow, D., A Bubbling Fluidization Model Using Kinetic-Theory of Granular Flow. *Aiche Journal* **1990,** *36* (4), 523-538.

Emmerich, F. G., Application of a cross-linking model to the Young's modulus of graphitizable and non-graphitizable carbons. *Carbon* **1995,** *33* (1), 47-50.

Ghadiri, M.; Cleaver, J. A. S.; Tuponogov, V. G.; Werther, J., Attrition of FCC powder in the jetting region of a fluidized bed. *Powder Technology* **1994,** *80* (2), 175-178.

Ghadiri, M.; Cleaver, J. A. S.; Yuregir, K. R.; O.E., Y. I., Attrition of sodium chloride crystals in a fluidized bed. In *Fluidization* Potter, O. E.; Nicklin, D. J., Eds. Engineering Foundation: Brisbane, Australia, 1992; Vol. VII, p 603.

Ghadiri, M.; Zhang, Z., Impact attrition of particulate solids. Part 1: A theoretical model of chipping. *Chemical Engineering Science* **2002,** *57* (17), 3659-3669.

Gidaspow, D., *Multiphase flow and fluidization : continuum and kinetic theory descriptions.* Academic Press: Boston, 1994; p xx, 467 p.

Griffith, A. A., The Phenomena of Rupture and Flow in Solids. *Philosophical Transactions of the Royal Society of London. Series A, Containing Papers of a Mathematical or Physical Character* **1921,** *221*, 163-198

Gunn, D. J., Transfer of heat or mass to particles in fixed and fluidised beds. *International Journal of Heat and Mass Transfer* **1978,** *21* (4), 467-476.

Gwyn, J. E., On Particle Size Distribution Function and Attrition of Cracking Catalysts. *Aiche Journal* **1969,** *15* (1), 35-&.

Hill, P. J.; Ng, K. M., Statistics of Multiple Particle Breakage. *Aiche Journal* **1996,** *42* (6), 1600-1611.

Hounslow, M. J.; Ryall, R. L.; Marshall, V. R., A discretized population balance for nucleation, growth, and aggregation. American Institute of Chemical Engineers: 1988; Vol. 34, pp 1821-1832.

Hulburt, H. M.; Katz, S., Some problems in particle technology: A statistical mechanical formulation. *Chemical Engineering Science* **1964,** *19* (8), 555-574.

Hulet, C.; Briens, C.; Berruti, F.; Chan, E. W., Effect of a shroud on entrainment into a submerged jet within a fluidized bed. *Chem. Eng. Process.* **2008,** *47* (9-10), 1435-1450.

Israelachvili, J. N., *Intermolecular and surface forces*. Second ed.; Academic Press: Toronto, 1991.

Kostoglou, M.; Dovas, S.; Karabelas, A. J., On the steady-state size distribution of dispersions in breakage processes. *Chemical Engineering Science* **1997,** *52* (8), 1285-1299.

Kumar, S.; Ramkrishna, D., On the solution of population balance equations by discrettization .1. A fixed pivot technique. *Chemical Engineering Science* **1996,** *51* (8), 1311-1332.

Li, F.; Briens, C.; Berruti, F.; McMillan, J., Study of solids entrainment into attrition jets in fluidized beds. In *Fluidization XIII*, Kim, S. D.; Kang, Y.; Lee, J. K.; Seo, Y. C., Eds. Engineering Conferences International: Gyeong-ju, Korea, 2010a.

Li, F.; Briens, C.; Berruti, F.; McMillan, J., Penetration of high velocity horizontal gas jets into a fluidized bed at high temperature. In *Fluidization XIII*, Kim, S. D.; Kang, Y.; Lee, J. K.; Seo, Y. C., Eds. Engineering Conferences International: Gyeong-ju, Korea, 2010b; Vol. XIII.

Marchisio, D. L.; Vigil, R. D.; Fox, R. O., Implementation of the quadrature method of moments in CFD codes for aggregation-breakage problems. *Chemical Engineering Science* **2003,** *58* (15), 3337-3351.

McGraw, R., Description of aerosol dynamics by the quadrature method of moments. *Aerosol Sci. Technol.* **1997,** *27* (2), 255-265.

McMillan, J.; Briens, C.; Berruti, F.; Chan, E., High velocity attrition nozzles in fluidized beds. *Powder Technology* **2007a,** *175* (3), 133-141.

McMillan, J.; Briens, C.; Berruti, F.; Chan, E., Particle attrition mechanism with a sonic gas jet injected into a fluidized bed. *Chemical Engineering Science* **2007b,** *62* (14), 3809-3820.

Merry, J. M. D., Penetration of a Horizontal Gas Jet into a Fluidised Bed. *Transactions of the Institution of Chemical Engineers and the Chemical Engineer* **1971,** *49* (4), 189-&.

Moreno-Atanasio, R.; Ghadiri, M., Mechanistic analysis and computer simulation of impact breakage of agglomerates: Effect of surface energy. *Chemical Engineering Science* **2006,** *61* (8), 2476-2481.

Pougatch, K.; Salcudean, M.; McMillan, J., Simulation of particle attrition by supersonic gas jets in fluidized beds. *Chemical Engineering Science* **2010,** *65* (16), 4829-4843.

Rajniak, P.; Dhanasekharan, K.; Sinka, C.; MacPhail, N.; Chern, R., Modeling and measurement of granule attrition during pneumatic conveying in a laboratory scale system. *Powder Technology* **2008,** *185* (3), 202-210.

Ramkrishna, D., *Population Balances*. Academic Press, Inc: New York, 2000.

Randolph, A. D.; Larson, M. A., *Theory of Particulate Processes*. Academic Press, Inc.: Toronto, 1988.

Ranz, W. E., Friction and transfer coefficients for single particle and packed beds. *Chem Eng Progress* **1952,** *48* (5), 247-253.

Taghipour, F.; Ellis, N.; Wong, C., Experimental and computational study of gas-solid fluidized bed hydrodynamics. *Chemical Engineering Science* **2005,** *60* (24), 6857-6867.

Vaux, W. G. K., Dale L. In *Particle attrition in fluid-bed processes*, Fluidization Grace, J. R. M., J. M. , Ed. Plenum Press: 1980.

Vigil, R. D.; Ziff, R. M., On the stability of coagulation--fragmentation population balances. *Journal of Colloid and Interface Science* **1989,** *133* (1), 257-264.

Wan, B.; Ring, T. A., Verification of SMOM and QMOM population balance modeling in CFD code using analytical solutions for batch particulate processes. *China Particuology* **2006,** *4* (5), 243-249.

Werther, J.; Xi, W., Jet attrition of catalyst particles in gas fluidized beds. *Powder Technology* **1993,** *76* (1), 39-46.

Wiederhorn, S. M., Fracture Surface Energy of Glass. *Journal of the American Ceramic Society* **1969,** *52* (2), 99-105.

Zenz, F. A.; Kelleher, E. G., STUDIES OF ATTRITION RATES IN FLUID-PARTICLE SYSTEMS VIA FREE FALL, GRID JETS, AND CYCLONE IMPACT. *Journal of powder & bulk solids technology* **1980,** *4* (2-3), 8.

Ziff, R. M., NEW SOLUTIONS TO THE FRAGMENTATION EQUATION. *J. Phys. A-Math. Gen.* **1991,** *24* (12), 2821-2828

Chapter 7

7 Experimental and Numerical Study of Twin-Jet Nozzle in Particle Attrition Process

7.1 Abstract

The convergent-divergent nozzle is popularly used in a number of industrial applications. For example, in the fluid coking process, a convergent-divergent nozzle is employed to control the particle size distribution in a reacting system. Studies for aerospace applications have found that twin-jet nozzles enhance flow mixing, entrainment, and jet thrust. Therefore, the aim of the present study is to investigate the fluid dynamic mechanism of twin-jet nozzles and their practical application to particle attrition in fluidized beds. Numerical investigations demonstrate that the twin-jet can enhance particle entrainment and momentum transfer in fluidized beds. These aspects have been applied to attrition experiments in a fluidized bed. Experimental results found that the grinding efficiency is consistently about 30% higher with twin-jet nozzles of the appropriate geometry. Protruding twin-jet nozzles entrain more particles into the jet cavity resulting in a higher grinding efficiency, when compared to non-protruding nozzles. Modeling confirmed the experimental results.

7.2 Introduction

The convergent-divergent nozzle is used in various industrial processes such as coal combustion, grinding, and fluid coking. Recent studies have been performed on jet attrition of fluidized particles, using supersonic, convergent-divergent nozzles. De Michele et al. (1976) developed the turbulent jetting region and jet model for axisymmetric based on the extension of the theory of turbulent submerged jets in fluidized beds. Merry suggested that the majority of solids entrainment occurs in the potential zone region, with particles accelerating within the jet cavity downstream (Merry, 1971). Bentham et al. (2004) asserted that the particle breakage mechanism of subsonic jets involves the particles entrained in the jet. According to another study by McMillan et al. (2007b), particles entrained into the jet are accelerated by the high velocity gas within the jet cavity, and then collide with slow moving particles near the tip of the jet cavity.

Since the convergent-divergent nozzles are more efficient than regular nozzles, they require less steam to achieve the same attrition rate (McMillan et al., 2007a).

Most recently, many studies have focused on how to enhance particle attrition with supersonic jets. Smith et al. (1992) suggested that the grinding efficiency could be enhanced by accelerating the particles into the grinding zone with velocity vectors more closely aligned with the axes of the nozzle; therefore, an accelerator tube was introduced downstream of the attrition nozzle. McMillan et al. (2006) found that a shroud around the exit of the attrition nozzle significantly improved the attrition rate by increasing solids entrainment into the jet. Li et al. (2010a) have demonstrated that the entrainment efficiency is affected significantly by gas jet properties. When using a given mass flowrate of gas, at the same pressure, several smaller size nozzles would provide a higher global entrainment of particles into the jets than a single large nozzle. However, non-interacting small nozzles provided less attrition than a large nozzle with the small total gas flowrate, presumably because particles did not accelerate to as high a velocity in their shorter jet cavities.

In the aerospace research area, twin-jets have attracted more attention because that they can be employed for enhancing mixing, controlling noise, and developing jet thrust. Lin and Sheu (1991) found that the twin jet configuration increases entrainment by enhancing the mixing between the jet and ambient fluids. Wlezien (1989) found that the interaction of two supersonic jets is strongly related to the nozzle spacing and jet Mach number. Moustafa (1994) further claimed that the structure of twin-jet flow is dependent upon the pressure ratio as well as the ratio of nozzle spacing. Koller-Milojevic and Shneider (1993) also found that enhanced entrainment occurred with twin-jet flow.

This paper investigates whether, by using two closely spaced small nozzles, which provide two initially separated jets that combine at a certain distance downstream of the nozzle tips, the higher entrainment efficiency of small nozzles could be combined with the high particle velocities of large jets. The main objective of the present study was to investigate the fluid dynamics of twin-jet nozzle and the practical application of twin-jet nozzle on particle attrition in a high temperature fluidized bed. The work was subdivided into two tasks. First, a numerical study was conducted to investigate the fundamental characteristics of twin-jet nozzle. In particular, the twin-jet nozzle was compared to a single nozzle with the same operating conditions, using various spacing sizes, nozzle pressure ratios (NPR), and nozzle configurations.

After the numerical simulation of twin-jet nozzles, some attrition experiments were carried out to validate the simulation results. The ultimate goal was to develop a suitable model that can be used to provide information that is difficult to measure experimentally and thus maximize the particle attrition performance.

7.3 Hydrodynamic theory

The two approaches of numerically modeling multiphase systems are the Eulerian-Eulerian model and the Eulerian-Lagrangian model. The Eulerian-Eulerian model is adopted in the present work, because the Eulerian-Eulerian model assumes the solid phase and gas phase can be treated mathematically as interpenetrating continua. Conservation equations for each phase are derived to obtain equations in mass, momentum, and energy. These equations are closed by constitutive relations that are obtained from the granular kinetic theory for granular flows. The kinetic theory of granular flow (KTGF) can be used to describe particle interactions in a bubbling fluidized bed where particles are in random motion state and can collide with other particles in binary collisions (Ding and Gidaspow, 1990; Gidaspow, 1994).

7.3.1.1   Conservation of Mass

Because no mass transfer occurs between the two phases (gas and solid), the continuity equation is:

$$\frac{\partial}{\partial t}(\varepsilon_q \rho_q) + \nabla(\varepsilon_q \rho_q \vec{u}_q) = 0$$

(7.1)

7.3.1.2   Conservation of Momentum

The momentum equation is:

$$\frac{\partial}{\partial t}(\varepsilon_s \rho_s \vec{u}_s) + \nabla(\varepsilon_s \rho_s \vec{u}_s \vec{u}_s) = -\varepsilon_s \nabla p + \nabla \cdot \overline{\overline{\tau}}_s + \varepsilon_s \rho_s \vec{g} +$$

$$\sum_{p=1}^{n} K_{ls}(\overline{u_l} - \overline{u_s})$$

(7.2)

where $\overline{\overline{\tau}}_q$ is the qth phase stress-strain tensor

$$\overline{\overline{\tau}}_q = \varepsilon_q \mu_q (\nabla \vec{u}_q + \nabla \vec{u}_q^T) + \varepsilon_q (\lambda_q - \frac{2}{3}\mu_q)\nabla \cdot \vec{u}_q \overline{\overline{I}}$$

(7.3)

Here μ_q and λ_q are the shear and bulk viscosity of phase q.

$K_{ls}(=K_{sl})$ is the interphase momentum exchange coefficient, more details described at next section.

7.3.1.3   Fluid-Solid Momentum Transfer and Exchange Coefficient

The fluid-solid exchange coefficient K_{sl} can be written in the following general form:

$$K_{sl} = \frac{\varepsilon_s \rho_s f}{\tau_s} \tag{7.4}$$

where f is defined differently for the different exchange-coefficient models, and τ_s is the particle relaxation time.

$$\tau_s = \frac{\rho_s d_s^2}{18\mu_l} \tag{7.5}$$

where d_s is the particle diameter

Syamlal-O'Brien model (Syamlal, 1987)

$$K_{ls} = \frac{3}{4} \frac{C_D}{v_{r,s}^2} \frac{\rho_g |\vec{v}_s - \vec{v}_g|}{d_s} \alpha_g \alpha_s \tag{7.6}$$

$$f = \frac{C_D \operatorname{Re}_s \varepsilon_g}{24 v_{r,s}^2} \tag{7.7}$$

$$C_D = \left(0.63 + \frac{4.8}{\sqrt{\operatorname{Re}_s / v_{r,s}}}\right)^2 \tag{7.8}$$

$$\operatorname{Re}_s = \frac{\rho_g d_s |\vec{v}_s - \vec{v}_g|}{\mu_g} \tag{7.9}$$

$$v_{r,s} = 0.5(A - 0.06 \operatorname{Re}_s + \sqrt{(0.06 \operatorname{Re}_s)^2 + 0.12 \operatorname{Re}_s (2B - A) + A^2}) \tag{7.10}$$

$$A = \alpha_g^{4.14}$$

$$B = \begin{cases} \varepsilon_g^{C1} & \varepsilon_g \geq 0.85 \\ C_2 \varepsilon_g^{1.28} & \varepsilon_g < 0.85 \\ default\ value: \ C_1 = 2.65\ and\ C_2 = 0.8 \end{cases}$$

Wen and Yu model

$$K_{ls} = \frac{3}{4} C_D \frac{\alpha_s \alpha_l \rho_l \left| \vec{v}_s - \vec{v}_l \right|}{d_s} \alpha_l^{-2.65}$$

(7.11)

$$C_D = \frac{24}{\alpha_l \, Re_s} \left[1 + 0.15 (\alpha_l \, Re_s)^{0.687} \right]$$

(7.12)

Gidaspow model

when $\alpha_g > 0.8$ then:

$$K_{sl} = \frac{3}{4} C_D \frac{\alpha_s \alpha_l \rho_l \left| \vec{v}_s - \vec{v}_l \right|}{d_s} \alpha_l^{-2.65}$$

(7.13)

Where

$$C_D = \frac{24}{\alpha_l \, Re_s} \left[1 + 0.15 (\alpha_l \, Re_s)^{0.687} \right]$$

(7.14)

When $\alpha_l \leq 0.8$ then:

$$K_{sl} = 150 \frac{\alpha_s (1 - \alpha_l) \mu_l}{\alpha_l d_s^2} + 1.75 \frac{\rho_l \alpha_s \left| \vec{v}_s - \vec{v}_l \right|}{d_s}$$

(7.15)

In dense fluidized beds it is recommended to use Gidaspow drag law model.

7.3.1.4   The conservation of Energy

$$\frac{\partial}{\partial t} (\varepsilon_q \rho_q h_q) + \nabla (\varepsilon_q \rho_q \vec{u}_q h_q) = -\varepsilon_q \frac{\partial p_q}{\partial t} + \overline{\overline{\tau}}_q : \nabla \vec{u}_q - \nabla \vec{q}_q + S_q +$$

$$\sum_{p=1}^{n} (Q_{pq} + \dot{m}_{pq} h_{pq} - \dot{m}_{qp} h_{qp})$$

(7.16)

In fluidized beds, the energy transfer between particles and gas is more complex than which in a fixed bed because of the motion of the suspended particles and gas bubbles (Chen, 2005). Three heat transfer mechanisms are involved in fluidized beds: gas-particle convection, particle-particle conduction, and particle radiation. The heat transfer coefficient of a bubbling fluidized bed is used for all three cases, with the surface area of particles defined as:

$$h_p = \frac{Q}{A(T_p - T_g)}$$

(7.17)

A dimensionless Nusselt number, $Nu_p = h_p D / k$, indicates the relationship of the fluid thermal conductivity k and a characteristic length D that specified for each flow system (Bird et al, 2002). Ranz and Marshall (1952) presented a correlation for estimating the Nusselt number in fixed beds:

$$Nu_p = 2 + 0.6 \, Re_p^{0.5} \, Pr_g^{0.33} \tag{7.18}$$

here, Pr is the Prandtl number.

The Nusselt number correlation by Gunn (1978) could estimate the heat transfer for the fixed and fluidized beds, typically for a porosity range of 0.35-1.0 and Reynolds number of up to 1×10^5.

$$Nu = (7 - 10\alpha_f + 5\alpha_f^2)(1 + 0.7 \, Re_p^{0.2} \, Pr^{1/3}) + (1.33 - 2.4\alpha_f + 1.2\alpha_f^2) \, Re_p^{0.7} \, Pr^{1/3} \tag{7.19}$$

In the present investigation, the Gunn correlation was used in all numerical simulation involving energy exchange.

7.3.1.5   Constitutive Equation

Solid pressure

The solid pressure is composed of a kinetic term and a second term due to particle collision:

$$p_s = \alpha_s \rho_s \Theta_s + 2\rho_s (1 + e_{ss}) \alpha_s^2 g_{0,ls} \Theta_s \tag{7.20}$$

Radial Distribution Function

$$g_0 = \left[1 - \left(\frac{\alpha_s}{\alpha_{s,max}} \right)^{\frac{1}{3}} \right]^{-1} \tag{7.21}$$

Kinetic Viscosity

There are two options for prediction of the Kinetic viscosity by FLUENT:

Syamlal et al:

$$\mu_{s,kin} = \frac{\alpha_s d_s \rho_s \sqrt{\Theta_s \pi}}{6(3 - e_{ss})} \left[1 + \frac{2}{5}(1 + e_{ss})(3e_{ss} - 1)\alpha_s g_{0,ss} \right] \tag{7.22}$$

Gidaspow et al:

$$\mu_{s,kin} = \frac{10 d_s \rho_s \sqrt{\Theta_s \pi}}{96 \alpha_s (1 + e_{ss}) g_{0,ss}} \left[1 + \frac{4}{5}\alpha_s g_{0,ss}(1 + e_{ss}) \right]^2 \alpha_s \tag{7.23}$$

Bulk Viscosity (Lun et al)

$$\lambda_s = \frac{4}{3}\alpha_s d_s \rho_s g_{0,ss}(1+e_{ss})\left(\frac{\Theta_s}{\pi}\right)^{1/2} \tag{7.24}$$

Frictional viscosity

In present work, Schaeffer's expression was used:

$$\mu_{s,fr} = \frac{p_s \sin\phi}{2\sqrt{I_{2D}}} \tag{7.25}$$

where p_s is the solids pressure, ϕ is the angle of internal friction, and I_{2D} is the second invariant of the deviatoric stress tensor.

Granular Temperature

The granular temperature of solid phase is defined to be is proportional to the kinetic energy of the random motion of the particles.

$$\frac{3}{2}\left[\frac{\partial}{\partial t}(\rho_s\alpha_s\Theta_s) + \nabla\cdot(\rho_s\alpha_s\vec{v}_s\Theta_s)\right] = (-p_s\bar{I}+\bar{\tau}s):\nabla\vec{v}_s + \nabla\cdot\left(k_{\Theta_s}\nabla\Theta_s\right) - \gamma_{\Theta_s} + \phi_{ls} \tag{7.26}$$

where

$(-p_s\bar{I}+\bar{\tau}s):\nabla\vec{v}_s$ = the generation of energy by the solid stress tensor

$k_{\Theta_s}\nabla\Theta_s$ = the diffusion of energy (k_{Θ_s} is the diffusion coefficient)

γ_{Θ_s} = the collisional dissipation of energy

ϕ_{ls} = the energy exchange between the gas phase and the solid phase

The diffusion coefficient of granular temperature calculated according Syamlal-O'Briens is:

$$k_{\Theta_s} = \frac{15d_s\rho_s\alpha_s\sqrt{\Theta_s\pi}}{41(41-33\eta)}\left[1+\frac{12}{5}\eta2(4\eta-3)\alpha_s g_{0,ss} + \frac{16}{15\pi}(41-33\eta)\eta\alpha_s g_{0,ss}\right] \tag{7.27}$$

The diffusion coefficient of granular temperature calculated according to Gidaspow is:

$$k_{\Theta_s} = \frac{150d_s\rho_s\sqrt{\Theta_s\pi}}{384(1+e_{ss})g_{0,ss}}\left[1+\frac{6}{5}\alpha_s g_{0,ss}(1+e_s)\right]^2 + 2\rho_s\alpha_s^2 d_s(1+e_{ss})g_{0,ss}\sqrt{\frac{\Theta_s}{\pi}} \tag{7.28}$$

Lun et al. (1984) developed the following expression for calculating the collisional dissipation energy:

$$\gamma_{\Theta m} = \frac{12(1-e_{ss}^2)g_{0,ss}}{ds\sqrt{\pi}}\rho_s\alpha_s^2\Theta_s^{3/2} \tag{7.29}$$

7.3.1.6 Turbulence Models

The *k-ε* dispersed turbulence model was used in present work because the concentration of the secondary phase is dilute. The model is applicable when there is obviously a primary continuous phase and other phases are dispersed.

Turbulence in the primary phase

The turbulent predictions are obtained:

$$\frac{\partial}{\partial t}\left(\alpha_q \rho_q k_q\right) + \nabla \cdot \left(\alpha_q \rho_q \vec{U}_q k_q\right) = \nabla \cdot \left(\alpha_q \frac{\mu_{t,q}}{\sigma_k} \nabla k_q\right) + \alpha_q G_{k,q} - \alpha_q \rho_q \varepsilon_q + \alpha_q \rho_q \Pi_{kq} \tag{7.30}$$

$$\frac{\partial}{\partial t}\left(\alpha_q \rho_q \varepsilon_q\right) + \nabla \cdot \left(\alpha_q \rho_q \vec{U}_q \varepsilon_q\right) = \nabla \cdot \left(\alpha_q \frac{\mu_{t,q}}{\sigma_\varepsilon} \nabla \varepsilon_q\right) + \alpha_q \frac{\varepsilon_q}{k_q}\left(C_{1\varepsilon} G_{k,q} - C_{2\varepsilon} \rho_q \varepsilon_q\right) + \alpha_q \rho_q \Pi_{\varepsilon q}$$

$$\tag{7.31}$$

Here Π_{kq} *and* $\Pi_{\varepsilon q}$ represent the effect of the dispersed phases on the continuous phase, and $G_{k,q}$ is the production of turbulent kinetic energy.

$$\Pi_{kq} = \sum_{p=1}^{M} \frac{K_{pq}}{\alpha_q \rho_q}\left(k_{pq} - 2k_q + \vec{v}_{pq} \cdot \vec{v}_{dr}\right) \tag{7.32}$$

$$\Pi_{\varepsilon q} = C_{3\varepsilon} \frac{\varepsilon_q}{k_q} \Pi_{kq} \tag{7.33}$$

where $C_{3\varepsilon} = 1.2$

Turbulence in the Dispersed Phase

$$\tau_{F,pq} = \frac{\alpha_q \rho_q}{K_{pq}}\left(\frac{\rho_p}{\rho_q} + C_V\right) \tag{7.34}$$

There are three common turbulent *k-ε* models: the standard, RNG; and realizable. In the present work, the standard k-ε model is used for simulation due to excellent performance for a wide range of turbulent flows. The standard k-ε model consists by the turbulence kinetic energy k and dissipation rate ε.

$$\frac{\partial}{\partial t}(\rho k) + \frac{\partial}{\partial x_i}(\rho k u_i) = \frac{\partial}{\partial x_i}\left[\left(\mu + \frac{\mu_t}{\sigma_k}\right)\frac{\partial k}{\partial x_j}\right] + G_k + G_b - \rho \varepsilon - Y_M + S_k \tag{7.35}$$

$$\frac{\partial}{\partial t}(\rho \varepsilon) + \frac{\partial}{\partial x_i}(\rho \varepsilon u_i) = \frac{\partial}{\partial x_i}\left[\left(\mu + \frac{\mu_t}{\sigma_\varepsilon}\right)\frac{\partial \varepsilon}{\partial x_j}\right] + C_{1\varepsilon}\frac{\varepsilon}{k}(G_k + C_{3\varepsilon} G_b) - C_{2\varepsilon}\rho\frac{\varepsilon^2}{k} + S_\varepsilon \tag{7.36}$$

7.4 **Numerical simulations**

7.4.1   **Computational domains**

Three-dimensional fluidized bed domains with various geometries of twin-jet and single nozzles were used to study the features of the interactions between the two flows of the twin-jet as well as between the jet and the ambient fluid. The simulations were conducted using the commercial CFD code ANSYS Fluent 12.0. Figur**e 7.1** shows the computational 3-D domain for simulating the twin-jet at turbulent state, including the domain inside the nozzle and the ambient region around the nozzle outlet, while Figure **7.2** shows the computational 3-D domain for simulating the twin-jet in a gas-solid fluidization system.
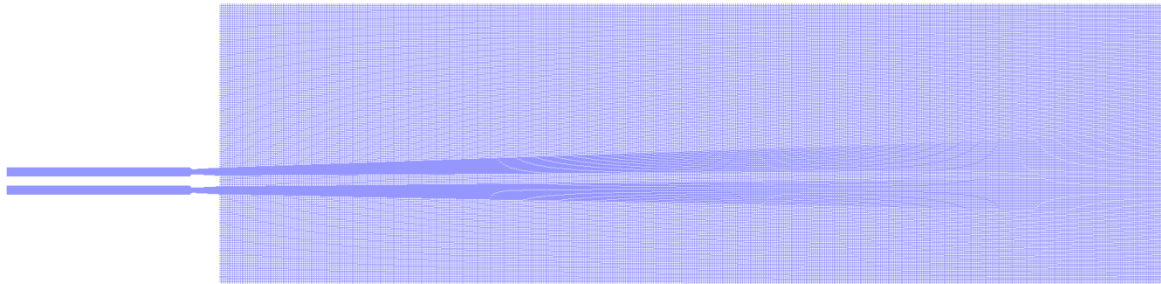
Figure 7.1 Computational domain and grid size for twin-jet at turbulent state
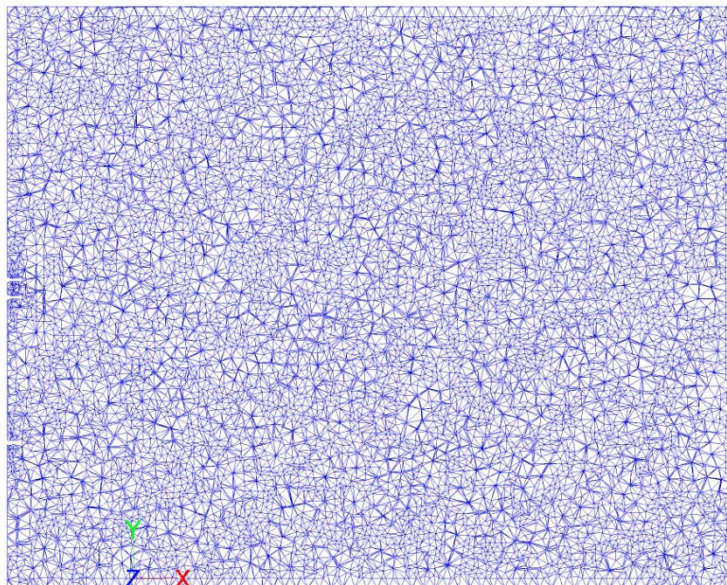
Figure 7.2 Computational domain and grid size for twin-jet in a fluidized bed

7.4.2 Operating parameters of the hot bed

Table 7.1 Simulation model parameters

Description	Value
Gas density	Incompressible & compressible
Particle density	Petroleum coke: 1450 kg/m^3
Mean particle diameter	Petroleum coke: 120 μm
Restitution coefficient	0.90
Initial solids packing	0.40
Superficial gas velocity	0.1 m/s – 0.3 m/s
Time step size	0.001 s
Maximum number of iterations	100
Convergence criteria	10^{-6}

Table 7.2 Configuration of secondary phase

Primary phase	Air
Secondary Phase	Petroleum coke
Granular	Activate
Granular temperature model	Phase property
Particle diameter	120 μm
Granular viscosity	Gidaspow
Granular bulk viscosity	Lun-et-al
Friction viscosity	Schaeffer
Angle of internal friction	30°
Friction pressure	Based-ktgf

Frictional modulus	Derived
Friction packing limit	0.61
Granular temperature	Algebraic
Solids pressure	Syamlal-O'Brien
Radial distribution	Lun-et-al
Elasticity modulus	derived
Packing limit	0.63

7.4.3   Boundary and initial conditions

The boundary conditions for the gas and solid phases are summarized in Table 7.3 and Table 7.4, respectively.

Table 7.3 Gas phase boundary conditions in Attrition Model

Name	Type	Value
Fluidization gas inlet	Mass flowrate inlet (mass flux)	V_g=0.10 -0.30 m/s
	Intensity and hydraulic diameter	4% Turbulent intensity; 0.17 m Hydraulic diameter
Bed out	Pressure outlet	P_{out} = 101325 MPa
	Intensity and hydraulic diameter	2% backflow turbulent intensity; 0.17 m Backflow hydraulic diameter
Nozzle inlet	Mass flow inlet	Varies with attrition pressures and attrition nozzles
	Pressure inlet	0.7 MPa - 2.1 MPa
	Turbulent intensity	4%
	Diameter (throat)	1.2 mm to 2.4 mm

Table 7.4 Solid phase boundary conditions in Attrition Model

Name	Type	Value
Fluidization gas inlet	Mass flowrate inlet (mass flux)	V_s=0.3 m/s
	Intensity and hydraulic diameter	4% Turbulent intensity; 0.17 m Hydraulic diameter
Bed out	Pressure outlet	P_{out} = 0 psig
	multiphase	Backflow volume fraction: 0
Nozzle inlet	Mass flow inlet	0
	Pressure inlet	0
	Volume fraction	0

7.4.4　Sensitivity study of mesh sizes

To study the sensitivity of the computational domain in relation to the mesh sizes of the simulation model, three different mesh sizes were chosen corresponding to cell numbers of 183 391, 287 770, and 410 539 respectively. The simulations ran for a period of 10 s real-time simulation for ensuring a statistical steady state. All the simulations were performed at a fluidization velocity of 0.30 m/s, with the Gidaspow drag model and 0.90 of restitution coefficient. To assess the mesh size sensitivity, solids velocity along the x-axial of single jet was predicted by simulation model. The Figure 7.3 shows the predicted results for the solid velocity distribution with the single jet with a 3.4 mm throat diameter. It can be observed that the medium mesh size corresponding to 287 770 cells and the fine mesh size corresponding to 410 539 cells provided similar results. Considering the computational cost, a mesh size corresponding to 287 770 cells was used in most of the subsequent simulation work.
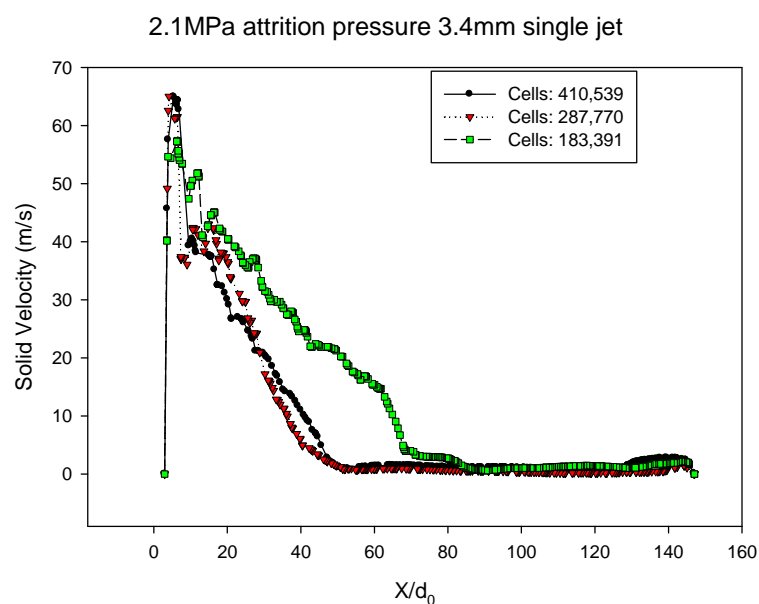
Figure 7.3 Mesh size sensitivities of solid velocity distribution in the single jet.

7.5 Experimental setup

Attrition experiments were carried out in a high temperature fluidized bed with a height of 1.23 m and a rectangular cross-section of 0.10 m × 0.50 m (Figure 7.4). The bed particles were typically heated up to 500°C with an in-bed electrical heater. Cold gases were injected into the hot fluidized bed via a convergent-divergent attrition nozzle located on the sidewall of the fluidized bed at a distance of 0.127m above the gas sparger. The operating temperature was

varied from ambient temperature to 500°C, while the cold gas pressure upstream of the supersonic nozzle ranged from 689 to 2068 kPa.
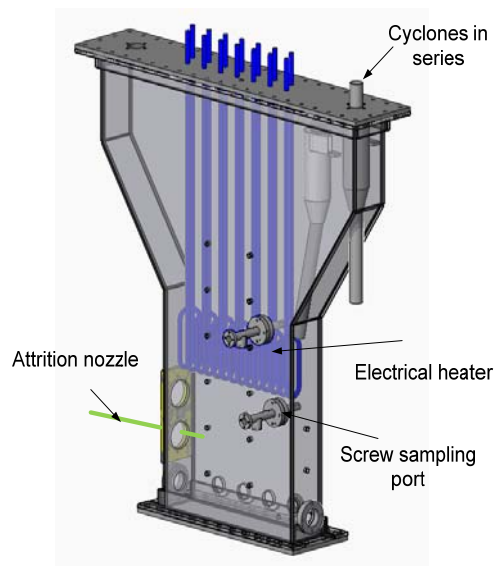

Figure 7.4 Schematic diagram of the hot fluidized bed

Figures 7.5 to 7.7 illustrate the single jet and twin-jet nozzles used in the present investigation, which are located inside the bed at a 0.127 m height above the fluidizing gas distributor. The twin-jet attrition nozzles were designed and fabricated specifically for determining the performances of twin-jet in jet-induced attrition experiments. The twin-jet nozzles used in experiments have the same Mach number and gas flowrate as the single nozzles. Since the nozzle spacing ratios affect the performance of the twin-jet nozzles, three different centre-to-centre spacing ratios were chosen, s/d, 4.0, 5.2, and 6.5, respectively. Meanwhile, two different geometries of twin-jet nozzles, extended twin-jet and flush twin-jet, were used in the present work, as shown in Fig.7.6 and Fig. 7.7.

Figure 7.5 A kind of convergent-divergent Nozzle used in the experiments
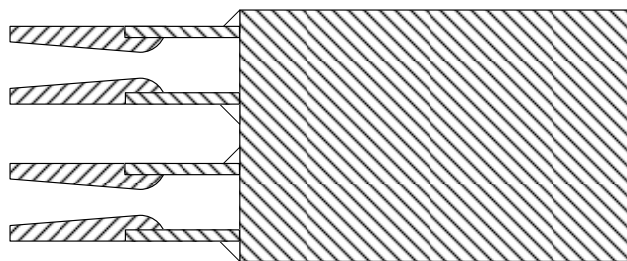
Figure 7.6 Scheme of extend twin-jet supersonic nozzle(s/p=4.0,5.2, 6.5)
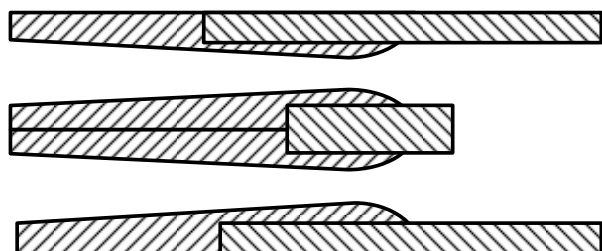
Figure 7.7 Scheme of flush twin-jet supersonic nozzle (s/p=4.0).

During each attrition run, bed particle samples were taken from the bed through sampling ports equipped with extraction screws and fines samples were collected from cyclones at regular intervals. After sampling, the particle size distribution of each sample was measured with a laser diffraction analyzer (HELOS of Sympatec Ltd).

A specific fluidized bed with two compartments was used for the solids entrainment measurements, as shown in Figure 7.8. The fluidized bed is constructed of polycarbonate, has a rectangular cross-section of 1.2 m × 0.1 m, and is 2.3 m tall. The bed is divided into two equal compartments by a partition wall, with an opening fitted with a draft tube. The fluidization velocity in each compartment is independently controlled by sonic nozzles and pressure regulators. A VTL (vertical transport line) unit is installed in the fluidized bed; it is comprised of a nozzle, a vertical riser, an elbow, a disengaging cyclone, and a downer with one 1 m length of sight glass and one pinch valve. A shroud installed around the VTL nozzle was used to maximize solids flow through the VTL. The bed solids could, thus, be pneumatically transported from the left side of bed to the right side through the VTL, while solids were conveyed back from the right side to left side by the supersonic nozzle through the draft tube connecting the two compartments. In each experiment, the gas flow through the VTL nozzle was adjusted until the bed levels in both compartments of the column became the same, as indicated by a zero differential pressure between the two compartments, and remained steady. The flowrate of solids entrained into the

jet and carried from the right hand side compartment to the left hand side compartment was, then, equal to the solids flowrate through the VTL, which could be accurately measured by closing the pinch valve and monitoring the rise of the solids level through the sight glass, using a camera. More details for solids entrainment measurement are described in the previous work (Li et al., 2010a).
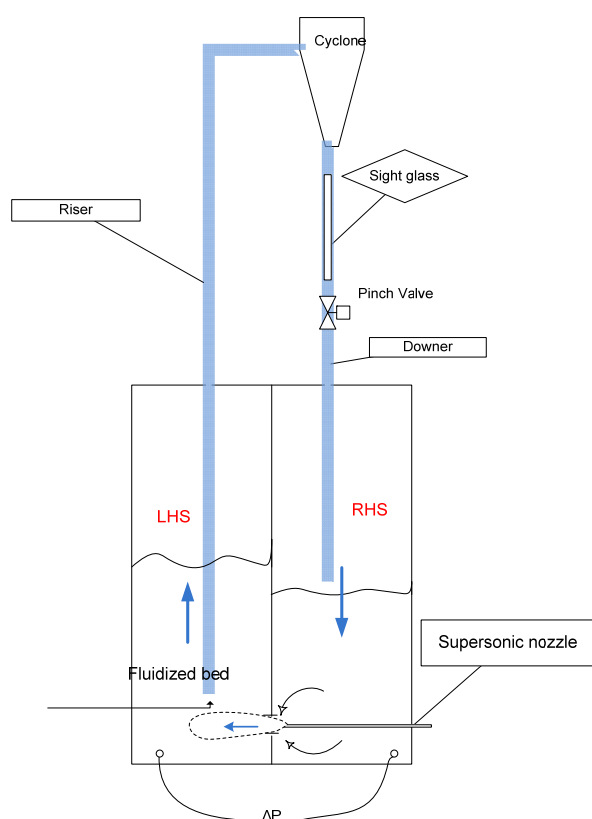

Figure 7.8 The fluidized bed with the Vertical Transport Line.

7.6 **Results and discussion**

7.6.1   **Results of numerical simulation:**

In this section, results predicted for the interaction characteristics of twin-jet nozzle are reviewed. As discussed earlier, the entrainment of particles in a jet was found to be a major factor in particle attrition. As seen in Figure 7.9, Merry proposed that the majority of entrainment occurs at the potential core region of a horizontal jet in a fluidized bed (Merry, 1971). Here, the

potential zone of turbulent free jet is defined as a core of flow in which the velocity remains constant and equal to the jet exit velocity, as shown in Figure 7.10 (Rajaratnam, 1976). Davies (1972) suggests that the length of potential zone is about 6.4 jet diameters, followed by a transition zone of about 8 jet diameters.
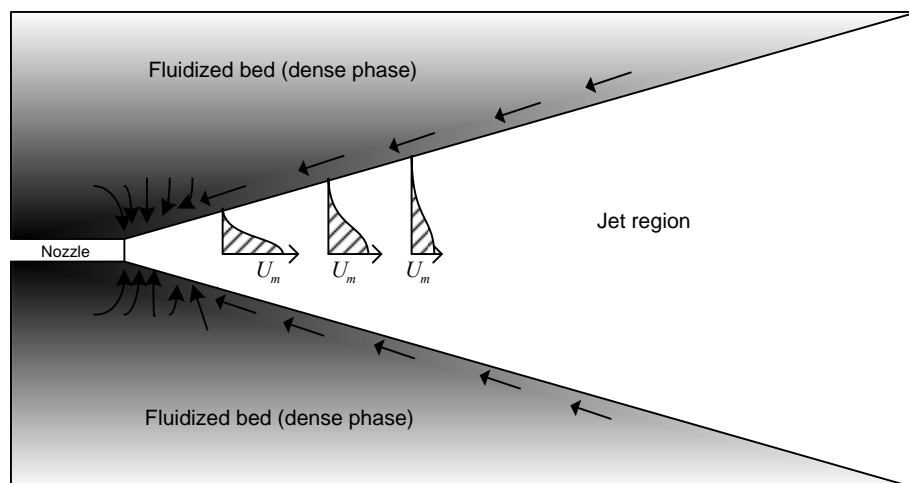

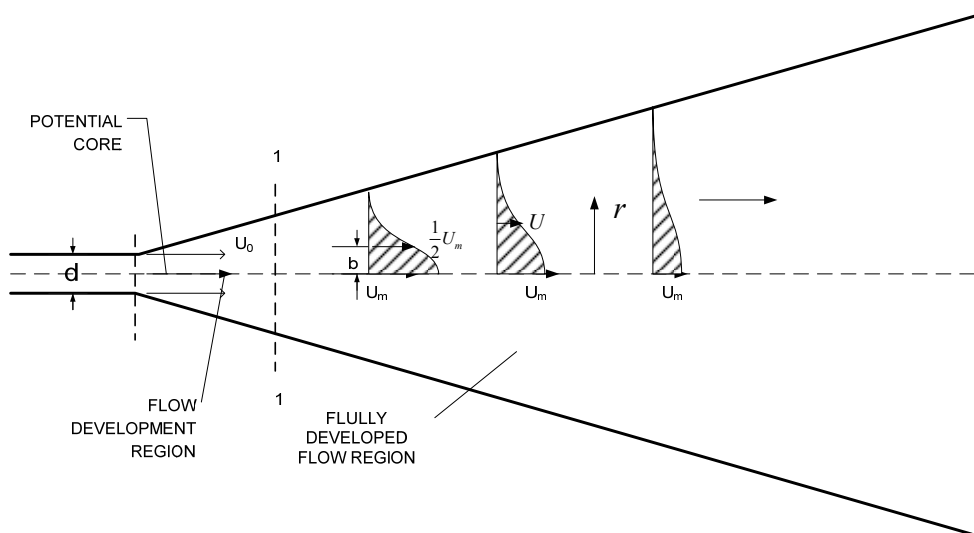**Figure 7.9 Solid entrainment tracks in the injection region (adapted from Merry, 1971)**

Figure 7.10 Configuration of turbulent jets (adapted from Rajaratnam, 1976)

De Michele and Massimilla (1976) proposed an equation to predict the penetration of the potential core in gas-solid systems:

$$L_p = \frac{d_0}{0.378 \lg(\rho_B / \rho_g)} \tag{7.37}$$

They further declared that there was a considerable reduction in the length of the potential core of a gas jet in fluidized beds, since its length to diameter ratio is only about 0.5 instead of 6.4-8 in a gas.

In the investigation of multiple jets, Raghunathan and Reid (1981) believe that the noise reduction in multiple jets is mostly caused by the enhancement of mixing and entrainment from the surrounding medium. This suggests that the interaction of two supersonic jets is probably an effective approach to enhance solids entrainment and momentum transport between gas and solids. Lin and Sheu (1991) proposed that the flow field of a twin-jet can be defined by three regions: the convergent region, the merging region, and the combined region, as shown in Figure 7.11.
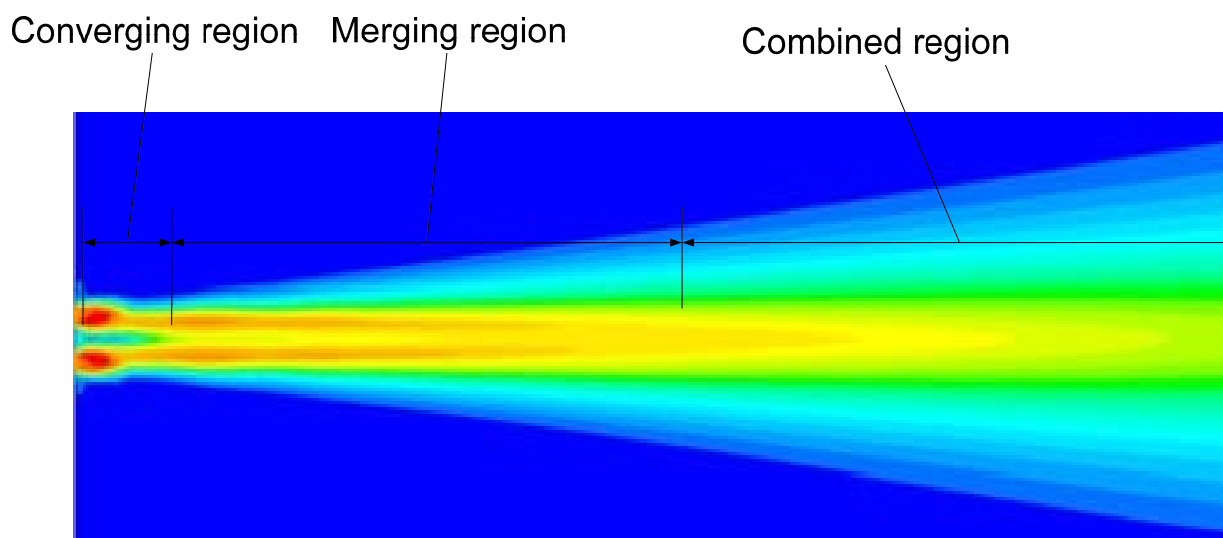
Figure 7.11 Interaction of two free jets with three regions

In order to assess the interaction characteristics between two flows of twin-jets nozzle, numerical simulations were carried out with the multiphase Eulerian-Eulerian Model that was described earlier.

7.6.1.1   Potential zone and turbulent developing area of twin free jets:

Figure 7.12 illustrates that the mean velocity profile of two supersonic nozzles in the x-y two-dimension plane, with A_e/A_t = 2.8, NPR=21, and 5.2 of nozzle centre-to-centre spacing. The velocity profile to a single supersonic nozzle are given in Figure 7.13, with the same operating

conditions of $A_e/A_t = 2.8$ and $p_0/p_a = 20$. Meanwhile, the throat diameter of the single nozzle D is equal to $\sqrt{2}d$, where d is the throat diameter of each small nozzle of the twin-jet. In the present work, the potential core region of the jet is defined as the region downstream of the nozzle tip where turbulent flow is developing. The potential core region of the twin-jet can be observed to be shorter but wider than for the single nozzle. Closer observation of the region near the nozzle tips, in Figure 7.14 and Figure 7.15, shows that increasing the nozzle pressure ratio can increase the length of the potential core due to the shock wave of expanded jets.
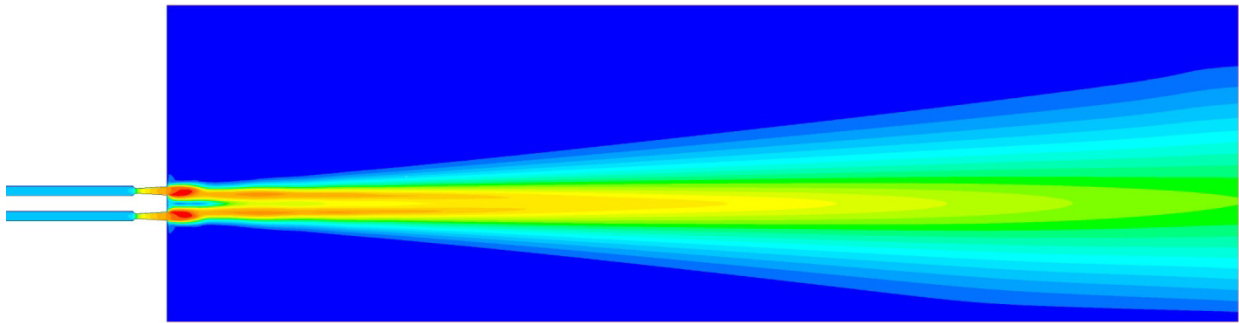
Figure 7.12 Velocity profile of twin nozzles as free jets (with $A_e/A_t = 2.8$, $p_0/p_a = 20$, s/d= 5.2).
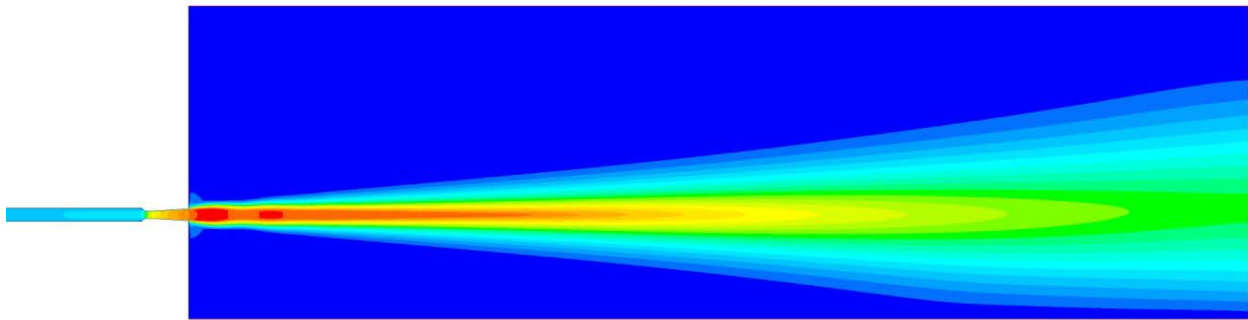
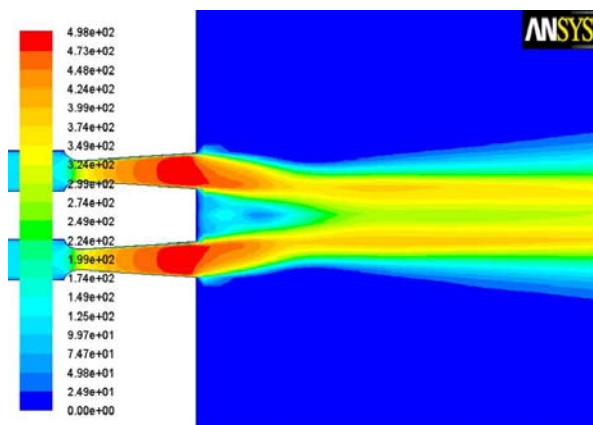**Figure 7.13 Velocity profile of single nozzle as a free jet ($A_e/A_t = 2.8$, $p_0/p_a = 20$)**

Figure 7.14 Velocity profile of twin free jets(with $A_e/A_t = 2.8$, $p_0/p_a =7$, s/d=4.0)
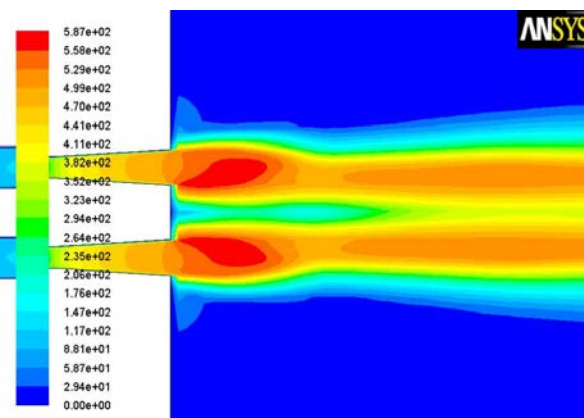
Figure 7.15 Velocity profile of twin free jets(with $A_e/A_t = 2.8$, $p_0/p_a =20$, s/d=4.0)

7.6.1.2   Mean gas velocity distributions

The major parameters governing the features of a supersonic twin-jet are nozzle pressure ratio (p_0/p_a), throat/exit area ratio, and nozzle centre-to-centre spacing (s/d). Figure 7.16 to Figure 7.19 show the mean axial velocity contour plots for twin-jet with the same pressure ratio and area ratio, but various nozzle spacings. The exit velocities for all three spacing values are the same magnitude. It is can be observed that the mean velocity of the twin-jet is symmetric with x-axial and the nozzle spacing has a dramatic effect on how the two jets mix and merge. Particularly, the two jets mix and merge into a single jet faster for smaller nozzle spacings.
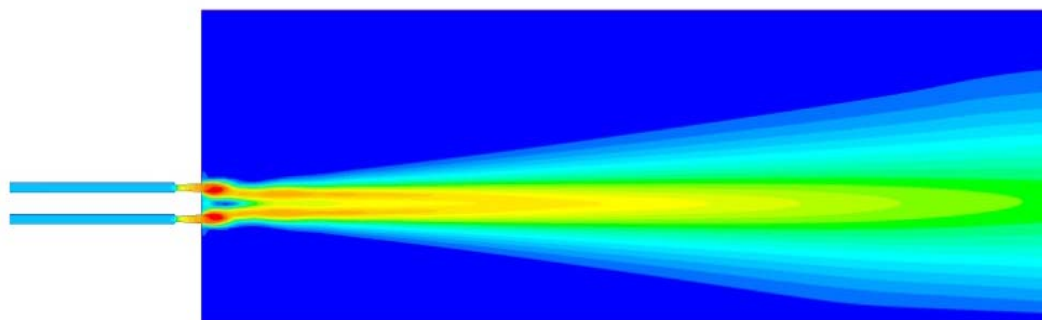

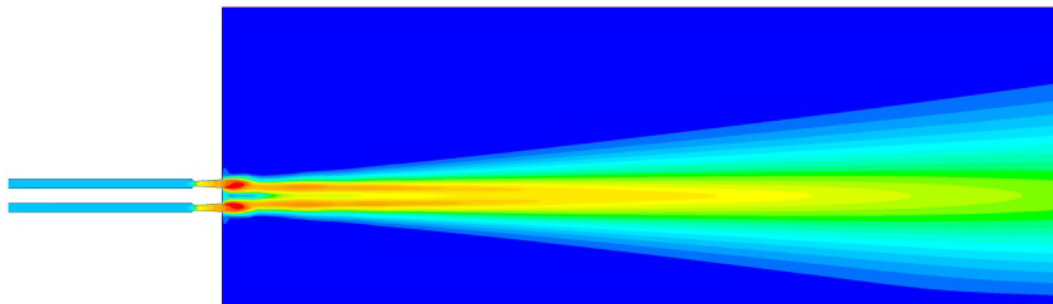**Figure 7.16 Velocity distribution of twin jets with 6.5 spacing ratio at 2.1MPa inject pressure**

Figure 7.17 Velocity distribution of twin jets with 5.2 spacing ratio at 2.1MPa inject pressure
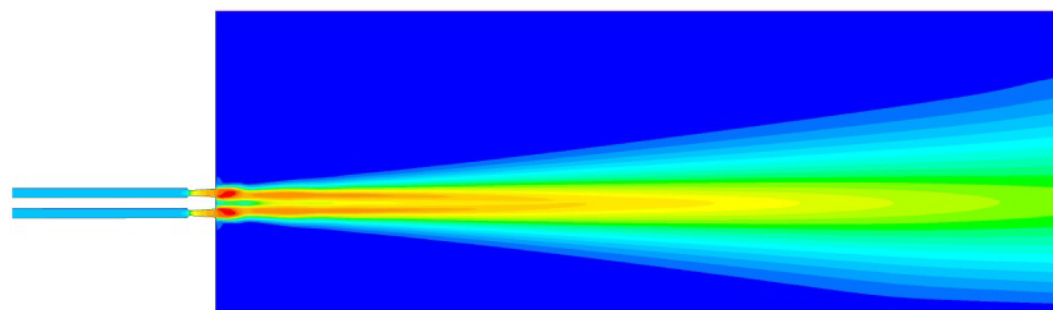

Figure 7.18 Velocity distribution of twin jets with 4 spacing ratio at 2.1MPa inject pressure
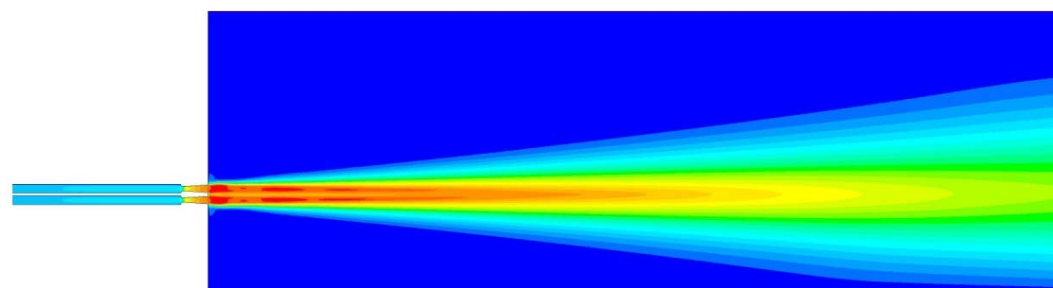

Figure 7.19 Velocity distribution of twin jets with 2.5 spacing ratio at 2.1MPa inject pressure

The variation of mean axial velocity along the jet centerlines is shown in Figure 7.20. It can be seen that the two jets develop the turbulent flow by shock wave in the potential zone, and then start to merge, reach a maximum value and then decrease as the single jet would. The single nozzle has a higher the peak centre-line velocity compared with the twin nozzle. In contrast to the single nozzle, the twin-jet nozzle was found to display a more significant velocity decay and lower intensity levels, which can be observed clearly in Figure 7.21 and Figure 7.22.
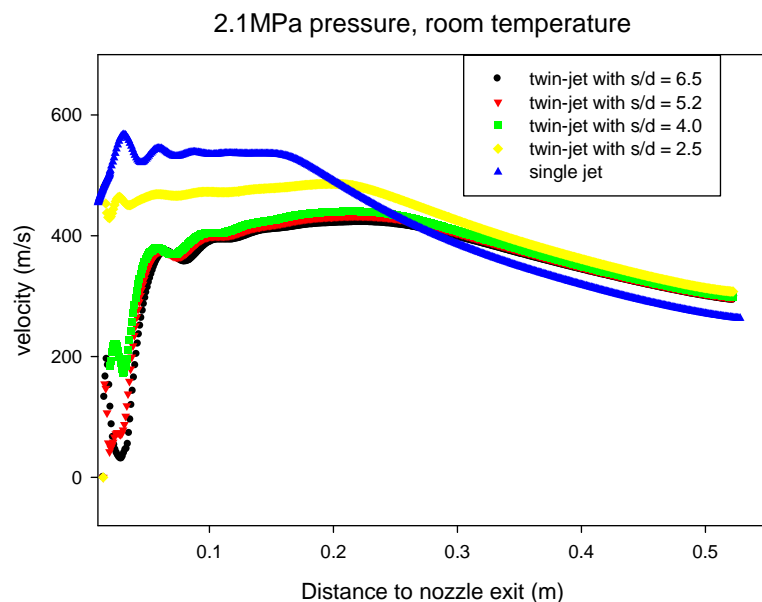
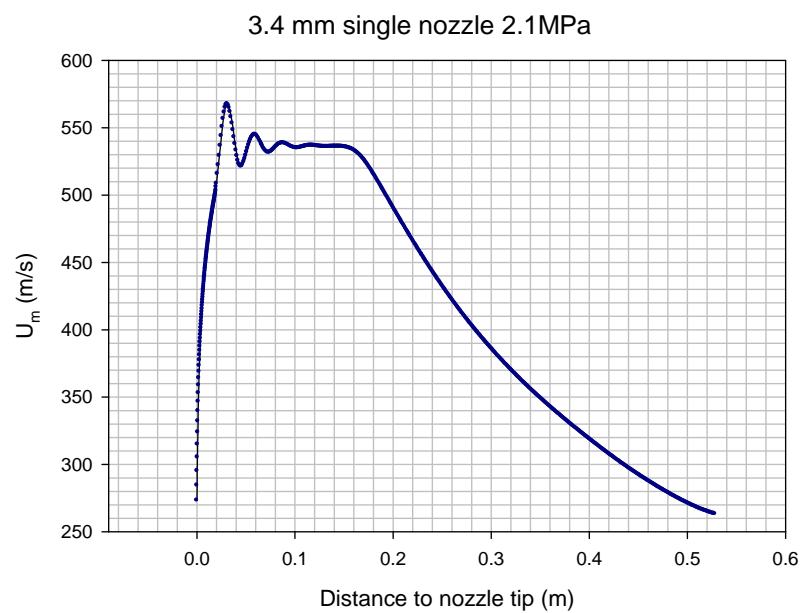**Figure 7.20 Axial velocity profiles at the jet centerline**

Figure 7.21 Axial velocity profile at the jet centerline for a single nozzle (3.4 mm single nozzle, 2.1 MPa attrition pressure)
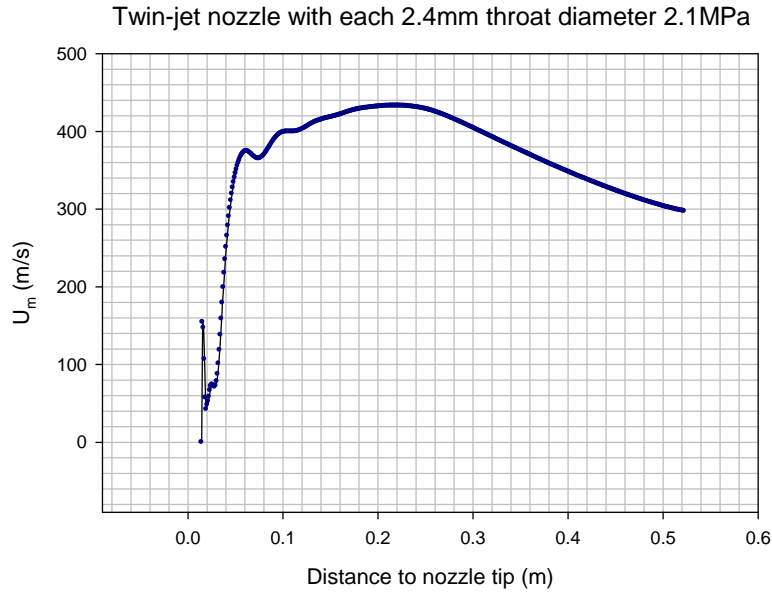
Twin-jet nozzle with each 2.4mm throat diameter 2.1MPa

Figure 7.22 Axial velocity profile at the jet centerline for a twin-jet nozzle (2.4 mm diameter, 2.1 MPa attrition pressure, s/d=5.2)

7.6.1.3   Solid velocity and solid temperature

A number of investigations were focused on the interaction characteristics of gas and solid phases when the twin-jet was used as supersonic jets in a fluidized bed. Figure 7.23 illustrates the contours of solid velocity for both twin-jet nozzle and single nozzle. It can be observed that the solid velocities are higher for twin-jet nozzle due to the mixture and combination of two jets. The predicted results of a single-jet are compared with the results of twin-jet of various spacing values in Figure 7.24. It shows that the twin-jet with a small spacing of 4 and the single-jet have higher particle velocities in merging area but with their velocity decreases faster with distance from the nozzle tip. Moreover, Figure 7.25 illustrates that the solids velocity increases with increasing attrition pressure.
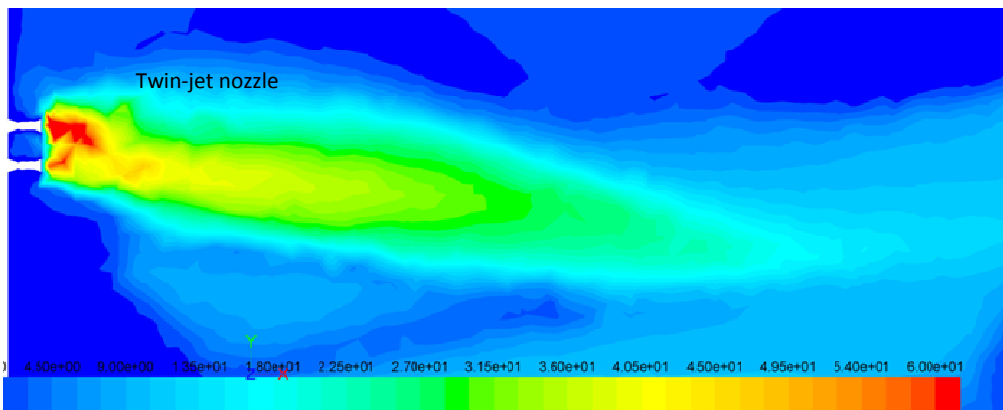
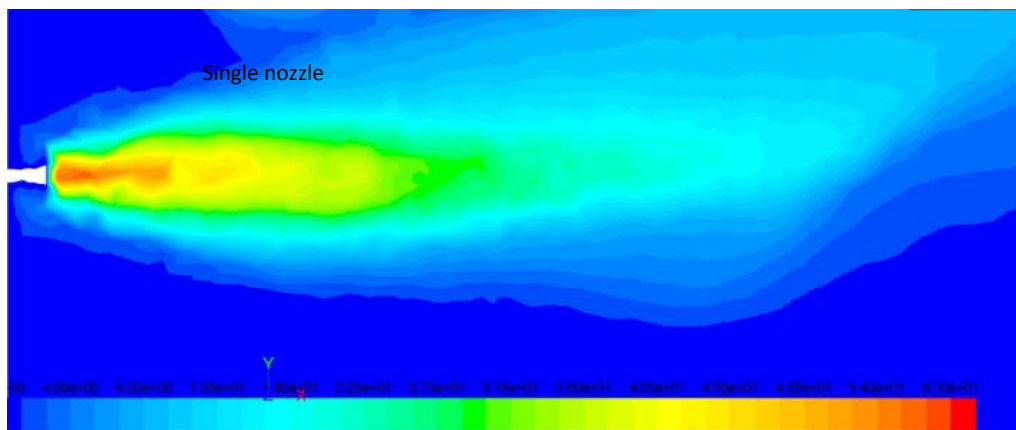Figure 7.23a:Contour of solid velocity (twin-jet)

Figure 7.23b:Contour of solid velocity (single-jet)

Figure 7.23 Contours of solid velocity of attrition nozzles in fluidized beds (2.1MPa attrition pressure, 2.4 mm twin-jet nozzle and 3.4 mm single nozzle)
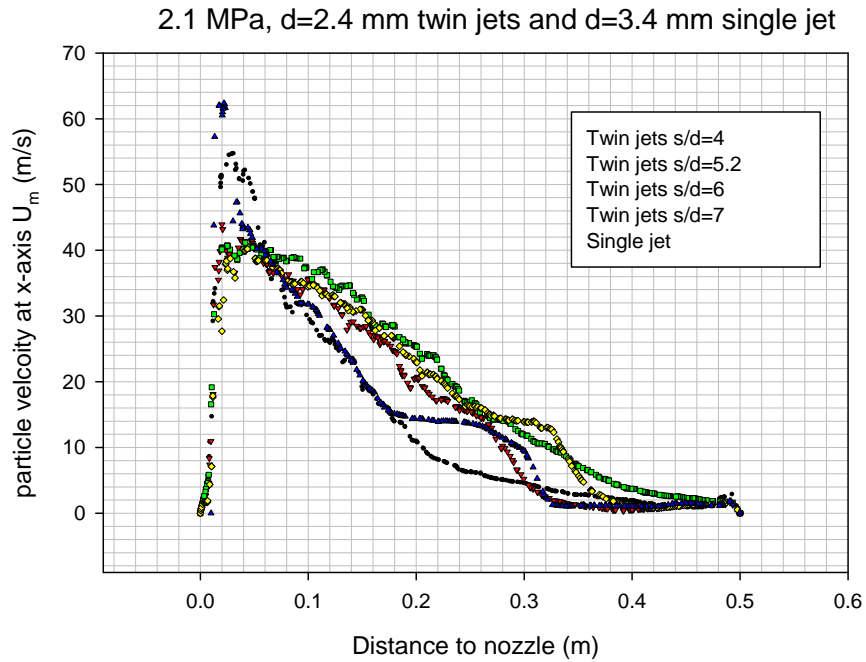
2.1 MPa, d=2.4 mm twin jets and d=3.4 mm single jet

Twin jets s/d=4
Twin jets s/d=5.2
Twin jets s/d=6
Twin jets s/d=7
Single jet

Figure 7.24 Comparison of particle velocity at the jet centerline for various jet configurations

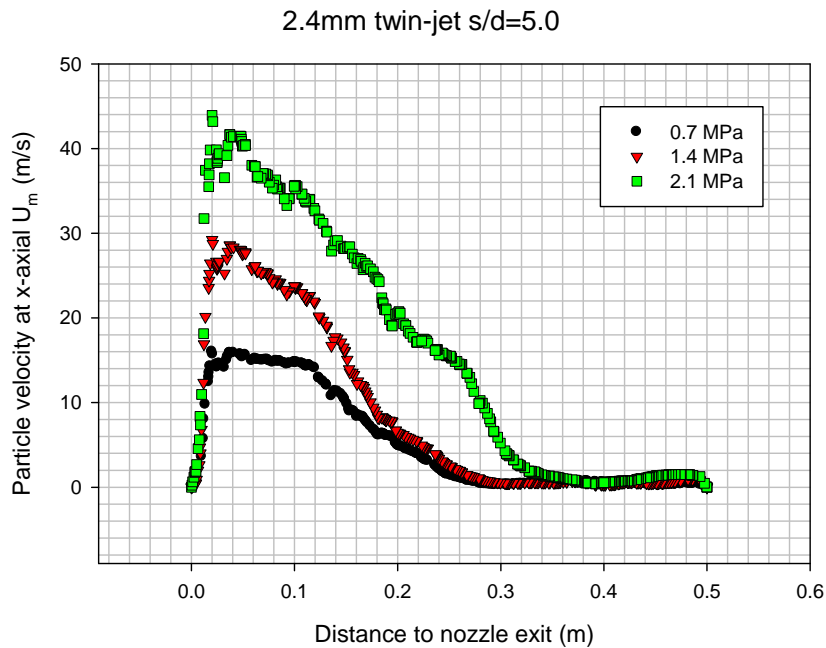## 2.4mm twin-jet s/d=5.0

- 0.7 MPa
- 1.4 MPa
- 2.1 MPa

Figure 7.25 Particle velocity in the centerline of jet at various jet pressures (s/d=5.2).

The kinetic theory of granular flow could be used to describe the flow behaviour of a fluid-solid mixture. Ogawa et al. (1980) suggested that the mechanical energy of granular flow is first

converted to random particle fluctuations and then dissipated into internal energy. In the kinetic theory of granular flow, the granular temperature of particles is defined as (Gidaspow, 1994):

$$\Theta = \frac{1}{3}\langle c^2 \rangle$$

(7.38)

where c denotes the instantaneous solids velocity.

In this work, the granular temperature is used to gauge the momentum and energy transformation in supersonic jet area. As illustrated in Figure 7.26, the twin jet has a much higher granular temperature at the potential core region when compared with the single jet at the same operating conditions. The intense particle velocity is expected at mixing region of twin-jet due to the enhanced momentum transfer between particle and solid phases caused by the interaction of the two nozzle flows. It can be assumed that the twin-jet achieves higher momentum transfer efficiency. Figure 7.27 shows the particle tracks in the vicinity of the twin-jet.
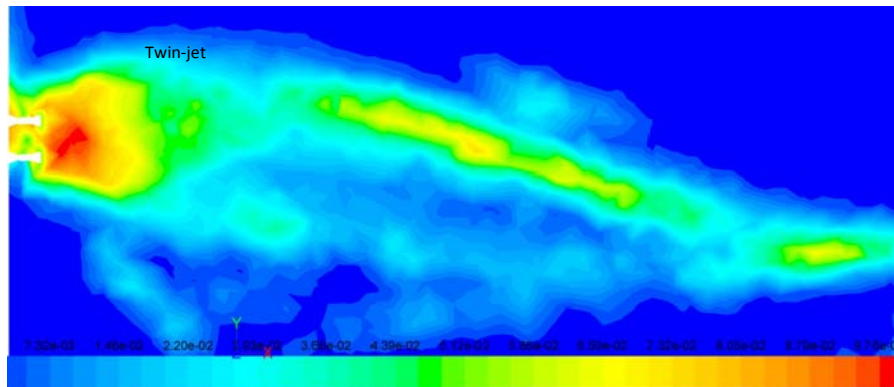

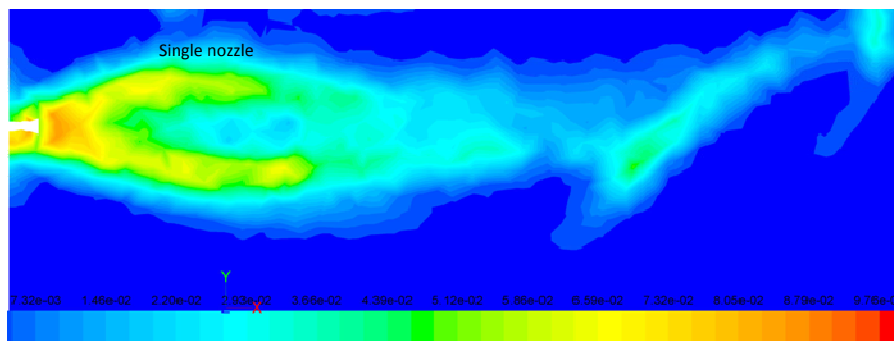Figure 7.26a:Contour of solids granular temperature (twin-jet)

Figure 7.26b:Contour of solids granular temperature (single-jet)

Figure 7.26 Contours of solids granular temperature with twin-jet nozzle and single jet.
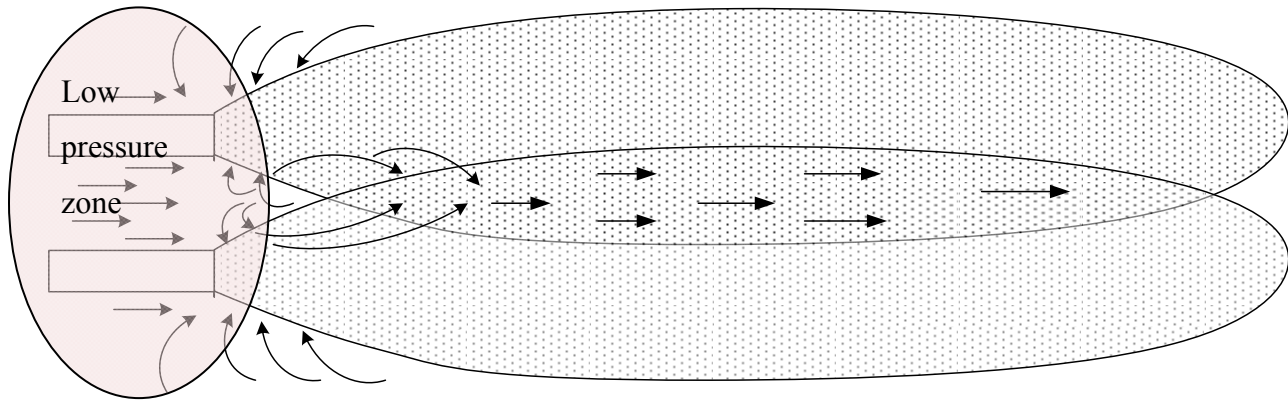
Figure 7.27 The entrained solid tracks in void vicinity of twin-jet

The numerical study of the twin-jet interaction shows that the region enclosed between the two jets develops a low-pressure zone as seen in Figure 7.27, which can promote the entrainment in potential cores and the jet shear layers. In particular, the space between the two jets promotes particle entrainment due to more space area and low pressure.

7.6.2   Experimental Results

A number of attrition experiments were performed in hot fluidized bed by twin-jet and single jet to compare with the simulation results. The main goal was to investigate if the twin-jet features found in the numerical study could promote particle attrition in a fluidized bed. The particle grinding efficiency was chosen as the criterion to assess the particle attrition in the present study. The particle grinding efficiency was first introduced by McMillan (2007a), as a ratio of the new surface area created per mass of attrition gas used. The grinding efficiency was determined from the bed particle and cyclone fines samples:

$$\eta(m^2/kg) = \frac{a_{bed}^f + a_{fines}^f - a_{bed}^i}{m_{attr}} \tag{7.39}$$

7.6.2.1   Influence of jet centre-to-centre spacing ratio

Due to the crucial roles of the jet spacing ratio in the dynamics of the twin-jet nozzle, three centre-to-centre spacing ratios were chosen in testing, which are 4, 5.2, and 6.5, respectively. The experimental results show that the twin-jets nozzle with 5.2 spacing ratio displayed a remarkable increase in grinding efficiency (Figure 7.28). The grinding efficiency is consistently about 30% higher with this twin-jet nozzle when compared with the single nozzle, when both nozzles had

the same exit properties, as shown in Figure 7.29. The benefits of the twin-jet nozzle seem stronger at higher nozzle pressures. Meanwhile, experiments also suggest that the attrition nozzles with spacing ratio of 4.0 and 6.5 have little influence on the grinding efficiency. In Figure 7.30, the same trend can be observed for attrition tests at the room temperature.
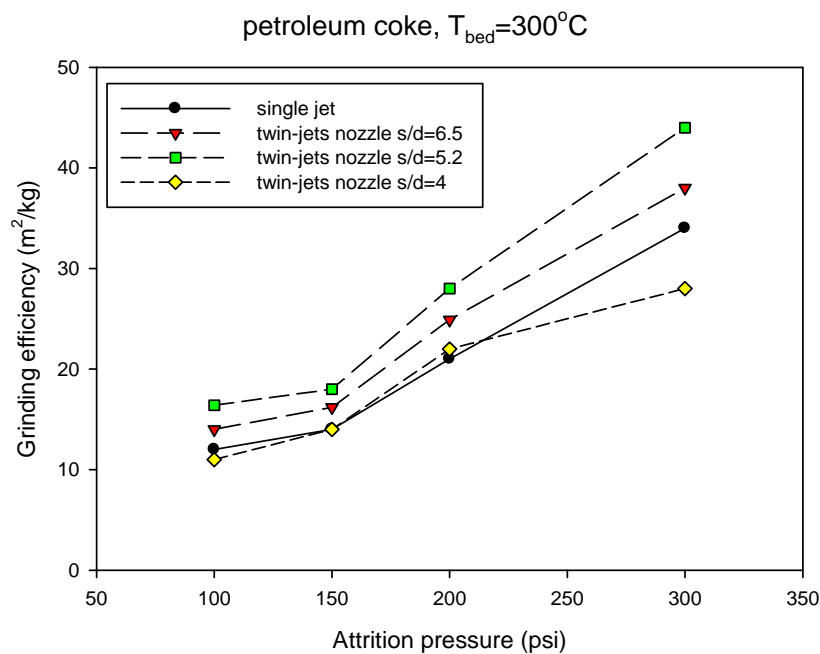
Figure 7.28 Influence of centre-to-centre spacing ratio of twin-jet nozzle on grinding efficiency in fluidized bed
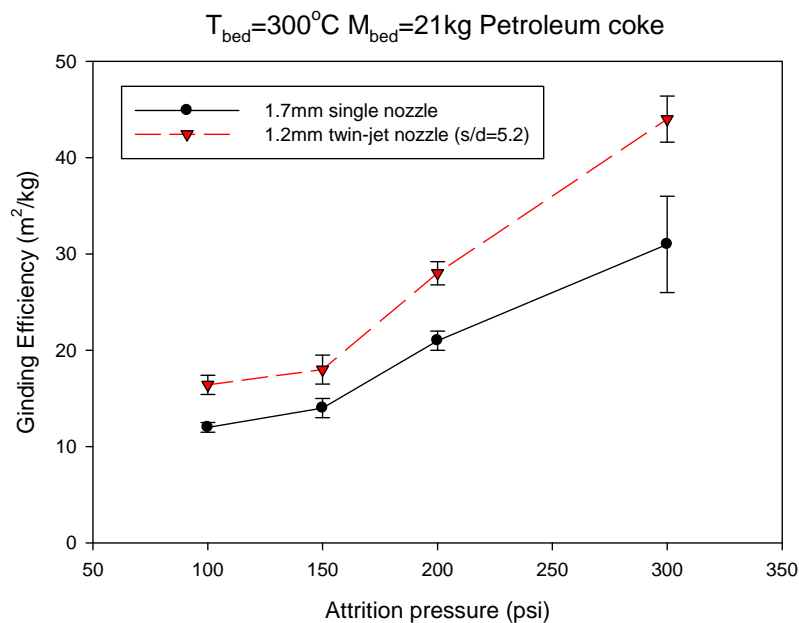
Figure 7.29 Comparison of performance of twin-jet nozzle (s/d=5.2) with single nozzle in attrition experiments.
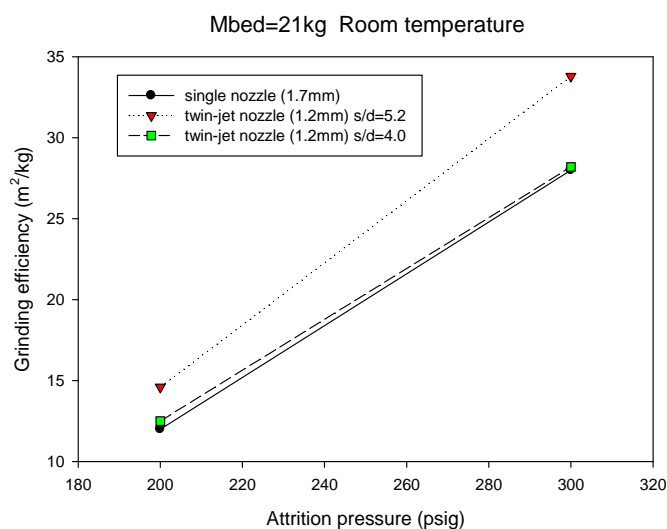
Figure 7.30 Comparison of performance of twin-jet nozzle with single nozzle in attrition experiments at room temperature.

7.6.2.2   Influence of jet orientation on the grinding efficiency

Tests showed that the nozzle orientation had little influence on the grinding efficiency of particle attrition in fluidized beds, as shown in Figure 7.31 and Figure 7.32.

Figure 7.31 Orientations of twin-jet nozzles

T_{bed}=300°C, m_{bed}=21kg, U_g-U_{mf}=0.20 m/s,Syncrude coke

Figure 7.32 Influence of twin-jet orientation on the grinding efficiency.

7.6.2.3   The influence of properties of twin-jet nozzle on grinding efficiency

In order to further study and integrate the effects of properties of twin-jet nozzles on particle attrition in fluidized beds, three operating conditions were chosen to carry out experiments (see Table 7.5). Due the excellent performance of the spacing ratio at 5.2, this spacing ratio was used in subsequent tests.
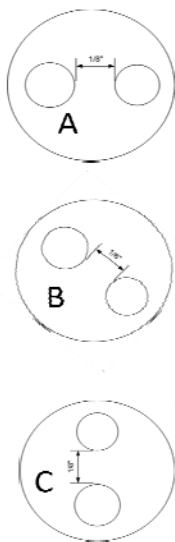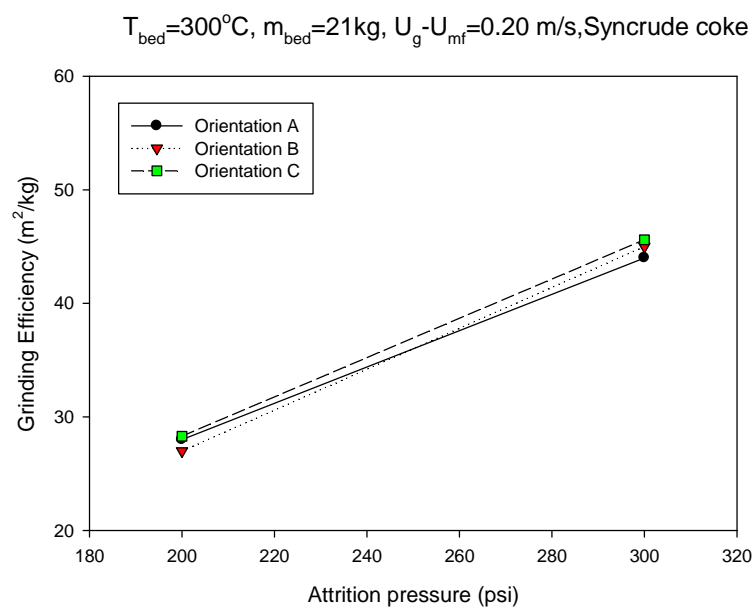
Table 7.5 Three operation conditions for attrition experiments

	Nozzle	Diameter (mm)	Mach Number	Cross-section area (m^2)
Case A	Single-jet	1.2	2.58	1.13×10^{-6}
Case B	Single-jet	1.7	2.58	2.27×10^{-6}
Case C	Extended twin-jet	1.2 (each, 5.2 nozzle central-to-central spacing ratio)	2.58	2.26×10^{-6}

Figure 7.33 shows the results of the attrition experiments for all three cases. The twin-jet nozzle gave the highest grinding efficiency. To continue investigate the solids entrainment for these cases, as seen Figure 7.34 and Figure 7.35, the twin-jet entrained more particles in jet from ambient system. However, the solids entrainment and entrainment efficiencies of twin-jet are lower than those for two isolated single nozzles.
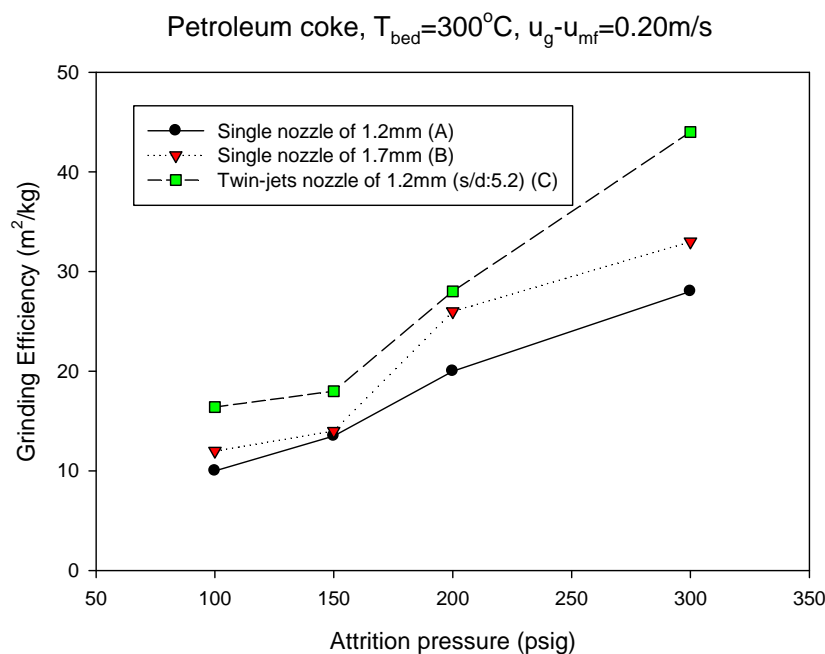

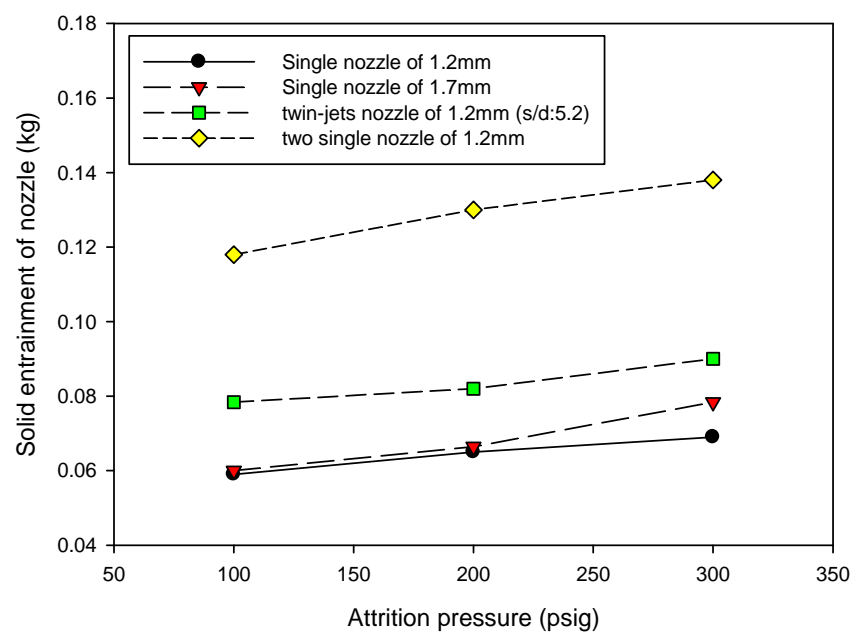**Figure 7.33 Performance of particle attrition with various nozzles**

Figure 7.34 Solids entrainment of nozzle with various nozzles
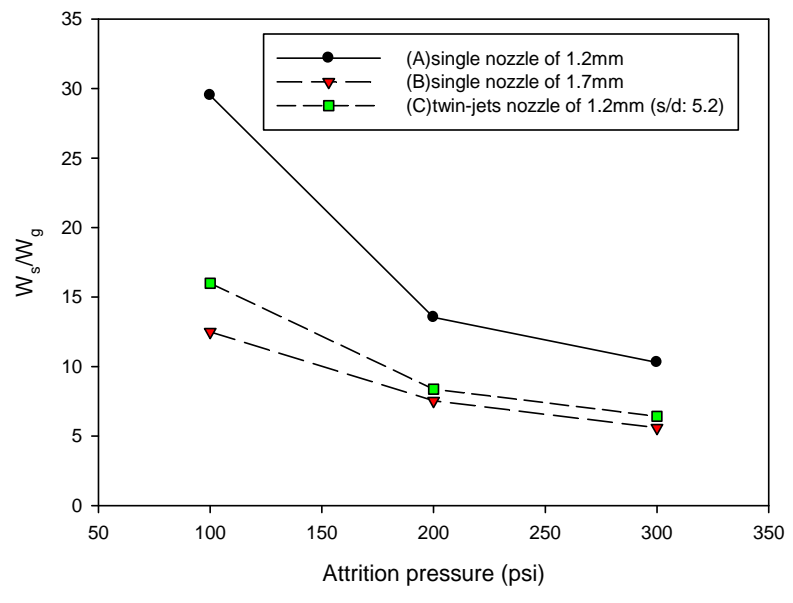

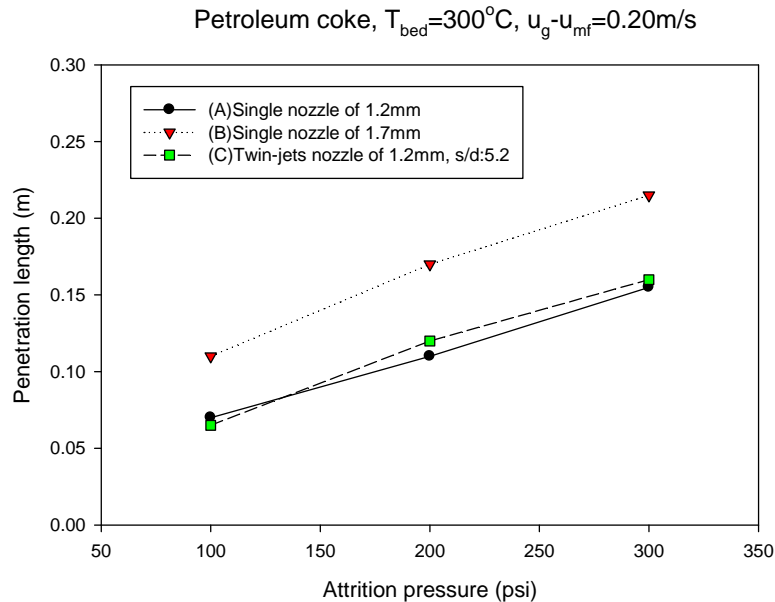**Figure 7.35 Particle entrainment efficiency with various nozzles**

Figure 7.36 Jet penetration lengths with various nozzles.

Figure 7.36 shows that the penetration length with the 1.2 mm twin-jet nozzle is similar to the penetration length with the single nozzle. Thereby, the twin-jet nozzle gives a shorter jet than the single nozzle with the same cross-section area. This is probably because the twin-jet entrains more solids from ambient system, which enhances the momentum and energy transfer between high speed gas jet and entrainment solids, and finally boosts the particle attrition; less energy is then available for penetration.

7.6.2.4   The influence of geometry of twin-jet on grinding efficiency

A specific geometry of a flush twin-jet was chosen to investigate the effect of the nozzle configuration on particle grinding efficiency, as shown in Figure 7.7. This typical twin-jet nozzle is flush with the conduit tip. Figure 7.37 shows the attrition experimental results using the single jet and the flush twin-jet (s/d=4.0). Moreover, it is known at previous section that the 1.2 mm twin-jet attrition nozzle with spacing ratio of 4.0 provides the similar grinding efficiency with the 1.7 mm single attrition nozzle at room temperature, as seen Figure 7.30. Therefore, it can be concluded that the flush twin-jet (s/d=4.0) contributes lower grinding efficiency than the single nozzle as well as the extended twin-jet (s/d=4.), with the same Mach number and the same operation conditions. It is probably because the flush geometry limits particle entrainment from the space between the nozzles.
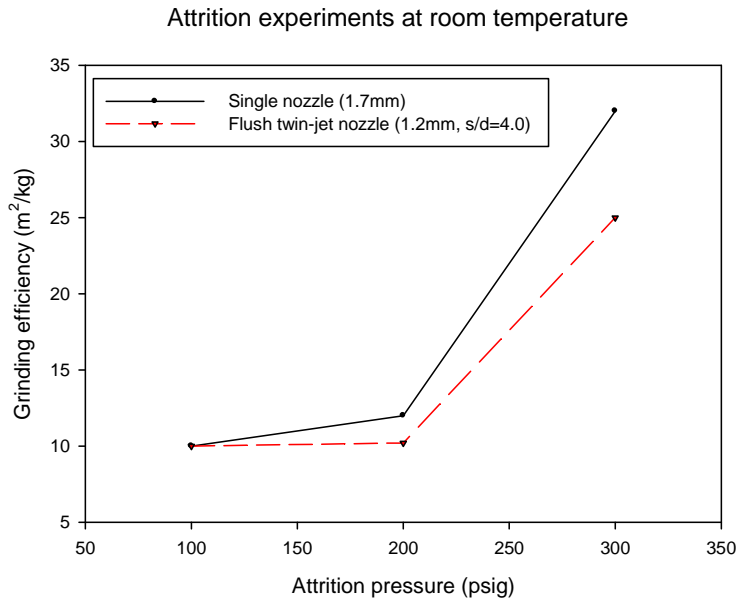
Attrition experiments at room temperature

Figure 7.37 Effect of nozzle geometry on grinding efficiency (s/d=4.0)

7.7 Conclusions

In the present study, the interaction features of twin supersonic jets have been simulated. The simulation results revealed that the twin-jet can enhance particle entrainment and momentum transportation into the jet cavity.

These aspects have been validated by attrition experiments in a fluidized bed. The extended twin-jet nozzle with the optimal spacing had a grinding efficiency that was about 30% higher than with a single nozzle. The benefits of the twin-jet nozzle seem stronger at higher nozzle pressures and high temperature. The extended twin-jet nozzles entrain more ambient solids to the jets compared with the single nozzle when they have the same flowrate. However the penetration length of a twin-jet nozzle is shorter than that of a single nozzle.

Experiments also suggest that the spacing ratio of twin-jet has significant effects on the particle grinding efficiency. The optimum nozzle spacing to nozzle diameter ratio was about 5.2, and nozzles with a spacing ratio of 4.0 or 6.5 had little impact on grinding efficiency. Other twin jet geometry parameters also play a crucial role in jet attrition. When compared to the extended twin-jet, the flush twin-jet has negative effect on the particle entrainment and grinding efficiency. The space between the two nozzles of the extended twin-jet nozzle allows more particles to be entrained into the jet.

7.8 Acknowledgements

7.9 Notation

a	Surface area of particles
A	Area (m^2)
A_e	Area of nozzle exit (m^2)
A_t	Area of nozzle throat (m^2)
C_D	Drag coefficient
c	Instantaneous solids velocity (m/s)
d	Diameter (m)
e_{ss}	Coefficient of restitution
f	Drag function for the different exchange-coefficient models
$g_{0,ss}, g_0$	Radial distribution function
G_b	Generation of turbulence kinetic energy due to buoyancy
G_k	Generation of turbulence kinetic energy due to the mean velocity
h	Heat transfer coefficient ($W/M^2 \cdot K$)
L_p	Length of the jet potential core (m)
k	Turbulence kinetic energy per unit mass (J/kg)
K_{sl}, K_{ls}	Fluid-solid exchange coefficient
K_{gs}	Gas-solid exchange coefficient
$k_{\Theta_s} \nabla \Theta_s$	Diffusion of energy
m	Mass (g, kg)
$\dot{m}$	Mass flow rate (kg/s)
NPR	Nozzle pressure ratio
Nu	Nusselt number
p_0	Upstream pressure of nozzle (Pa)
p_a	Ambient pressure (Pa)

p	Pressure (Pa)
p_s	Solid pressure
Pr	Prandtl number
Q	Flow rate of enthalpy (W)
q	Heat flux (W/m^2)
Re	Reynolds number
s	Nozzle centre-to-centre spacing (m)
s/d	Ratio of nozzle spacing to nozzle diameter
u, v, w	Velocity (m/s)
u_{mf}	Minimum fluidization velocity (m/s)
u_g	Bed fluidization velocity (m/s)
U$_0$	Gas velocity at nozzle exit (m/s)
U$_m$	Gas velocity on jet axis (m/s)
$v_{r,s}$	The terminal velocity correlation for the solid phase
Y$_M$	Contribution of the fluctuating dilatation in compressible turbulence to the overall dissipation rate

Greek letters

α	Volume fraction
γ_{Θ_s}	Collisional dissipation of energy
ε	Volume fraction
ε	Turbulent dissipation rate (m^2/s^3)
η	Grinding efficiency
Θ_s	Granular temperature
λ_q	Bulk viscosity (Pa-s)
λ_s	Bulk Viscosity (Pa-s)
μ	Dynamic viscosity (Pa-s)
μ_q	Shear viscosity (Pa-s)
$\mu_{s,kin}$	Kinetic Viscosity (Pa-s)
$\mu_{s,fr}$	Frictional viscosity (Pa-s)
τ_s	Particle relaxation time (Eq. 7.5)
$\overline{\overline{\tau_q}}$	Stress-strain tensor
ρ	Density (kg/m^3)
ρ_B	Bed density (kg/m^3)
ρ_s	Particle density (kg/m^3)
σ	Turbulent Prandtl number
ϕ_{ls}	Energy exchange between the gas phase and the solid phase

1-21

7.10 **References**

Anderson, E. A.; Spall, R. E., Experimental and numerical investigation of two-dimensional parallel jets. *J. Fluids Eng.-Trans. ASME* **2001,** *123* (2), 401-406.

Bentham, A. C.; Kwan, C. C.; Boerefijn, R.; Ghadiri, A., Fluidised-bed jet milling of pharmaceutical powders. *Powder Technology* **2004,** *141* (3), 233-238.

Bird, R. B. B.; Warren E. Stewart; Lightfoot, E. N., *Transport phenomena*. John Wiley & Sons, Inc: New York : , c2007. , 2002.

De Michele, G.; Elia, A.; Massimilla, L., INTERACTION BETWEEN JETS AND FLUIDIZED-BEDS. *Quaderni Dell Ingegnere Chimico Italiano* **1976,** *12* (6), 155-162.

Ding, J.; Gidaspow, D., A Bubbling Fluidization Model Using Kinetic-Theory of Granular Flow. *Aiche Journal* **1990,** *36* (4), 523-538.

Gidaspow, D., *Multiphase flow and fluidization : continuum and kinetic theory descriptions*. Academic Press: Boston, 1994; p xx, 467 p.

Gunn, D. J., Transfer of heat or mass to particles in fixed and fluidised beds. *International Journal of Heat and Mass Transfer* **1978,** *21* (4), 467-476.

Kollermilojevic, D.; Schneider, W., FREE AND CONFINED JETS AT LOW REYNOLDS-NUMBERS. *Fluid Dyn. Res.* **1993,** *12* (6), 307-322.

Li, F.; Briens, C.; Berruti, F.; McMillan, J. In *Study of solids entrainment into attrition jets in fluidized beds*, Fluidization XIII, Gyeong-ju, Korea, Kim, S. D.; Kang, Y.; Lee, J. K.; Seo, Y. C., Eds. Engineering Conferences International: Gyeong-ju, Korea, 2010a; pp 201-208.

Lun, C. K. K.; Savage, S. B.; Jeffrey, D. J.; Chepurniy, N., Kinetic Theories for Granular Flow - Inelastic Particles in Couette-Flow and Slightly Inelastic Particles in a General Flowfield. *J. Fluid Mech.* **1984,** *140* (MAR), 223-256.

McMillan, J. Characterization of the interactions between high velocity jets and fluidized particles. The University of Western Ontario, London, Canada, 2006.

McMillan, J.; Briens, C.; Berruti, F.; Chan, E., High velocity attrition nozzles in fluidized beds. *Powder Technology* **2007a,** *175* (3), 133-141.

McMillan, J.; Briens, C.; Berruti, F.; Chan, E., Particle attrition mechanism with a sonic gas jet injected into a fluidized bed. *Chemical Engineering Science* **2007b,** *62* (14), 3809-3820.

Merry, J. M. D., Penetration of a Horizontal Gas Jet into a Fluidised Bed. *Transactions of the Institution of Chemical Engineers and the Chemical Engineer* **1971,** *49* (4), 189-&.

Moustafa, G. H., EXPERIMENTAL INVESTIGATION OF HIGH-SPEED TWIN JETS. *Aiaa J.* **1994,** *32* (11), 2320-2322.

Ogawa, S.; Umemura, A.; Oshima, N., On the equations of fully fluidized granular materials. *Zeitschrift für Angewandte Mathematik und Physik (ZAMP)* **1980,** *31* (4), 483-493.

Ranz, W. E., Friction and transfer coefficients for single particle and packed beds. *Chem Eng Progress* **1952,** *48* (5), 247-253.

Smith, J. M.; Van Ness, H. C.; Abbott, M.; Van Ness, H., *Introduction to Chemical Engineering Thermodynamics*. McGaw-Hill: 2005.

Taghipour, F.; Ellis, N.; Wong, C., Experimental and computational study of gas-solid fluidized bed hydrodynamics. *Chemical Engineering Science* **2005,** *60* (24), 6857-6867.

Thies, A. T.; Tam, C. K. W., Computation of turbulent axisymmetric and nonaxisymmetric jet flows using the Kappa-epsilon model. *Aiaa J.* **1996,** *34* (2), 309-316.

Wlezien, R. W., NOZZLE GEOMETRY-EFFECTS ON SUPERSONIC JET INTERACTION. *Aiaa J.* **1989,** *27* (10), 1361-1367.

Chapter 8

8 Conclusions and Recommendations

8.1 Conclusions

1. The particle grinding efficiency from a horizontal supersonic nozzle in a hot fluidized bed is strongly dependent on the solid, bed and nozzle properties when the particle attrition is trigged. Larger scale nozzles, operating with a high flowrate of a low molecular weight gas at high temperature provide the highest grinding efficiency. In particular, increasing the operating temperature enhances particle grinding dramatically. The study also suggests that fragmentation is the dominant mechanism in supersonic induced particle attrition in a high temperature fluidized bed.

2. The study shows that the larger nozzles have a higher attrition efficiency than small-scale size nozzles due to the longer penetration length. Longer jets provide more opportunities for particle-particle collisions and give enough time for the large particles to accelerate to a high velocity. Larger attrition nozzles operating at a higher flowrate or attrition steam pressure are recommended for the fluid coking process.

3. The major factors that affect the particle grinding efficiency include particle entrainment into the jet and the jet penetration. Increasing the particle entrainment efficiency is an efficient way to improve the particle grinding efficiency. A novel measuring technique was employed successfully in the study of solids entrainment of a supersonic attrition nozzle in a high temperature fluidized bed. Smaller nozzles provide a higher entrainment efficiency, but a lower attrition efficiency. Solids entrainment is therefore an important factor but not as important as the jet penetration.

4. A thermal technique was developed to measure the penetration length of horizontal supersonic nozzles in a high temperature fluidized bed. The jet penetration length increases with increasing nozzle throat diameter, increasing gas density, and decreasing

particle density. The bed operating temperature is found to have a minimal influence on the penetration length of a supersonic nozzle.

5. A new and improved empirical correlation has been proposed to predict the penetration length of horizontal supersonic jet at high temperature, derived with a variety of nozzle sizes, gas properties, and operating temperatures. The correlation, based on the Froude number, gave predictions that agreed well with the experimental data.

6. A three-dimensional numerical model was developed to simulate a horizontal convergent-divergent attrition jet in a high temperature fluidized bed. The predicted results of jet penetration lengths are in very good agreements with the experimental data and the correlation predictions. The simulation results have also demonstrated that the fluidization velocity and bed temperature have a little influence on jet penetration length. Finally, the hypothesis was proposed that the behavior of a horizontal convergent-divergent nozzle is similar to an inclined buoyant jet in a uniform stagnant environment. The velocity and density profiles follow the Gaussian function distributions.

7. A jet-induced attrition model in fluidized beds at high temperature has been proposed and developed. The model is coupled Eulerian-Eulerian multiphase model with population balance method. Moreover, particle-particle interactions are described with the kinetic theory of granular flow. Experimental results with a hot fluidized bed were used to determine and modify the critical parameters of model. It is found that the best prediction was obtained using the Ghadiri breakage kernel, generalized daughter size distribution function, and discrete solution method. Moreover, the breakage constant of the Ghadiri breakage kernel increases with increasing temperature.

8. Using twin supersonic nozzles provides a way to combine the large entrainment rate achieved with small nozzles with the long jet penetration obtained with large nozzles. Research focused on the interaction features of twin supersonic jets and their application to particle attrition in a fluidized bed. The twin-jet nozzle with the best geometry demonstrates the highest grinding efficiency among all cases: it is consistently about 30%

higher than with a single nozzle. Moreover, the benefits of the twin-jet nozzle seem stronger at higher nozzle pressures and high temperature. The twin-jet nozzles entrain more ambient solids to the jets compared with the single nozzle with the same flowrate, but their jet penetration is shorter than for a single nozzle. Experiments also suggest that the spacing of the twin nozzles has significant effects on the particle grinding efficiency.

9. The twin nozzles geometries play a crucial role in the mechanism of jet-induced particle breakage. For the extended twin-jet, the space between the two nozzles allows more particles to be entrained into the jet. In contrast, the geometry of the flush twin-jet has a negative effect on the particle entrainment and grinding efficiency.

8.2 Recommendations

1. A new modified correlation based on the Froude number was developed to predict the penetration length of a horizontal supersonic nozzle. The hypothesis of buoyant jet and Gaussian distribution of velocity profile is useful to justify why the penetration length of a horizontal supersonic nozzle can be predicted with the Froude number. In future work, a global semi-empirical correlation probably can be derived from the theory of buoyant jet to model the jet penetration in gas-solid fluidized beds regarding to various particles and operating conditions.

2. Data analysis with the method of moments shows that a higher attrition temperature leads to a higher grinding efficiency and coarser attrition products. It would be interesting to continue to study the influence of attrition temperature on the final particle size distribution.

3. In the present study, the extended twin-jet performed better than the flush twin-jet. Further work should expand the investigation of the influence of geometry of a single nozzle on solid entrainment in jet.

4. Future work is required to develop a semi-empirical breakage kernel and to improve optimization procedure for more precise prediction of particle attrition from a convergent-divergent nozzle in fluidized beds at high temperature.

Curriculum Vitae

Name: Feng Li

Post-secondary Education and Degrees:
Southern Yangtze University, China
Wuxi, Jiangsu, China
1986-1990 B.A.

The University of Western Ontario
London, Ontario, Canada
2006-2007 M.Eng.

Honours and Awards:
Western Engineering Scholarship
2007-2011

Accelerate Internship Project Award (MITACS)
2010

Related Work Experience
Teaching Assistant
The University of Western Ontario
2007-2011

Research Assistant
The University of Western Ontario
2007-2011

Visiting Research Engineer
Syncrude Research Centre, Edmonton
May 2010 - Aug 2010

Process Engineer & Project Engineer
Greenapple Chemical, Inc.
2001-2004

Process Engineer
Wuxi Chemical Industry Group Co. Ltd.
1990-2001

Publications:

Li, F.; Briens, C.; Berruti, F.; McMillan, J., *Study of solids entrainment into attrition jets in fluidized beds*. Fluidization XIII Proceeding, Kim, S. D.; Kang, Y.; Lee, J. K.; Seo, Y. C., Eds. Engineering Conferences International: Gyeong-ju, Korea, 2010a.

Li, F.; Briens, C.; Berruti, F.; McMillan, J., *Penetration of high velocity horizontal gas jets into a fluidized bed at high temperature*. Fluidization XIII Proceeding, Kim, S. D.; Kang, Y.; Lee, J. K.; Seo, Y. C., Eds. Engineering Conferences International: Gyeong-ju, Korea, 2010b

Li, F., McMillan, J., Mueller, E., *Study of particle attrition process in commercial fluid Cokers*. Syncrude Research Department Progress Report, 39 (09), p. 49-66, 2010c.